NASA Conference Publication 10124

Seals Flow Code Development–92

Proceedings of a workshop held at
NASA Lewis Research Center
Cleveland, Ohio
August 5–6, 1992

NASA

NASA Conference Publication 10124

Seals Flow Code Development–92

Proceedings of a workshop held at
NASA Lewis Research Center
Cleveland, Ohio
August 5–6, 1992

NASA
National Aeronautics and
Space Administration

Office of Management

Scientific and Technical
Information Program

1992

CONTENTS

SUMMARY

A two-day workshop was held at the NASA Lewis Research Center on August 5 and 6, 1992. The intent of the workshop was to inform the technical community of the seal code development activity sponsored by NASA Lewis and to provide a forum for participants to exchange information on respective activities in seals. We thank the workshop presenters, the participants and the peer committee for their contributions.

Three codes were disseminated to the technical community for beta testing. They are the ICYL (cylindrical seal in incompressible fluids), GCYL (cylindrical seal in compressible fluids) and SPIRALG (spiral grooved gas seal) code. Close to thirty companies requested these codes at the workshop.

Several needs, shortcomings, and problem areas have been delineated from the workshop on the NASA Lewis seals contract with Mechanical Technology Incorporated. The deficiencies include: validation data sets, convection flow contributions (inlet, inertia, turbulence, body forces), surface distortions, dynamics matrices in the CFD code, computational efficiency (speed, storage, hardware), and awareness of current seal user requirements and projected needs.

The positive aspects, however, must not be overlooked. The codes are being worked into a transportable user friendly format. They are available for members of the peer committee and beta-users to apply toward their particular area of expertise. The findings from beta-testing need to be reported to enhance program effectiveness. This will be an on-going activity throughout this contract.

Workshop Chairs:

Anita D. Liang
Robert C. Hendricks

OVERVIEW

SEALS FLOW CODE DEVELOPMENT WORKSHOP

and

BRUSH SEALS SYSTEM WORKSHOP

AUGUST 5-6, 1992

NASA LEWIS RESEARCH CENTER

AEROSPACE TECHNOLOGY DIRECTORATE SPACE PROPULSION TECHNOLOGY DIVISION NASA Lewis Research Center

PROGRAM OBJECTIVE - Develop Codes for Analyzing and Designing Optimized Advanced Seals for Future Aerospace and Advanced Rocket Engine Systems

- OVERVIEW OF NASA CONTRACT NAS3-25644
- CURRENT ISSUES
- PROGRAM STATUS

AEROSPACE TECHNOLOGY DIRECTORATE
SPACE PROPULSION TECHNOLOGY DIVISION
NASA Lewis Research Center

PROGRAM SCOPE

- SEVEN YEAR EFFORT (NASA Contract NAS3-25644)
- PARALLEL PATHS - Scientific Code and Industrial Codes
- DEVELOPMENT OF A KNOWLEDGE-BASED SYSTEM
- TECHNOLOGY TRANSFER VIA WORKSHOPS
- CODE VALIDATION VIA PUBLISHED DATA, IN-HOUSE TEST WORK AND COOPERATIVE PROGRAMS

TEAM MEMBERS

NASA LeRC	MTI	CFDRC
Julie Carlile	Bharat Aggarwal	Mahesh Athavale
Bob Hendricks	Tony Artiles	Andrzej Przekwas
Anita Liang	Wilbur Shapiro	Ashok Singhal
Margaret Proctor		

AEROSPACE TECHNOLOGY DIRECTORATE
SPACE PROPULSION TECHNOLOGY DIVISION
NASA Lewis Research Center

PROGRAM ORGANIZATION

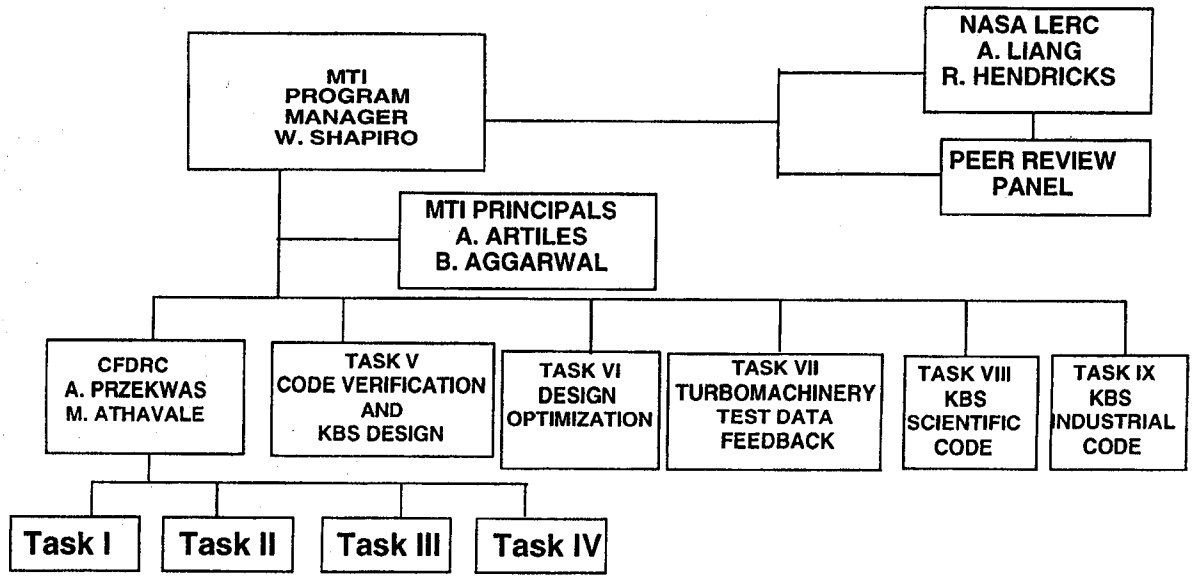

Task 1 Cylindrical Seals Code
Task II Cylindrical Code Augmentation (Labyrinth, Honeycomb, Damper, Brush)
Task III Face, Wave, Grooved Seals
Task IV Tip, Contact, Non-Continuous Seals

MAJOR TECHNICAL ACTIVITIES

1. DEVELOPMENT OF ANALYTICAL CODES
2. DEVELOPMENT OF EXPERT SYSTEMS
3. INTEGRATION OF CODES AND EXPERT SYSTEMS INTO ONE SINGLE FRAMEWORK

AEROSPACE TECHNOLOGY DIRECTORATE SPACE PROPULSION TECHNOLOGY DIVISION NASA Lewis Research Center

CODE DEVELOPMENT

INDUSTRIAL CODES -	TWO-DIMENSIONAL CODES FOR DIFFERENT TYPES OF SEALS
SCIENTIFIC CODE -	A THREE-DIMENSIONAL CFD CODE FOR SEAL ANALYSIS
SEAL TYPES -	Cylindrical, bushing and ring, face, labyrinth, tip, damping, brush, electro-fluids, and "smart"

INDUSTRIAL KBS

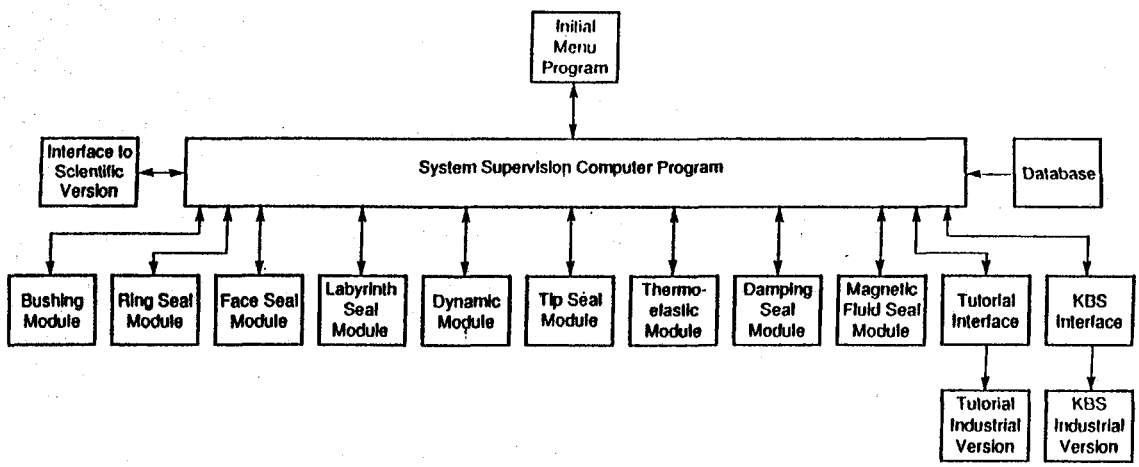

AEROSPACE TECHNOLOGY DIRECTORATE
SPACE PROPULSION TECHNOLOGY DIVISION
NASA Lewis Research Center

SCIENTIFIC KBS

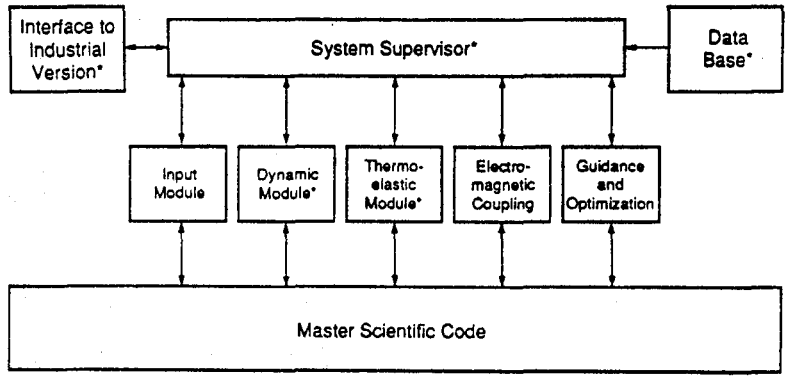

*Common with Industrial Knowledge-Based System

A MODULAR KNOWLEDGE-BASED SYSTEM

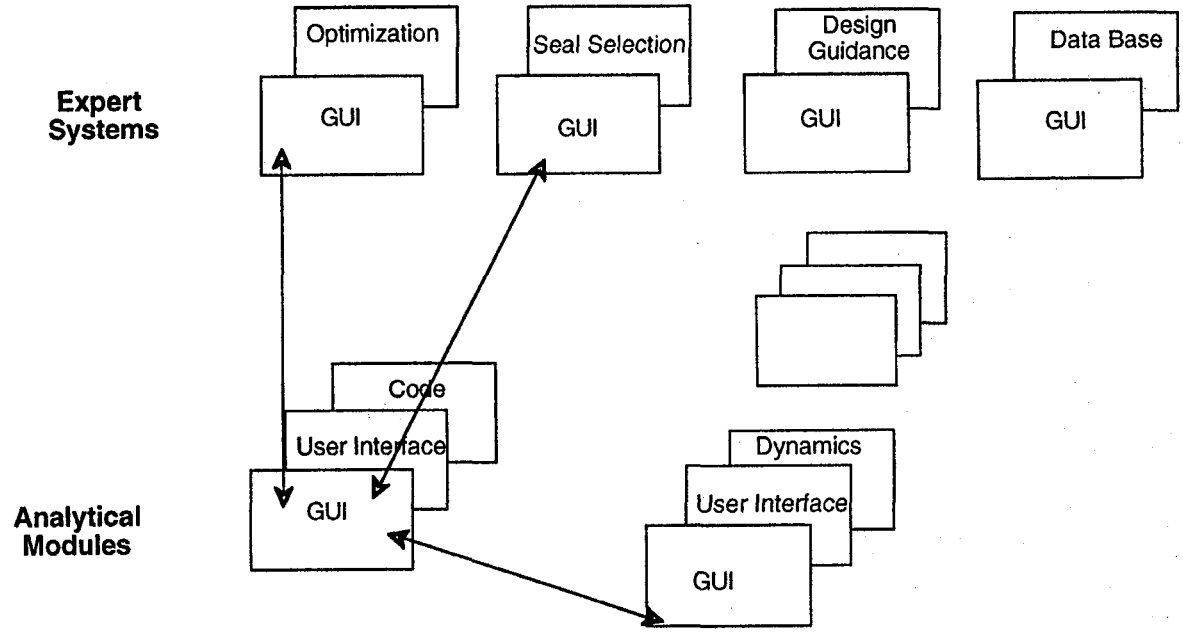

Level of Communications Between Modules - - GUI

AEROSPACE TECHNOLOGY DIRECTORATE
SPACE PROPULSION TECHNOLOGY DIVISION
NASA Lewis Research Center

MAJOR ISSUE FROM 1991

- PORTABILITY OF THE KBS

COMPUTER SYSTEM CONSIDERATIONS

- A DESK-TOP SYSTEM (FOR ALL USER TYPES)
- SUFFICIENT MEMORY FOR CODE EXECUTION AND FOR MULTITASKING
- I/O COMMUNICATIONS WITH THE SCIENTIFIC CODE
- COMPUTING POWER FOR GUI
- PORTABLE SOFTWARE DEVELOPMENT TOOLS
- PRICING

AEROSPACE TECHNOLOGY DIRECTORATE SPACE PROPULSION TECHNOLOGY DIVISION NASA Lewis Research Center

COMPUTER SYSTEMS

PERSONAL COMPUTERS WITH OS/2 OPERATING SYSTEM

- Intel 30386 or Higher
- Math Coprocessor
- 8 Megabytes of RAM
- 80 Megabyte hard drive

UNIX WORKSTATIONS

- 16 Megabytes of RAM

MACINTOSH/IBM INTEGRATED SYSTEM

PORTABILITY OF SOFTWARE

Fortran and C for Codes

GUI - User Interface and C++ compatible with OS/2 Presentation Manager and OSF/MOTIF

Expert Systems - NEXPERT or CLIPS

AEROSPACE TECHNOLOGY DIRECTORATE SPACE PROPULSION TECHNOLOGY DIVISION NASA Lewis Research Center

STATUS

- SEVERAL INDUSTRIAL CODES HAVE BEEN PRODUCED AND READY FOR DISSEMINATION
- A 3D CFD CODE FOR CYLINDRICAL SEALS HAS BEEN COMPLETED
- THE KNOWLEDGE-BASED SYSTEM FRAMEWORK HAS BEEN DEFINED
- RESULTS AND STATUS OF THE PROGRAM HAVE BEEN REPORTED IN SEVERAL MAJOR CONFERENCES
- SEVERAL COOPERATIVE PROGRAMS HAVE BEEN ESTABLISHED
- A TECHNOLOGY TRANSFER PLAN HAS BEEN FORMULATED

CODE DELIVERABLES

	CODE OR MODULE	APPROXIMATE DELIVERY DATE	
1.	CFD Cylindrical Code	02/01/92	(09/92)
2.	Augmented CFD Cylindrical Module	02/01/94	
3.	CFD Code, Face, Wave, Non-Continuous Module	09/01/95	
4.	CFD, Tip, Contact, Non-Continuous Module	09/01/96	
5.	GJOURN	02/01/91	
6.	ICYL	03/01/91	(07/92)
7.	SPIRALG	04/01/91	
8.	IFACE	02/01/92	
9.	GFACE	03/01/92	(10/92)
10.	SPIRALI	04/01/92	
11.	FACEDY	02/01/93	
12.	RINGDY	03/01/93	
13.	LABYRINTH	04/01/93	
14.	FACECON	02/01/94	
15.	DISTORTION	04/01/94	
16.	Additional Codes	04/01/95	
17.	Industrial KBS	04/01/96	
18.	Scientific KBS	04/01/96	

AEROSPACE TECHNOLOGY DIRECTORATE SPACE PROPULSION TECHNOLOGY DIVISION NASA Lewis Research Center

NEAR TERM ACTIVITIES

CONTINUE CODE DEVELOPMENT

ADD TURBULENCE AND INERTIA IN COMPRESSIBLE CODES

DEVELOP USER INTERFACE FOR THE CFD CODE

DEVELOP GRAHICAL USER INTERFACE

DEVELOP EXPERT SYSTEMS

92P48

Industrial Code Development

Presented by

W. Shapiro and A. Artiles
Mechanical Technology Incorporated
Latham, New York

Presented to

NASA Seals Workshop
Contract NAS3-25644

5 August 1992

OBJECTIVES

- Compile and generate sets of verified 2D and simplified 3D or 1D codes
- Codes are intended for expeditious parametric studies, analysis, and design of a wide variety of seals
- Integration is accomplished by the industrial KBS; additional functions of the KBS are:
  - User-friendly interaction
  - Contact sensitive and hypertext help
  - Design guidance
  - Expandable data base

CODE DELIVERABLES

Code Module	Approximate Delivery Date	
GCYL (Gas Cylindrical)	02/01/91	←
ICYL (Incompressible Cylindrical)	03/01/91	←
SPIRALG (Gas Spiral Groove)	04/01/91	←
CFD Cylindrical Code	07/31/92	←
IFACE (Incompressible Face)	12/31/92	←
GFACE (Gas Face)	12/31/92	←
SPIRALI (Incompressible Spiral Groove)	12/31/92	←
FACEDY (Face Dynamics)	09/30/93	←
RINGDY (Ring Dynamics)	09/30/93	←
LABYRINTH (Gas)	09/30/93	←
Augmented CFD Cylindrical Module	02/01/94	
FACECON (Face Contact)	02/01/94	
DISTORTION (Thermoelastic Distortion)	04/01/94	
Additional Codes: Brush Damping Seal	04/01/95	
CFD Code, Face, Wave, Groove Module	09/01/95	
Industrial KBS	04/01/96	←
Scientific KBS	04/01/96	←
CFD, Tip, Contact, Noncontinuous Module	09/01/96	

Computer Code GCYL Gas Cylindrical Seals

GCYL CAPABILITIES

- ❑ Varying geometries
- ❑ Variable or constant grid (30 × 74)
- ❑ Shaft eccentricity and misalignment
- ❑ Specified boundary pressures and periodic boundary conditions
- ❑ Symmetry in axial direction
- ❑ Determining load (function of displacement) or seal position to satisfy given load
- ❑ Choice of English or SI units
- ❑ Frequency-dependent stiffness and damping coefficients
- ❑ Inlet and outlet inertia*
- ❑ Turbulence*

*To be added.

CYLINDRICAL GEOMETRIES

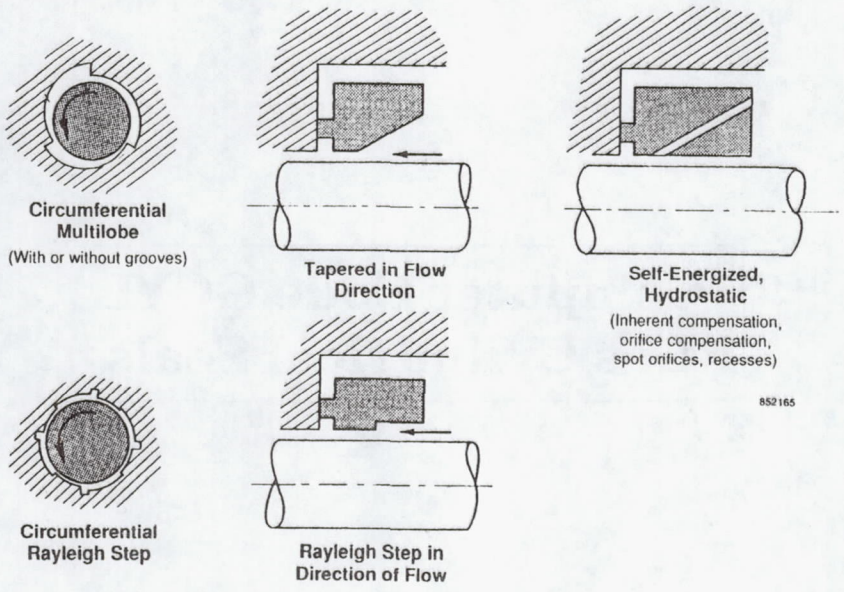

SEGMENTED RING SEAL

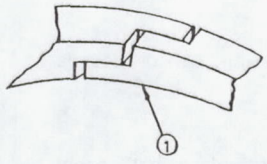

Item	Description	Material
1	Segmented Ring Rayleigh Step	Carbon
2	Spring-Radial	Inconel X-750
3	Spring-Axial	Inconel X-750
4	Housing	Stainless Steel 17-4 PH
5	Cover	Stainless Steel 17-4 PH
6	Stop Pin	Stainless Steel 17-4 PH
7	Seal	Teflon
8	Sleeve	Inconel 718 Hard Chromium Plated

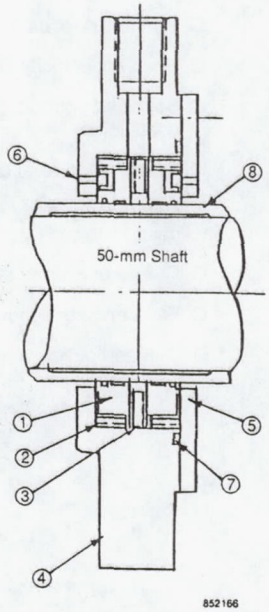

GCYL OUTPUT

- Clearance distribution
- Pressure distribution
- Leakage at specified flow paths
- Load and load angle
- Righting moments
- Viscous dissipation
- Cross-coupled, frequency-dependent stiffness and damping coefficients
- Plotting routines (pressure and clearance distribution)

COMPRESSIBLE REYNOLDS' EQUATION

$$\frac{\partial}{\partial\theta}\left(PH^3\,\frac{\partial P}{\partial\theta}\right)+\frac{\partial}{\partial Z}\left(PH^3\,\frac{\partial P}{\partial Z}\right)=\Lambda\,\frac{\partial\,(PH)}{\partial\theta}+\frac{\partial\,(PH)}{\partial T}$$

where:

$$Z = z/R,\ H = h/C_o,\ T = t/t_o,\ P = p/p_o,$$

$$\Lambda = \frac{6\mu\omega R^2}{p_o C_o^2},\quad t_o = \frac{12\mu R^2}{p_o C_o^2}$$

INTEGRAL FORMAT

$$\int \nabla \cdot \vec{Q} dA = \oint \vec{Q} \cdot \vec{n}\, dS = \frac{\partial}{\partial T} \int (PH)\, dA$$

where:

$$\vec{Q} = H^3\, P\, \frac{\partial P}{\partial \theta} + \Lambda\, (PH)$$

ASSUMPTIONS

- Laminar flow

  $$\tau = \mu \frac{dV}{dy}, \frac{dV}{dy} = U/h$$

  where:

  τ = Shear stress
  μ = Viscosity
  V = Fluid velocity
  U = Slider velocity
  y = Film height

- Inertia is small and neglected compared to viscous shear
- Pressure across film is constant
- Height of film is small compared to other geometric dimensions; curvature is ignored
- Viscosity is constant
- Gas is iosothermal

TURBULENCE

- $Re = \frac{\rho U h}{\mu} \geq 1000$

  Where:

  ρ = Density
  U = Surface velocity
  h = Film thickness
  Re = Reynolds number

- The most common approach to turbulence is to use G factors that modify the viscosity. G factors are dependent on the Reynolds number and pressure gradients

  — Couette Reynolds number: $Re = h R\omega\rho/\mu$

  — Poiseuille Reynolds number: $Re^* = h^3 \mid \vec{\nabla}P \mid \rho/\mu^2$

  — $G_x = \text{Min}\,[G_x\,(Re), G_p\,(Re^*)]$

  — $G_z = \text{Min}\,[G_z\,(Re), G_p\,(Re^*)]$

UNWRAPED SEAL SURFACE

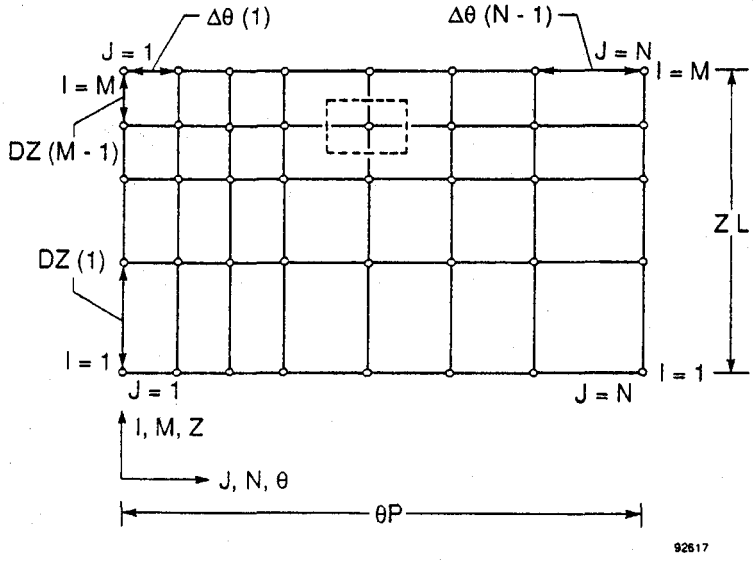

FLOW BALANCE CELL

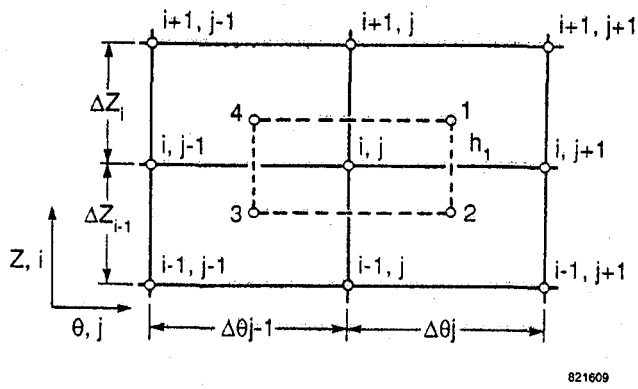

FLOW BALANCE CONTROL VOLUME

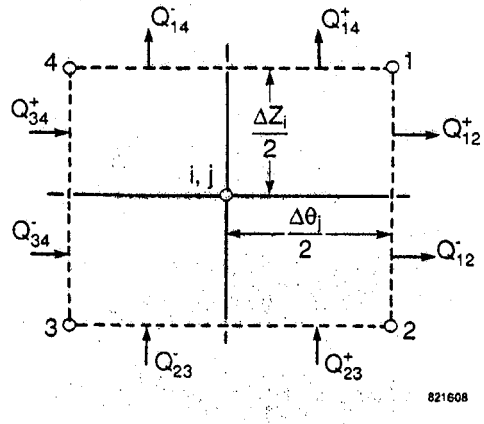

FLOW BALANCE EQUATION

$$Q_{12}\frac{\Delta Z_i}{2} + Q_{12}^{-}\frac{\Delta Z_{i-1}}{2} + Q_{14}^{+}\frac{\Delta\theta_j}{2} + Q_{14}^{-}\frac{\Delta\theta_{j-1}}{2} - Q_{34}^{+}\frac{\Delta Z_i}{2} - Q_{34}^{-}\frac{\Delta Z_{i-1}}{2}$$

$$- Q_{23}^{+}\frac{\Delta\theta}{2} - Q_{23}^{-}\frac{\Delta\theta_{j-1}}{2} = -\frac{1}{4}(\Delta\theta_j + \Delta\theta_{j-1})(\Delta Z_i + \Delta Z_{i-1})\frac{\partial H_{ij}}{\partial t}$$

$$+ Q_{source}$$

Where, for example

$$Q_{12}^{+} = \frac{-H_1^3\, G_x\,(P_{i,j+1} - P_{i,j})}{\Delta\theta_j} + \Lambda\, P_{12}\, H_1$$

and

$$P_{12} = \frac{P_{i,j} + P_{i,j+1}}{2}$$

NEWTON-RAPHSON LINEARIZATION

$$F_{ij}\,(P_1, P_2, P_3, \ldots P_k, \ldots P_9) = 0$$

- The partial derivatives for the Newton-Raphson linearization may be calculated numerically:

$$\frac{\partial F_{ij}}{\partial P_k} = \Big\{F_{ij}\,(P_1, P_2, \ldots P_k + \varepsilon/2, \ldots P_9) - F_{ij}\,(P_1, P_2, \ldots P_k - \varepsilon/2, \ldots P_9)\Big\}/\varepsilon$$

- Then the linear equation for determining iterated pressures is:

$$F_{ij}\,(\text{old}) + \sum_{k=1}^{9}\frac{\partial F_{ij}}{\partial P_k}\,(\text{old})\,(P_k\,(\text{new}) - P_k\,(\text{old})) = 0$$

- The equation is put into the matrix format where P_j is the current pressure being solved for

$$[C_i]\,\{P_i\} + [E_i]\,\{P_{i-1}\} + [D_i]\,\{P_{i+1}\} = \{R_i\}$$

The system of equations is solved by the column matrix method.

FREQUENCY-DEPENDENT SPRING AND DAMPING COEFFICIENTS

$$\int \vec{\nabla} \cdot \vec{Q} dA = \oint \vec{Q} \cdot \vec{n}\, ds = -\frac{\partial}{\partial T} \int (1 + P)\, H dA$$

- Introduce the RHS and perturb clearance and pressure

  $H = e^{i\sigma t}$, $P' = Pe^{i\sigma t}$

  then, perturb the resulting equation with respect to eccentricity to obtain

  $$\frac{\partial P}{\partial \varepsilon_k}$$

- The real part of the derivative with respect to eccentricity integrated over the area is stiffness. While the imaginary part divided by σ and integrated over the area is damping

FREQUENCY-DEPENDENT SPRING AND DAMPING COEFFICIENTS (continued)

$$\int \vec{\nabla} \cdot \vec{Q} dA = \oint \vec{Q} \cdot \vec{n}\, ds = -\frac{\partial}{\partial T} \int (1 + P)\, H dA$$

- The final set of linear difference equations for the complex stiffness pressure derivatives $\{P^{k,l}\}$ are obtained

$$[C^{*l}]\{P_j^{k,l}\} + [\hat{E}^l]\{P_{j-1}^{k,l}\} + [\hat{D}^l]\{P_{j+1}^{k,l}\} = \{R^{j,k}\} - [\hat{C}^{j,k}]\{\hat{P}_j\} - [\hat{E}^{j,k}]\{\hat{P}_{j-1}\} - [\hat{D}^{j,k}]\{\hat{P}_{j+1}\}$$

where:

$$[C^{*l}] = [\hat{C}^l] + i\sigma[\bar{C}^l]$$

$$\{R^{j,k}\} = \{\hat{R}^{j,k}\} - i\sigma\{\bar{R}^{j,k}\}$$

$$\bar{R}_i^{j,k} = A_{ij} \frac{\partial H_{ij}}{\partial \varepsilon_k} (1 + P_{ij})$$

$$\bar{C}_{ij}^{l} = HC_1 A_1 + HC_2 A_2 + HC_3 A_3 + HC_4 A_4$$

$$[\hat{C}^{j,k}] = \frac{[\hat{C}^l]_{\varepsilon_k + \eta} - [\hat{C}^l]\,|_{\varepsilon_k}}{\eta}$$

- The system of equations is solved by the column method in a directly analogous manner to that used in solving the steady-state equation. The principal difference is that all the matrix operations are performed using complex arithmetic.

STIFFNESS AND DAMPING COEFFICIENTS

Speed (rpm)		48,000	48,000
Excitation Frequency (rpm)		48,000	0
Stiffness Coefficients			
Principal X (lb/in.)	KXX =	0.965	5885
Cross coupled (lb/in.)	KXY =	1942	7267
Cross coupled (lb/rad)	KXA =	0.730	-0.239
Cross coupled (lb/rad)	KXB =	1.291	1.298
Cross coupled (lb/in.)	KYX =	1040	-7116
Principal Y (lb/in.)	KYY =	17,670	13,050
Cross coupled (lb/rad)	KYA =	1.450	3.258
Cross coupled (lb/rad)	KYB =	0.448	1.877
Cross coupled (in.-lb/in.)	KAX =	0	0
Cross coupled (in.-lb/in.)	KAY =	0	0
Principal A (in.-lb/rad)	KAA =	639	421
Cross coupled (in.-lb/rad)	KAB =	72	192
Cross coupled (in.-lb/in.)	KBX =	0	0
Cross coupled (in.-lb/in.)	KBY =	0	0
Cross coupled (in.-lb/rad)	KBA =	-194	-294
Principal B (in.-lb/rad)	KBB =	221	134
Damping Coefficients			
Principal X (lb-sec/in.)	DXX =	1.658	1.406
Cross coupled (lb-sec/in.)	DXY =	-0.7059	-1.859
Cross coupled (lb-sec/rad)	DXA =	0	0
Cross coupled (lb-sec/rad)	DXB =	0	0
Cross coupled (lb-sec/in.)	DYX =	0.918	3.012
Principal Y (lb-sec/in.)	DYY =	1.521	1.897
Cross coupled (lb-sec/rad)	DYA =	0	0
Cross coupled (lb-sec/rad)	DYB =	0	0
Cross coupled (in.-lb-sec/in.)	DAX =	0	0
Cross coupled (in.-lb-sec/in.)	DAY =	0	0
Principal A (in.-lb-sec/rad)	DAA =	0.090	0.1130
Cross coupled (in.-lb-sec/rad)	DAB =	-0.031	-0.047
Cross coupled (in.-lb-sec/in.)	DBX =	0	0
Cross coupled (in.-lb-sec/in.)	DBY =	0	0
Cross coupled (in.-lb-sec/rad)	DBA =	0.026	0.039
Principal B (in.-lb-sec/rad)	DBB =	0.067	0.069

360° cylindrical seal; L = 1 in.; D = 1 in.; C = 0.001 in.;
$\mu = 3 \times 10^{-9}$ lb-sec/in.^{2}; 0 gage pressure at both ends

INLET INERTIA

$$Q = G\, C_D\, A_o\, P_s \left\{ \left(\frac{P_R}{P_s}\right)^{2/\gamma} \left[1 - \left(\frac{P_R}{P_s}\right)^{\frac{\gamma-1}{\gamma}} \right] \right\}^{1/2}$$

where:

- C_D = Coefficient of discharge
- A_o = Orifice area, $in.^2$
- P_s = Upstream pressure, psia
- P_R = Downstream pressure, psia
- γ = Ratio of specific heats
- G_c = Gas constant, $sec^2/°R$
- θ = Absolute gas temperature
- Q = Orifice flow, lb/sec

$$\text{If } \left(\frac{P_R}{P_s}\right) \leq P_{CR}, \text{ then } \left(\frac{P_R}{P_s}\right) = P_{CR}$$

where:

$$P_{CR} = \left[\frac{2.0}{(\gamma + 1)}\right]^{\left(\frac{\gamma}{\gamma-1}\right)}$$

INTERNAL HALVING ROUTINE

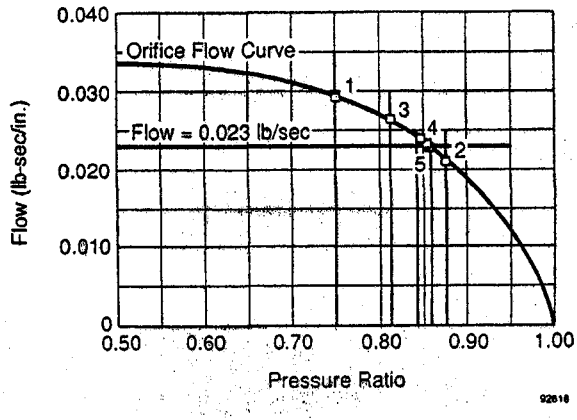

Computer Code SPIRALG
Spiral-Groove Gas Seals

SPIRAL-GROOVE FACE SEAL

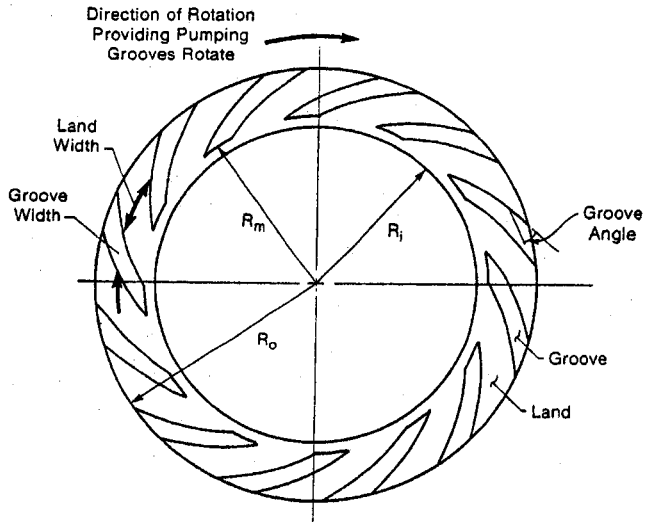

Groove Angle = α
Groove Depth = GD
Land Width/Groove Width = γ

872565-2

SPIRAL-GROOVE CYLINDRICAL SEALS

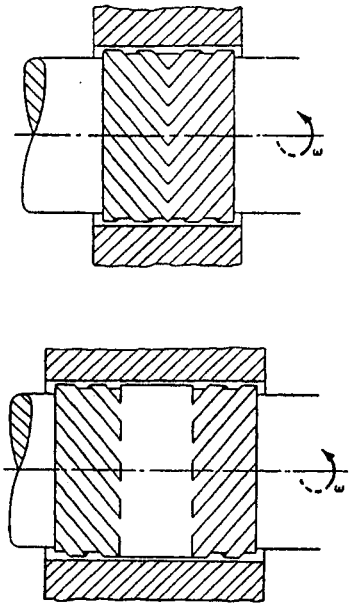

CAPABILITIES

- Shaft seals and face seals
- Compressible flow
- Finite eccentricity and misalignment
- Four degrees of freedom for shaft seals (three for face seals)
- Frequency-dependent dynamic coefficients
- Arbitrary end pressures
- Predicts load, flow, power loss, dynamic coefficients, shaft displacements, and minimum film thickness

ASSUMPTIONS

- Laminar isothermal flow
- No fluid inertia
- Ideal gas law
- Thin film approximations are valid
- Narrow groove theory
- Linearized time dependence
- Ideal surfaces

TECHNICAL FEATURES

- Finite misalignment
- General algorithm for treating frequency-dependent dynamic coefficients
- Either forces or displacements may be specified in all degrees of freedom
- Optional implementation of automatic numerical damping algorithm
- Optional implementation of Romberg extrapolation algorithm

COORDINATE REFERENCE FRAMES

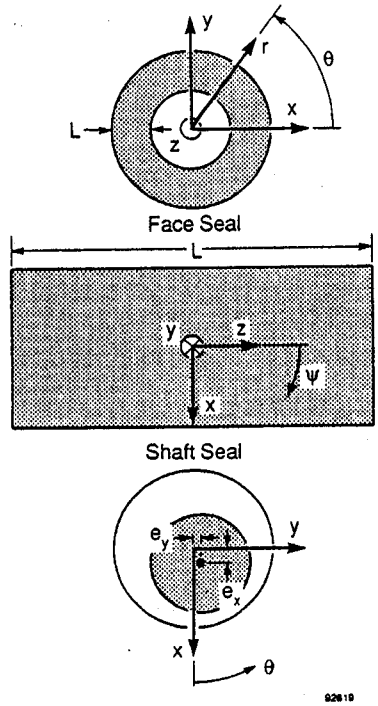

ECCENTRIC SPIRAL-GROOVED SHAFT SEAL

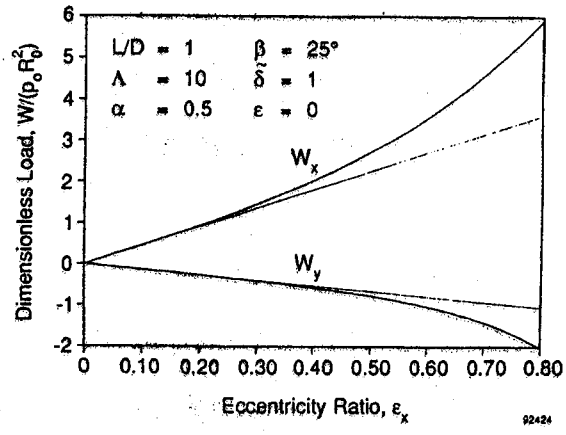

SPIRALG THEORY

GLOBAL AND LOCAL PRESSURES

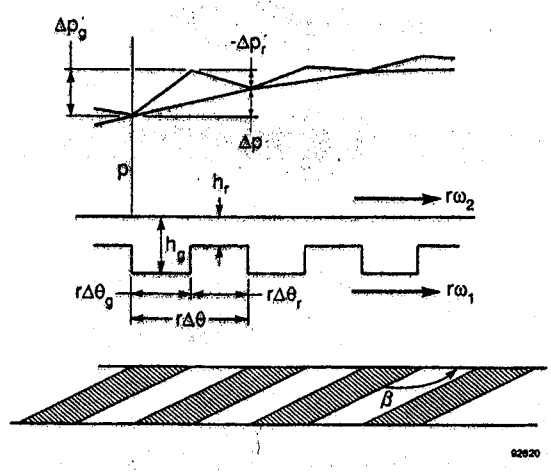

GLOBAL AND LOCAL PRESSURE GRADIENTS

- When the number of grooves becomes large, the sawtooth portion of the local pressure variation may be approximated with linear representations

$$\frac{\Delta p}{\Delta \theta} = \frac{\Delta p_g'}{\Delta \theta} + \frac{\Delta p_r'}{\Delta \theta} = \left(\frac{\partial p'}{\partial \theta}\right)_g \frac{\Delta \theta_g}{\Delta \theta} + \left(\frac{\partial p'}{\partial \theta}\right)_r \frac{\Delta \theta_r}{\Delta \theta}$$

$$\frac{\Delta \theta_g}{\Delta \theta} = \alpha \text{ and } \frac{\Delta \theta_r}{\Delta \theta} = 1 - \alpha$$

$$\frac{\partial p}{\partial \theta} = \alpha \left(\frac{\partial p'}{\partial \theta}\right)_g + (1 - \alpha) \left(\frac{\partial p'}{\partial \theta}\right)_r$$

- The corresponding relationship in the traverse direction,

$$\frac{\partial p}{\partial s} = \alpha \left(\frac{\partial p'}{\partial s}\right)_g + (1 - \alpha) \left(\frac{\partial p'}{\partial s}\right)_r$$

  is obtained in a similar manner.

- The remaining two equations required to solve for the four local pressure derivatives are obtained from continuity considerations.

CONTINUITY CONDITIONS

- Continuity of pressure at groove-ridge interface

$$\frac{\cos \beta}{r} \left(\frac{\partial p'}{\partial \theta}\right)_g + \sin \beta \left(\frac{\partial p'}{\partial s}\right)_g = \frac{\cos \beta}{r} \left(\frac{\partial p'}{\partial \theta}\right)_r + \sin \beta \left(\frac{\partial p'}{\partial s}\right)_r$$

- Continuity of flow at groove-ridge interface

$$- \frac{h_g^3}{12 \mu} \left[\frac{\sin \beta}{r} \left(\frac{\partial p'}{\partial \theta}\right)_g - \cos \beta \left(\frac{\partial p'}{\partial s}\right)_g\right]$$

$$+ \frac{h_g}{2} r(\omega_2 - \omega_1) \sin \beta$$

$$= - \frac{h_r^3}{12 \mu} \left[\frac{\sin \beta}{r} \left(\frac{\partial p'}{\partial \theta}\right)_r - \cos \beta \left(\frac{\partial p'}{\partial s}\right)_r\right]$$

$$+ \frac{h_r}{2} r(\omega_2 - \omega_1) \sin \beta$$

- Four equations in four unknown local derivatives that can be solved for in terms of global derivatives

FLOW EQUATIONS

- The transverse flow across a ridge groove pair is

$$q_s = -\frac{h_g^3}{12\mu}\frac{p}{p_o}\alpha\left(\frac{\partial p'}{\partial s}\right)_g - \frac{h_r^3}{12\mu}\frac{p}{p_o}(1-\alpha)\left(\frac{\partial p'}{\partial s}\right)_r$$

- Similarly, the flow in the theta or parallel direction is

$$q_\theta = -\frac{h_g^3}{12\mu}\frac{p}{p_o}\alpha\frac{1}{r}\left(\frac{\partial p'}{\partial \theta}\right)_g$$

$$-\frac{h_r^3}{12\mu}\frac{p}{p_o}(1-\alpha)\frac{1}{r}\left(\frac{\partial p'}{\partial \theta}\right)_r$$

$$+ r\frac{\omega_1+\omega_2}{2}\frac{p}{p_o}\left[\alpha h_g + (1-\alpha)h_r\right]$$

- The squeeze film flow is

$$q_A = -\frac{1}{p_o}\left(p\left[\alpha h_h + (1-\alpha)h_r\right]\right)$$

- The global flows are expressed in terms of local derivatives, which, in turn, are functions of global derivatives. Thus, global parameters can be used throughout.

DIMENSIONLESS FLOWS

$$Q_\theta = -(1+P)\left[H_r^3\left(k_2\frac{\partial}{\partial S} + \frac{k_3}{R}\frac{\partial}{\partial\theta}\right)P + \Lambda_\delta k_4 R\sin\beta - \Lambda(\alpha\tilde{\delta} + H_r)R\right]$$

$$Q_s = -(1+P)\left[H_r^3\left(k_1\frac{\partial}{\partial S} + \frac{K_2}{R}\frac{\partial}{\partial\theta}\right)P - \Lambda_\delta K_4 R\cos\beta\right]$$

where:

$$P = \frac{p-p_o}{p_o} \qquad R = \frac{r}{R_o}$$

$$\vec{Q} = \frac{12\mu R_o}{C^3 p_o}\vec{q} \qquad \tilde{t} = \frac{\omega}{2\Lambda}t$$

$$H_r = \frac{h_r}{C} \qquad \Gamma = \frac{h_g}{h_r}$$

$$S = \frac{s}{R_o}$$

and

$$\Lambda = \frac{6\mu\omega R_o^2}{p_o C^2} \qquad \tilde{\delta} = \frac{h_g - h_r}{C}$$

$$\Lambda_\delta = \Lambda\tilde{\delta}\tilde{\omega}\alpha(1-\alpha)\sin\beta \qquad \alpha = \frac{l_g}{l_r + l_g}$$

$$\tilde{\omega} = \frac{\omega_2 - \omega_1}{\omega}$$

k VECTOR

- The column matrix containing spiral-groove coefficients, $k_i(\alpha, \beta, \Gamma)$, is:

$$k = \begin{bmatrix} \dfrac{\alpha(1-\alpha)(\Gamma^3-1)^2 \sin^2\beta + \Gamma^3}{(1-\alpha)\Gamma^3 + \alpha} \\ \dfrac{\alpha(1-\alpha)(\Gamma^3-1)^2 \sin\beta\cos\beta}{(1-\alpha)\Gamma^3 + \alpha} \\ \dfrac{\alpha(1-\alpha)(\Gamma^3-1)^2 \cos^2\beta + \Gamma^3}{(1-\alpha)\Gamma^3 + \alpha} \\ \dfrac{(\Gamma^3-1)}{(1-\alpha)\Gamma^3 + \alpha} \\ \dfrac{(1-\alpha)\Gamma + \alpha}{\Gamma} \\ \dfrac{(\Gamma-1)\sin\beta}{(1-\alpha)\Gamma^3 + \alpha} \\ \dfrac{\alpha(1-\alpha)(\Gamma^3-1)\sin\beta\cos\beta}{(1-\alpha)\Gamma^3 + \alpha} \\ \dfrac{\alpha(1-a)(\Gamma^3-1)(\Gamma-1)\cos\beta + \alpha\Gamma + (1-\alpha)\Gamma^3}{(1-\alpha)\Gamma^3 + \alpha} \end{bmatrix}$$

k VECTOR

- The column matrix containing spiral-groove coefficients, $k_i(\alpha, \beta, \Gamma)$, is:

$$k = \begin{bmatrix} \dfrac{\alpha(1-\alpha)(\Gamma^3-1)^2 \sin^2\beta + \Gamma^3}{(1-\alpha)\Gamma^3 + \alpha} \\ \dfrac{\alpha(1-\alpha)(\Gamma^3-1)^2 \sin\beta\cos\beta}{(1-\alpha)\Gamma^3 + \alpha} \\ \dfrac{\alpha(1-\alpha)(\Gamma^3-1)^2 \cos^2\beta + \Gamma^3}{(1-\alpha)\Gamma^3 + \alpha} \\ \dfrac{(\Gamma^3-1)}{(1-\alpha)\Gamma^3 + \alpha} \\ \dfrac{(1-\alpha)\Gamma + \alpha}{\Gamma} \\ \dfrac{(\Gamma-1)\sin\beta}{(1-\alpha)\Gamma^3 + \alpha} \\ \dfrac{\alpha(1-\alpha)(\Gamma^3-1)\sin\beta\cos\beta}{(1-\alpha)\Gamma^3 + \alpha} \\ \dfrac{\alpha(1-\alpha)(\Gamma^3-1)(\Gamma-1)\cos\beta + \alpha\Gamma + (1-\alpha)\Gamma^3}{(1-\alpha)\Gamma^3 + \alpha} \end{bmatrix}$$

CELL CONTROL VOLUME

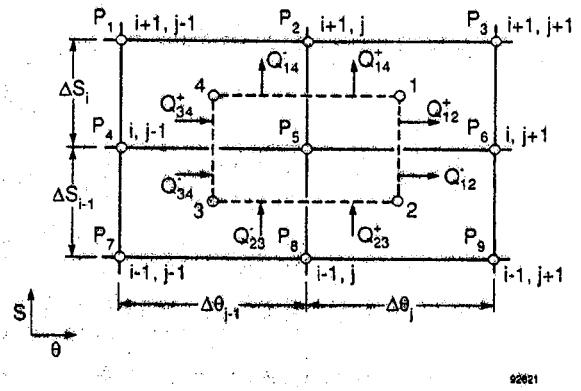

NEWTON-RAPHSON ITERATION

Flow Balance

$$\dot{Q}_{12}\Delta\bar{S}_{12} + Q^{+}_{12}\Delta\bar{S}^{+}_{12} + Q^{+}_{14}\Delta\bar{S}^{+}_{14}\ \dot{Q}_{14}\Delta\bar{S}_{14} - Q^{+}_{34}\Delta\bar{S}^{+}_{34} -$$

$$- \dot{Q}_{34}\Delta\bar{S}_{34} - \dot{Q}_{23}\Delta\bar{S}_{23} - Q^{+}_{23}\Delta\bar{S}^{+}_{23} =$$

$$= - \frac{\partial}{\partial \bar{t}} (1 + P_{ij}) (\alpha\tilde{\delta} + H_r)_{i+1/2,\, j+1/2}\ \Delta\bar{A}_1$$

$$+ (\alpha\tilde{\delta} + H_r)_{i+1/2,\, j-1/2}\ \Delta\bar{A}_4 + (\alpha\tilde{\delta} + H_r)_{i-1/2,\, j-1/2}\ \Delta\bar{A}_3$$

$$+ (\alpha\tilde{\delta} + H_r)_{i-1/2,\, j+1/2}\ \Delta\bar{A}_2$$

For Steady State, RHS = 0

$$F_{ij} (H_r, P_1, P_2, P_3, P_4, P_5, P_6, P_7, P_8, P_9) = 0$$

Apply Newton-Raphson

$$F_{ij} + \sum_{k=1}^{9} \frac{\partial F_{ij}}{\partial P_k} \left(P_k^{new} - P_k\right) = 0$$

where:

$$\frac{\partial F_{ij}}{\partial P_k} = \frac{F_{ij} (H_r, P_1, \ldots, P_k + \eta, \ldots, P_9) - F_{ij} (H_r, P_1, \ldots, P_9)}{\eta}$$

NEWTON-RAPHSON ITERATION

Flow Balance

$$Q^-_{12}\Delta\bar{S}^-_{12} + Q^+_{12}\Delta\bar{S}^+_{12} + Q^+_{14}\Delta\bar{S}^+_{14}\ Q^-_{14}\Delta\bar{S}^-_{14} - Q^+_{34}\Delta\bar{S}^+_{34} -$$

$$- Q^-_{34}\Delta\bar{S}^-_{34} - Q^-_{23}\Delta\bar{S}^-_{23} - Q^+_{23}\Delta\bar{S}^+_{23} =$$

$$= -\frac{\partial}{\partial\tilde{t}}\left\{(1 + P_{ij})\left[(\alpha\tilde{\delta} + H_r)_{i+1/2,\,j+1/2}\ \Delta\bar{A}_1\right.\right.$$

$$+ (\alpha\tilde{\delta} + H_r)_{i+1/2,\,j-1/2}\ \Delta\bar{A}_4 + (\alpha\tilde{\delta} + H_r)_{i-1/2,\,j-1/2}\ \Delta\bar{A}_3$$

$$\left.\left. + (\alpha\tilde{\delta} + H_r)_{i-1/2,\,j+1/2}\ \Delta\bar{A}_2\right]\right\}$$

For Steady State, RHS = 0

$$F_{ij}\ (H_r, P_1, P_2, P_3, P_4, P_5, P_6, P_7, P_8, P_9) = 0$$

Apply Newton-Raphson

$$F_{ij} + \sum_{k=1}^{9}\frac{\partial F_{ij}}{\partial P_k}\left(P_k^{new} - P_k\right) = 0$$

where:

$$\frac{\partial F_{ij}}{\partial P_k} = \frac{F_{ij}\ (H_r, P_1, \ldots, P_k + \eta, \ldots, P_9) - F_{ij}\ (H_r, P_1, \ldots, P_9)}{\eta}$$

COLUMN MATRIX FORMAT

- Generate system of equations in the following format:

$$[C^j]\left\{P_j^{new}\right\} + [E^j]\left\{P_{j-1}^{new}\right\} + [D^j]\left\{P_{j+1}^{new}\right\} = \{R^j\}$$

where:

$$C^j_{i,\,i+k} = \frac{\partial F_{ij}}{\partial P_{i+k,\,j}}$$

$$E^j_{i,\,i+k} = \frac{\partial F_{ij}}{\partial P_{i+k,\,j-1}}$$

$$D^j_{i,\,i+k} = \frac{\partial F_{ij}}{\partial P_{i+k,\,j+1}}$$

$k = -1, 0, 1;\ i = 2, \ldots, M - 1$

- The interior elements of the column vector $\{R^j\}$ are

$$R^j_i = \sum_{k=-1}^{1}\left(C^j_{i,i+k}\ P_{i+k,\,j} + E^j_{i,i+k}\ P_{i+k,\,j-1} + D^j_{i,i+k}\ P_{i+k,\,j+1}\right) - F_{ij}$$

- Equations solved by column or transfer matrix method

FLOW DIAGRAM FOR LOGIC USED IN SUBROUTINE SPIRAL

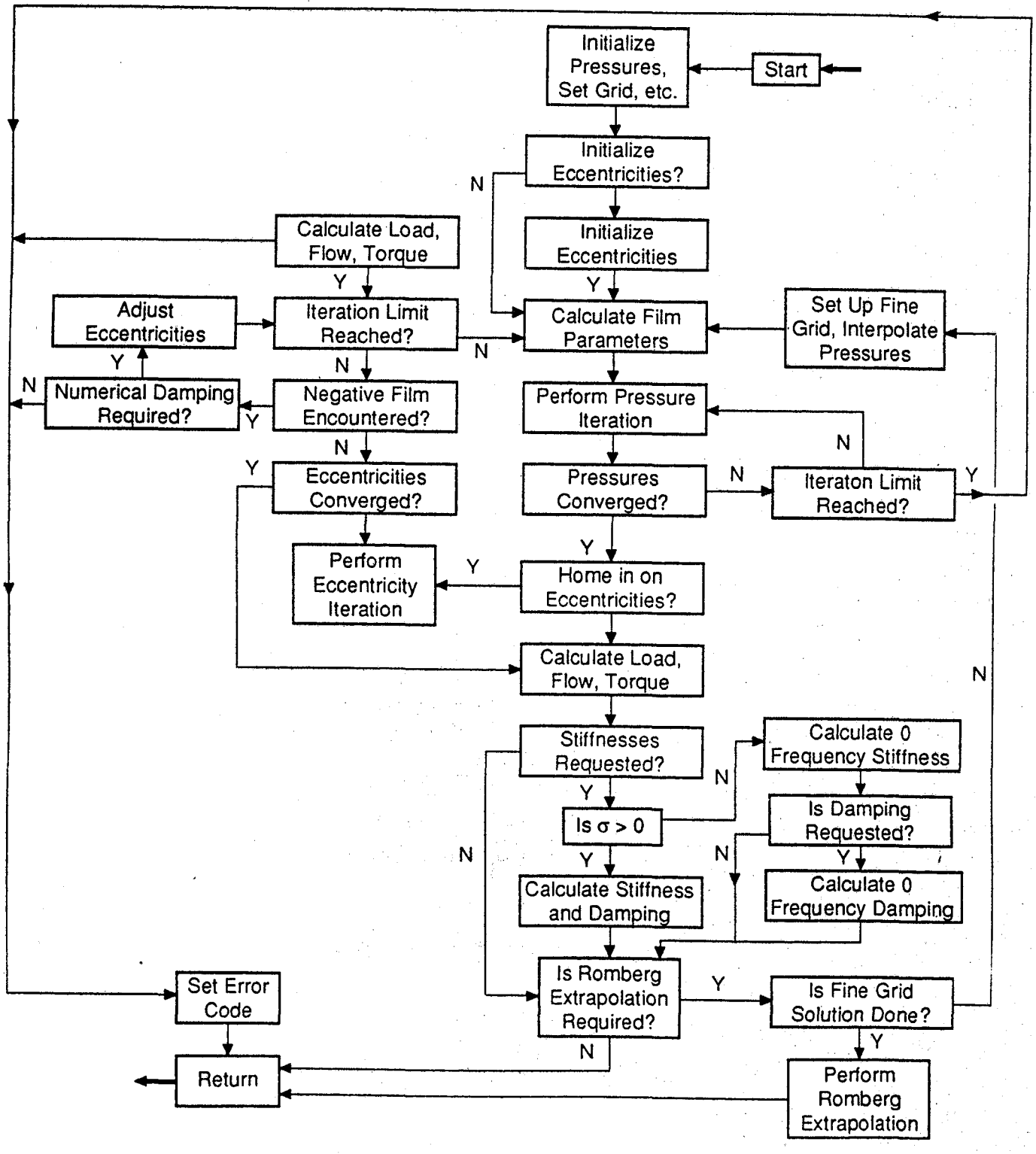

Mechanical Technology Incorporated
92P48

92773(M)

Computer Code GFACE
Gas Face Seals

GFACE CAPABILITIES

- Varying geometries
- Variable or constant grid (30 × 74)
- Shaft eccentricity and misalignment
- Specified and periodic boundary conditions
- Determining performance as a function of position or position to satisfy a given load
- Frequency-dependent stiffness and damping coefficients
- English or SI units

FACE SEAL CONFIGURATIONS

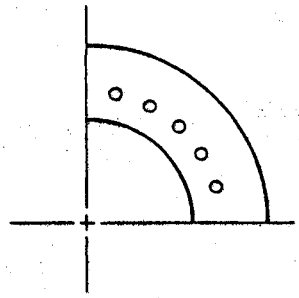

Hydrostatic

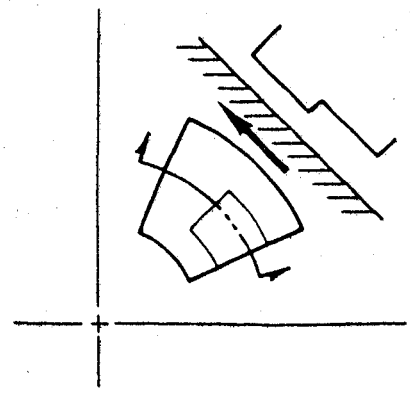

Circumferential
Rayleigh Step

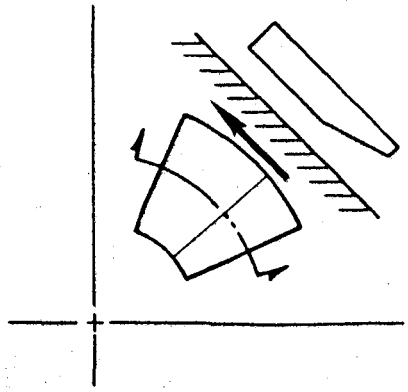

Circumferential
Tapered Land

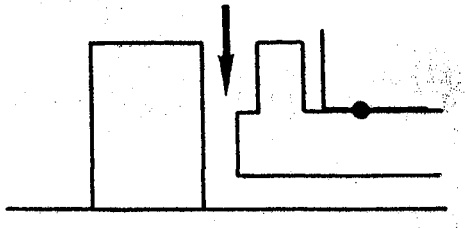

Radial Rayleigh Step

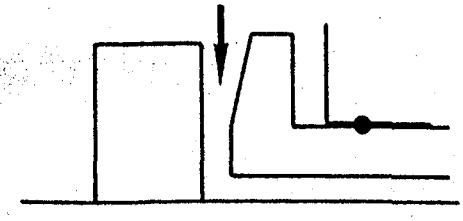

Radial Tapered Land

86265 - 1

POLAR GRID MESH SYSTEM

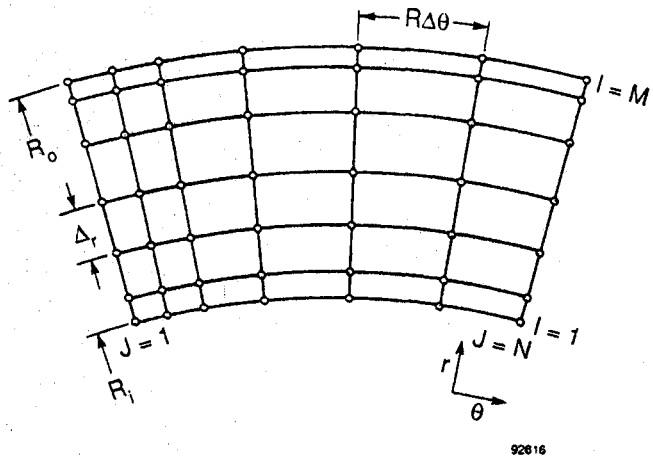

COORDINATE SYSTEM FOR GFACE

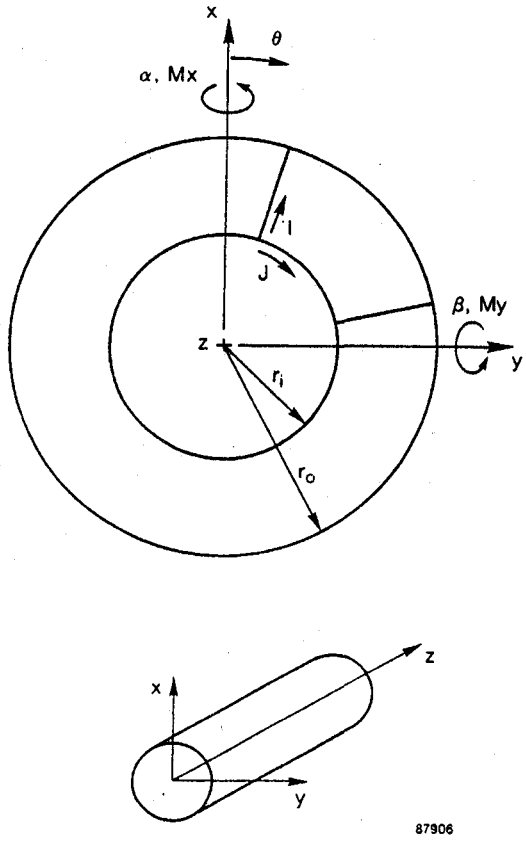

GFACE THEORY

REYNOLDS' EQUATION

$$\frac{\partial}{\partial R}\left(R\,PH^3\,\frac{\partial P}{\partial R}\right)+\frac{1}{R}\,\frac{\partial}{\partial \theta}\left(PH^3\,\frac{\partial p}{\partial \theta}\right)=\Lambda\,\frac{\partial (PH)}{\partial \theta}+\frac{\partial (PH)}{\partial T}$$

where:

$$R = r/r_o,\ H = h/C_o,\ T = t/t_o,\ P = p/p_o,$$

$$\Lambda = \frac{6\,\mu\omega r_o^2}{p_o C_o^2},\quad t_o = \frac{12\,\mu r_o^2}{p_o C_o^2}$$

FLOW-BALANCE CELL AND ASSOCIATED GRID NETWORK

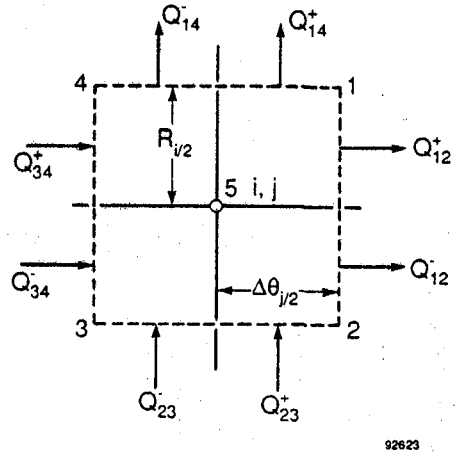

FLOW-BALANCE ACROSS CELL

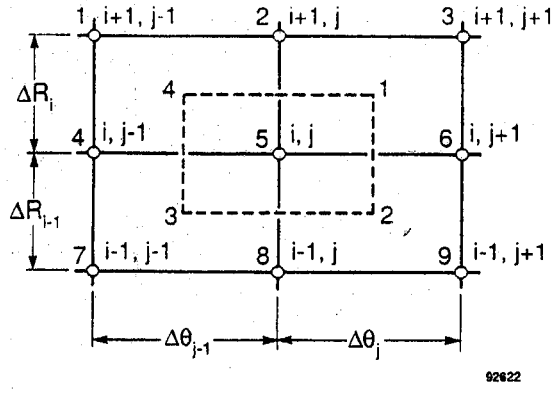

MASS FLOW BALANCE

- The net flow through a cell can be expressed as:

$$Q^{+}_{12}\frac{\Delta R_i}{2} + Q^{-}_{12}\frac{\Delta R_{i-1}}{2} + Q^{+}_{14}\frac{\Delta\theta_j}{2} + Q^{-}_{14}\frac{\Delta\theta_{j-1}}{2}$$

$$-Q^{+}_{34}\frac{\Delta R_i}{2} - Q^{-}_{34}\frac{\Delta R_{i-1}}{2} - Q^{+}_{23}\frac{\Delta\theta_j}{2} - Q^{-}_{23}\frac{\Delta\theta_{j-1}}{2} = Q_{in}$$

- Q^{+}_{12} means the mass flow per unit length across the plus side of cell boundary 1-2, etc.
- The Q's are dimensionless mass flow per unit length, except for Q_{in}, which is a dimensionless source inlet flow.
- In the θ direction:

$$Q = -\frac{PH^3}{R}\frac{\partial P}{\partial\theta}\frac{\Delta R}{2} + \Lambda\, RPH\,\frac{\Delta H}{2}$$

- In the R direction:

$$Q = PH^3\, R\,\frac{\partial P}{\partial R}\,\frac{\Delta\theta}{2}$$

CELL PRESSURES AND DERIVATIVES

- Q is defined as:

$$Q = \frac{12\,\mu G_c T_a\, q}{p_o^2 C_o^3}$$

- Pressures are taken as the average pressure across the boundary. For example:

$$P_{12} = \frac{P_{i,j} + P_{i,j+1}}{2}$$

and

$$\left.\frac{\partial P}{\partial \theta}\right|_{12} = \frac{P_{i,j+1} - P_{i,j}}{\Delta\theta_j}$$

EXTERNAL MASS FLOW

$$Q_{in} = OFC \times A_o \times P_S' \left\{ \left(\frac{P_R'}{P_S'}\right)^{2/\gamma} \left[1 - \left(\frac{P_R'}{P_S'}\right)^{\frac{\gamma-1}{\gamma}} \right] \right\}^{1/2}$$

where:

$$OFC = \frac{12\,\mu C_d}{p_o C_o^2} \sqrt{\frac{2\,\gamma G_c T_a}{\gamma - 1}}$$

$A_o = \pi\, d_o\, H_5$ for inherent compensation

$$A_o = \frac{\pi\, d_o^2}{4\, C_o}$$ for orifice compensation

FLOW CHOKING

$$\text{If } \left(\frac{P_R'}{P_S'}\right) \leq P_{CR}, \text{ then } \left(\frac{P_R'}{P_S'}\right) = P_{CR}$$

where:

$$P_{CR} = \left[\frac{2.0}{(\gamma + 1)}\right]^{\frac{\gamma}{(\gamma - 1)}}$$

Also, if

$$\frac{P_R'}{P_S'} > 1.0, \quad \frac{P_R'}{P_S'} = \frac{1}{P_R'/P_S'}, \quad \text{and } P_S' = P_R',$$

then this condition implies backflow through the orifice.

NEWTON-RAPHSON ITERATION ON FLOW BALANCE EQUATION

$$f_{i,j}^{(old)} + \sum_{k=1}^{5} \frac{\partial f_{i,j}^{(old)}}{\partial P_K} \left(P_K^{(new)} - P_K^{(old)}\right) = 0$$

where the partial derivatives are explicitly determined, e.g.,

$$\frac{\partial f_{i,j}}{\partial P_K} = \frac{f(P_1, P_2, \ldots P_K + \varepsilon/2 \ldots P_5)_{i,j} - f(P_1, P_2, \ldots P_K + \varepsilon/2, \ldots P_5)_{i,j}}{\varepsilon}$$

COLUMN MATRIX FORMAT

- The linearized Newton-Raphson equations may be written in the form:

$$C_j P_j + E_j P_{j-1} + D_j P_{j+1} = R_j$$

- The column method is used to solve the new pressures in the set of m x n equations.

VISCOUS POWER LOSS

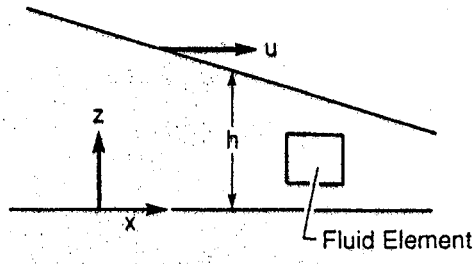

a) Seal Interface

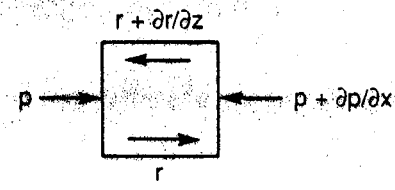

b) Fluid Element

92624

VISCOUS FRICTION TORQUE

$$T_F = \frac{T_f}{p_o\, CR_o^2} = \int\int \frac{H}{2}\frac{\partial p}{\partial \theta}\, Rd\theta\, dR + \int\int \frac{\Lambda}{6}\frac{R^2}{H}\, Rd\theta dR$$

FLOW ACROSS CIRCUMFERENTIAL LINE

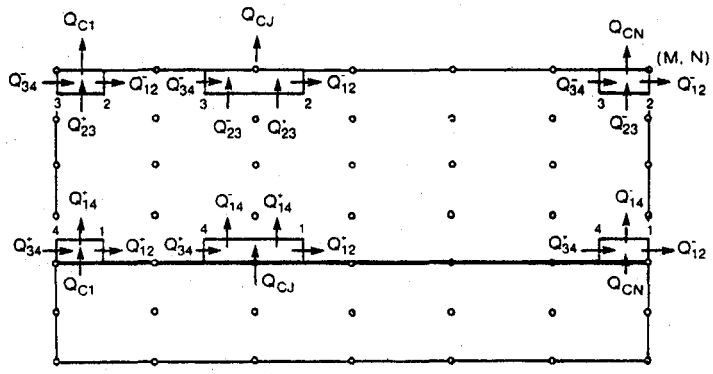

861603

FLOW ACROSS AXIAL LINE

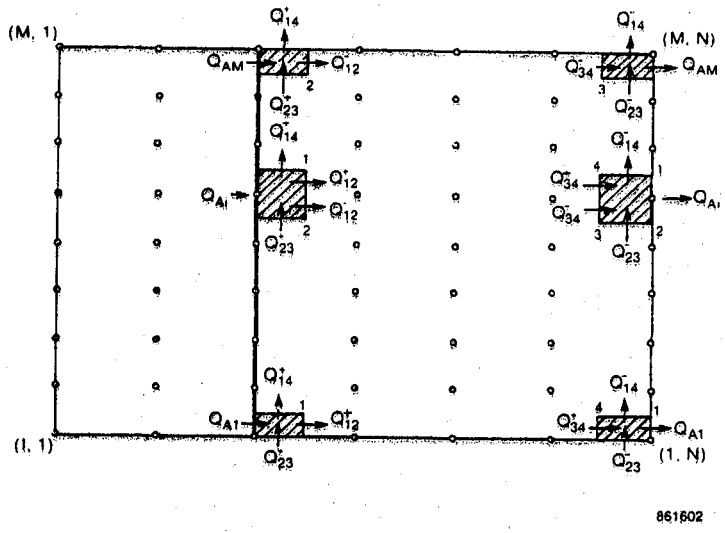

NONUNIFORM CLEARANCE GEOMETRIES

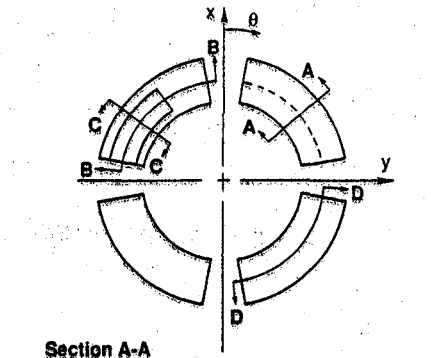

Section A-A

- Radial Taper: Type 1
- Radial Taper: Type 2

Section B-B

- Rayleigh Step

Section C-C

- Rayleigh Step

Section D-D

- Circumferential Taper

MISALIGNED RAYLEIGH-STEP CLEARANCE DISTRIBUTION

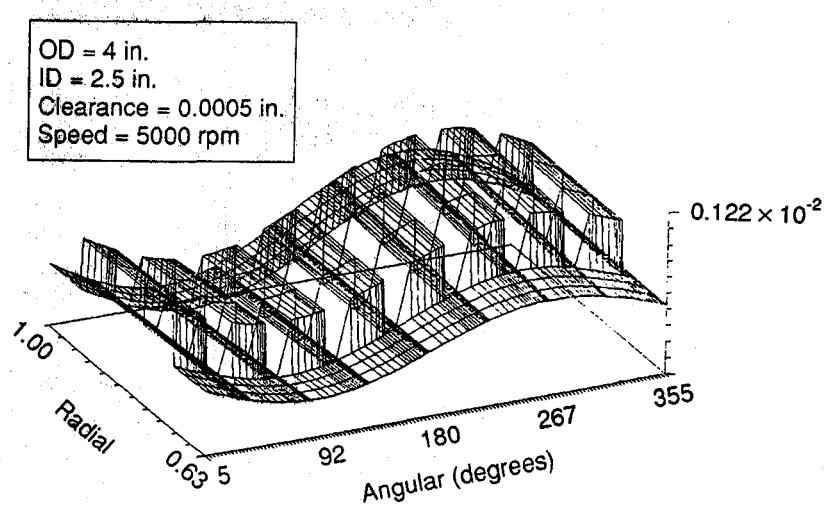

MISALIGNED RAYLEIGH-STEP PRESSURE DISTRIBUTION

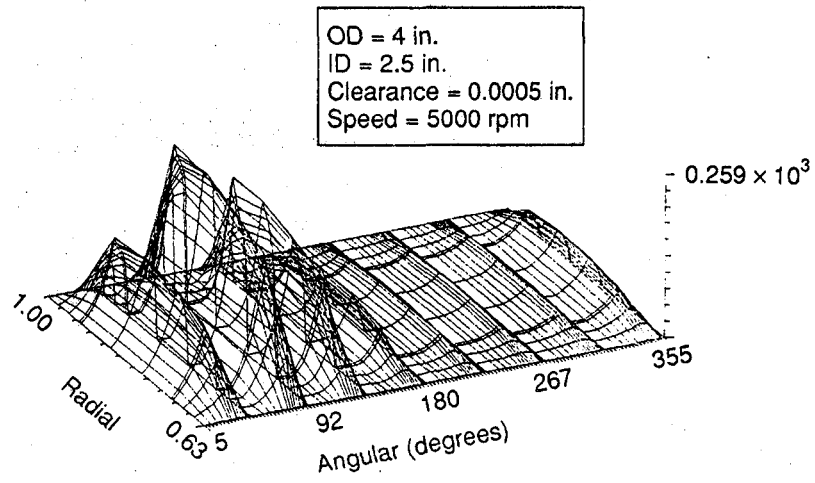

DOUBLE TAPERED-LAND CLEARANCE DISTRIBUTION

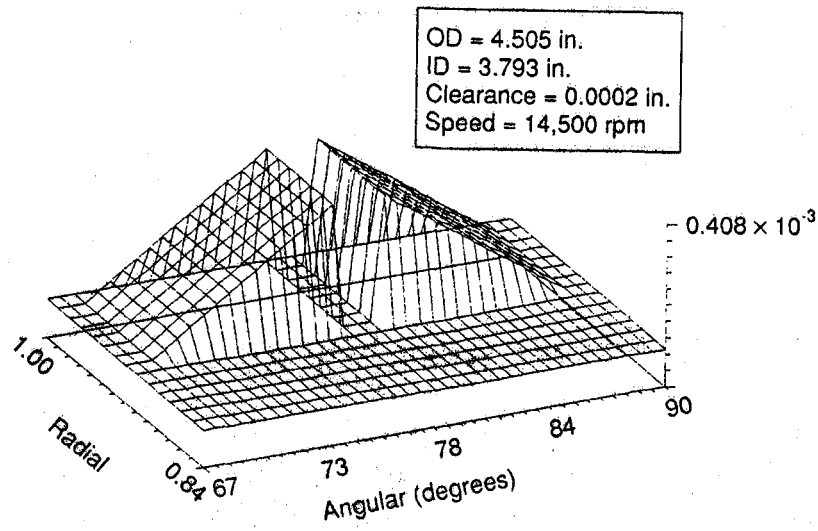

DOUBLE TAPERED-LAND PRESSURE DISTRIBUTION

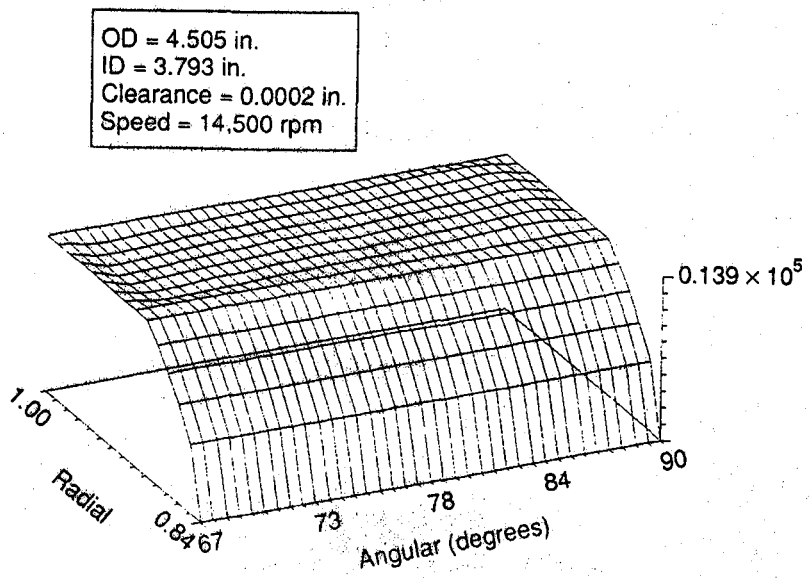

STATUS OF INDUSTRIAL CODES

	ICYL	GCL	SPIRALG	IFACE	GFACE	SPIRALI
Formulation	C	C	C	C	C	C
Coding	C	C	C	P	P	C
Documentation	C	C	C			C
KBS Integration	C	C	C			

C = Complete

P = In preparation

ICYL = Incompressible Cylindrical Code

GCYL = Gas Cylindrical Code

SPIRALG = Gas Spiral-Groove Code

IFACE = Incompressible Face Seal Code

GFACE = Gas Face Seal Code

SPIRALI = Incompressible Spiral-Groove Code

INCOMPRESSIBLE FLOW CODES ☞ OVERVIEW

W. Shapiro
Mechanical Technology Incorporated
Latham, New York

- OVERVIEW 3 CODES:
  - Capabilities
  - Status
- **ICYL** ☞ Cylindrical Seals
  - Introduction
  - Assumptions
  - Formulation & Solution Method
- **SPIRALI** ☞ Spiral Groove Seals (Cylindrical and Face)
  - Introduction
  - Assumptions
  - Formulation & Solution Method
- **IFACE** ☞ Face Seals
  - Examples

INCOMPRESSIBLE FLOW CODES ☛ CAPABILITIES

		ICYL	IFACE	SPIRALI
Geometry		Cylindrical	Face	Both
Turbulent Flow		Yes	Yes	Yes
Inertia	Inlets	Yes	Yes	Yes
	Film	No	No	Yes
Film thickness		Arbitrary	Arbitrary	Axis-symmetric
Eccentricity		Finite	Finite	Perturbation
Pressure Pockets		Yes	Yes	No
Spiral Grooves		No	No	Yes

INCOMPRESSIBLE FLOW CODES ☛ STATUS

	ICYL	IFACE	SPIRALI
Formulation	Complete	Complete	Complete
Coding	Complete	In Progress	Complete
Documentation	Complete		Complete
KBS Interface	Complete		

Incompressible **Cyl**indrical Program ☛ Capabilities

ICYL by Dr. Antonio Artiles

- 2-D cylindrical geometry.
- Rotation of rotor and housing.
- Roughness of rotor and housing.
- Laminar or turbulent flow.
- Inertia pressure drop at inlets to fluid film
  - from pressurized pockets
  - from seal ends
- Arbitrary film thickness distribution
  - steps
  - pockets (pressurized or not)
  - tapers
  - preloaded arcs
- Rotor position relative to housing described by four degrees of freedom
  - 2 translational
  - 2 rotational
- User specifies:
  - Rotor lateral position –or– External forces
  - Rotor angular position –or– External moments
  - Pocket pressures –or– orifice size
- Dynamic coefficients
  - 16 stiffness
  - 16 damping
  - critical mass

Incompressible **Cyl**indrical Program ☛ Assumptions

- Isothermal and incompressible flow
- Turbulence: bulk flow model with separate friction factors
- Fluid inertia effects at film entrance use loss coefficients.
- Fluid inertia effects in the film (additional to those inherent in turbulence) are negligible.
- Pressurized pockets deep (constant pressure)
- Surface roughness $<<$ film thickness $<<$ seal dimensions
- Wall roughness is isotropic

CYLINDRICAL SEAL GEOMETRY SCHEMATIC

(CONCENTRIC ALIGNED POSITION)

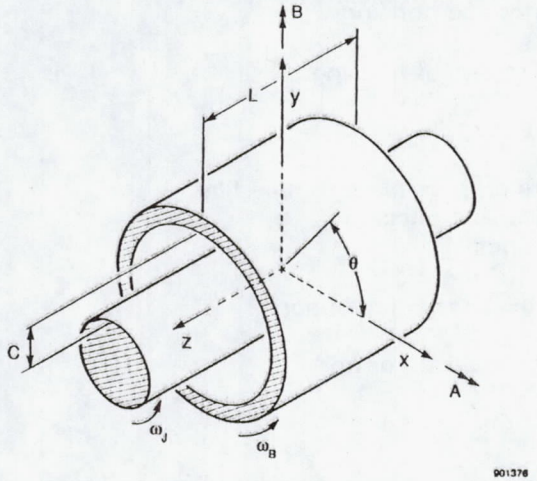

SCHEMATIC ILLUSTRATING ROTOR LATERAL AND ANGULAR DISPLACEMENTS

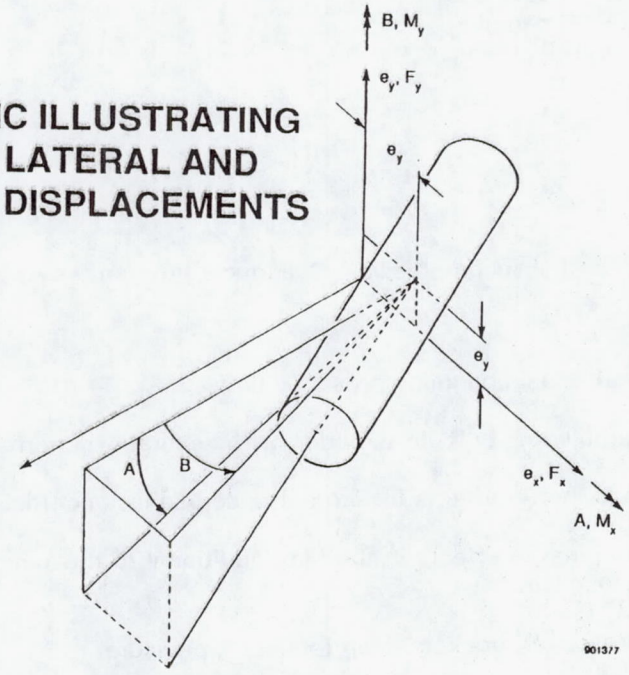

AXIAL CROSS SECTION OF SEAL WITH ECCENTRIC ROTOR

(FILM THICKNESS EXAGGERATED)

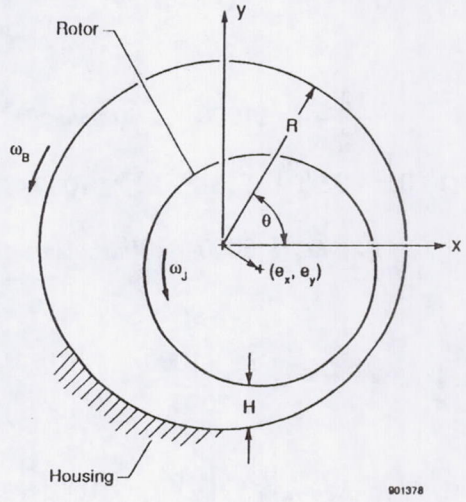

ICYL Program ☛ Governing Equations

Film thickness

$$H = H_o - (e_x + ZB)\cos\theta - (e_y - ZA)\sin\theta$$

$$\frac{\partial H}{\partial t} = -\left(\frac{\partial e_x}{\partial t} + Z\frac{\partial B}{\partial t}\right)\cos\theta - \left(\frac{\partial e_y}{\partial t} - Z\frac{\partial A}{\partial t}\right)\sin\theta$$

momentum

$$\frac{(f_j Re_j + f_b Re_b)}{2} U = -\frac{H^2}{\mu R}\frac{\partial P}{\partial \theta} + \frac{(Re_j f_j U_j + Re_b f_b U_b)}{2}$$

$$\frac{(f_j Re_j + f_b Re_b)}{2} V = -\frac{H^2}{\mu}\frac{\partial P}{\partial Z}$$

continuity

$$\frac{1}{R}\frac{\partial}{\partial \theta}(UH) + \frac{\partial}{\partial Z}(VH) + \frac{\partial H}{\partial t} = 0$$

Reynolds numbers, friction factors

$$Re_i = \frac{\rho H}{\mu}\sqrt{(U-U_i)^2 + V^2}$$

$$f_i = \begin{cases} \dfrac{12}{Re_i}, & Re_i \le 1000 \qquad (laminar) \\ \dfrac{12}{Re_i}(1 - 3\xi^2 + 2\xi^3) + f_i^*(3\xi^2 - 2\xi^3), & 1000 < Re_i < 3000 \\ f_i^*, & Re_i \ge 3000 \qquad (turbulent) \end{cases}$$

$$\xi \equiv \frac{Re_i - 1000}{2000}$$

$$f_i^* = 0.001375\left[1 + \left(\frac{10^4 e_i}{H} + \frac{10^6}{4\,Re_i}\right)^{\frac{1}{3}}\right]$$

Reynolds numbers, friction factors

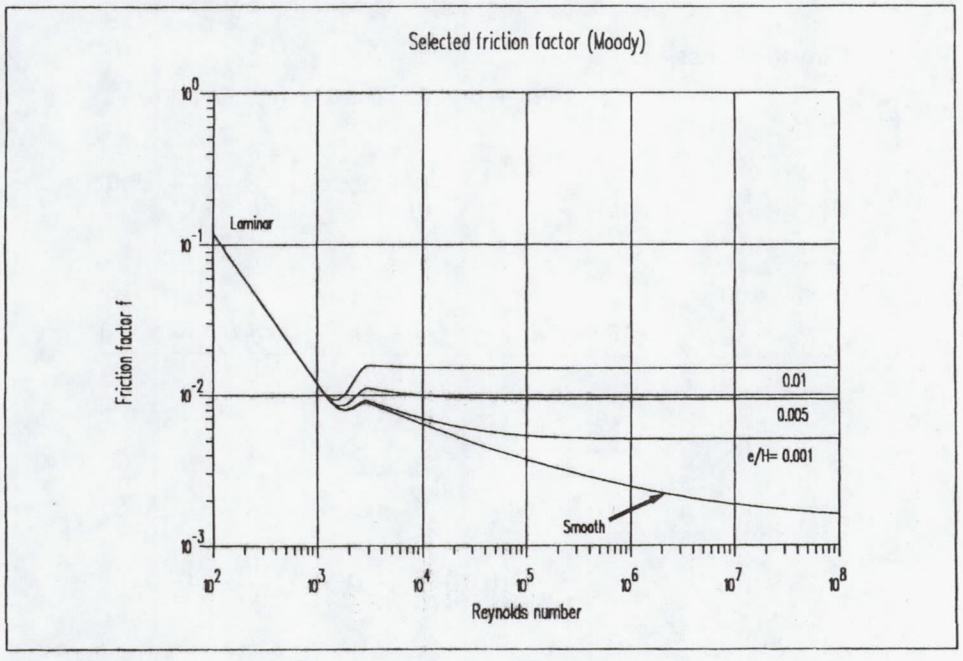

circumferential ends:

$$P(Z, \theta_s) = 0 \text{ and } P(Z, \theta_e) = 0,$$

or periodic boundary conditions:

$$P(Z, \theta_s) = P(Z, \theta_e) \text{ and } U(Z, \theta_s) = U(Z, \theta_e).$$

left end: $P(-L/2,\theta) = P_l - K_e \, \frac{1}{2}\rho V_n^2.$

right end: $P(L/2,\theta) = P_r - K_e \, \frac{1}{2}\rho V_n^2,$

or mid-length symmetry:

$$V(0,\theta) = 0$$

pocket boundaries: $P(Z,\theta) = P_p - K_e \, \frac{1}{2}\rho V_n^2.$

Pressurized Pockets

orifice pressure drop:

$$P_s - P_p = sgn(Q_r) \frac{\rho}{2}\left(\frac{Q_r}{A_o C_d}\right)^2$$

orifice flow:

$$Q_r = \oint_{S_p} H \, \vec{V}\cdot\hat{n} \, dS + \int_{A_p} \frac{\partial H}{\partial t} \, dA$$

Discretization of continuity equation

$$-\oint_{S_c} \boldsymbol{v}\cdot\hat{\boldsymbol{n}}\, dS = \int_{A_c} \frac{\partial h}{\partial \tau}\, dA$$

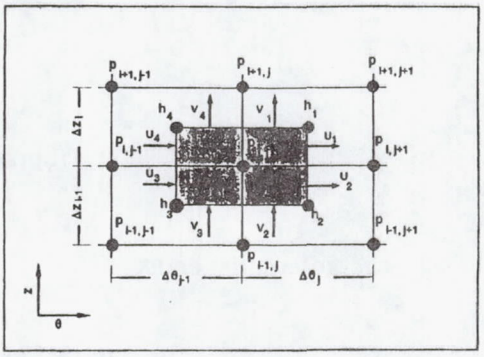

$$F_{i,j} = \frac{\Delta z_i}{2}(u_1 h_1 - u_4 h_4) + \frac{\Delta z_{i-1}}{2}(u_2 h_2 - u_3 h_3) +$$
$$+ \frac{\Delta\theta_j}{2}(v_1 h_1 - v_2 h_2) + \frac{\Delta\theta_{j-1}}{2}(v_4 h_4 - v_3 h_3) -$$
$$- \frac{1}{4}\frac{\partial h_{i,j}}{\partial \tau}(\Delta z_i + \Delta z_{i-1})(\Delta\theta_j + \Delta\theta_{j-1}) = 0$$

Discretization of continuity equation at pressurized boundaries

$$F_{i,j} = p_b - p_{i,j} - \Lambda_c \max(0, v_n)^2$$
$$= 0$$

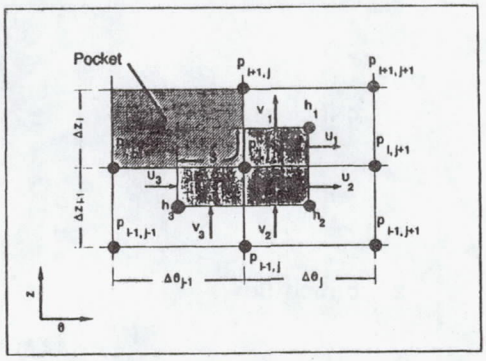

$$v_n = \left[\frac{\Delta z_i}{2}(u_1 h_1) + \frac{\Delta z_{i-1}}{2}(u_2 h_2 - u_3 h_3) + \frac{\Delta\theta_j}{2}(v_1 h_1 - v_2 h_2) - \frac{\Delta\theta_{j-1}}{2}(v_3 h_3) -\right.$$
$$\left. - \frac{\partial h_{i,j}}{\partial \tau}\frac{(\Delta z_i + \Delta z_{i-1})\Delta\theta_j + \Delta z_{i-1}\Delta\theta_{j-1}}{4}\right] + \left[\frac{(\Delta\theta_{j-1} + \Delta z_i)h_{i,j}}{2}\right]$$

Evaluation of velocity components

$$G_u\left[\frac{\partial p}{\partial \theta}, u, v\right] \equiv \frac{f_j Re_j + f_b Re_b}{2} u + 12h^2 \frac{\partial p}{\partial \theta} - (Re_j f_j \Lambda_j + Re_b f_b \Lambda_b) = 0,$$

$$G_v\left[\frac{\partial p}{\partial z}, u, v\right] \equiv \frac{f_j Re_j + f_b Re_b}{2} v + 12h^2 \frac{\partial p}{\partial z} = 0,$$

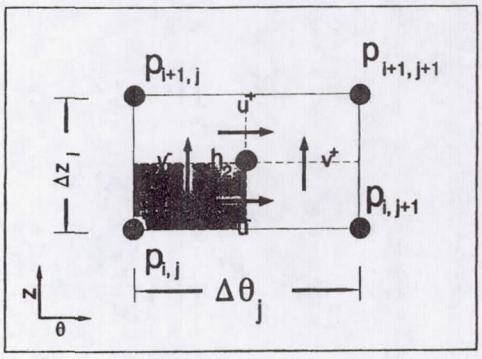

$$Re_j = \frac{Re_o^* h}{12}\sqrt{(u - 2\Lambda_j)^2 + v^2},$$

$$Re_b = \frac{Re_o^* h}{12}\sqrt{(u - 2\Lambda_b)^2 + v^2},$$

Evaluation of velocity components

$$G_u\left[\frac{p_{i,j+1} - p_{i,j}}{\Delta \theta_j},\ u^-,\ \frac{v^- + v^+}{2}\right] = 0$$

$$G_v\left[\frac{p_{i+1,j} - p_{i,j}}{\Delta z_i},\ \frac{u^- + u^+}{2},\ v^-\right] = 0$$

$$G_u\left[\frac{p_{i+1,j+1} - p_{i+1,j}}{\Delta \theta_j}, u^+, \frac{v^- + v^+}{2}\right] = 0$$

$$G_v\left[\frac{p_{i+1,j+1} - p_{i,j+1}}{\Delta z_i}, \frac{u^- + u^+}{2}, v^+\right] = 0$$

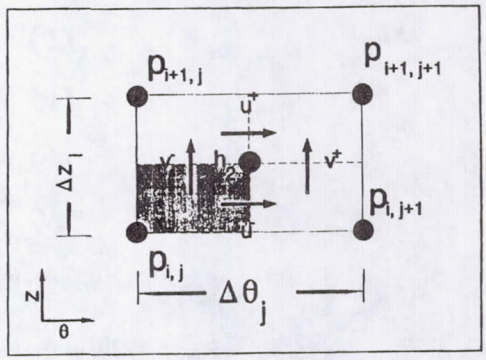

ICYL: Forces, Moments, Torque

$$\begin{Bmatrix} F_x \\ F_y \\ M_x \\ M_y \end{Bmatrix} = \int_{-L}^{L} \int_{\theta_s}^{\theta_e} P \begin{Bmatrix} \cos\theta \\ \sin\theta \\ -Z\sin\theta \\ Z\cos\theta \end{Bmatrix} R\,d\theta\,dZ$$

$$\vec{T} = T\hat{e}_z = \iint_{A_f} \vec{r} \times \vec{t}\; dA$$

$$= R \iint_{A_f} \hat{e}_r \times (\bar{\tau} \bullet \hat{e}_r)\; dA$$

$$T = \frac{P_o R^2}{2C_o} \iint_{A_f} \{ h \frac{\partial p}{\partial \Theta} - \frac{f_j R_j (u - 2\Lambda_j) - f_b R_b (u - 2\Lambda_b)}{72h} \}\; d\theta\, dZ$$

Solution of Rotor position and pocket pressures.

$$f_x(r) = -f_{xg}$$

$$f_y(r) = -f_{yg}$$

$$m_x(r) = -m_{xg}$$

$$m_y(r) = -m_{yg}$$

$$p_s - p_{p1} = sng(q_{r1})\,\Lambda_{r1}\,(q_{r1})^2, \quad \textit{for pocket 1,}$$

$$p_s - p_{p2} = sng(q_{r2})\,\Lambda_{r2}\,(q_{r2})^2, \quad \textit{for pocket 2, etc.}$$

SPIRALI (Spiral Groove Incompressible Flow) ☞ Introduction

SPIRALI by Dr. Jed Walowit

Spiral groove seals

- Provide:
  - ■ stability
    - □ increase in-phase[1] component of force
    - □ decrease out-of-phase component of force
  - ■ load support
  - ■ sealing (pumping against pressure gradient)
- Cylindrical seals → symmetric grooves pump against each other
- Face seals → grooves pump against dam region

[1] with the displacement

SPIRALI ☞ Basic Assumptions

- Isothermal and incompressible flow
- Turbulence: Hirs bulk flow model generalized for separate friction factors
- Film discontinuities use loss coefficients. Inertia effects (additional to those inherent in turbulence) throughout film.
- Circumferential and transient effects use small perturbations to a steady state first order solution for a concentric, aligned seal.
- surface roughness $<<$ film thickness $<<$ seal dimensions
- Narrow groove theory
  - ○ neglects edge effects and local inertia effects[2]
  - ○ valid for large number of grooves ($>> 2\pi\sin\beta$)
- Machined surfaces are axisymmetric (except spiral grooves)

[2] due to groove to groove pressure variations

SPIRALI ☞ Coordinate system

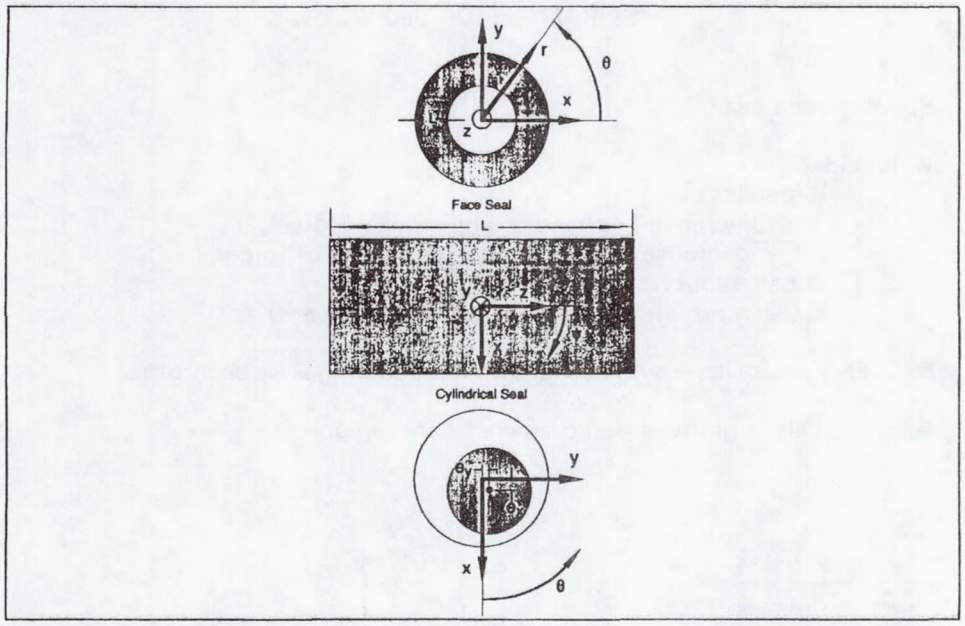

SPIRALI ☞ Quadratic film variation

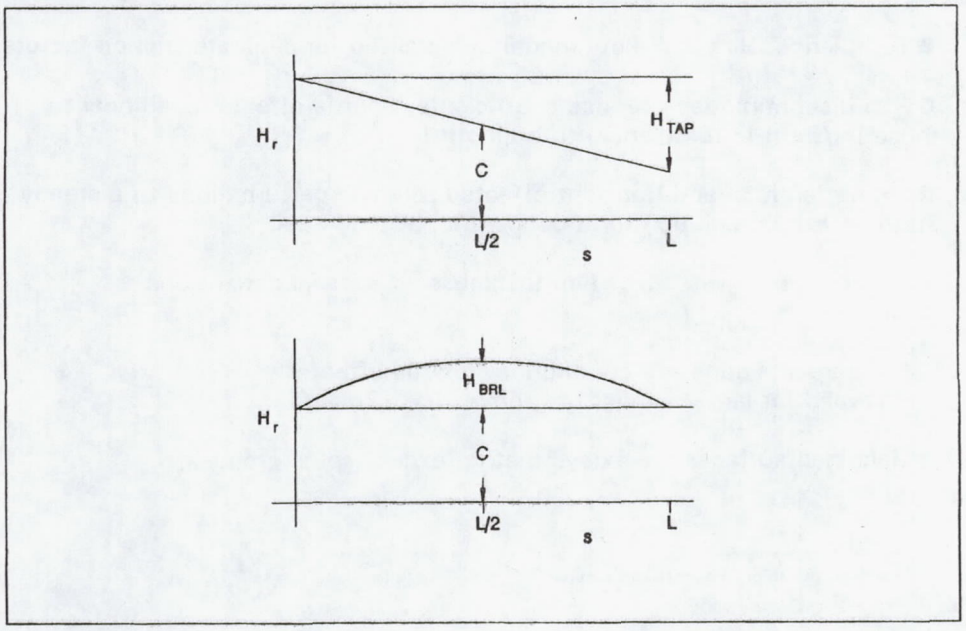

SPIRALI ☞ INTEGRATED EQUATIONS

MOMENTUM (Θ AND s DIRECTIONS):

$$\rho h\left(\frac{\partial u}{\partial t} + v\frac{\partial u}{\partial s} + \frac{u}{r}\frac{\partial u}{\partial \theta} + \frac{uvl_f}{r}\right) = -\frac{h}{r}\frac{\partial p}{\partial \theta} + (\vec{\tau}_b - \vec{\tau}_a)\cdot\vec{i} \quad ,$$

$$\rho h\left(\frac{\partial v}{\partial t} + v\frac{\partial v}{\partial s} + \frac{u}{r}\frac{\partial v}{\partial \theta} - \frac{u^2 l_f}{r}\right) = -h\frac{\partial p}{\partial s} + (\vec{\tau}_b - \vec{\tau}_a)\cdot\vec{j} \quad .$$

CONTINUITY:

$$\frac{1}{r}\frac{\partial}{\partial s}(rvh) + \frac{1}{r}\frac{\partial}{\partial \theta}(uh) + \frac{\partial h}{\partial t} = 0 \quad .$$

SPIRALI ☞ Shear stresses, shear factors, and Reynolds numbers

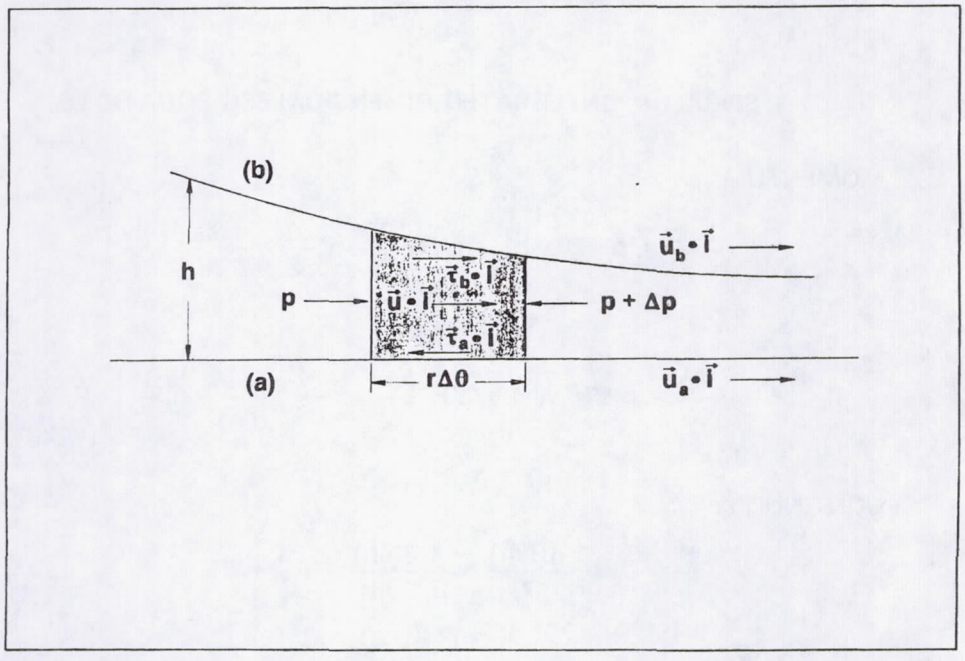

SPIRALI ☛ Shear stresses, shear factors, and Reynolds numbers

$$\vec{\tau}_a = \frac{1}{2}\rho\,|\vec{u}-\vec{u}_a|\;\; f_a\!\left(\frac{2h\rho\,|\vec{u}-\vec{u}_a|}{\mu}\right)(\vec{u}-\vec{u}_a) =$$
$$= \frac{1}{4}\frac{\mu}{h}R_a\;\; f_a(R_a)\;(\vec{u}-\vec{u}_a)\quad ,$$

$$f_a(R_a) = n_0 R_a^{\,m_0}\;,\quad f_b(R_b) = n_0 R_b^{\,m_0}$$

$$R_a = 2h\,|\vec{u}-\vec{u}_a|\,\rho/\mu\;\;,\qquad R_b = 2h\,|\vec{u}-\vec{u}_b|\,\rho/\mu\;\;.$$

	Laminar	Turbulent
n_0	24.0	0.0751
m_0	-1	-0.25

SPIRALI ☛ INTEGRATED DIMENSIONLESS EQUATIONS

MOMENTUM:

$$-\frac{1}{\tilde{r}}\frac{\partial\tilde{p}}{\partial\theta} = \tilde{p}^*\Phi(\tilde{u},\tilde{v},\tilde{h}) + \tilde{p}^*R^*\left(\frac{\partial\tilde{u}}{\partial\tilde{t}} + \tilde{v}\frac{\partial\tilde{u}}{\partial S} + \frac{\tilde{u}}{\tilde{r}}\frac{\partial\tilde{u}}{\partial\theta} + l_f\frac{\tilde{u}\tilde{v}}{\tilde{r}}\right)\;,$$

$$-\frac{\partial\tilde{p}}{\partial S} = \tilde{p}^*\Psi(\tilde{u},\tilde{v},\tilde{h}) + \tilde{p}^*R^*\left(\frac{\partial\tilde{v}}{\partial\tilde{t}} + \tilde{v}\frac{\partial\tilde{v}}{\partial S} + \frac{\tilde{u}}{\tilde{r}}\frac{\partial\tilde{v}}{\partial\theta} - l_f\frac{\tilde{u}^2}{\tilde{r}}\right)\;,$$

CONTINUITY:

$$\frac{1}{\tilde{r}}\frac{\partial(\tilde{r}\tilde{v}\tilde{h})}{\partial S} + \frac{1}{\tilde{r}}\frac{\partial(\tilde{u}\tilde{h})}{\partial\theta} + \frac{\partial\tilde{h}}{\partial\tilde{t}} = 0$$

SPIRALI ☛ INTEGRATED DIMENSIONLESS EQUATIONS

where

$$\Phi(\tilde{u},\tilde{v},\tilde{h}) = \frac{(\tilde{u} - \tilde{r}\tilde{\omega})R_a f_a(R_a) + \tilde{u}R_b f_b(R_b)}{\tilde{h}^2} ,$$

and

$$\Psi(\tilde{u},\tilde{v},\tilde{h}) = \frac{R_a f_a(R_a) + R_b f_b(R_b)}{\tilde{h}^2}\tilde{v} .$$

SPIRALI ☛ Boundary conditions

u_{in}, p_{in} at seal inlet:

$$\tilde{u} = \tilde{u}_{in} ,$$

$$\tilde{p} = \tilde{p}_{in} - \frac{1}{2}\tilde{\rho}^* R^* (1 + \zeta)\tilde{v}^2 \quad @ \; S = S_{in} .$$

p_{ex} at exit:

$$\tilde{p} = \tilde{p}_{ex} \quad @ \; S = S_{ex} .$$

S_{in} depends on flow direction. S_{ex} at the opposite side from S_{in}.

SPIRALI ☞ Continuity conditions

At $s = s_j$:

$$(h + \Delta h)v_J = hv \quad ,$$

$$p_J + \frac{1}{2}\rho v_J^2 = p + \frac{1}{2}\rho v^2(1 + \xi) \quad .$$

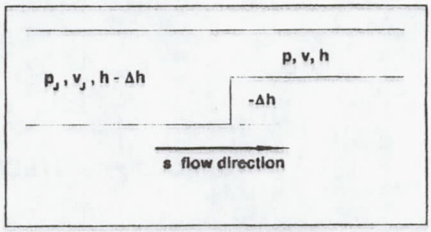

Jump in film thickness.

$$\xi = \begin{cases} \zeta(R,\tilde{h},\tilde{v}) & , \ \Delta\tilde{h} < 0 \text{ (contraction)} \\ \left(1 - \dfrac{\tilde{h}}{\tilde{h} - \Delta\tilde{h}}\right)^2 & , \ \Delta\tilde{h} \geq 0 \text{ (expansion)} \end{cases} \quad .$$

SPIRALI ☞ Stator with inward pumping grooves

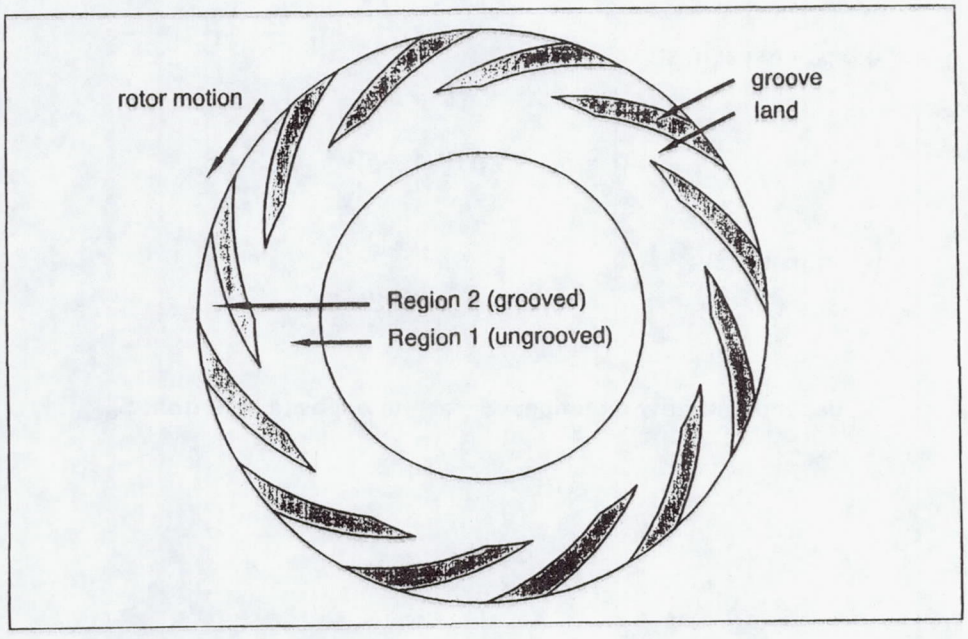

SPIRALI ☛ Spiral groove parameters, global and local pressures

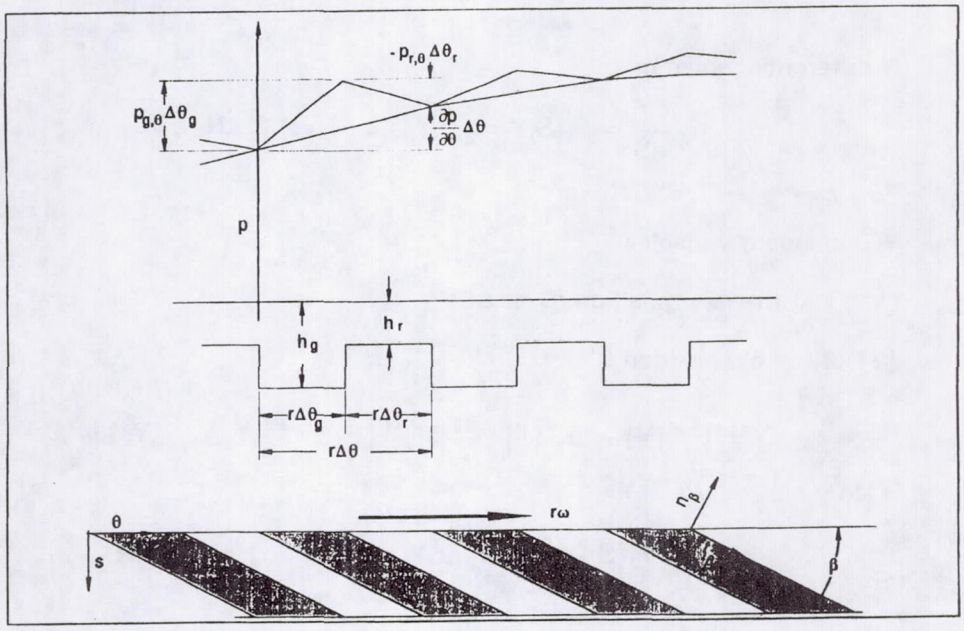

SPIRALI ☛ First order equations

First order variables, $\tilde{H}(S)$, $\tilde{P}(S)$, $\tilde{U}(S)$ and $\tilde{V}(S)$:

$$\Phi^*(\tilde{U},\tilde{V},\tilde{H},l_f) + R^*\tilde{V}\frac{d\tilde{U}}{dS} = 0 \quad ,$$

$$-\frac{d\tilde{P}}{dS} = \tilde{\rho}^*\Psi^*(\tilde{U},\tilde{V},\tilde{H},l_f) + \tilde{\rho}^*R^*\tilde{V}\frac{d\tilde{V}}{dS} \quad ,$$

$$\frac{d(\tilde{r}\tilde{H}\tilde{V})}{dS} = 0 \quad .$$

Closed form solution:

$$\tilde{V} = \frac{\tilde{r}_{in}\tilde{H}_{in}\tilde{V}_{in}}{\tilde{r}\tilde{H}} \quad ,$$

SPIRALI ☞ Semi-Implicit Algortihm

N differential equations:

$$\frac{dY_i}{dS} = F_i(S,Y_1,Y_2,...,Y_N) \ , \quad i = 1,2,...,N \ ,$$

Y_i dependent variables

$\{Y^{new}\}$ at the new position $(S + \Delta S)$

$\{Y\}$ at the old position **S**

$$\{Y^{new}\} = \{Y\} + \Delta S\left([I] - \frac{\Delta S}{2}[k]\right)^{-1}\left\{F\left(S+\frac{\Delta S}{2},Y_1,Y_2,...,Y_N\right)\right\} \ ,$$

$$k_{ij} = \frac{\partial}{\partial Y_j}F_i\left(S + \frac{\Delta S}{2},Y_1,Y_2,...,Y_j,...,Y_N\right) \ , \quad i,j = 1,2,...,N \ .$$

SPIRALI ☞ Second order equations

$$\tilde{h} = \tilde{H}(S) + \tilde{h}'(S,\theta,\tilde{t}) \ , \quad \tilde{u} = \tilde{U}(S) + \tilde{u}'(S,\theta,\tilde{t}) \ ,$$
$$\tilde{v} = \tilde{V}(S) + \tilde{v}'(S,\theta,\tilde{t}) \ , \quad \tilde{p} = \tilde{P}(S) + \tilde{p}'(S,\theta,\tilde{t}) \ .$$

$$-\frac{1}{\tilde{r}\tilde{\rho}^*}\frac{\partial\tilde{p}'}{\partial\theta} = R^*\left(\frac{\partial\tilde{u}'}{\partial\tilde{t}} + \tilde{V}\frac{\partial\tilde{u}'}{\partial S} + \frac{d\tilde{U}}{dS}\tilde{v}' + \frac{\tilde{U}}{\tilde{r}}\frac{\partial\tilde{u}'}{\partial\theta}\right) + \Phi^*_{\tilde{U}}\tilde{u}' + \Phi^*_{\tilde{V}}\tilde{v}' + \Phi^*_{\tilde{H}}\tilde{h}' \ ,$$

$$-\frac{1}{\tilde{\rho}^*}\frac{\partial\tilde{p}'}{\partial S} = R^*\left(\frac{\partial\tilde{v}'}{\partial\tilde{t}} + \tilde{V}\frac{\partial\tilde{v}'}{\partial S} + \frac{d\tilde{V}}{dS}\tilde{v}' + \frac{\tilde{U}}{\tilde{r}}\frac{\partial\tilde{v}'}{\partial\theta}\right) + \Psi^*_{\tilde{U}}\tilde{u}' + \Psi^*_{\tilde{V}}\tilde{v}' + \Psi^*_{\tilde{H}}\tilde{h}' \ ,$$

$$\tilde{V}\frac{\partial(\tilde{r}\tilde{h}')}{\partial S} + \frac{d\tilde{V}}{dS}\tilde{r}\tilde{h}' + \tilde{r}\tilde{H}\frac{\partial v'}{\partial S} + \frac{d(\tilde{r}\tilde{H})}{dS}\tilde{v}' + \tilde{U}\frac{\partial\tilde{h}'}{\partial\theta} + \tilde{H}\frac{\partial\tilde{u}'}{\partial\theta} + \tilde{r}\frac{\partial\tilde{h}'}{\partial\tilde{t}} = 0 \ .$$

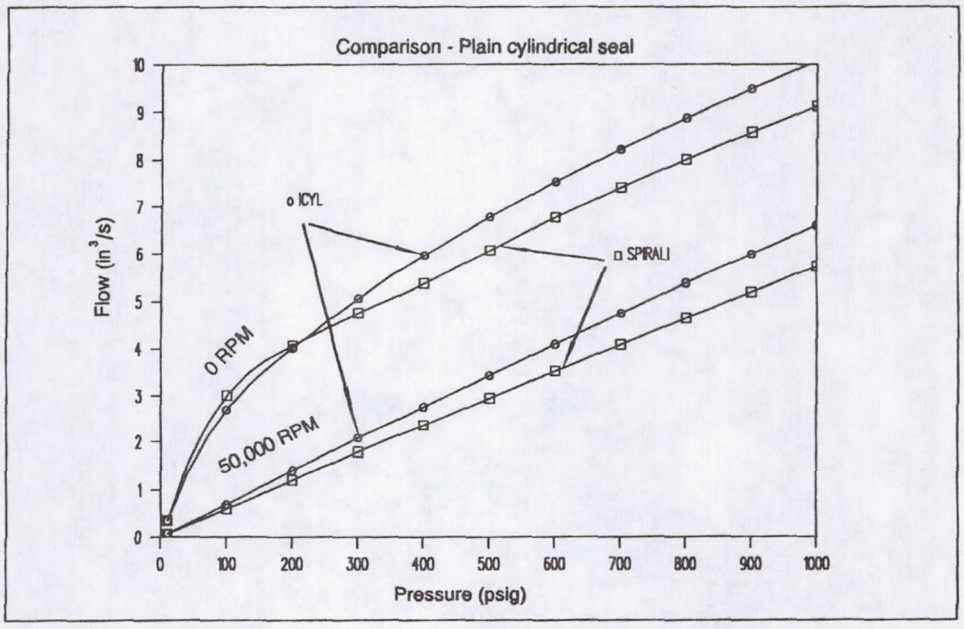

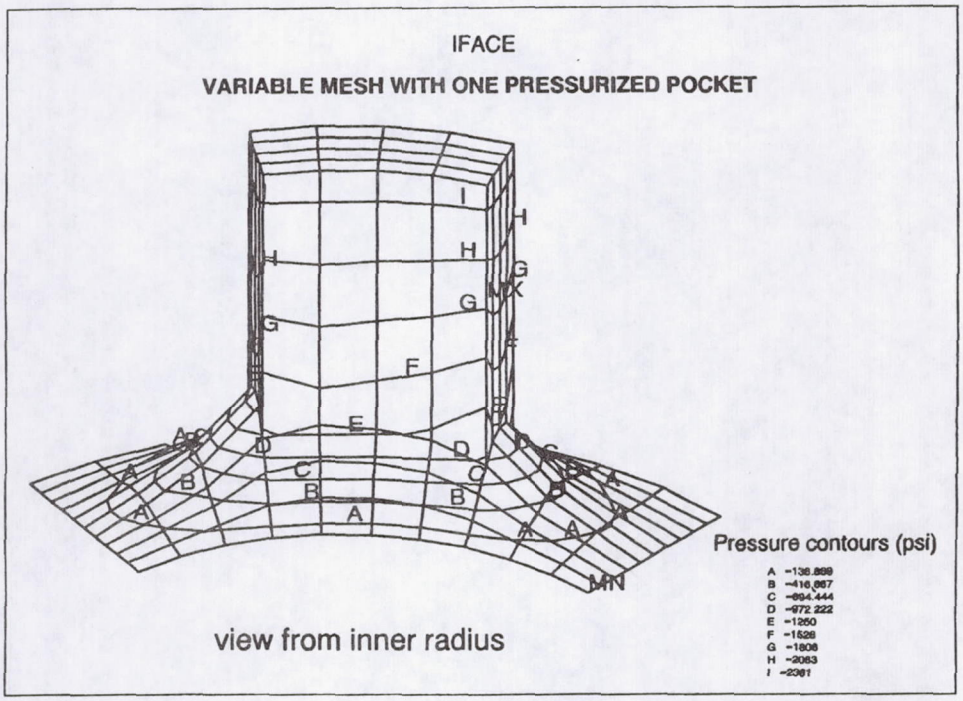

Preceding Page Blank

CFD Research Corporation
3325-D Triana Blvd. ■ Huntsville, AL 35805 ■ (205) 536-6576 ■ FAX: (205) 536-6590

CFDRC

DEVELOPMENT OF A CFD CODE FOR ANALYSIS OF FLUID DYNAMIC FORCES IN SEALS

Presentation by
A.J. Przekwas and M.M. Athavale
CFD Research Corporation
Huntsville, AL

Presented at
Second Seals Flow Code Development Workshop
NASA Lewis Research Center
Cleveland, OH

August 5, 1992

P-4115 7/01

OUTLINE

CFDRC

- Objectives
- Status Report
- Code Capabilities
- Rotordynamic Coefficient Methods
- Test Results
- Conclusions

P-4115-7/02

OBJECTIVE OF THE PROGRAM

CFDRC

- Develop Scientific 3D CFD Code for (CFDRC)
  - Prediction of Flow and Dynamics in Various Seals
  - Contribute to Data Base
  - Accuracy Standard for Industrial Design Codes
- Compile and Generate Set of Verified Industrial Codes (MTI)
- Seal Design Configuration with (MTI)
  - Knowledge Based System (KBS)
  - CAD/CAM and Visualization Tools

P-4115-7/03

OBJECTIVES

CFDRC

- Develop Verified CFD Code for Analyzing Seals
- Required Features Include:
  - Applicability to a Wide Variety of Seal Configurations, such as: Cylindrical, Labyrinth, Face, Tip and Brush Seals
  - Accuracy of Predicted Flow Fields and Dynamic Forces
  - Efficiency (Economy) of Numerical Solutions
  - Reliability (Verification) of Solutions
  - Ease-of-Use of the Code (Documentation, Training)
  - Integration with KBS

P-4115-7/04

CFD CODE REQUIREMENTS

CFDRC

- Scientific Code Required Capabilities
  - 3D N-S Analysis in BFC Grids
  - Stationary and Rotating Frames
  - Incompressible and Compressible Flows
  - Variable Physical Properties
  - Steady-State and Transient Solutions
  - Rotordynamic Coefficients
  - Interfaces with Advanced Preprocessing (Grid-GUI) and Postprocessing Packages

P-4116-7/05

SCIENTIFIC CFD CODE DEVELOPMENT

CFDRC

Task 1: Develop a 3D CFD Code for Cylindrical Seals
- for Annular, Tapered, Stepped
- Verification of Code Accuracy
- Rotordynamic Coefficient Calculations

Task 2: Augmentation of Code for Labyrinth and Damper Seals

Tasks 3 & 4: Augmentation for Other Seal Configurations

Note: Starting CFD Code = REFLEQS (developed by CFDRC under a contract from NASA MSFC/ED32)

P-4115-7/06

STATUS - 1991 WORKSHOP

CFDRC

AT 1991 WORKSHOP - 2D CAPABILITIES

- Colocated Grid Formulation for BFC Grids
- Strong Conservative Formulation of Momentum Equations with Cartesian Components
- Choice of SIMPLE, Modified SIMPLEC
- Higher Order Accurate Temporal Differencing
- Higher Order (2nd, 3rd) Spatial Discretizations Available
- Rotating Grid System for Stator-Rotor Configurations
- Moving Grid Options for Arbitrary Rotor Whirling Analysis

P-4115 7/07

CURRENT STATUS

CFDRC

Accomplishments Since Last Workshop

- All Numerical Models Transferred to 3-D
  - colocated variables
  - higher-order schemes, *etc.*
- Rotordynamic Coefficient Calculation Methods
  - circular whirl
  - moving grid (numerical scheme)
- Seal Specific User Interface
  - grid generation
  - preprocessing

P-4115 7/08

CURRENT CODE CAPABILITIES

CFDRC

- **Seals Code has:**
  - **Finite Volume, Pressure-Based Integration Scheme**
  - **Colocated Variables with Strong Conservation Approach**
  - **High-Order Spatial Differencing - up to Third-Order**
  - **Up to Second-Order Temporal Differencing**
  - **Comprehensive Set of Boundary Conditions**
  - **Variety of Turbulence Models (k-ε, Low Re k-ε, multiple scale k-ε)**
  - **Moving Grid Formulation for Arbitrary Rotor Whirl**
  - **Two Possible Ways to Calculate Rotordynamics: (i) Circular Whirl (ii) Shaker Method (moving grid)**

P-4115-7/09

CODE SYSTEM ENVIRONMENT

CFDRC

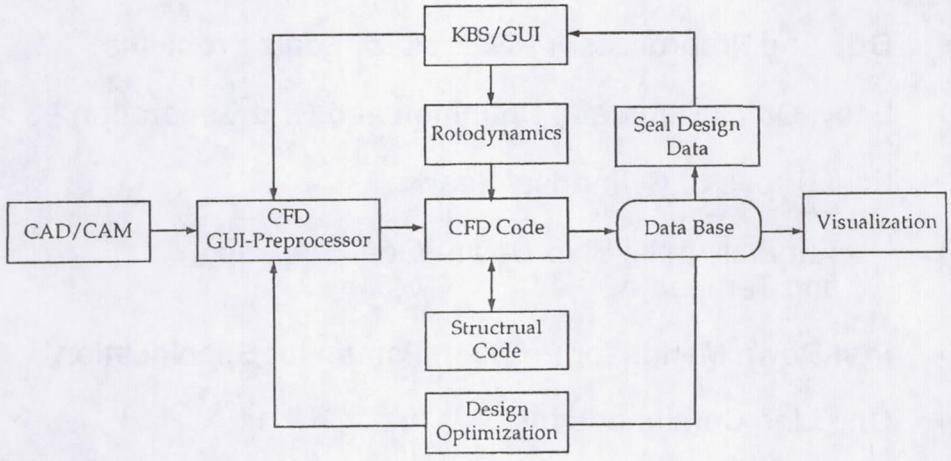

P-4115-7/10

FLOW SOLVER STRUCTURE

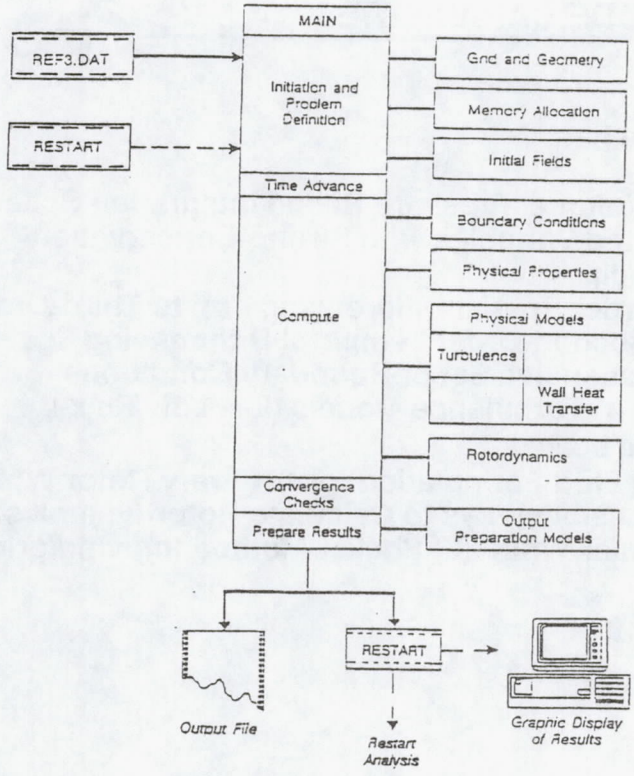

P-4115-7/11

SEAL SPECIFIC CAPABILITIES

- GUI and Preprocessor - Geared for Seals Problems
- Easy, Quick Geometry Definition and Grid Generation
- Four Types of Cylindrical Seals:
  - Annular, Axial Step-Down, Axial Step-Up, and Tempered
- Pull-Down Menus for Problem Parameter Specification
- One Line Commands for
  - Automatic Grid generation
  - Integrated Quantities: Rotor Loads, Torque, *etc.*
  - Rotordynamic Coefficient

P-4115-7/12

ROTORDYNAMIC COEFFICIENTS

CFDRC

- Relation Between Fluid Reaction Force and Rotor Motion
  - Small Perturbations
  - For Nominal, Centered, Rotor Position

$$\begin{bmatrix} -Fy \\ -Fz \end{bmatrix} = \begin{bmatrix} K & k \\ -k & K \end{bmatrix} \begin{bmatrix} y \\ z \end{bmatrix} + \begin{bmatrix} C & c \\ -c & C \end{bmatrix} \begin{bmatrix} \dot{y} \\ \dot{z} \end{bmatrix} + \begin{bmatrix} M & 0 \\ 0 & M \end{bmatrix} \begin{bmatrix} \ddot{y} \\ \ddot{z} \end{bmatrix}$$

- K, k -- Direct and Cross-Coupled Stiffness Coefficients
- C, c -- Direct and Cross-Coupled Damping Coefficients
- M -- Lumped Mass (Direct Inertia) Coefficient

P-4115-7/13

ROTORDYNAMIC COEFFICIENT - METHODS

CFDRC

$$\begin{bmatrix} -Fy \\ -Fz \end{bmatrix} = \begin{bmatrix} K & k \\ -k & K \end{bmatrix} \begin{bmatrix} y \\ z \end{bmatrix} + \begin{bmatrix} C & c \\ -c & C \end{bmatrix} \begin{bmatrix} \dot{y} \\ \dot{z} \end{bmatrix} + \begin{bmatrix} M & 0 \\ 0 & M \end{bmatrix} \begin{bmatrix} \ddot{y} \\ \ddot{z} \end{bmatrix}$$

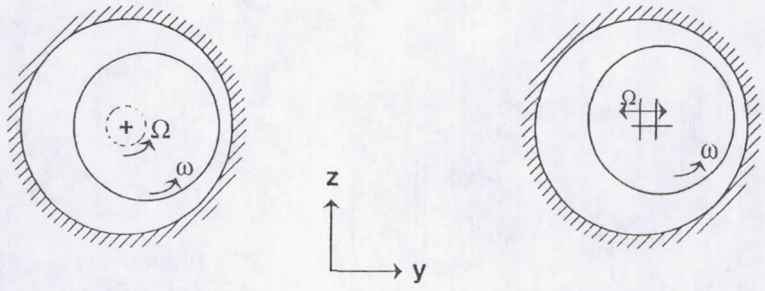

Circular Whirl Orbit Method

"Numerical Shaker" Method (with moving grid)

P-4115-7/14

CIRCULAR WHIRL METHOD

CFDRC

- Rotating Frame $\rightarrow$ Quasi-Steady Solutions
- Calculate Quasi-Steady Solutions
  - 4 or More Whirl Frequencies, Ω_i
  - Integrate Pressures for each Ω_i to Generate Rotor Loads, Fy and Fz
- Curve Fit to Calculate Rotordynamic Coefficients:

  - $Fy = + K + c\Omega - M\Omega^2$
  - $Fz = - k + C\Omega$

P-4115-7/15

NUMERICAL SHAKER METHOD

CFDRC

Two Approaches to Calculate Coefficients

Integrated Approach

$$F_Y = F_{YS}\, sin(\Omega t) + F_{YC}\, cos(\Omega t)$$

$$F_Z = F_{ZS}\, sin(\Omega t) + F_{ZC}\, cos(\Omega t)$$

Successive Time Step Approach

$$\begin{bmatrix} F_{Y1} \\ F_{Z1} \\ F_{Y2} \\ F_{Z2} \end{bmatrix} = \begin{bmatrix} y_1 & 0 & \dot{y}_1 & 0 \\ 0 & -y_1 & 0 & -\dot{y}_1 \\ y_2 & 0 & \dot{y}_2 & 0 \\ 0 & -y_2 & 0 & -\dot{y}_2 \end{bmatrix} \begin{bmatrix} K' \\ k \\ C \\ c \end{bmatrix}$$

$$K' = K + M\,\Omega^2$$

P-4115-7/16

Horizontal Displacement Definition

$$Y = A\, sin(\Omega t) + B\, cos(\Omega t)$$

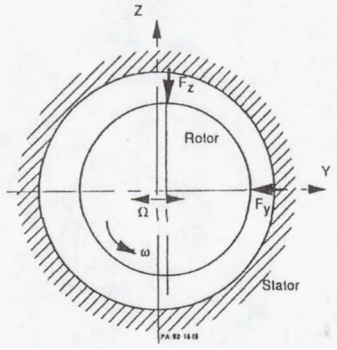

Ω = Shaker Frequency
ω = Rotor Speed

CODE ACCURACY CHECK & VALIDATION

CFDRC

- Extensive Validation Effort
  - Checkout Problems
  - Benchmark Problems
  - Validation Problems
  - Field Problems

P-4115-7/17

CODE ACCURACY AND VALIDATION

CFDRC

- Partial List of Relevant Test Cases
  - Flows in Pipes, Channels, Very Narrow Annulii
  - 2D and 3D Driven Cavity Flows
  - Laminar Flows: Wedge, Duct to 90° Bend
  - Rotating Flows: Disk in a Cavity, Stator-Rotor Config.
  - Turbulent Flows in Annular and Laybrinth Seals (Texas A&M)
  - Flow in Journal Bearings

P-4115-7/18

DESCRIPTION OF THE FLOW PROBLEM

CFDRC

- Simplified Turbine Cavity Problem:
  - 90 x 130 grid
  - Central Differencing
  - k-ε Turbulence Model
- Cooling Flow Rate Parameter

$$C_Q = Q/(R\nu)$$

where
Q = volumetric flow rate
ν = kinematic viscosity
R = cavity radius

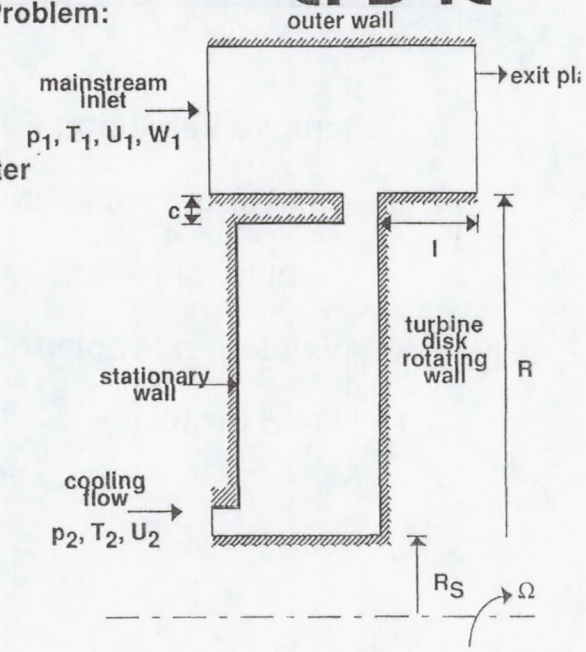

P 4115 7/20

NUMERICAL RESULTS

CFDRC

Streamlines

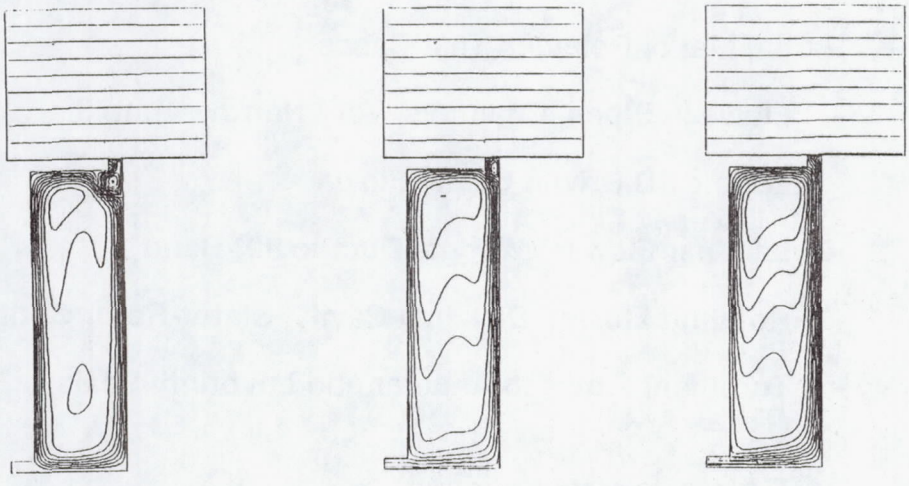

$C_Q = 1500$ $C_Q = 7200$ $C_Q = 13000$

P 4115 7/21

Computational results

Cavity temperatures at three cooling flow rates

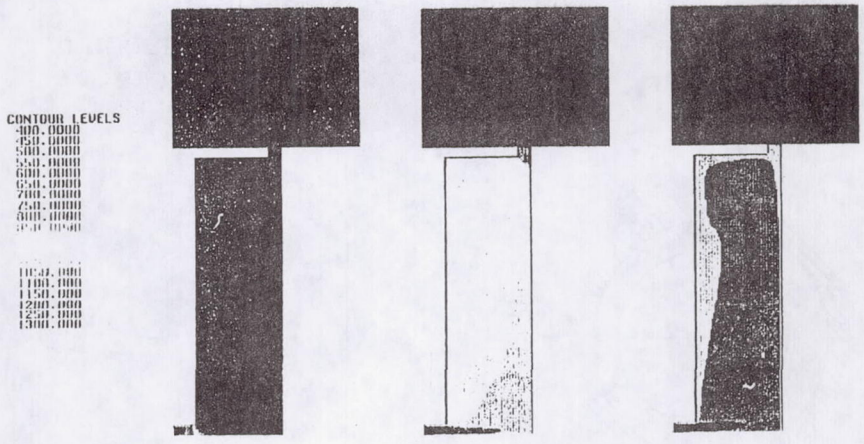

21% design | Design | 189% design

SAMPLE PROBLEM DEFINITION

CFDRC

- Annular Seal Geometry (After Nordmann, 1987)
  - RotorRadius 23.5 mm., Nominal Clearance 200μm
  - Seal Length 23.5 mm.
  - Rotor Speed 1000-5000 rpm
- Flow Conditions
  - Specified ΔP Across the Seal
  - Specified Inlet Loss Coefficient
  - Water Density 996 Kg/m^3, viscosity 0.7 x 10^{-3} N-s/m
- Computational Parameters
  - k-ε Turbulence Model
  - $N_x * N_r * N_\theta = 10 * 5 * 30$ Computational Grid
  - 40 Time Steps per Cycle

P 4115 7/19

FLUID REACTION FORCES

CFDRC

- Rotor Speed 3000 rpm., Ω = 40 cps.

Geometry

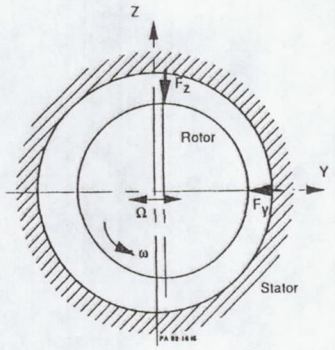

Time Variation of Fluid Forces

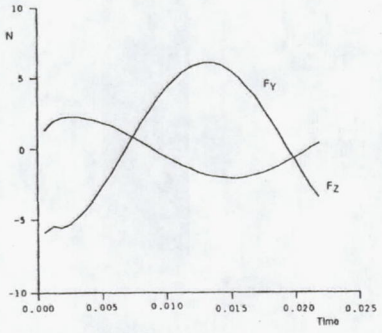

PA 92-16PFV12

ROTORDYNAMIC COEFFICIENTS

CFDRC

Time Variation of Stiffness Coefficients

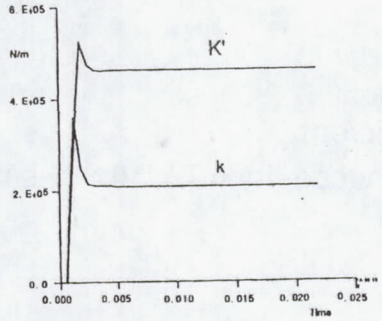

Mass Parameter

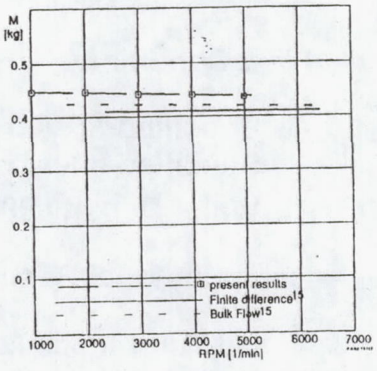

PA 92-16PFV12

STIFFNESS COEFFICIENTS

CFDRC

Direct

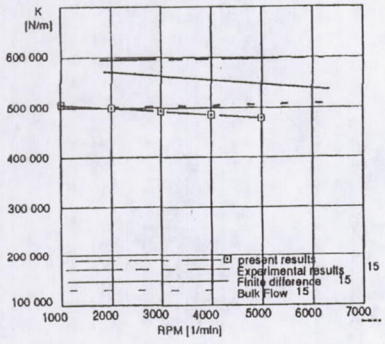

Cross-Coupled

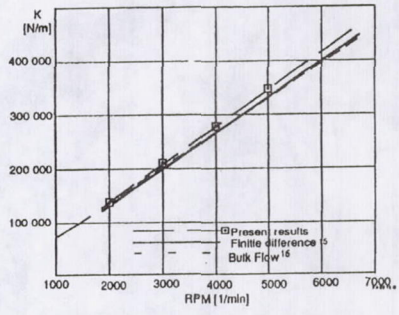

PA 92-16PR/12

DAMPING COEFFICIENTS

CFDRC

Direct

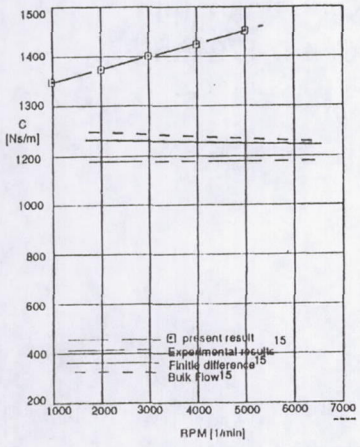

Cross-Coupled

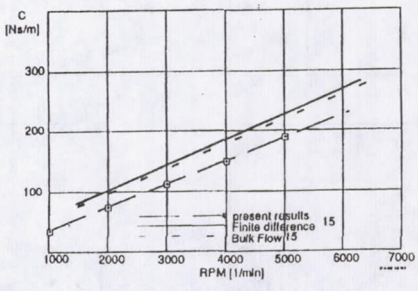

PA 92-16PR/12

Time-dependent pressure field, t=nT.

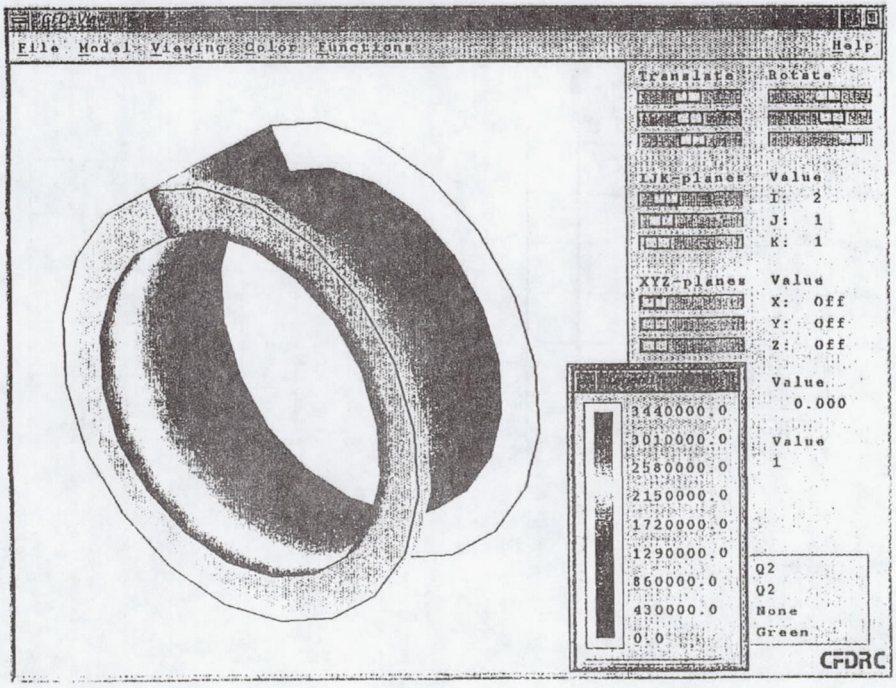

TAPERED GAS SEAL (NELSON, 1985)

CFDRC

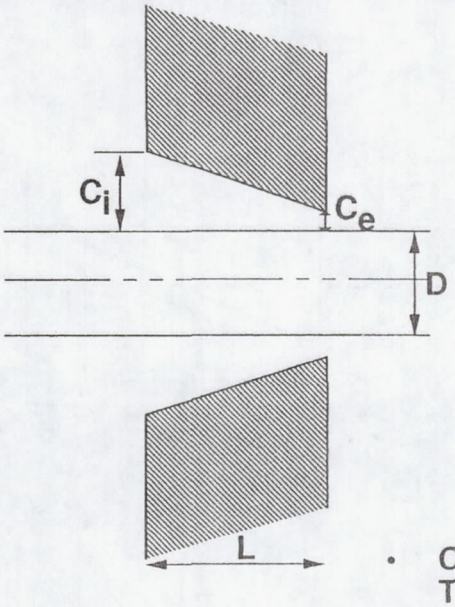

D = 65.0 mm
C_e = 0.086 mm
C_i = 0.172 mm
3 L/D ratios: 0.1, 0.2, 0.4

- Compressible, Turbulent, Transonic Flow

P 4116 7/25

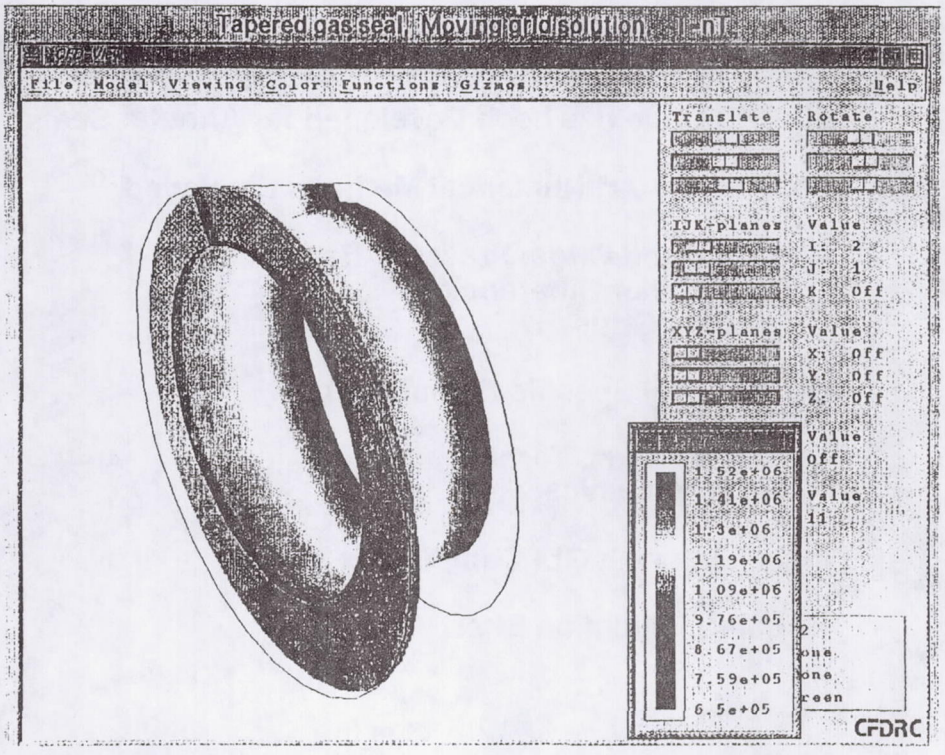

TAPERED GAS SEAL - RESULTS

Moving Grid Method

CFDRC

L/D	K N/m	k N/m	C N-s/m	c N-s/m	Exit Mach Number
0.1	948000	19700	11.5	0.016	1.00
	1150000	15429	9.94	0.043	1.00
0.2	1700000	75700	43.9	0.073	0.96
	2125500	60886	38.62	0.09	0.97
0.4	2880000	267000	152	0.27	0.83
	3553200	233820	145.9	0.57	0.83

Nelson, 1985 Present Results

P-4115-7/22

CONCLUDING REMARKS

CFDRC

- 3D CFD Code has been Developed for Annular Seals
- State-of-the-Art Numerical Methods Employed
  - Colocated Grids, Pressure-Based
  - High Order Differencing
  - Moving Grids
- Several Seal Specific Parameters
  - Rotor Loads, Torque, *etc*
  - Rotordynamics
- Initial Link with GUI Completed
- Ongoing Validation Effort

P-4115-7/23

CONCLUDING REMARKS (CONTINUED)

CFDRC

- Continue Code Testing & Validation
- Add Treatment for Inlet/Exit Regions
  - Geometry Definition
  - Grid Generation
- Code Extensions
  - Augmentation of Code for Labyrinth Seals
  - Treatment of Damper Seals
- Identified Needs
  - Multi-Domain Capability for Proper Treatment of Inlet/Outlet Plenums
  - Two-Layer k-ε Model for Near-Wall Treatment

P-4115-7/24

Seal Analysis Codes: KBS User Interface

Presented by:

Bharat B. Aggarwal
Lynn Cowper

Mechanical Technology Inc.

Seal Analysis Codes: KBS User Interface

Overview

- KBS Executive
  - Access all seal analysis codes
  - Utility services like printing, browsing, plotting, etc.
  - System maintenance and configuration
- Industrial Codes
  - Prepare input files for analysis codes
  - Run analysis code
- Scientific Code
  - User input tailored for specific seal configurations
  - Four types of Cylindrical seals implemented. Others to be added in phases.
  - Prepare input files for preprocessor
  - Run the preprocessor
  - Communication capabilities to be added later

Seal Analysis Codes: KBS User Interface

KBS System Implementation

- Portability Requirements
  - User interest in Unix at the last workshop
  - Elected to support both OS/2 and Unix
  - Unix support for OSF/Motif environment only
- Implementation Strategy
  - C++ and Commonview 3.0 class libraries from Glockenspiel
  - Portable to several Unix platforms with OSF/Motif interface
  - NASA will support IBM, HP, and SUN workstations

Seal Analysis Codes: KBS User Interface

KBS System Requirements

- IBM PC Users
  - Intel 80386 (with 80387) or 80486 based machine
  - 8 Mb RAM
  - 80 Mb Hard Disc
  - OS/2 Version 2.0
  - Will continue supporting OS/2 version 1.3 for another year
- Workstation Users
  - IBM RS/6000, SUN, or HP 700 series workstations
  - 24 Mb RAM
  - 200 Mb Hard Disc
  - Unix with OSF/Motif user interface

Seal Analysis Codes: KBS User Interface

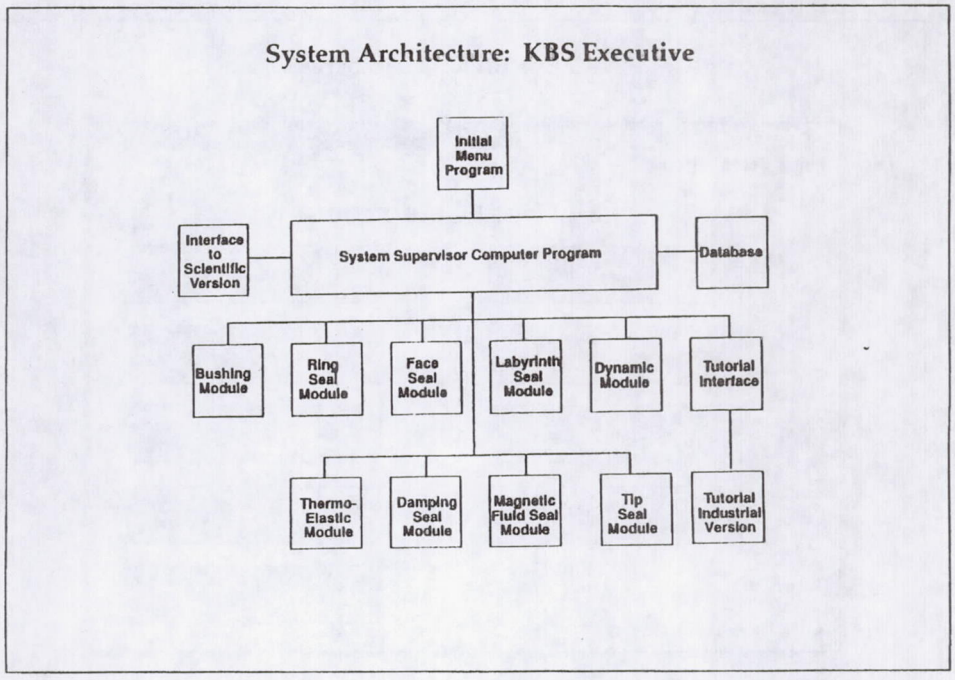

Seal Analysis Codes: KBS User Interface

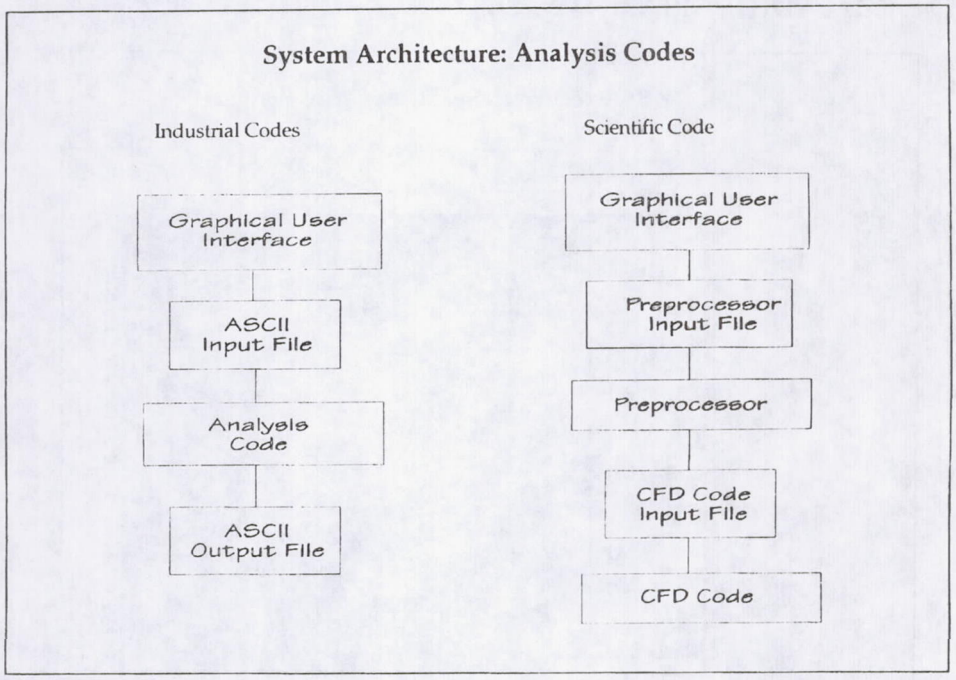

Seal Analysis Codes: KBS User Interface

KBS Executive: Main Screen

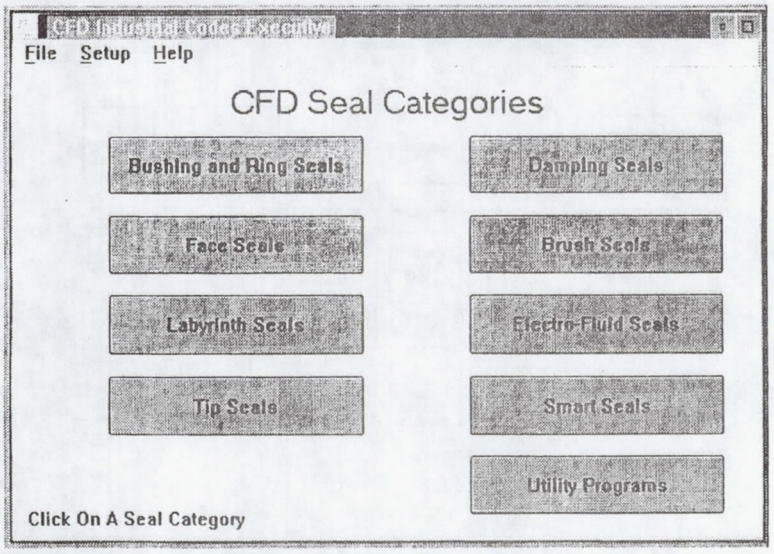

Seal Analysis Codes: KBS User Interface

KBS Executive: Seal Categories Screen

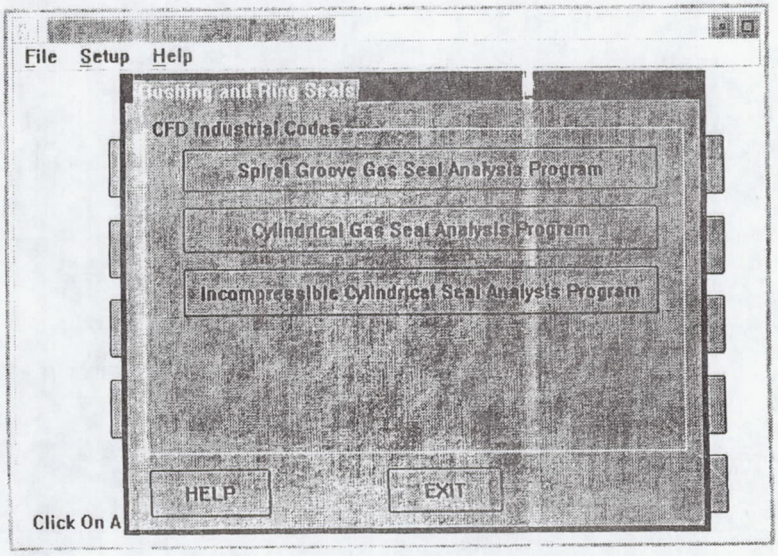

Seal Analysis Codes: KBS User Interface

Industrial Code GCYL: Main Screen

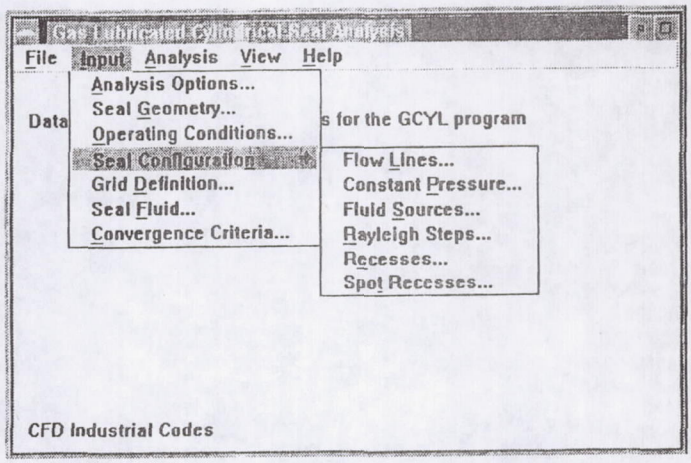

Seal Analysis Codes: KBS User Interface

Industrial Code GCYL: Analysis Options Screen

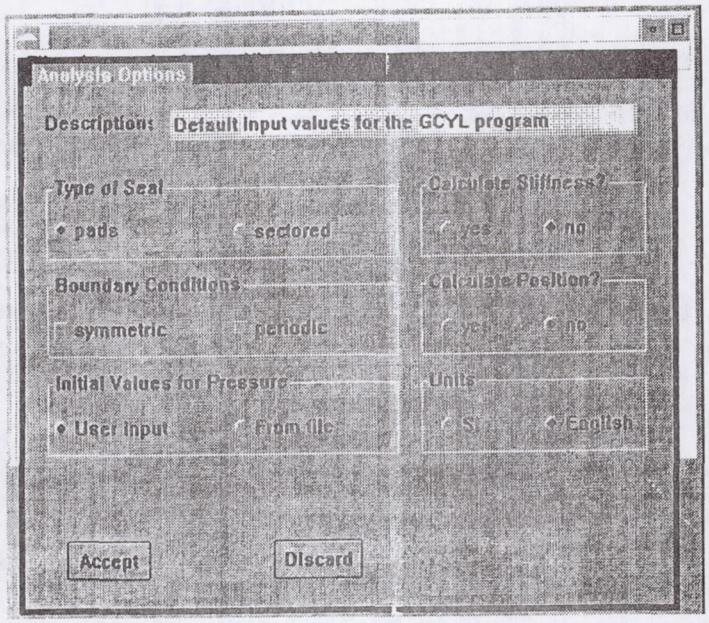

Seal Analysis Codes: KBS User Interface

Industrial Code GCYL: Typical Input Screen

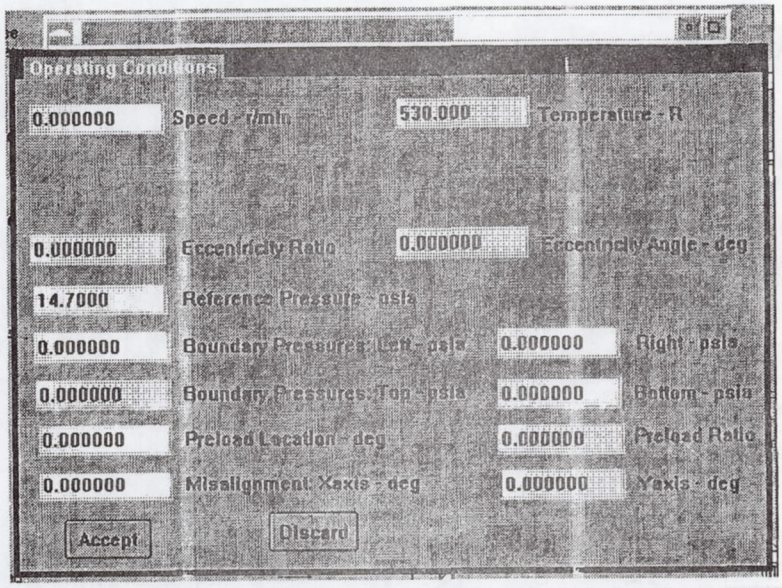

Seal Analysis Codes: KBS User Interface

Industrial Code GCYL: Help Screen

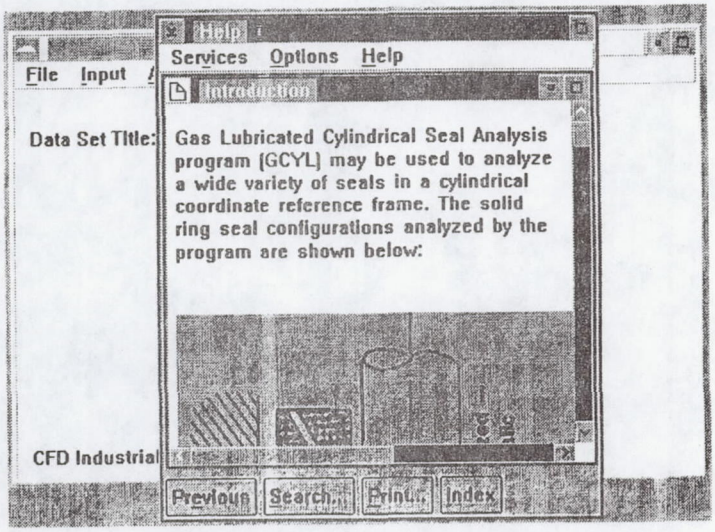

Seal Analysis Codes: KBS User Interface

Industrial Code GCYL: Plotting Program

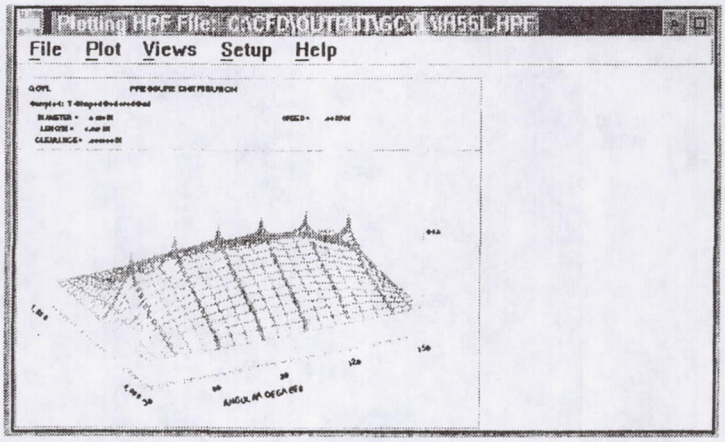

Seal Analysis Codes: KBS User Interface

Scientific Code: Main Screen

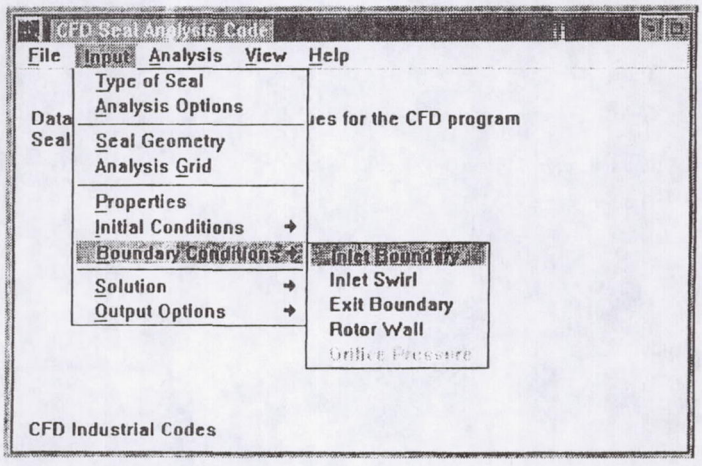

Seal Analysis Codes: KBS User Interface

Scientific Code: Seal Types

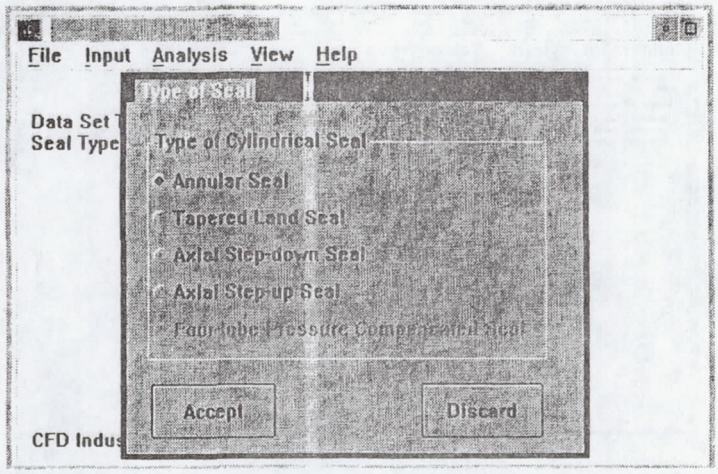

Seal Analysis Codes: KBS User Interface

Scientific Code: Analysis Options Screen

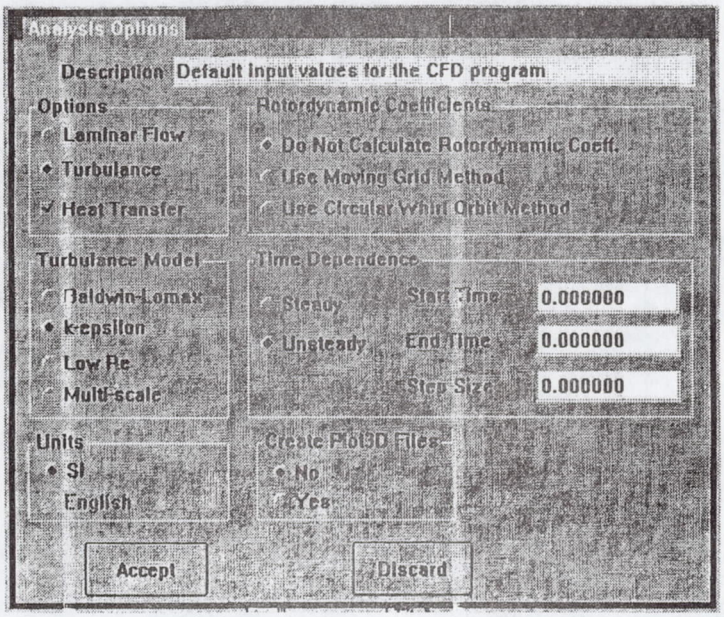

Seal Analysis Codes: KBS User Interface

Scientific Code: Typical Input Screen

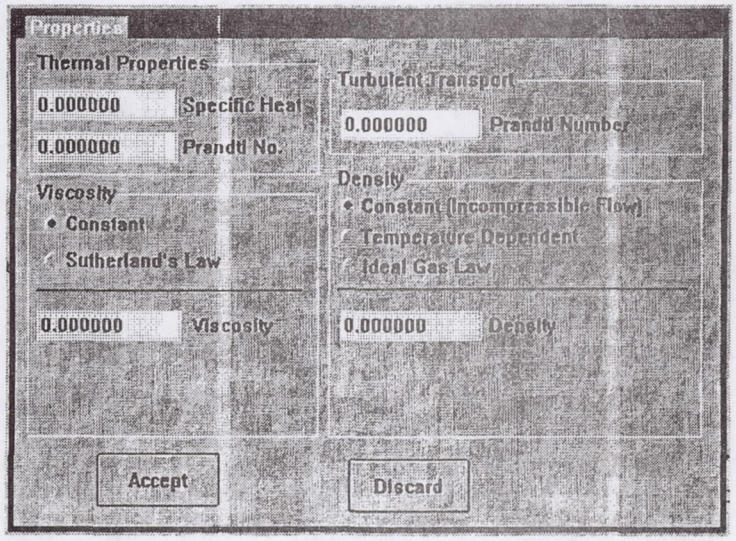

Seal Analysis Codes: KBS User Interface

Scientific Code: Solution Control Options

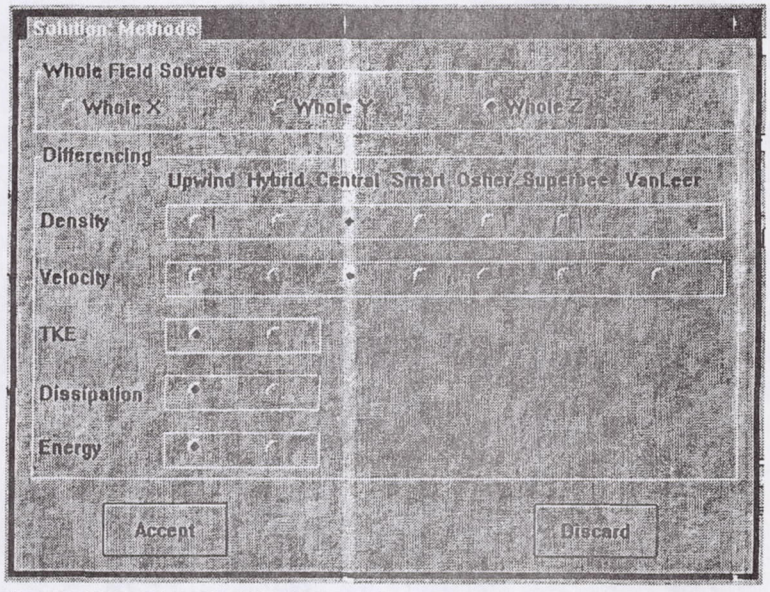

Seal Analysis Codes: KBS User Interface

Scientific Code: Output Options

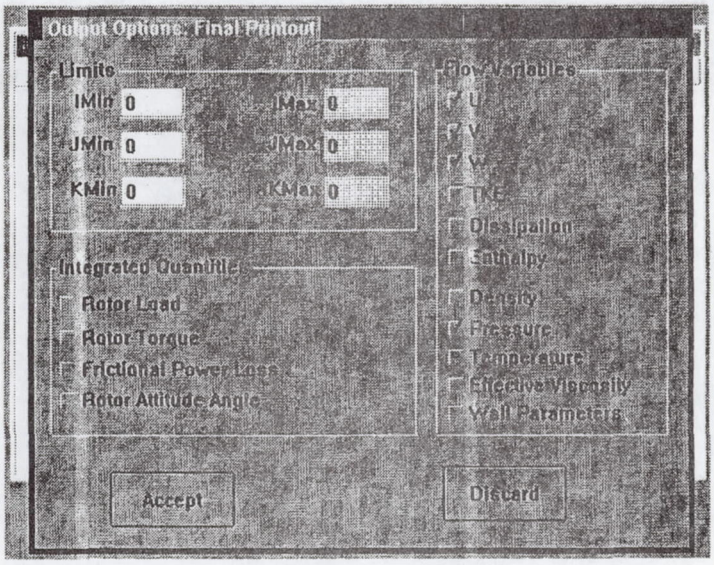

Seal Analysis Codes: KBS User Interface

Summary and Future Plans

- KBS implemented to support both OS/2 and Unix users
- Interactive graphics capability to be added to ease input
- Selection of a standard plot file format
- Implementation of database capability
- New codes to be added as they become available
- Enhancements based on user feedback

BRUSH SEAL BRISTLE FLEXURE AND HARD-RUB CHARACTERISTICS

Robert C. Hendricks, Julie A. Carlile, and Anita D. Liang
National Aeronautics and Space Administration
Lewis Research Center
Cleveland, OH 44135

SUMMARY

The bristles of a 38.1-mm (1.5-in.) diameter brush seal were flexed by a tapered, 40-tooth rotor operating at 2600 rpm that provided sharp leading-edge impact of the bristles with hard rubbing of the rotor lands. Three separate tests were run with the same brush accumulating over 1.3×10^9 flexure cycles while deteriorating 0.2 mm (0.008 in.) radially. In each, the test bristle incursion depth varied from 0.130 to 0.025 mm (0.005 to 0.001 in.) or less (start to stop), and in the third test the rotor was set 0.25 mm (0.010 in.) eccentric. Runout varied from 0.025 to 0.076 mm (0.001 to 0.003 in.) radially. The bristles wore but did not pull out, fracture, or fragment. Bristle and rotor wear debris were deposited as very fine, nearly amorphous, highly porous materials at the rotor groove leading edges and within the rotor grooves. The land leading edges showed irregular wear and the beginning of a convergent groove that exhibited sharp, detailed wear at the land trailing edges. Surface grooving, burnishing, "whipping," and hot spots and streaks were found. With a smooth-plug rotor, post-test leakage increased 30 percent over pretest leakage.

INTRODUCTION

High-performance, lightweight engines require compliant seal configurations to accommodate flexible interfaces. Thus, in many aircraft gas turbine engines and other turbomachines brush seal systems are being proposed to replace labyrinth seals because brush seals are compliant and reliable, leak less, cost less, and enhance rotor stability. Brush seals have been the subject of much recent seals research (refs. 1 to 20).

A brush seal system consists of the brush and a hardened rub ring and can be linear, circular, or contoured (see ref. 20 for a review). The bristles are oriented to make an angle of 30° to 50° with the interface, such as the rotor radius for a circular brush. This design allows the bristles to flex when rotor excursions occur without significant damage to either the rotor or the seal.

A typical brush seal configuration, figure 1 (courtesy of Cross Mfg. Ltd. (ref. 1)) consists of (1) a backing plate (like a sealing dam), (2) a circumferential or linear set of packed wires (fibers or bristles), (3) a pinch plate that serves as a retainer for the brush bristles, and (4) an outside diameter surface that fits tightly to the housing (insert in fig. 1). The flexibility of the fibers and implicitly the performance of this seal are governed by many factors as expressed in terms of similitude parameters (refs. 9 and 20). Among these factors are fiber length and diameter, inclination to the moving surface, surface speed, interface friction, seal diameter, fluid properties, packing density, modulus of elasticity, backing plate clearance, and preload or interference fit.

Typically for a circular brush, the wire or brush materials are superalloys and range from 0.05 to 0.07 mm (0.002 to 0.0028 in.) in diameter. The bristles are approximately 0.96 mm (0.38 in.) long and are aligned at 30° to 50° to the shaft in the direction of rotation. Nominally, there are 98 bristles/mm (2500 bristles/in.) of circumference. The interface is characterized by a smooth (4 to 20 rms), hardened rub surface on the shaft (e.g., Al_2O_3 or for short duration the uncoated shaft itself). Because brush seals are contact seals with radial interferences ranging from zero to more than 0.25 mm (0.01 in.), ceramic

coatings and superalloy materials are often used to enhance life and minimize wear at elevated surface speeds, temperatures, and pressure drops.

Although brush seals show great promise for future applications, it must be acknowledged that brush seals are most effective as contact seals and that life and wear rates are major concerns. Whereas bristle blowout will cause excessive leakage, bristle loss and debris have a potential for destructive impact on the powerplant. Thus, the issues of bristle pullout, surface rubbing, bristle wear, and debris are qualitatively addressed in this paper.

The authors are aware that other data exist for ranges of interference fits and other configurations, but the results are proprietary.

APPARATUS

The "drill press" apparatus was similar to that described in reference 2. In the tests of reference 2 the 38.1-mm (1.5-in.) diameter brush seal was fixed in a pressure vessel and the rotor was a smooth-surface, tapered plug turning at 400 rpm. Leakage data at various interferences and eccentricities have been reported (ref. 19).

In the tests described herein the 38.1-mm (1.5-in.) diameter brush seal was again mounted in the pressure vessel that simulated the static housing; but for these tests flutes were machined the length of the plug rotor, providing a set of 40 lands and 40 grooves, or a 40-tooth rotor (fig. 2). The lands were 1.638±0.04 mm (0.0645±0.0015 in.) just above the groove at test 3 and 1.582±0.04 mm (0.0623±0.0015 in.) just below the groove at test 1; see rotor sketch on table I. The groove width (fig. 3) averaged 1.397 to 1.422 mm (0.055 to 0.056 in.) with further dimensions provided in tables I and II. Prior to testing the machining tool marks were clear, being axial in the grooves and circumferential on the lands. This rotor provided 40 impacts of the brush bristles per revolution and was rotated at 2600 rpm.

The 38.1-mm (1.5-in.) diameter brush seal (fig. 4) was damaged in a previous series of tests related to reference 2. The damaged section, although quite small and having a "chewed" appearance, increased seal leakage. The seal could no longer be used for leakage tests but was adequate for the tests herein.

The rotor was AISI 304 stainless steel, and the brush bristles were Haynes 25 in the annealed condition. When stainless steel is rubbed during a machining operation, it tends to change from a "gummy" machining material to a surface-work-hardened material. As a result the bristles would be expected to rub-machine the stainless steel, and in turn the stainless steel would be expected to abrasively remove the bristles.

In test 1 the interference was set at 0.025 to 0.050 mm (0.001 to 0.002 in.) with the groove depth at 0.05 to 0.08 mm (0.002 to 0.003 in.). As expected the bristles rub-machined the rotor.

For test 2 the plug rotor was reset to a portion of the surface that was unrubbed. At that point the groove depth was 0.08 to 0.13 mm (0.003 to 0.005 in.). The interference fit between the rotor lands and the brush was 0.05 to 0.08 mm (0.002 to 0.003 in.).

For test 3 the plug rotor was again reset to a portion of the surface that was unrubbed. The groove depth was 0.178 to 0.254 mm (0.007 to 0.010 in.). For this test the rotor was initially set 0.33 mm (0.013 in.) eccentric, but the rotor rubbed the fence (backing washer) slightly. The fence diameter was 39.2 mm (1.544 in.). The rotor was then reset to an estimated static eccentricity less than 0.25 mm

(<0.010 in.). The dynamic eccentricity was estimated to be less than 1 mm (<0.004 in.). No active clearance measurements were made during these tests; these estimates of eccentricities were made from post-test photographs and static measurements. These settings provided a test with significant rotor impacting and incursion at one portion of the seal and no rubbing contact diametrically opposite to that position.

In tests 1 and 2 the smooth rotor and the 40-tooth rotor were assumed to be interchangeable. The repositioning of the stator for test 3 introduced an unaccountable bias that was estimated in order to correlate the measured flow rates. For test 3 the smooth-rotor initial static eccentricity was estimated to be less than 0.15 mm (<0.006 in.), and after test 3 the estimated static eccentricity was less than 0.25 mm (<0.010 in.).

RESULTS

The results are separated into observations of (1) the brush bristle flexure cycles with associated interface damage to the brush seal and the rotor, and (2) the leakage or performance changes.

Bristle Flexure and Interface Damage

Visualization of the rotor-brush interface at creeping surface speeds (under 10 rpm) revealed little groove penetration. In the impact zone the brush stiffness and the low void did not permit a fully deflected or extended set of bristles at the interface. Instead the impact compacted the bristles in the circumferential direction into the brush and spread the bristles in the axial direction at rate of 40 times per revolution.

Time of testing and brush diameters before and after testing for the three tests are presented in table I; additional dimensions are given in table II. The diameters were obtained by inspecting the brush on an optical comparator before and after each test. The chewed area and a few stray wires served as reference positions for measurements.

Optical inspection of the grooves cut by the brush into the stainless steel rotor (test 1) showed that the cut converged from the leading edge to the trailing edge of the land as the wires (bristles) crossed the rotor (fig. 5). Wire grooves were clear cut and debris was evident, as is better shown in the enlargement (fig. 6).

The following groove extents in millimeters (inches) were measured in test 1:

Width at inlet	1.52 (0.06)
Width at center	1.3 (0.051)
Width at outlet	1.27 (0.05)

For test 2 the inlet region at the land leading edge was extensive and not readily characterized, but a general convergence pattern was evident. Similar behavior at the leading edge was noted for test 3.

In order to corroborate the optical results, profilometer results for a typical tooth of the 40-tooth rotor were taken. Wear area and groove depth estimates are provided in table III. Values for the extent of the groove in millimeters (inches) are shown in figures 7 to 9 at a resolution of 0.02 mm/division.

Width within 0.1 mm of inlet	0.9 (0.035)
Width at center	0.4 (0.016)
Width within 0.08 mm of outlet	0.27 (0.011)

It is evident that the optical values for groove extent were much larger than those from the profilometer. The problem is the scale used in defining the groove depth. For example, at a resolution of 0.01 mm/division the width at the center is 1.15 mm (0.045 in.), but at a resolution of 0.02 mm/division the width at the center is 0.4 mm (0.016 in.). At the smaller resolution the extent of the scratched interface generally agrees with the optical values, but at the larger resolution the extent of the scratched interface is not resolved (i.e., detail is lost).

For the surface asperity resolution used herein the optical method better defined the extent (width) of the damaged interface; the profilometer provided the depth. At one-half the depth resolution only the major grooving was defined.

The first profile, labeled "leading edge," was taken within 0.10 mm (0.004 in.) of the leading edge and shows a broad damage region with deep grooving for test 2 (fig. 8(a)) and test 3 (fig. 9(a)) but a minor amount of material damage for test 1 (fig. 7(a)). The material buildup adjacent to the groove of test 3 probably occurred during rotor-fence rub. The second profile, labeled "mid section," was taken midway between the tooth leading and trailing edges. The damage of test 2 (fig. 8(b)) and test 3 (fig. 9(b)) was severe, and a twofold cut has developed in the rotor during test 2. Again moderate damaged was noted for test 1 (fig. 7(b)). The third profile, labeled "trailing edge," was taken within 5 percent of the trailing edge. The grooving seen in the midsection profile carried through with perhaps some sharpness of the features near the trailing edge (figs. 7(c), 8(c), and 9(c) for tests 1, 2, and 3, respectively).

The brush bristle impact at the leading edge left material deposits that were magnetic (i.e., from the rotor) and rust color (probably Fe_3O_4) with a spongelike (or cauliflower) appearance (fig. 10); these deposits are readily seen at higher magnification (80X) in figure 11. Debris was generated by surface machining grooves, "whipping" of the leading edge, burnishing, and sharp trailing edges. The deposited materials were fine, porous, "greasy" to the fingers, and readily removed from the rotor; removal from the bristles was not straightforward. Standard degreasing cleaned but not thoroughly, and ultrasonic cleaning was not attempted. The reasoning was to see if these deposits would inhibit the responsive character of the bristles. The debris can affect both the response and the leakage, but neither effect was observed in these tests. Further work here is warranted.

These deposits also indicate rapid wear-in with a long oxidation period for the "machined out" material. The materials deposited on the groove wall at the land leading edge (fig. 11) and on the groove wall at the land trailing edge (fig. 12) had little or no structure; the defraction spectra were peakless.

It is speculated that the bristles were dragged across the land, with "machined" material adhering to the bristle and then "impacted" off the bristle at the leading edge of the next tooth. Some of the materials were deposited within the groove. Black nodule-like debris tended to adhere to the groove wall at the land trailing edge. This black material and rust-colored materials formed in the groove at the land leading edge.

Stainless steel work hardens so that the cut grooves were probably harder than the parent stainless steel and would wear the annealed Haynes 25 bristles. The smooth grooves, the hot spots, and the hot streaking may indicate that a thin layer of stainless steel flowed plastically as it was machined out (figs. 13 and 14). Because of the incursive impact of the toothed rotor and the heated interface, the

Haynes 25 bristles could lose strength, erode, fracture, or pull out as massive debris. But no pullouts or massive debris was found after any of the three tests. At higher magnification (200X) the tips still appear intact without fracture, but wear is evident and oxidation debris appears to be well adhered to the surface (fig. 15). As further evidence of the bristle wear an examination of the bristle tip surface revealed tip grooving (fig. 16), and the severe impacting on the bristles is shown by erratic wear notches on the bristle surface (fig. 17).

The trailing edge of the land was "cut" clean by the brush in all three tests (fig. 18) in stark contrast to the erratic leading-edge surface, which was whipped by the bristles (fig. 19). Of interest is the contrast between the land surface cuts. Test 1 surface cuts were a simple wear scar; those of tests 2 and 3 were multiple grooves with complex surfaces and burnishing (fig. 20). The most rotor damage appeared from test 2 and the most brush damage from test 3, where the rotor was set eccentric.

These tests, although preliminary and only qualitative, begin to mitigate the fear of brush seal disintegration through bristle flexing as over 1×10^9 cycles were sustained without failure, fracture, or pullout. However, the required flexures are at least an order of magnitude higher with parameters such as surface speed, temperature, pressure, and materials to be considered.

$$\text{Total flexures} = 222 \text{ hr} \times 60 \text{ min/hr} \times 40 \text{ teeth} \times 2600 \text{ rpm} = 1.38\times10^9$$

$$\text{Required eccentric shaft flexures} = 10\,000 \times 60 \times 1 \text{ (flexure/rotation)} \times 20\,000 \text{ rpm} = 12\times10^9$$

$$\text{Required rotor disk flexures} = 50 \times \text{eccentric shaft flexures}$$

However, bristle flexures raise an equally troubling concern over seal life, because brush seals do wear out. Once these seals begin to reach line-to-line contact, their leakage can be equivalent to that of an advanced labyrinth seal. The sealing margin and competitive edge of the worn brush seal begin to fade. New competitive (lower leakage) configurations for labyrinth, damper, honeycomb, feltmetal, and spiral-groove seals are under investigation. It is clear that long-duration testing at elevated surface speeds and working fluid temperatures are required.

Correlation of Leakage Data

Although not the primary objective of this experiment, overall changes in brush leakage were estimated from flow checks before and after testing. In order to determine these leakages the 40-tooth rotor was replaced with a smooth-surface, tapered rotor. Runout errors resulting from rotor interchange were unresolved as were those associated with the static eccentricity of test 3. Measurements characterizing the rotor and brush before and after testing are given in table I. The average depth of the brush-cut groove as well as the estimated clearances are given in tables II and III.

Leakage is characterized in figure 21 in terms of volumetric flow rate as a function of pressure drop across the brush seal before and after each of the three tests. Both pretest and post-test results are provided in the same figure. Because this brush seal was damaged (see APPARATUS section), absolute leakage measurements would require weighing, but the relative leakage should be accurate. The interference fits for the brush seal leakage data for pretests 1 and 2 were nearly the same, resulting in corresponding leakages. While taking data it was found that the brush would stiffen and the pressure drops would increase. Data points illustrating hystersis (typical in brush seals) are shown. After correcting the post-test 2 data for clearance, these test results agreed with those of post-test 1.

Setting the rotor eccentric in test 3 proved a major problem in cross correlating the leakage results. The estimated initial static eccentricity for the smooth rotor was less than 0.15 mm (0.006 in.), and the smooth rotor and the 40-tooth rotor were assumed to be interchangeable at the same spindle loading. However, the rotor rubbed the fence (backing washer) slightly, requiring an initial static eccentricity of 0.36 mm (0.014 in.) and implying a difference in spindle loading. The rotor was reset to an estimated eccentricity of less than 0.025 mm (0.010 in.). Post-test photographs indicated that the dynamic eccentricity was <0.10 mm (<0.004 in.) and clearly illustrated the fence rub (fig. 22).

For test 3 the repositioning of the stator and the differential spindle loading introduced an unaccountable bias that was difficult to estimate in correlating the leakage results. From the data of reference 19 a relation was found for the change in pressure as a function of eccentricity at a fixed volumetric flow rate. Using this relation and corrections for clearance and assuming a pretest static eccentricity of 0.15 mm (0.006 in.) and a post-test static eccentricity of 0.25 mm (0.010 in.) show that the results of test 3 were overcorrected by 20 percent with respect to the results of tests 1 and 2. Future testing requires instrumentation to overcome these positioning errors. Nevertheless, these leakage data indicate that under conditions of severe brush and rotor wear the brush seal leakage increased 30 percent. And, although brush seal performance degraded, the brush seal did not fail.

SUMMARY OF RESULTS

In three separate tests with a 40-tooth tapered stainless steel rotor operating at 2600 rpm and a 38.1-mm (1.5-in.) diameter brush seal with 0.07-mm (0.0028-in.) diameter annealed Haynes 25 bristles set at a nominal 0.076-mm (0.003-in.) radial interference for each test, the following results were obtained:

1. The bristles withstood over 1×10^9 cycles without pullout, fracture, or massive debris generation.

2. Rotor grooving up to 0.076 mm (0.003 in.) in depth radially with erratic "whipped" leading-edge surfaces followed by convergent grooving to a clean-cut trailing edge was commonplace for each of the three tests.

3. Most of the debris generated was a fine black material that appeared amorphous, but the rust-colored materials were iron rich and magnetic, implying Fe_3O_4. The debris was "cauliflower" in form and highly porous with low adhesion, except for that which was fine enough to adhere to the bristles. Those fines were not readily dislodged. Nonuniform fines (or oxidation) adhering to the bristles tended to separate the bristles, increasing porosity, and would enhance leakage paths.

4. Radial bristle losses up to 0.2 mm (0.008 in.) were demonstrated, which if left uncorrected would lead to equivalent or higher leakages than those of labyrinth seals. Bristle loss at elevated surface speeds and temperatures requires further study.

5. Generated debris can impair bristle motion and alter leakage, but within the limitations of this experiment these considerations were not a problem. They remain as issues to be resolved.

6. Under conditions of severe rotor-stator interface damage, the brush seal leakage performance degraded 30 percent, but the seal did not fail.

REFERENCES

1. Ferguson, J.G.: Brushes as High Performance Gas Turbine Seals. ASME Paper 88-GT-182, 1988.
2. Flower, R.: Brush Seal Development Systems. AIAA Paper 90-2143, 1990.
3. Chupp, R.; and Nelson, P.: Evaluation of Brush Seals for Limited Life Gas Turbine Engines. AIAA Paper 90-2140, 1990.
4. Holle, G.; and Krishnan, M.: Gas Turbine Engine Brush Seal Applications. AIAA Paper 90-2142, 1990.
5. Conner, K.J.; and Childs, D.W.: Brush Seal Rotordynamic Damping Characteristics. AIAA Paper 90-2139, 1990.
6. Hendricks, R.C., et al.: A Bulk Flow Model of a Brush Seal System. ASME Paper 91-GT-325, 1991.
7. Hendricks, R.C., et al.: Some Preliminary Results of Brush Seal/Rotor Interference Effects on Leakage at Zero and Low RPM Using a Tapered-Plug Rotor. AIAA Paper 91-3390, 1991. (Also NASA TM-104396, 1991.)
8. Chupp, R.; and Dowler, C.: Flow Coefficient for Brush Seals. Presented at the 28th Joint Propulsion Conference, Nashville, TN, July 6-8, 1992.
9. Hendricks, R.C., et al.: Brush Seals in Vehicle Tribology. Presented at the 13th Leeds-Lyon Symposium on Tribology, Leeds, England, 1990.
10. Gorelov, G.M., et al.: An Experimental Study of the Rate Characteristics of Brush Seals in Comparison With Labyrinth Seals. Aviats. Tekh., no. 4, 1988, pp. 43-46.
11. Braun, M.J.; Hendricks, R.C.; and Canacci, V.A.: Non-Intrusive Qualitative and Quantitative Flow Characterization and Bulk Flow Model for Brush Seals. Proceedings of Japan International Tribology Conference, ASME, New York, 1990, pp. 1611-1616.
12. Braun, M.J.; Hendricks, R.C.; and Canacci, V.A.: Flow Visualization in a Simulated Brush Seal. ASME Paper 90-GT-217, 1990.
13. Braun, M.J.; Hendricks, R.C.; and Canacci, V.A.: Flow Visualization and Quantitative Velocity and Pressure Measurements in Simulated Single and Double Brush Seals. STLE Tribol. Trans., vol. 34, Jan. 1991, pp. 70-80.
14. Braun, M.; Canacci, V.A.; and Hendricks, R.C.: Flow Visualization and Motion Analysis for a Series of Four Sequential Brush Seals. AIAA Paper 90-2482, 1990.
15. Mullen, R.L.; Braun, M.J.; and Hendricks, R.C.: Numerical Modeling of Flows in Simulated Brush Seal Configurations. AIAA Paper 90-2141, 1990.
16. Hendricks, R.C., et al.: Investigation of Flows in Bristle and Fiberglas Brush Seal Configurations. ISROMAC-4: The Fourth International Symposium of Transport Phenomena and Dynamics of Rotating Machinery, Hemisphere Publ., New York, 1992, pp. 315-325.
17. Carlile, J.A.; Hendricks, R.C.; and Yoder, D.A.: Brush Seal Leakage Performance With Gaseous Working Fluids at Static and Low Rotor Speed Conditions. NASA TM-105400, 1992.
18. Braun, M.J.; Hendricks, R.C.; and Yang, Y.: Effects of Brush Seal Morphology on Leakage and Pressure Drops. AIAA Paper 91-2106, 1991.
19. Schlumberger, J.A.; Proctor, M.; and Hendricks, R.C.: Eccentricity Effects on Leakage of a Brush Seal at Low Surface Speeds. NASA TM-105141, 1991.
20. Hendricks, R.C.; Carlile, J.A.; and Liang, A.D.: Some Sealing Concepts - A Review. Part A: Industrial, Proposed and Dynamic; Part B: Brush Seal Systems. ISROMAC-4: The Fourth International Symposium of Transport Phenomena and Dynamics of Rotating Machinery, Hemisphere Publ., New York, 1992, pp. 247-277.

TABLE I.—DIAMETRAL CHANGES AND TEST CYCLE TIMES FOR 38.1-mm (1.5-in.) DIAMETER BRUSH SEAL

[Seal fence inside diameter, 1.543±0.0005 in.]

	Position				Average
	Vertical	Horizontal	Vertical	Horizontal	
	Rotation, deg				
	0		45		
	Brush diameter (from optical comparator inspection), in.				
Before test 1	1.494	1.4918	1.4926	1.4945	1.4932
After test 1[a]	1.497	1.496	1.495	1.495	1.4958
Change, in.	0.003	0.0042	0.0024	0.0005	0.00255
Before test 2	1.495	1.495	1.497	1.496	1.4958
After test 2[b]	1.5058	1.5061	1.5041	1.5037	1.5049
Change, in.	0.0108	0.0111	0.0071	0.0077	0.00918
Before test 3	1.5058	1.5061	1.5041	1.5037	1.5049
After test 3[c]	1.504	1.514	1.512	1.5064	1.5091
Change, in.	−0.0018	0.0079	0.0079	0.0027	0.00418

[a]Total test time, 70.3 hr.

[b]Total test time, 43 hr.

[c]Total test time, 109 hr.

TABLE II.—ADDITIONAL TEST AND GEOMETRY INFORMATION

[Seal fence inside diameter, 1.543±0.0005 in. Dimensions are in inches.]

(a) 40-Tooth rotor

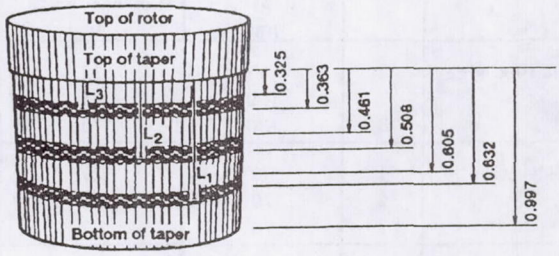

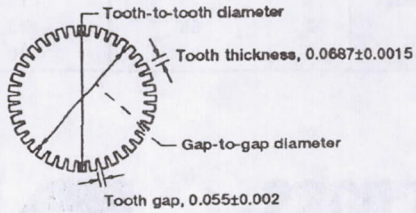

Position	Tooth-to-tooth diameter	Gap-to-gap diamter
Top of rotor	1.523±0.0005	1.485±0.0005
Bottom of rotor	1.491±0.003	1.483±0.003

Test case	Top-of-brush wear surface	Bottom-of-brush wear surface	Average
1	0.605	0.632	0.618
2	.461	.508	.484
3	.325	.303	.344

(b) Smooth rotor

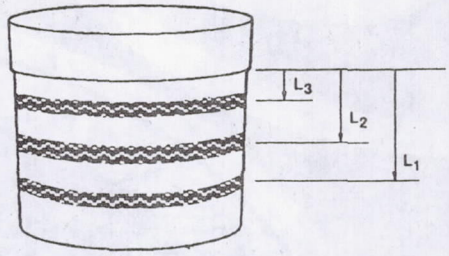

Test case	L[a]	Smooth-rotor diameter	Free brush diameter	Concentric radial clearance	Static eccentricity
Before test 1	L1	1.4992	1.4932	−0.0030	0
After test 1		1.4992	1.4958	−.0017	0
Before test 2	L2	1.5046	1.4958	−0.0044	0
After test 2		1.5046	1.5049	.0001	0
Before test 3	L3	1.5105	1.5049	−0.0028	0.013
After test 3		1.5105	1.5091	−.007	.013

[a]Corresponds to equivalent axial positions of 40-tooth rotor.

TABLE III.—PROFILOMETER RESULTS FOR 40-TOOTH ROTOR, TESTS 1, 2, AND 3

Location	Test	Peak groove depth, μm	Estimated average depth, μm	Wear area, μm^2
Leading edge	1	57	22	24 910
	2	130	95	141 680
	3	130	70	114 370
Midsection	1	30	17	7 652
	2	70	35	37 106
	3	70	27	56 493
Trailing edge	1	25	12	6 610
	2	65	35	48 649
	3	67	30	56 169

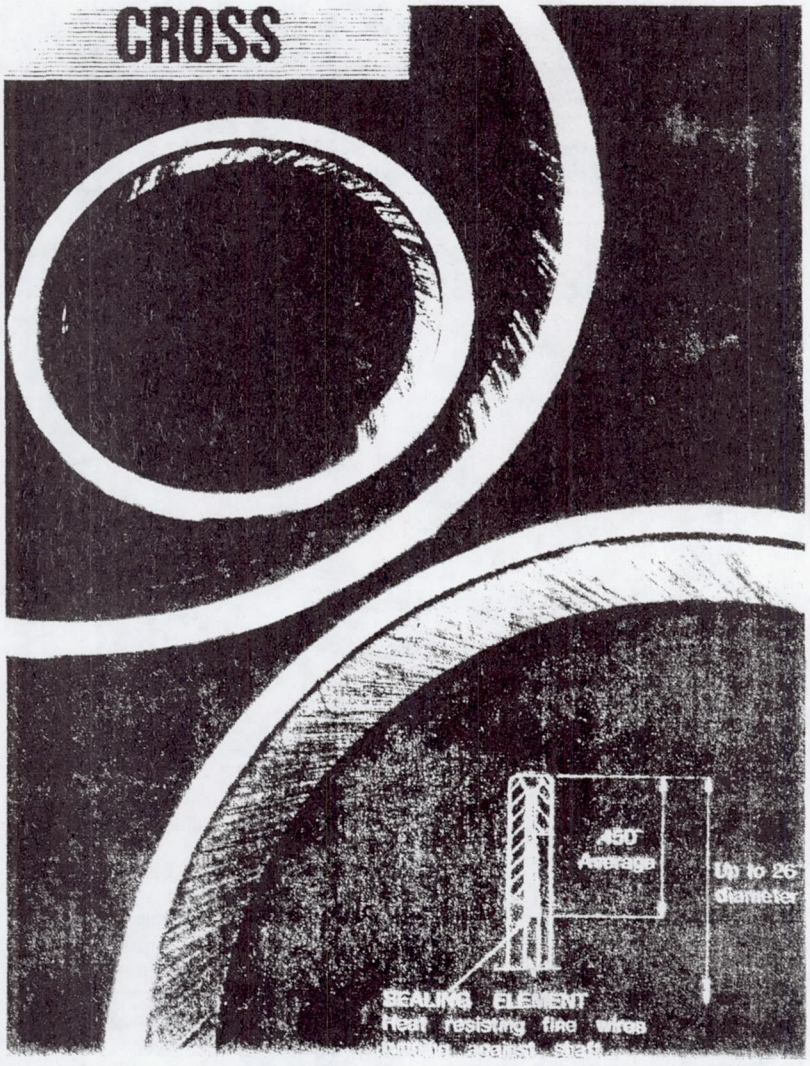

Figure 1.—Circular brush seal. (Courtesy of Cross Mfg. Ltd.)

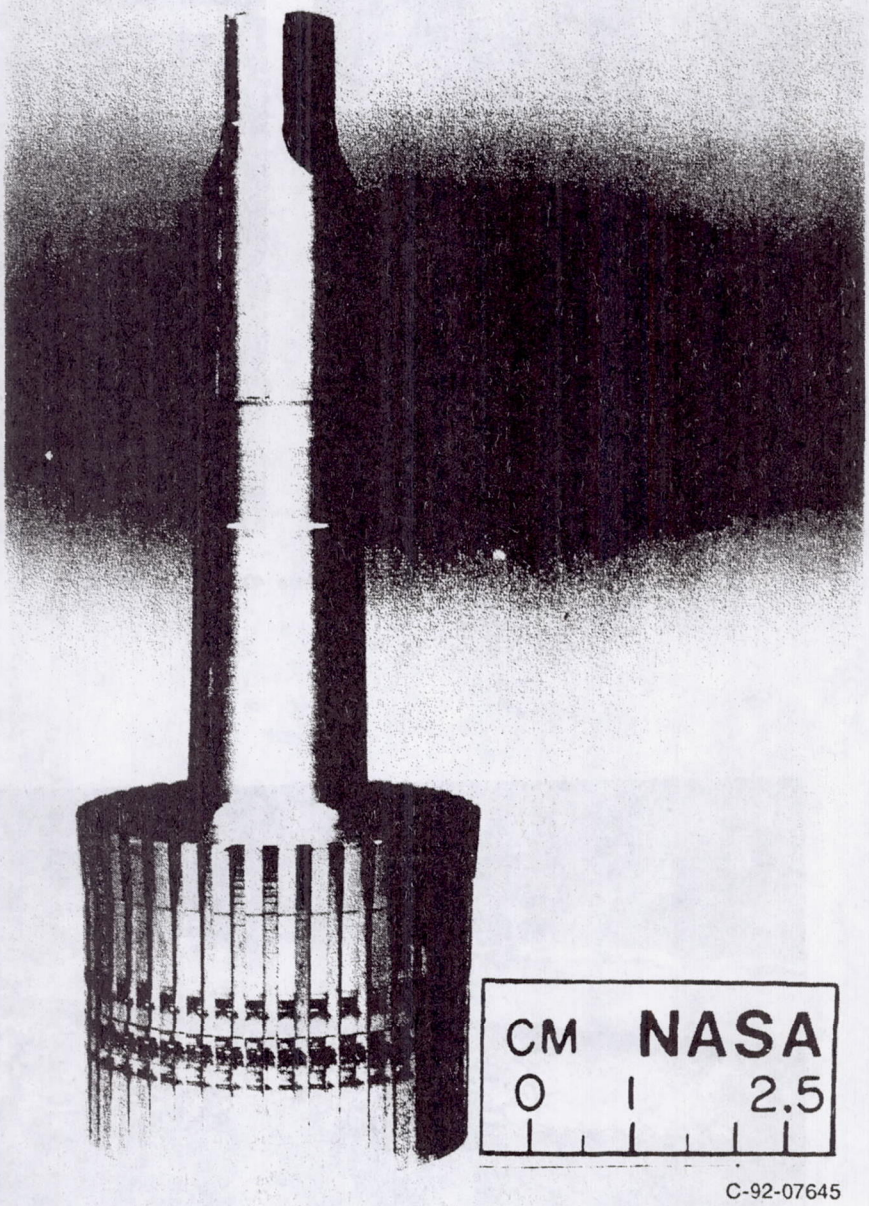

Figure 2.—Geometry of tapered, 40-tooth rotor.

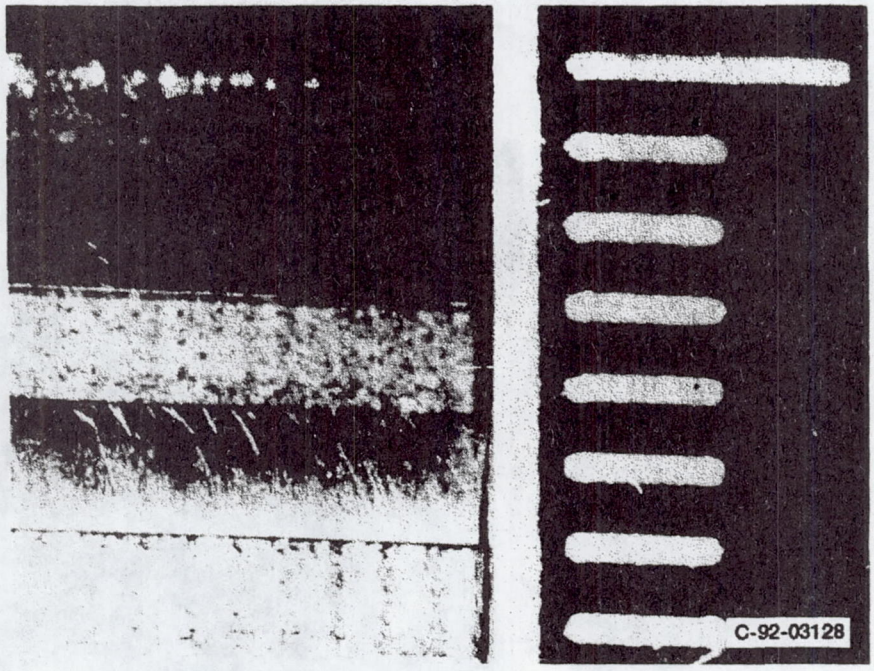

Figure 3.—Rotor prior to tests (40 lands).

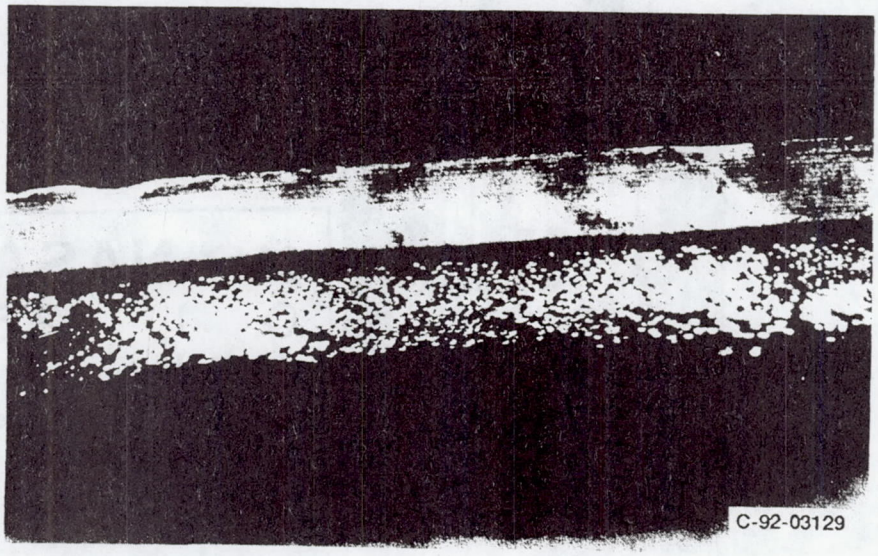

Figure 4.—Brush seal prior to tests (270° mark).

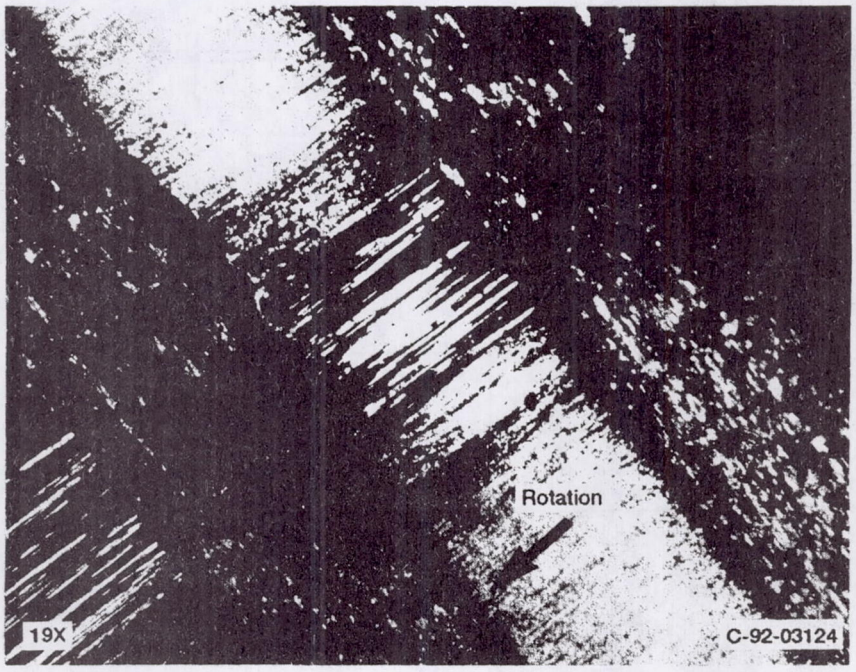

Figure 5.—Rotor surface after test 1. (Arrow shows direction of rotation.)

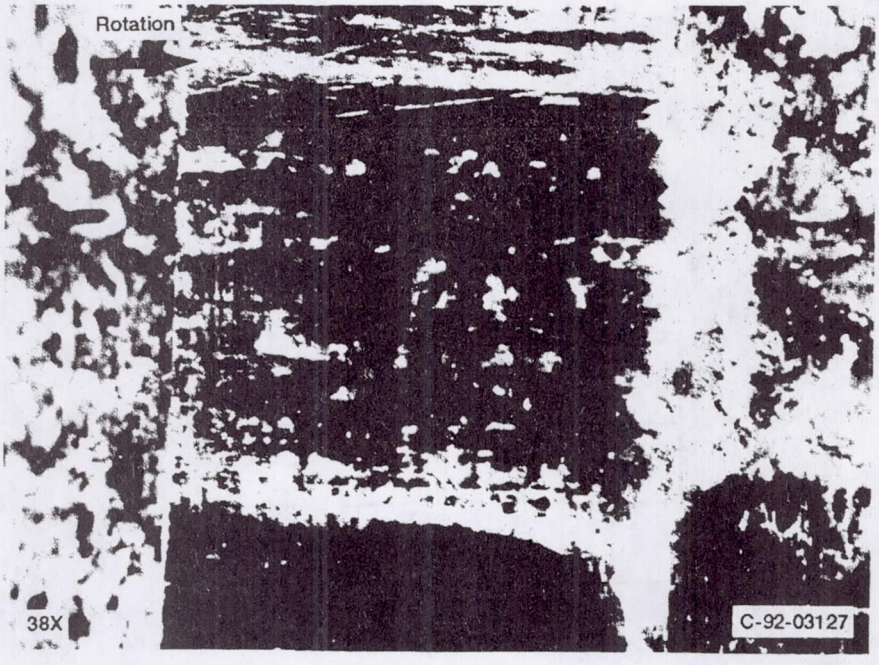

Figure 6.—Rotor land and groove after test 1.

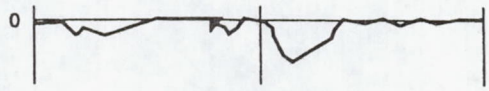

(c) Trailing edge.

(b) Midsection.

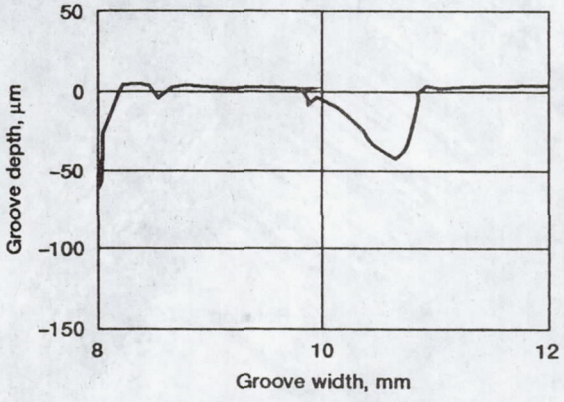

(a) Leading edge.

Figure 7.—Profilometer traces for 40-tooth rotor (test 1).

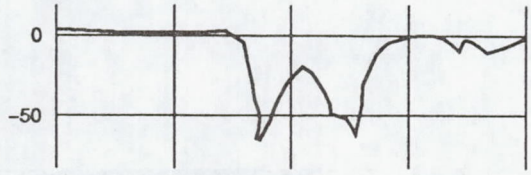

(c) Trailing edge.

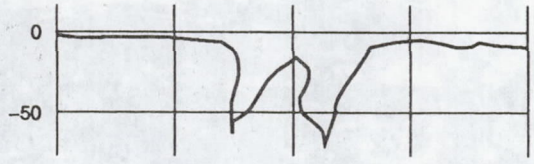

(b) Midsection.

(a) Leading edge.

Figure 8.—Profilometer traces for 40-tooth rotor (test 2).

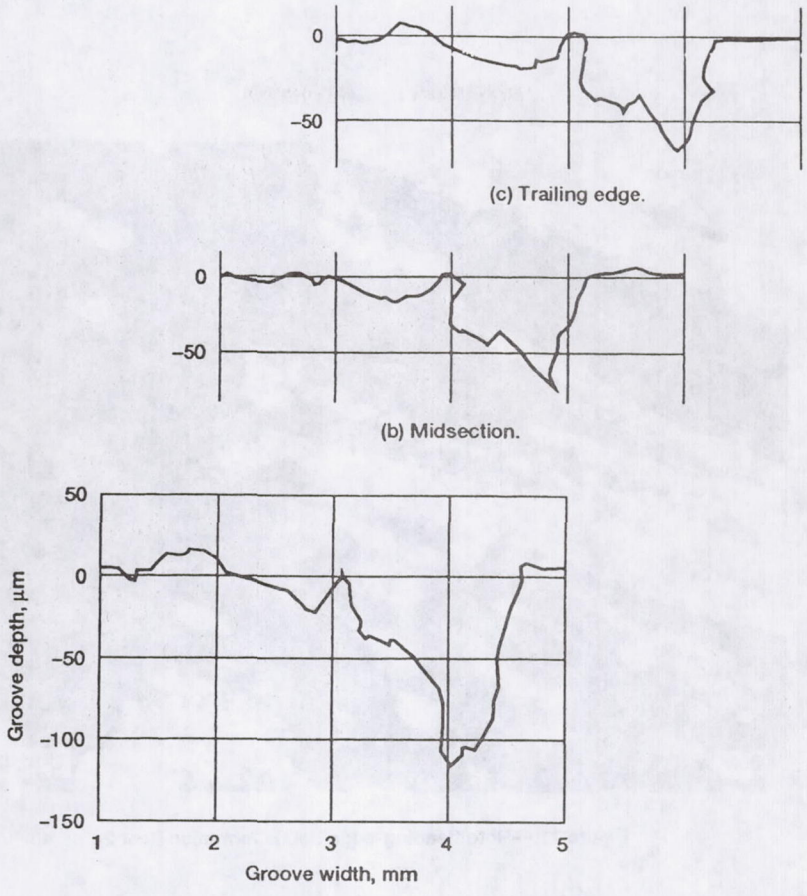

Figure 9.—Profilometer traces for 40-tooth rotor (test 3).

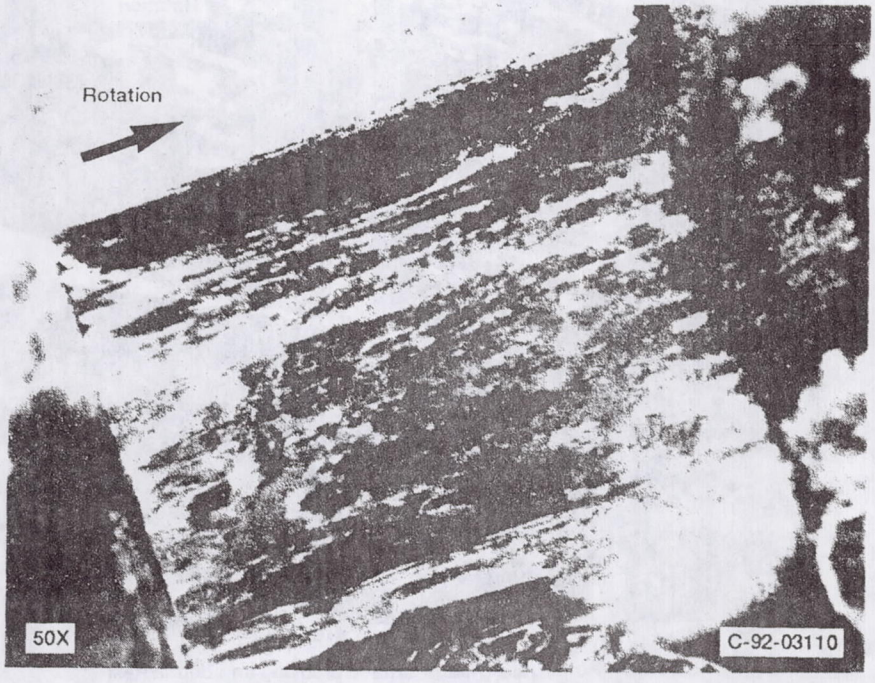

Figure 10.—Rotor land with debris and rub scars (test 2).

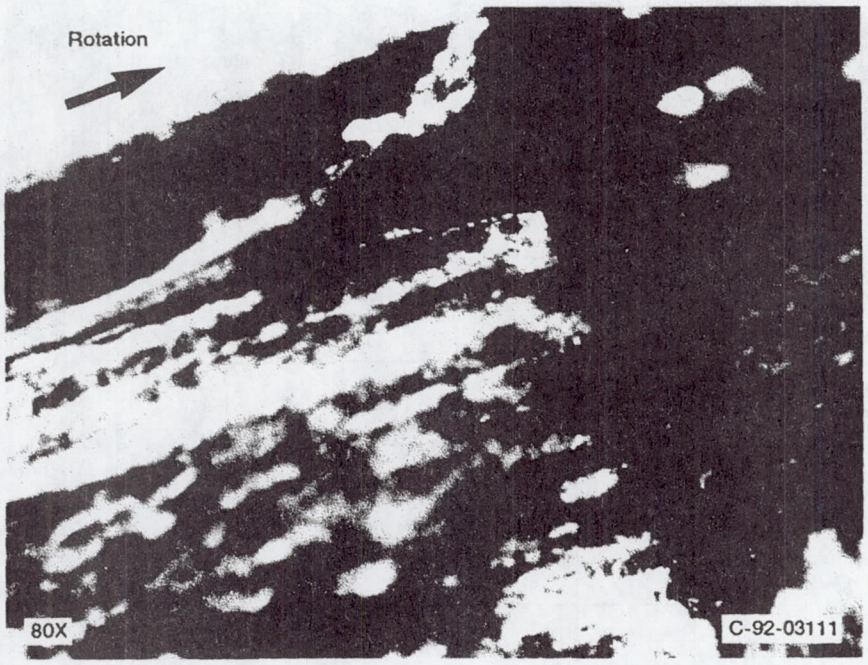

Figure 11.—Rotor leading-edge debris formation (test 2).

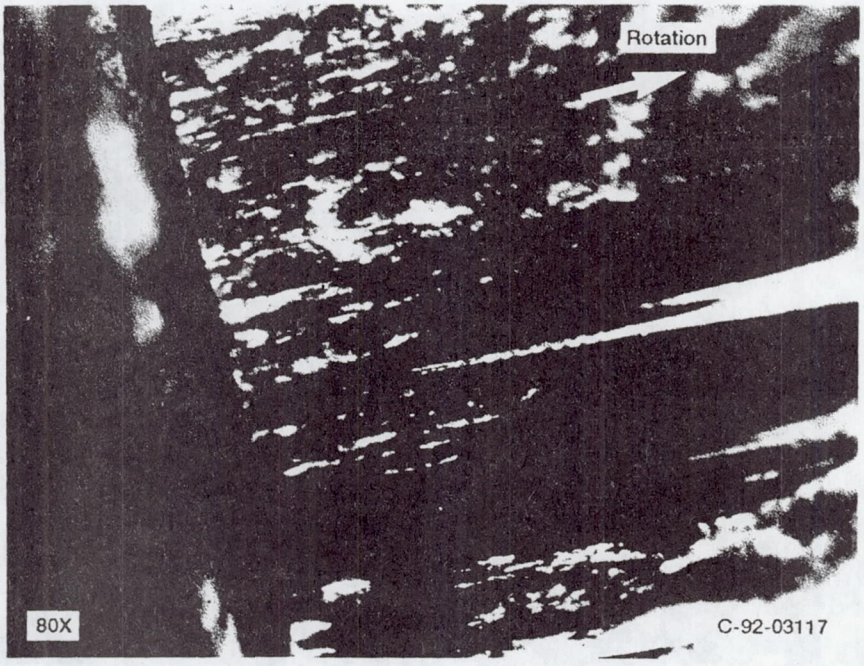

Figure 12.—Rotor trailing-edge surface grooving and debris (test 3).

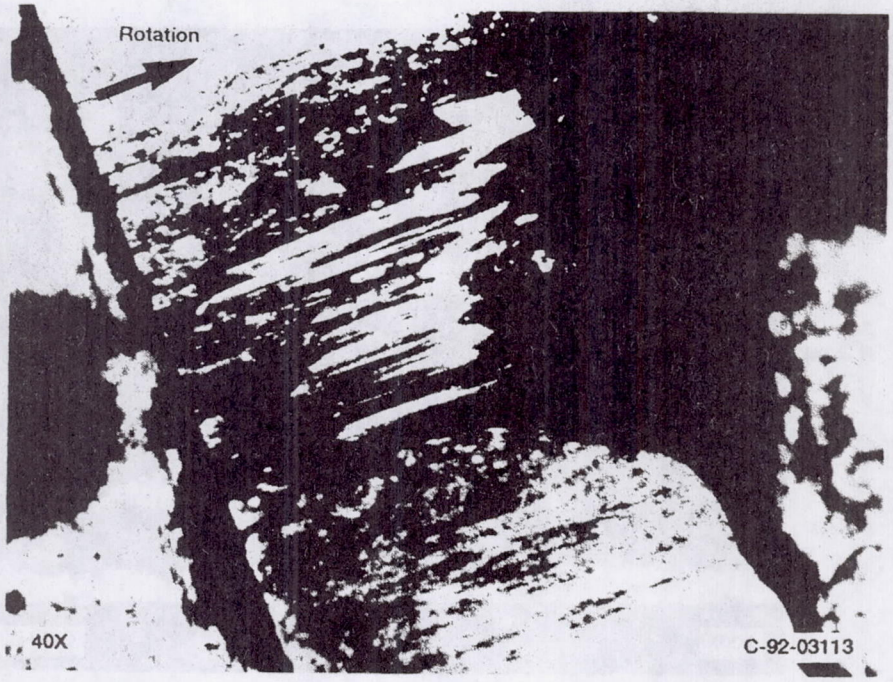

Figure 13.—Rotor leading edge, surface machining, and hot spots (test 3).

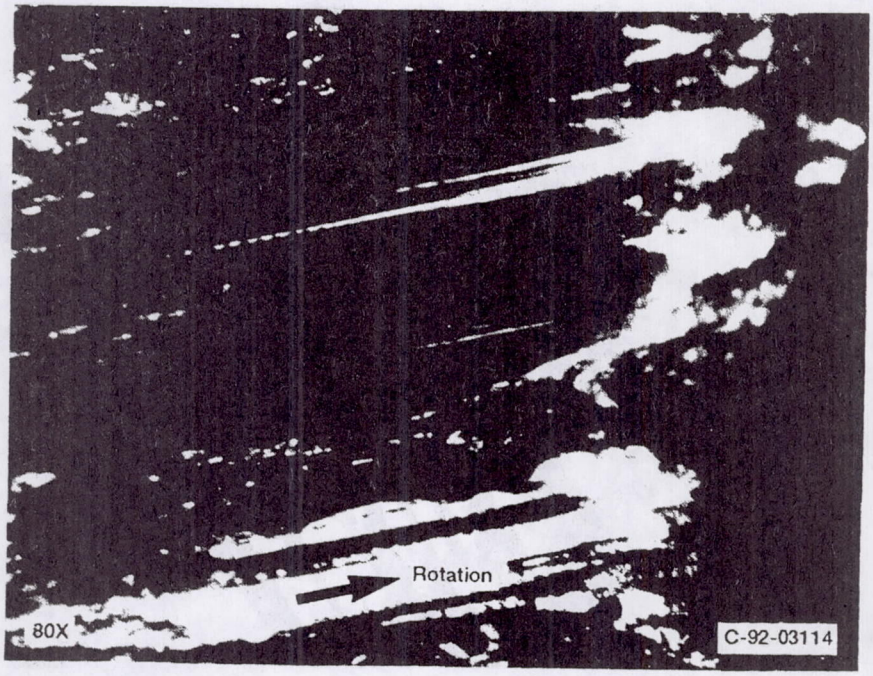

Figure 14.—Rotor land hot streaks, hot spots, and surface machining (test 3).

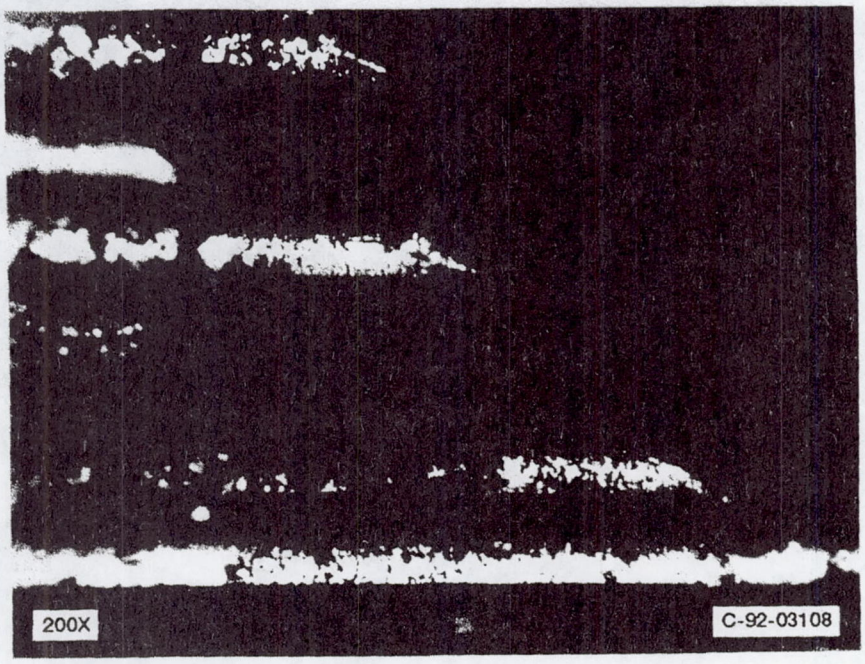

Figure 15.—Brush bristle tips with debris (test 1).

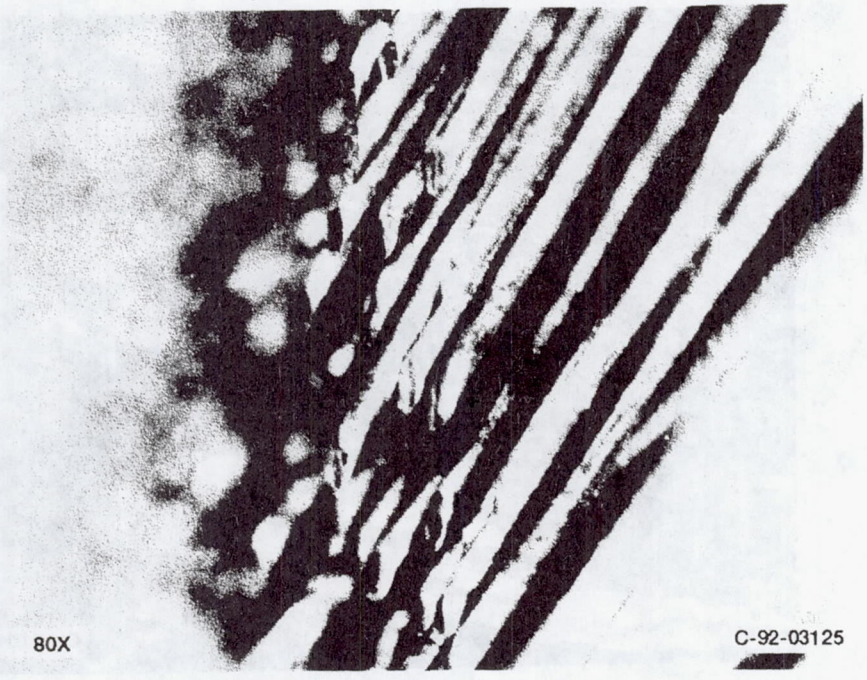

Figure 16.—Brush bristle tip wear patterns (test 2).

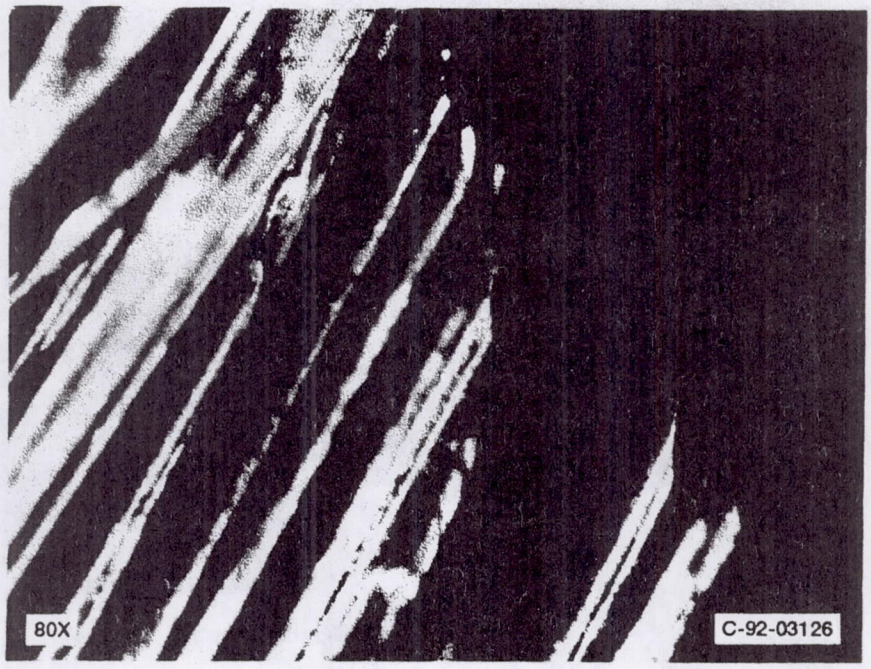

Figure 17.—Brush bristle tips and damage (test 1).

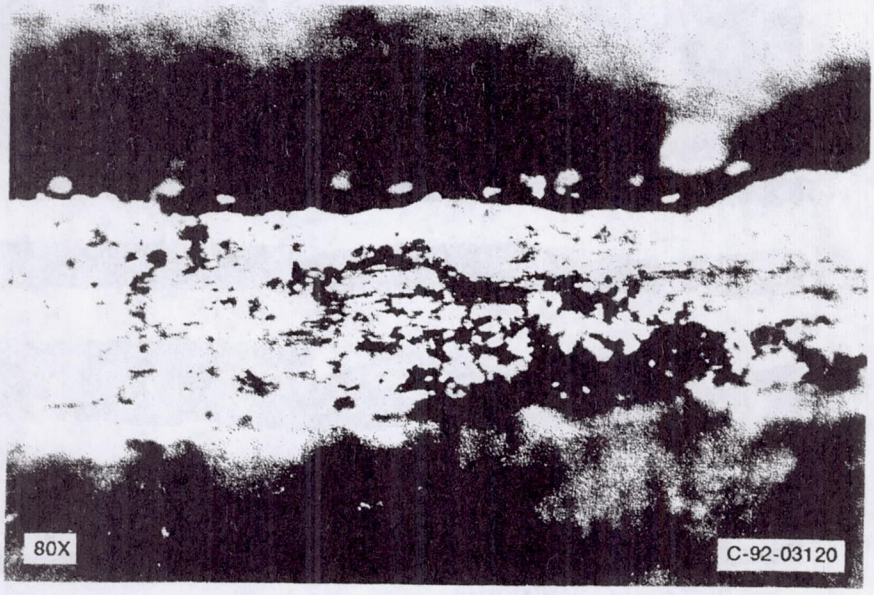

Figure 18.—Rotor trailing edge (test 3).

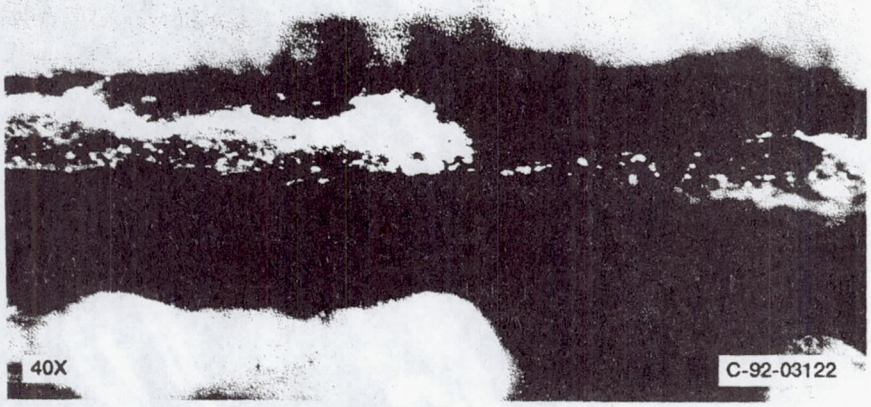

Figure 19.—Rotor leading edge (test 2).

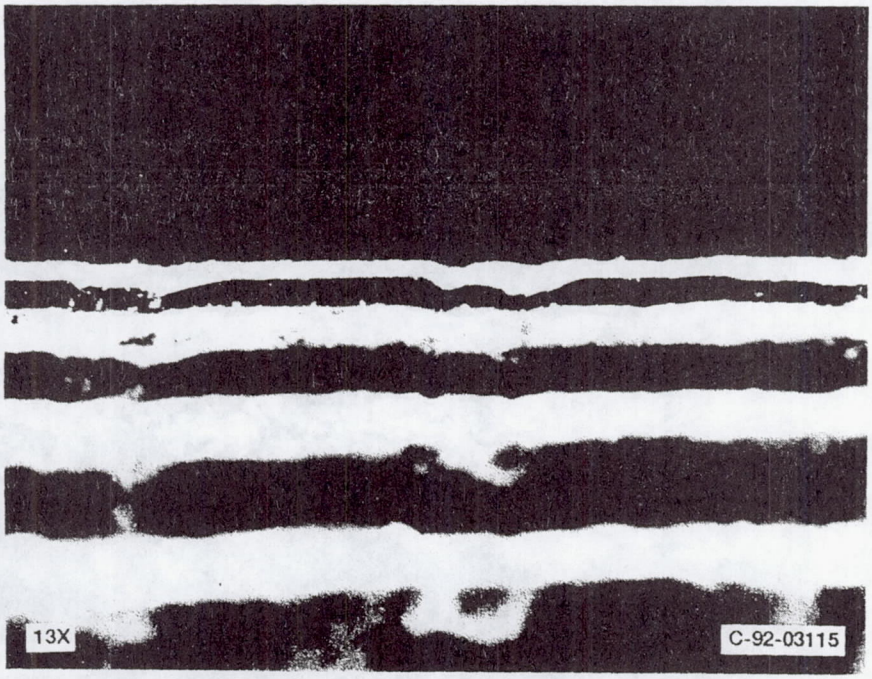

Figure 20.—Rotor trailing edge (tests 1, 2, and 3).

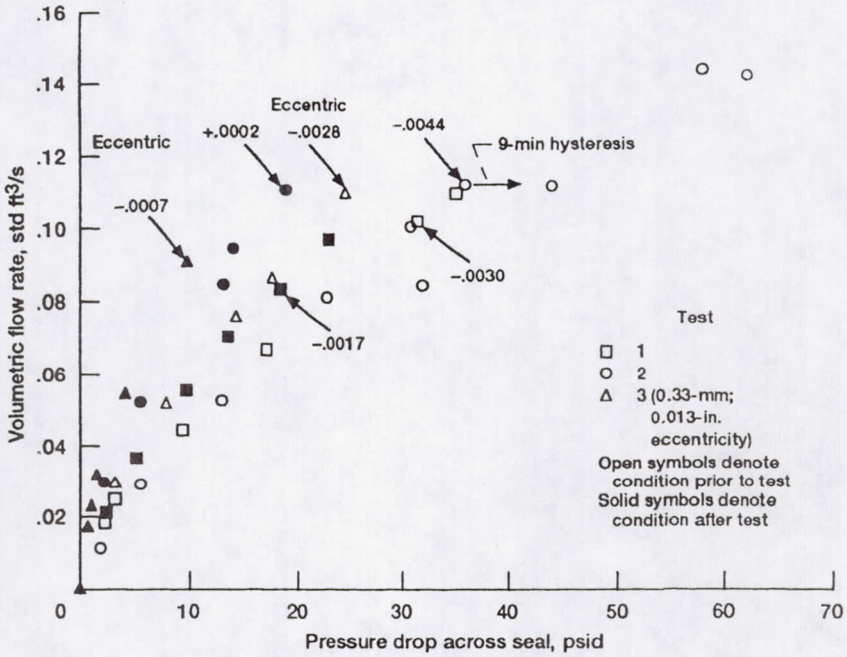

Figure 21.—Pre- and posttest leakage results for smooth rotor.

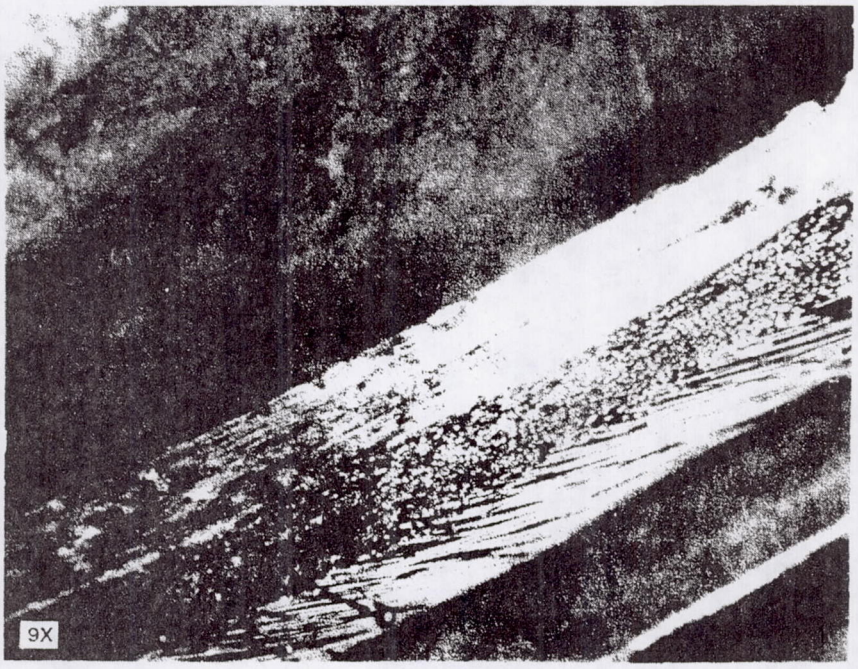

Figure 22.—Fence damage sustained during test 3.

INTEGRITY TESTING OF BRUSH SEAL IN A T-700 ENGINE

Robert C. Hendricks, Thomas A. Griffin, George A. Bobula, and Robert C. Bill
National Aeronautics and Space Administration
Lewis Research Center
Cleveland, Ohio, 44135

Harold W. Howe
Technetics Corporation
Deland, Florida

SUMMARY

A split-ring brush seal was fabricated, installed between two labyrinth-honeycomb shroud seals, and tested in the fourth-stage turbine of a T-700 engine. The annealed Haynes 25 bristles rubbed directly against the nonconditioned, irregular René 80 turbine blade shroud surface. A total of 21 hr of cyclic and steady-state data were taken with surface speeds to 335 m/s (1100 ft/s) and shroud temperatures to 620 °C (1150 °F). Wear appeared to be rapid initially, with an orange flash of hot brush fragments during the first engine startup, to minimal after 10 hr of operation. The brush survived the testing but experienced some bristle pullouts and severe bristle wear; some turbine interface wear and possible material transfer was noted. Future design concerns center on tribological behavior at the interface with or without lubricants.

INTRODUCTION

Engine testing of brush seals has been reported (e.g., Rolls Royce (ref. 1) and Allison (ref. 2)) that demonstrated performance increases relative to labyrinth seals. These brush seal systems had smooth rotor interfaces (<25 rms) and operated at moderate temperatures and surface speeds. Even though these tests were successful, concern over catastrophic failure of the brush, such as a loss of bristles when subjected to high surface speeds at elevated temperatures, has not been resolved.

The objectives of this program were first to demonstrate that a well-designed and manufactured brush seal could survive the "pounding" of an irregular rotor surface without catastrophic failure, second to illustrate the concept of running a combined brush and labyrinth seal system, and third to acquire metallographic data on bristles subjected to such an environment.

EXPERIMENTAL BRUSH CONFIGURATION AND INSTALLATION

A cross-sectional view of the split-ring brush seal configuration is illustrated in figure 1. A major problem in designing retrofit seals is consistency of hardware measurements, and for this experimental engine the seal was crafted to fit.

In order to fit into the existing T-700 engine fourth-stage turbine shroud, the design was required to fit into a radial clearance about half that normally used for brush seals. The 0.071-mm (0.0028-in.) diameter, Haynes 25 bristles were angled 43° to 50° to the interface with about 2500 per inch of circumference (98.4 per millimeter of circumference). The backing washer (or fence) was angled 19° to match the slope of the turbine shroud. The design clearance was −0.51 mm (−0.02 in.) but could range to −1.27 mm (−0.05 in.) diametral (the uncertainty reflecting that of the engine geometry) with an outside diameter of 333.9 mm (13.146 in.) and an inside diameter of 322.3 mm (12.690 in.).

Figure 2 shows several views of the split-ring brush seal, illustrating the joint and the restraining pin hole. Figure 3 shows the unusual brush cross section that was crafted to fit the turbine shroud between the two labyrinth-honeycomb seals. Figure 4 shows a closeup view of the installed brush; and figure 5, an overall view of the installed brush. Figure 6(a) shows the pressure tap locations in one of the shrouds. A thermocouple was installed in each shroud (fig. 6(b)); three of the four were functional. Figures 6(c) and (d) show views of the shroud ring and instrumentation lines.

Assembly of the turbine with the shroud required forcing the brush past the upstream labyrinth tooth without any visual or instrumented guidelines; see figure 7 (power turbine). Forcing the brush over the labyrinth tooth spread the bristles axially into the upstream direction. This type of spreading alters the bristle packing configuration, but the extent of alteration and the degree of spreading are unknown. Post-test results indicated that perhaps two to three upstream bristle rows remained spread with possibly one downstream bristle row in disarray. Still the brush was resilient because the remaining rows appeared to be in position. The flexibility of a brush seal and the abuse it can withstand appear to be significant.

With the brush installed, the turbine shaft was difficult to rotate, requiring 14.7 N-m (130 in.-lbf) of torque. This was a major concern because heat generation could be sufficient to melt the materials at the interface. The geared tooth rotor results (ref. 3), including material smearing, cutting, and local hot spots, indicate that high heat loads and temperatures could be present but would be confined to the interface, with the lowest heat-sinking element (the bristles) absorbing the energy. Therefore, the bristles would fail, but the effects on the power turbine should be benign.

ENGINE OPERATIONS

The T-700 turbine section was assembled and the brush seal test was "piggybacked" on the break-in of the engine. Operations consisted of the standard break-in procedures with data taken under both steady and cyclic conditions. The engine was operated a total of 21 hr, including break-in, steady state, and 10 hr of cycling between ground and flight idle (4-min ground idle and 5-min flight idle). Turbine speeds were 10 000 and 20 000 rpm, and average fourth-stage turbine shroud temperatures were 455 and 566 °C (850 and 1050 °F), respectively. Maximum shroud temperatures were limited to 621 °C (1150 °F). The turbine inlet temperatures were about 139 deg C (250 deg F) higher. The pressure drop measurements across the brush were up to 0.007 MPa (1 psia) and varied from shroud to shroud. An assessment of the effect of the brush seal on engine performance was inconclusive and remains to be investigated further. Neither radial nor axial positions of the rotor were monitored, but such position sensors should be an integral part of the engine dynamics.

Because of concern over the 14.7 N-m (130-in.-lbf) installed torque that was required to rotate the power turbine shaft, after about 10 hr of engine operations the compressor and the power turbine were decoupled. The turbine shaft turned freely but not in reverse. The turbine assembly has 50 shrouded blades with irregularities (radial, to 0.229 mm (0.009 in.); circumferential, to 0.076 mm (0.003 in.); and axial, to 0.051 mm (0.002 in.)) representing protrusions into the brush and the spaces between the blade pairs. It is not known how many cycles were required to "free the bristles," but at 10 000 rpm and with 24 irregular asperities impacting each bristle (4000 impacts/s at a surface speed of 168 m/s (550 ft/s)) it is assumed that brush break-in was rapid. The annealed Haynes 25 bristles rubbed against hardened René 80 blades and probably wore rapidly during the initial stages of engine break-in.

Furthermore, and of significance to engine designers, a flash was noted upon initial engine ignition that was concluded to be expulsion of brush fragments. This is important because critical components

must be protected against initially high levels of debris generation. Analysis of these and other fragments showed severe oxidation with some degree of stiffness remaining. These fragments are not passive debris; they can cause damage to critical components. The only debris noted in the gear-tooth rotor study (ref. 3) was a "lubricant powder." Thus, surface speed, rotor roughness, and brush construction play a major role in determining the spectrum of debris generation.

RESULTS AND DISCUSSION

In any potentially destructive situation one attempts to preserve the critical components. Brush bristle wear would degrade performance, but failure of the turbine or a shaft (depending on seal location) could result in engine loss, perhaps catastrophic. So the brush seal becomes the sacrificial component, not only in this case but when running against a coated shaft. The brush seal would then be replaced at discrete intervals, such as during overhauls.

For these tests the brush rubbed the turbine blade shroud asperities smooth and did provide a distinct wear track, perhaps through transfer of material. However, no direct damage was ascribed to the turbine blade shrouds. The engine was immediately returned to service.

Before proceeding to discuss post-test results, we return to the installation of the brush into the power turbine shroud. Figures 4, 5, and 7 show views of the installed brush seal. The brush was designed for an interference of 0.51 mm (0.020 in.) diametral. The actual interference could not be determined, but estimates of the pretest brush clearance were −0.51 to −1.27 mm (−0.02 to −0.05 in.) diametral. Measurements of the shrouds differed as did those for the rotor. Although the differences were only a few thousands of an inch (mils), they represented a significant percentage of the clearance gap. It was also determined that individual blade sets could have a step change of 0.229 mm (0.009 in.) from one blade set to the next. These surface irregularities are shown in the post-test photograph (fig. 8).

Upon initial engine startup, an orange burst was noted and was assumed to be expelled brush bristles (i.e., those that were inadequately attached, were pulled out by rotor irregularities, or were embedded within the blade row gaps during the blind installation and "snapped" or "yanked" or "bent" aside during engine break-in). Residual bristles from the exhaust were photographed (fig. 9). Although they appeared to be highly oxidized and stressed, they were curly and still wirey. The number of residual bristles decreased with operation until none were noted. It is assumed that at this time the bristles and the rotor were in nearly line-to-line contact (i.e., rubbed in). Precooling the bristles during the initial rub-in may mitigate bristle loss and the orange burst.

Turbine speeds to 20 000 rpm and shroud temperatures to 620 °C (1150 °F) were commonplace. These conditions provided an interface speed of 335 m/s (1100 ft/s) or a temperature-velocity (TV) product of over $(1100)^2$ with the global target of about $(1500)^2$ (in U.S. customary units, feet per second per degree F).

Further assessment of figure 8 shows that the leading edges of the blade sets were polished. Some brush wear was noted and expected because René 80 is hard relative to the annealed Haynes 25 and the heat-sinking capacity of the brush is very small relative to that of the rotating blade sets. The surface irregularities at the rubbing interface can be seen. Although there was some evidence of material transfer, no metallurgical samplings or rotor measurements were taken because of the tight program schedules for the engine operations. This was a major error; however, if there comes a time when the rotor can be

looked at, some of the transferred materials may be found still embedded in the rotor even after it has undergone other program tests for General Electric Co.

Figure 10 illustrates bristle spreading after testing, with a central core of bristles rubbed (probably clip cut and worn to shape). Although the environment was hostile, the brush did not disintegrate, but bristle pullout could be noted in a few places. Some upstream bristles (two or three rows) show spreading and perhaps one row downstream (toward the exhaust). The remainder of the bristles show wear (or cutting plus wear). Detailed estimates of the bristle stubble heights are given in figure 11(a) as taken from the set of photographs in figure 11(b) corresponding to positions (joint, J+1, J+1.5, J+2, J+2.5, J+3, J+3.5, J+4, and J+4.5) shown in figure 11(a). The last two photographs in figure 11(b) correspond to the minimum stubble height, where the rotor actually rubbed the fence (position J+3); the view is looking toward the bristle stubbles to show the rubbed fence. Figure 11(c) shows wear track and fence rub, and figure 11(d) shows the joint wear track.

The following measured diametral parameters in millimeters (inches) were used to establish seal clearances:

Pretest brush diameter (no taper)	321.79 (12.669)
Post-test brush diameter (tapered)	324.15 (12.762)
Differential	2.36 (0.093)
Pretest rub interface diameter	322.30 to 322.81 (12.689 to 12.709)
Brush pretest interference	0.51 to 1.27 (0.02 to 0.04)
Labyrinth cold clearance	2.29 to 2.46 (0.09 to 0.097)
Bright region diameter (fig. 8(a))	323.42 (12.733)
Differential	0.74 (0.029)
Stubble height (fig. 11(a))	0.71 (0.028)
Possible material transfer	0.25 to 0.5 (0.01 to 0.02)
Possible engine eccentricity	0 to 0.8 (0 to 0.03)
Blade shroud height variation	0 to 0.23 (0 to 0.009)

The average diametral clearance estimates in millimeters (inches) are as follows:

Pretest brush clearance	−0.51 to −1.3 (−0.02 to −0.04)
Post-test brush clearance	0 to 0.8 (0 to 0.03)
Post-test labyrinth clearance	2.3 to 2.5 (0.09 to 0.10)

The engine parameters are as follows:

Turbine speeds to 20 000 rpm, m/s (ft/s)	335 (1100)
Maximum turbine shroud temperatures, °C (°F)	620 (1150)
Temperature-velocity product (approximate; in U.S. customary units ft/s-°F; future target, $(1500)^2$)	$(1100)^2$

Details of the bristles (fig. 12) show an ingrained wear pattern that is characteristic of a high spot in the rotor which cuts a shallow groove as it wears in. Furthermore, the rotor ran eccentric with respect to the seal either during cycling or steady state or both. Plots of bristle measurements show rubbing of the seal ring at 180° to the pinned point and a step across the joint where the end of the split seal rubbed the rotor.

The blind installation and operation made it difficult to assess intermediate states of wear or the health of the brush or the turbine shroud/brush interface. Although accelerometer measurements were in bounds, no detailed information concerning the orbital dynamics was available.

Metallographic results (fig. 13) illustrate some material migration along the bristle and material transfer both from and to the surface. Material smears seem to be in line with a softer material rubbing a harder material even to the point of melting. Thus, one would conclude that the interface became very hot, but the interface followed the classic Block slider problem, where the penetration depth (radial) is very small. Thus, the thermal effect at the interface appeared to be topical, wearing the brush bristles until line contact with the rotor and smear transfer of both materials occurred. Such evidence is presented in figure 14, for an individual bristle that was clipped from the brush. The clipped end was removed from the interface, and the worn end is representative of interface materials. There are material smears, oxidized spots, and apparent pits. It is not clear how the irregularities of the interface affected these results, but it is clear that materials were transferred.

Metallographic analysis of the sectioned brush will be completed and reported later.

Derby and England (ref. 4) reported excellent brush bristle and coating wear for Alloy A (Ni-Cr-Al-base superalloy solid-solution strengthened) bristles and Triboglide coating. Alloy A is being used in gas turbine hot spots and develops a tenacious Cr_2O_3 and Al_2O_3, yittria-modified oxide layer. Triboglide is a chromium carbide (CrC) containing additives of 12 wt% barium and calcium fluoride solid lubricants. Triboglide is based on the work of Harold Sliney at NASA Lewis but has no silver additive. The tests were performed with 1200 °F air.

Atkinson and Bristol (ref. 5) report better wear for a cobalt alloy rubbing against chromium carbide at room temperature, but their high-temperature (480 °C) result shows nearly equivalent wear for either the cobalt- or the nickel-base alloy. However, the Co-alloy/CrC combination had less leakage under dynamic conditions and better wear at room temperature. The tests were conducted to simulate a CT7-9 compressor discharge seal. The brush was 129 mm in diameter and of standard Cross Mfg. construction.

It is apparent that the composition of both the coating and the bristles needs to be characterized with respect to the working fluid, the operating conditions, and the component life requirements. The importance of surface conditions must be emphasized. Wear decreases after operation because the brush rubs a smoother surface and bristle wear decreases line loading.

Obviously, tribological pairing is important and references 4 and 5 present a good initial look into these problems. Limitations on speed, temperature, and preloading have to be established. Furthermore, limitations on surface asperities have to be established for expedient or commercial engines even though it has been demonstrated that direct bristle rubbing of a smooth shaft could be acceptable for expedient engines (ref. 6).

SUMMARY OF RESULTS AND CONCLUSIONS

A split-ring brush seal installed between two labyrinth-honeycomb shroud seals was tested in the fourth-stage turbine of a T-700 engine. The following results were obtained and conclusions drawn:

1. Properly designed brush seals have sufficient integrity to withstand highly irregular surface operations at surface speeds to 335 m/s (1100 ft/s) and shroud temperatures to 620 °C (1150 °F) with a non-centered turbine orbit during steady and cyclic loading.

2. Upon initial engine startup, bristle debris can be expected mostly in the form of fines and some larger elements. The nature and amount of debris should depend on the construction, the surface characteristics (e.g., asperities), the temperature and velocity of the interface, and the bristle preload. Critical components must be protected.

3. The post-test clearance was estimated to be line to line to 0.8 mm (0.03 in.), indicating a well-worn but still functional seal configuration. Accurate determinations of the rotor and stator dimensions along with dynamic displacement measurements are necessary for assessing bristle wear characteristics and seal clearances. A plot of bristle stubble height versus circumferential position revealed some characteristics of the rotor and engine operations.

4. Wear is expected to be initially rapid, then steady, and subsequently decreasing with time of engine operation. Cyclic operations cause more rapid wear of the bristle/rotor interface. Material transfer, smearing, and pitting of the interface are commonplace.

5. Installation torques can be high, but rub-in torques are low. Rotor reversals are not permitted.

6. Tribological pairing is important, and limitations on speed, temperature, preload, and asperities have yet to be established even though direct rubbing of a smooth shaft of an expedient engine appears plausible.

7. Although high installation torques (14.7 N-m; 130 in.-lbf) probably contributed to high bristle wear, the effects on the power turbine were benign even though heat generation and shear were sufficient to transfer materials at the interface. The René 80 is hard and has large heat capacity, and the Haynes 25 bristles are annealed and have small heat capacity. Therefore, the brush bristles failed first.

8. The pressure drop measurements across the brush seal were up to 0.007 MPa (1 psia), but the effect of the brush seal on engine performance was inconclusive and requires further assessment. Radial and axial rotor sensor position monitoring is recommended.

9. Metallographic studies of the brush and rotor are being completed.

REFERENCES

1. Ferguson, J.G.: Brushes as High Performance Gas Turbine Seals. ASME Paper 88-GT-182, 1988.

2. Holle, G.; and Krishnan, M.: Gas Turbine Engine Brush Seal Applications. AIAA Paper 90-2192, 1990.

3. Hendricks, R.C.; Carlile, J.A.; and Liang, A.D.: Brush Seal Bristle Flexure and Hard Rub Characteristics. Presented at the NASA Lewis Research Center Seals Workshop, Cleveland OH, Aug. 5-6, 1992.

4. Derby, J.; and England, R.: Tribopair Evaluations of Brush Seal Applications. AIAA Paper 92-3715, 1992.

5. Atkinson, E.; and Bristol, B.: Effects of Material Choices on Brush Seal Performance, Lubr. Eng., vol. 48, no. 9, Sept. 1992, pp. 740-746.

6. Chupp, R.; and Nelson, P.: Evaluation of Brush Seals for Limited Life Gas Turbine Engines. AIAA Paper 90-2140, 1990.

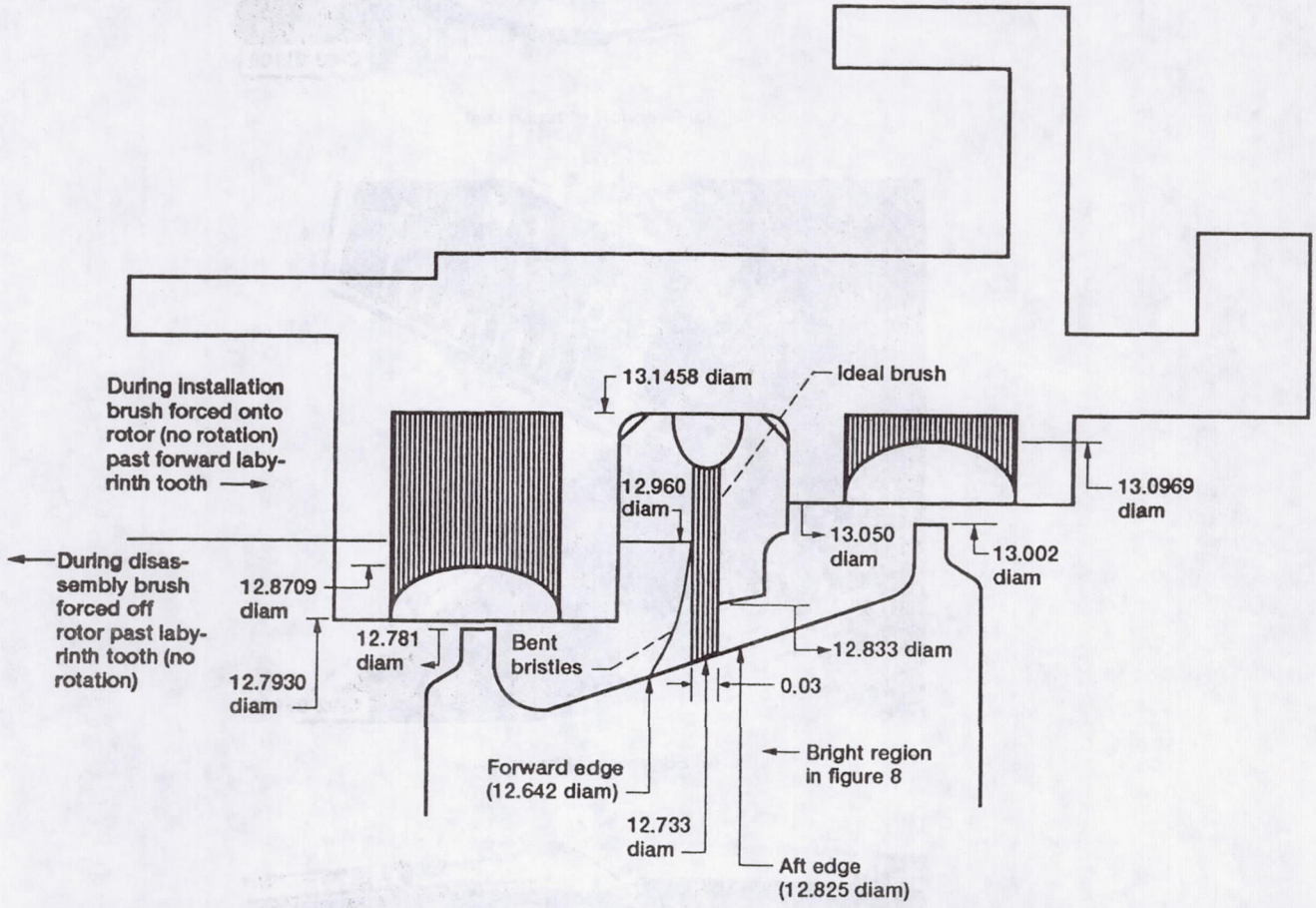

Figure 1.—Cross-sectional view of split-ring brush seal configuration. (Brush design with ~0.020 in. interference. Dimensions are in inches.)

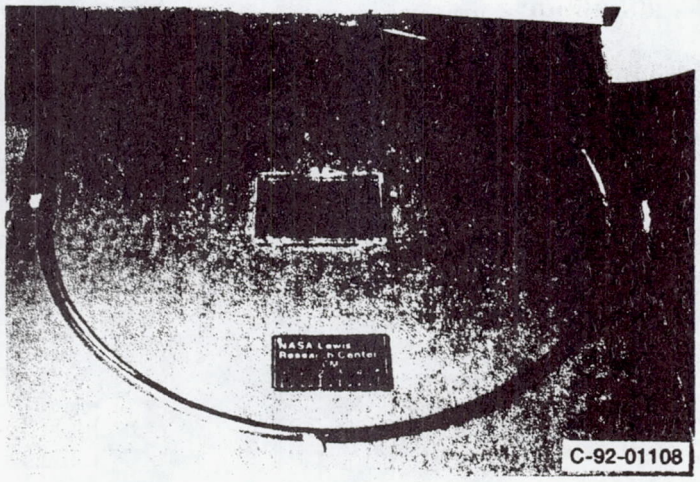

(a) Overview of brush seal.

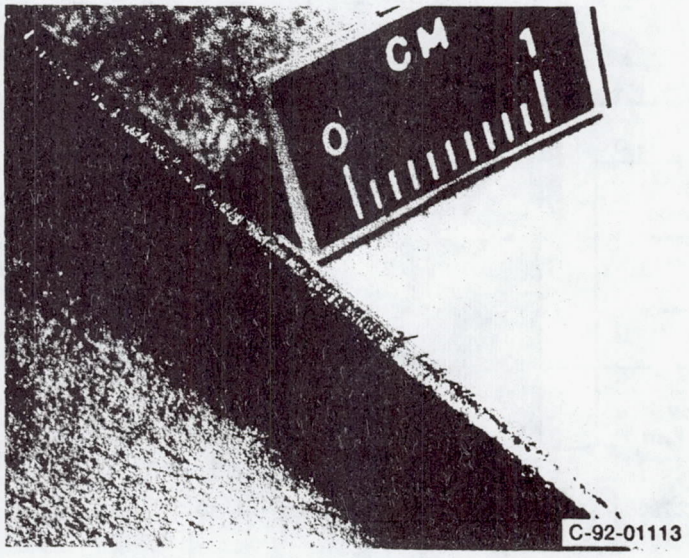

(b) Edge view of brush seal.

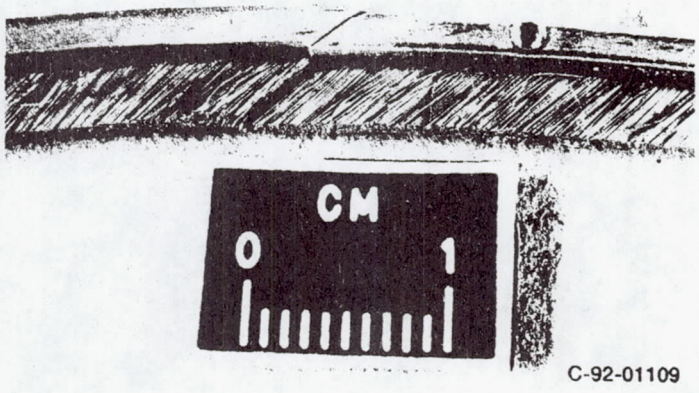

(c) Split end view.

Figure 2.—Split-ring brush seal.

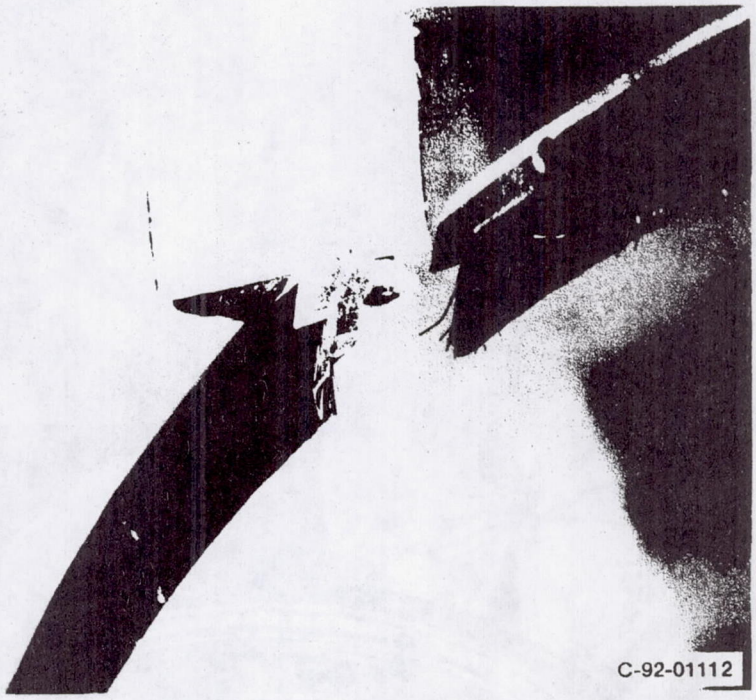

Figure 3.—Brush seal cross section crafted to fit turbine shroud between two labyrinth-honeycomb seals.

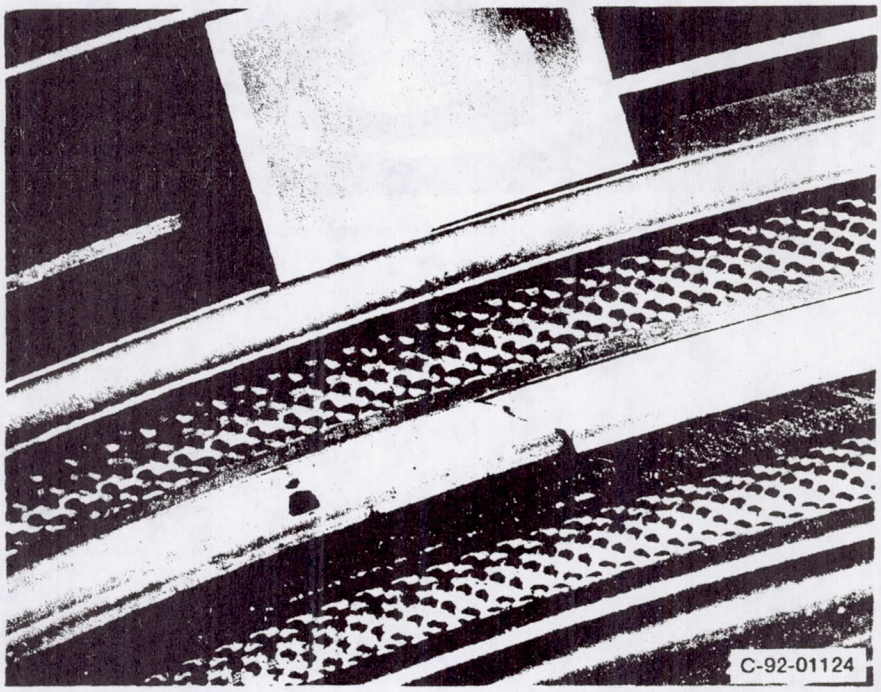

Figure 4.—View of installed brush seal.

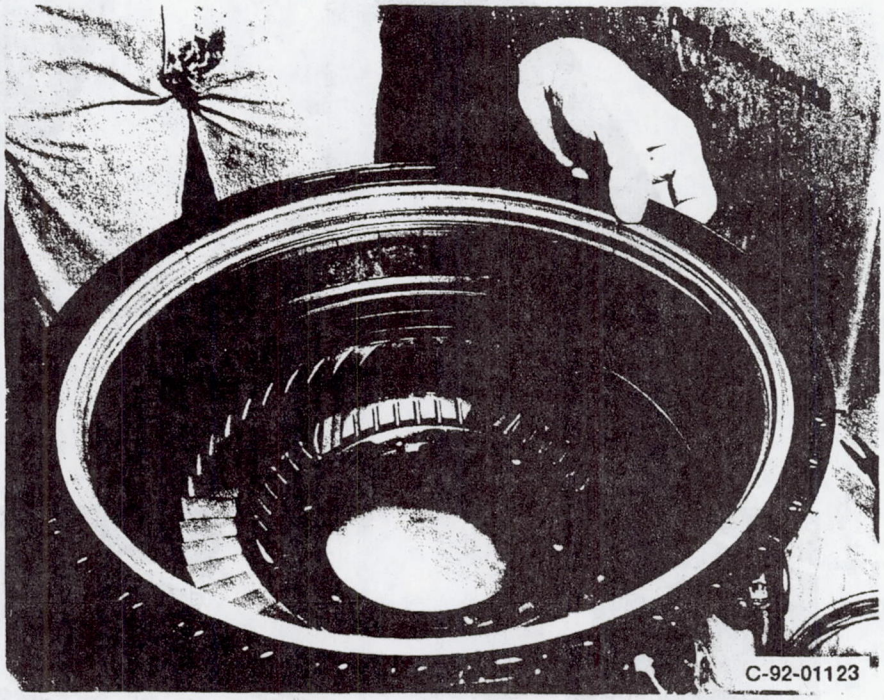

Figure 5.—Overview of installed brush seal and power turbine housing.

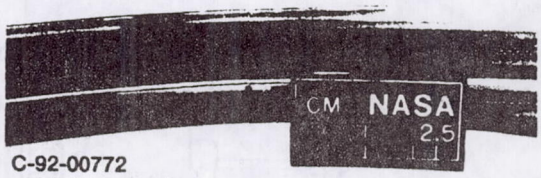

C-92-00772

(a) Pressure tap hole.

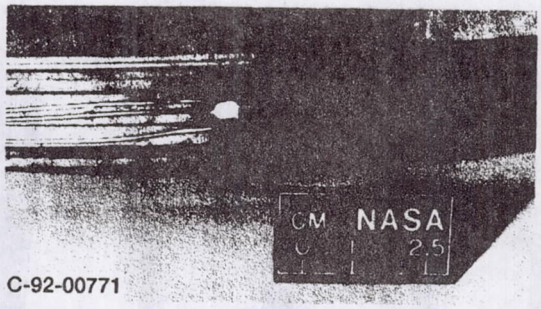

C-92-00771

(b) Thermocouple mount and pressure tap lines.

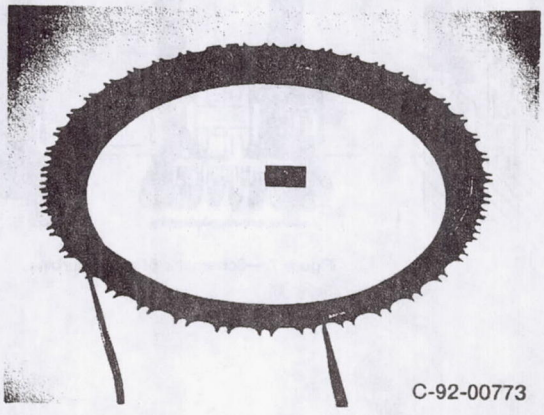

C-92-00773

(c) Shroud ring with three seal segments and instrumentation lines — downstream view.

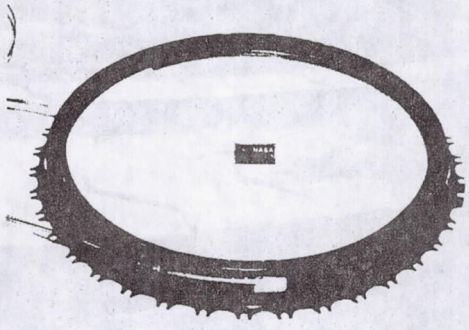

C-92-00774

(d) Shroud ring with three seal segments and instrumentation lines — upstream view.

Figure 6.—Pressure tap and thermocouple locations on shroud seal.

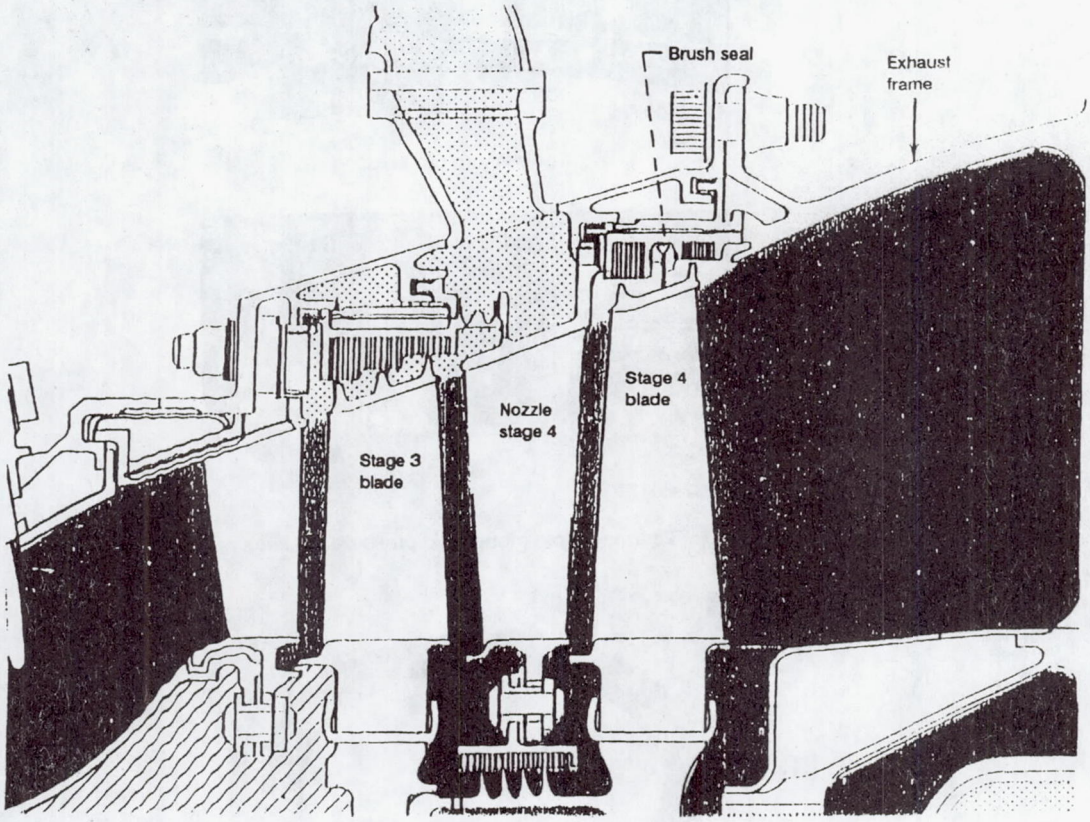

Figure 7.—Schematic of power turbine.

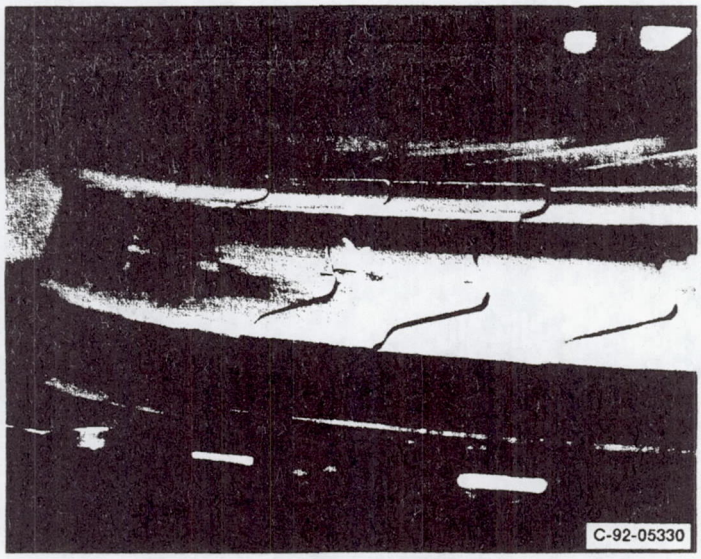

Figure 8.—Fourth-stage turbine after testing, showing polishing of leading edges.

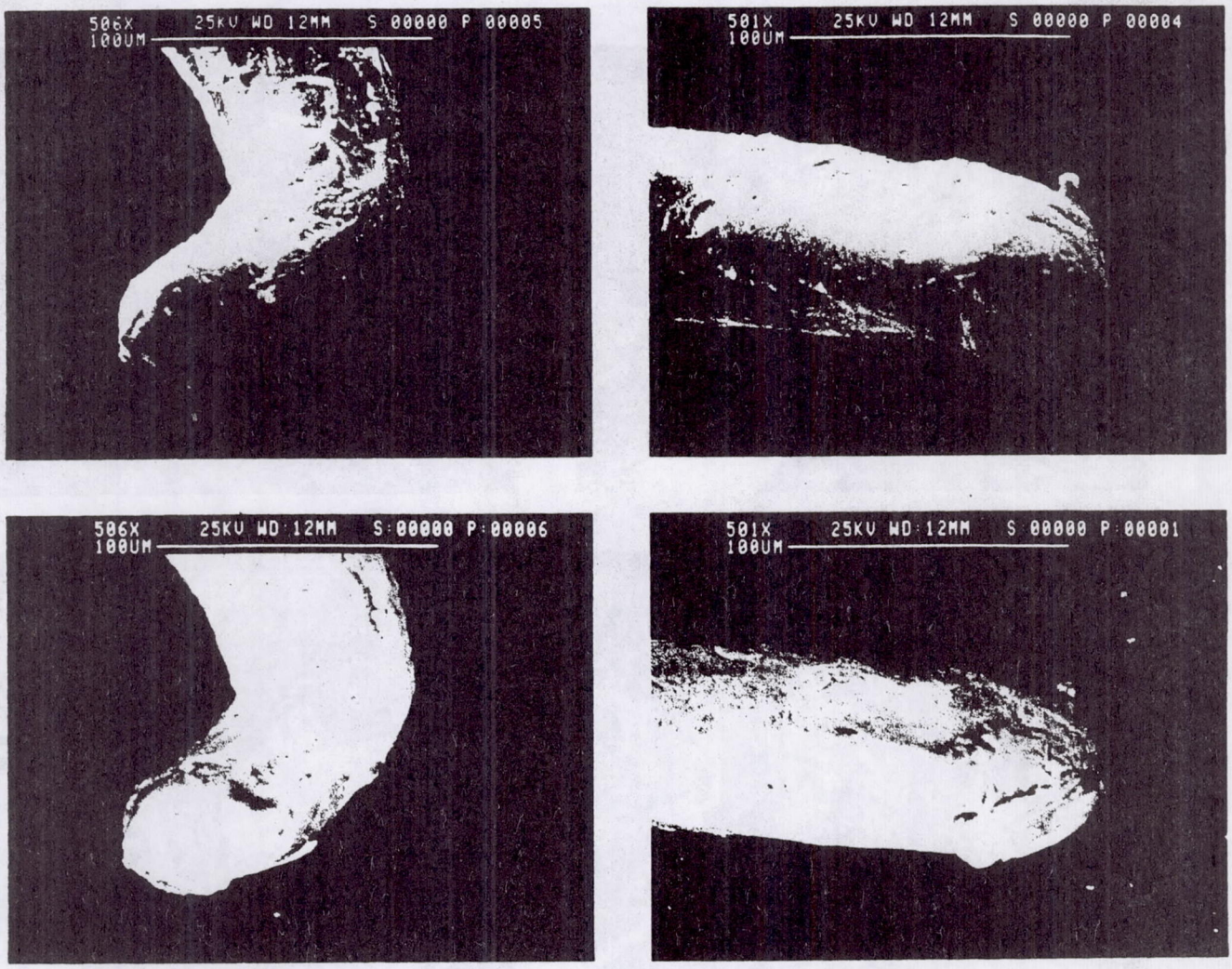

(a) Typical bristle tips.

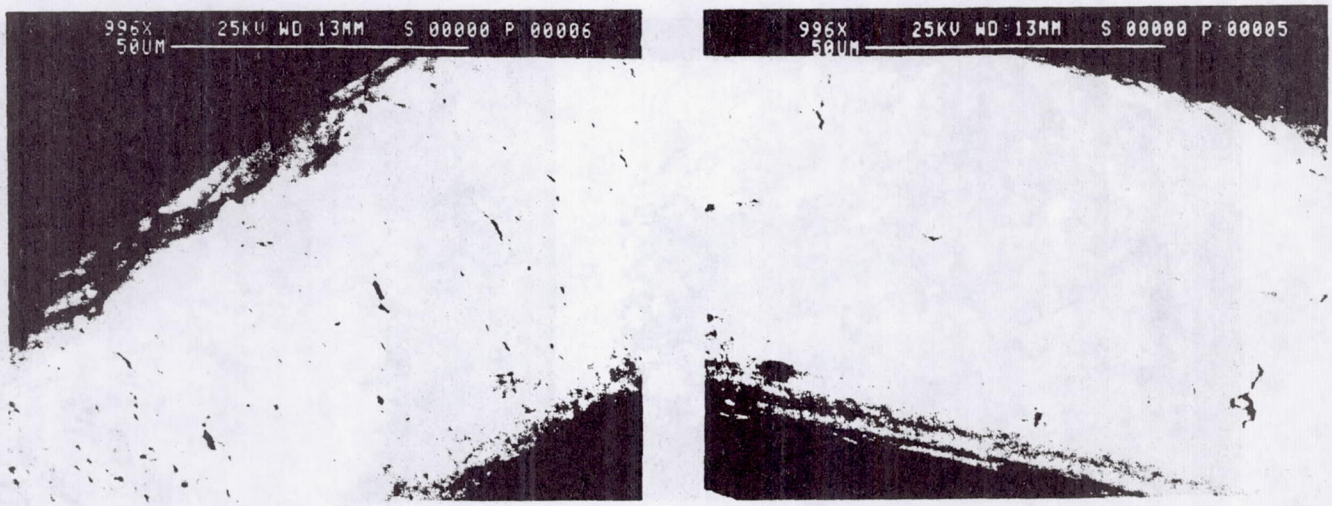

(b) Surface features.

Figure 9.—Typical brush seal debris found in engine exhaust duct.

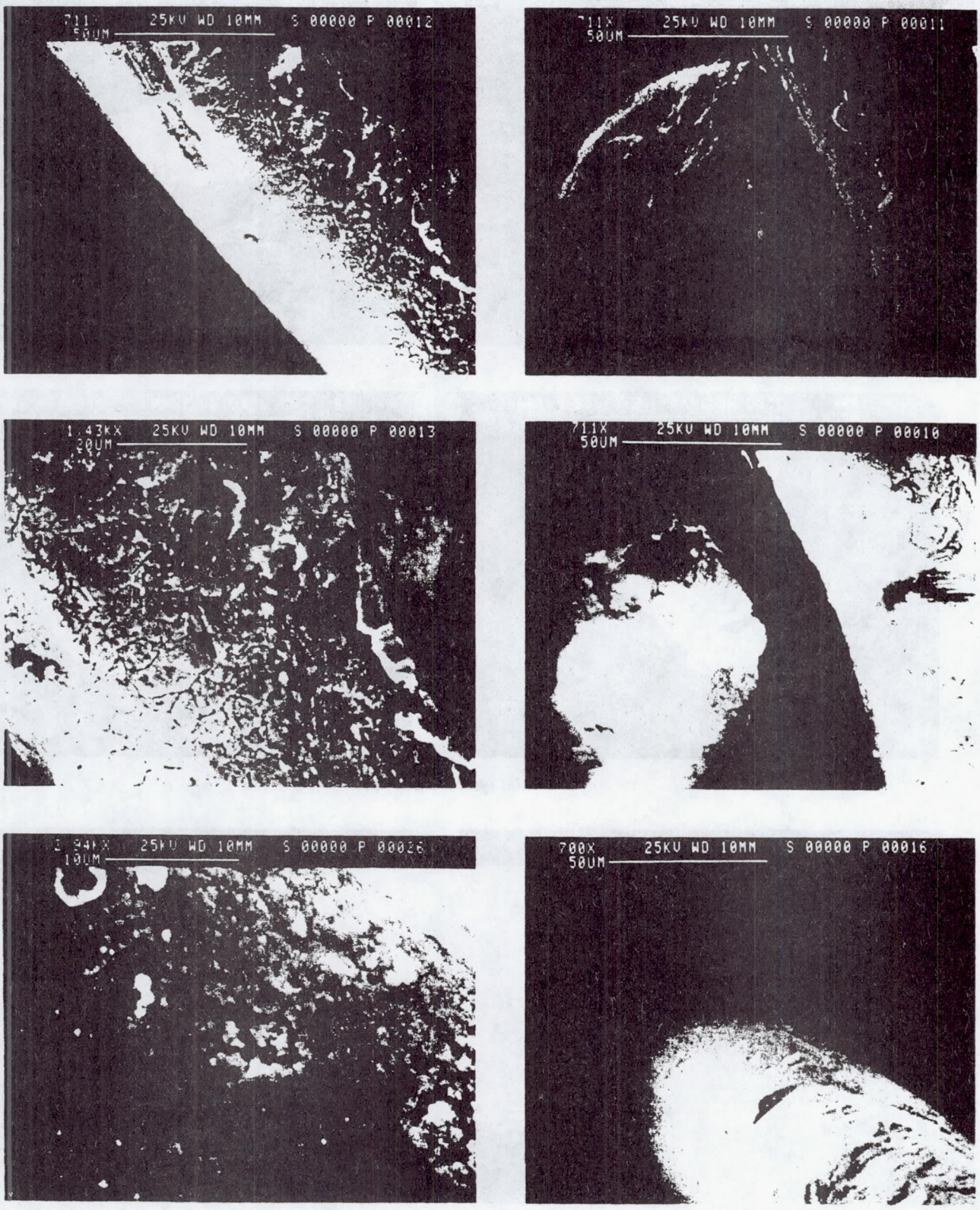

(b) Continued.

Figure 9.—Continued.

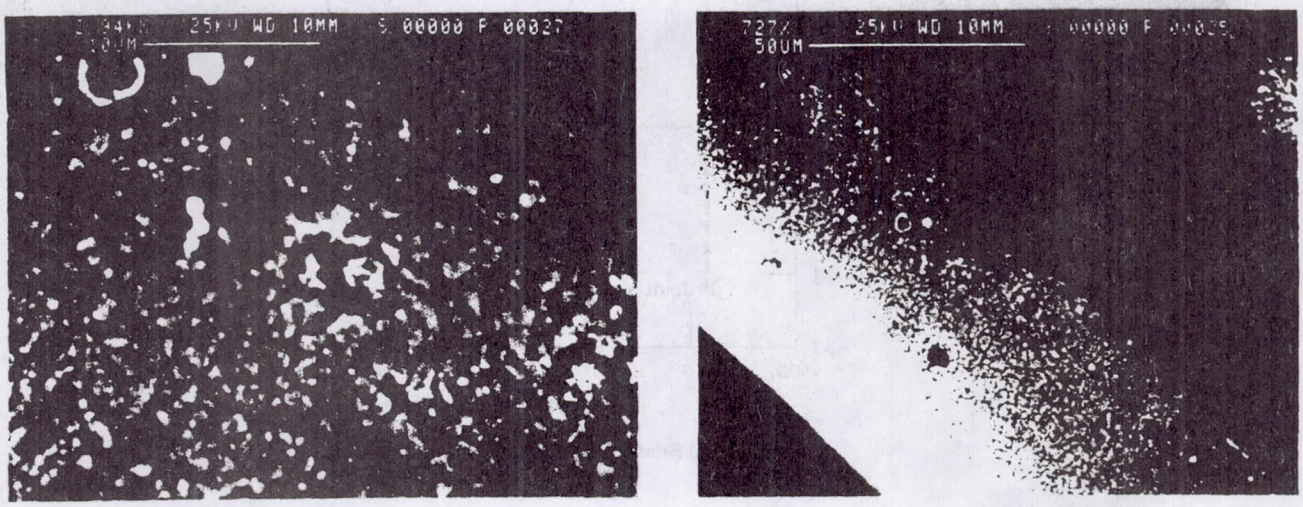

(b) Concluded.

Figure 9.—Concluded.

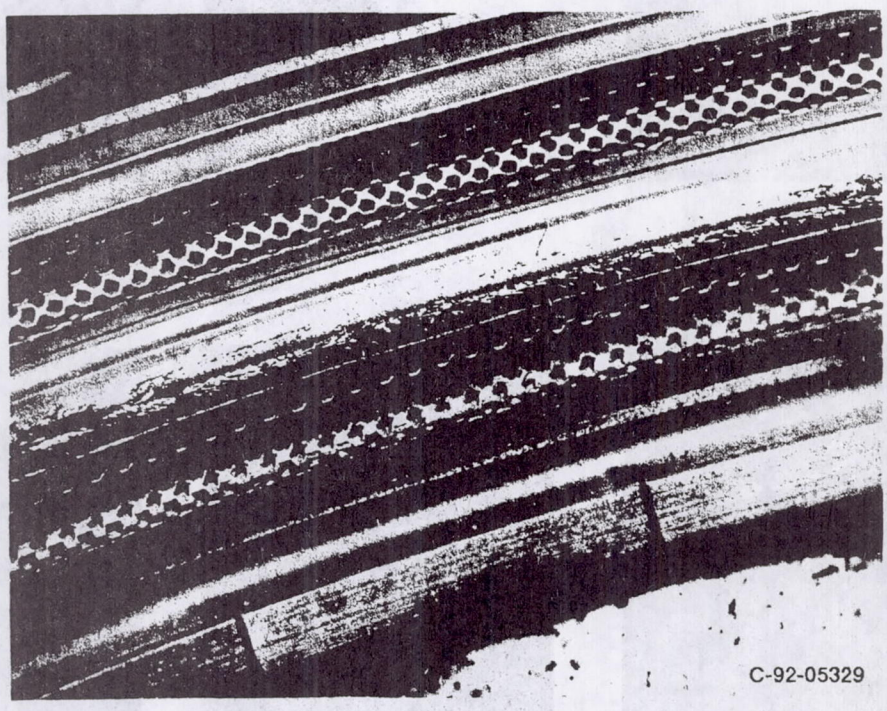

Figure 10.—Post-test view of brush seal showing bristle spreading and core of rubbed bristles.

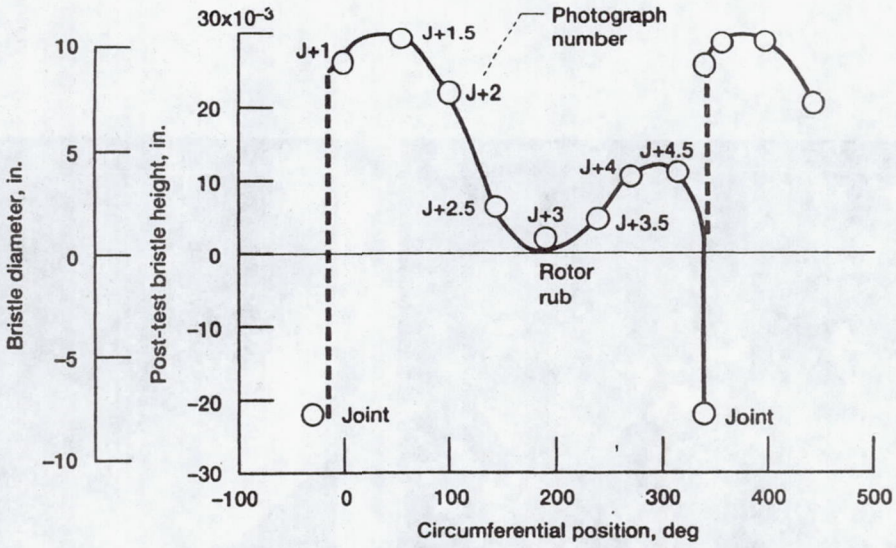

(a) Bristle height versus circumferential position.

Joint. J + 1. J + 1.5.

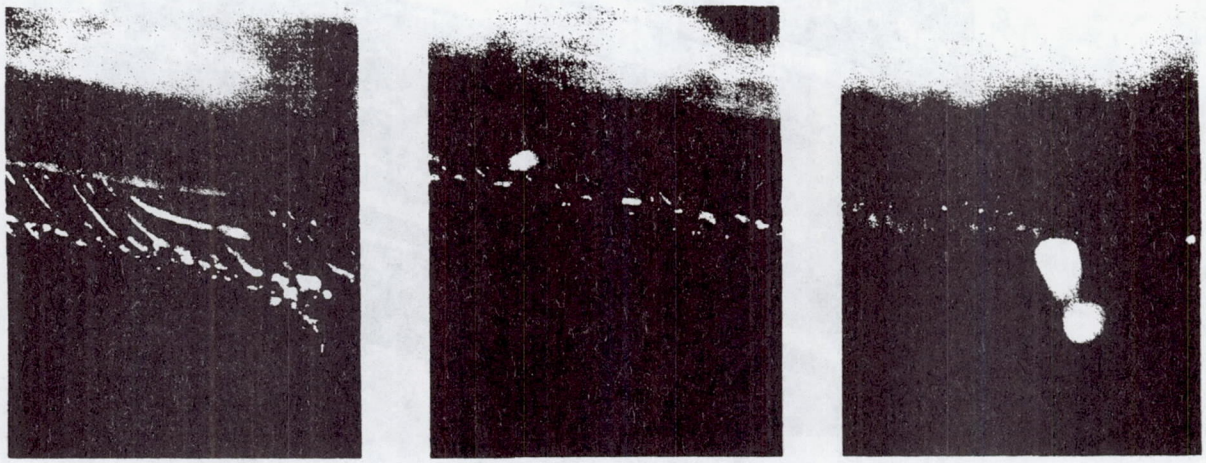

J + 2. J + 2.5. J + 3.

(b) Bristles at backing washer.

Figure 11.—Post-test bristle stub height and backing washer rub. Bristle diameter, 0.0028 in.

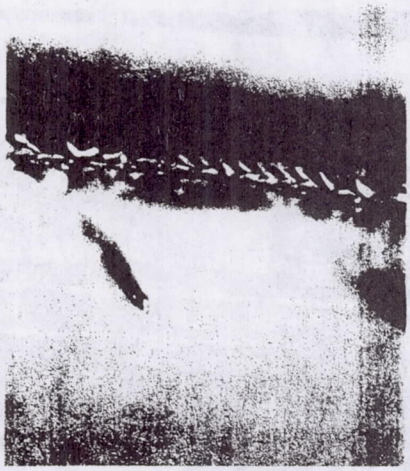

J + 3.5.

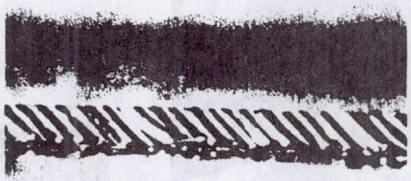

J + 4.

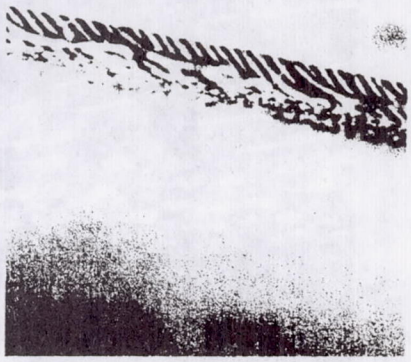

J + 4.5.

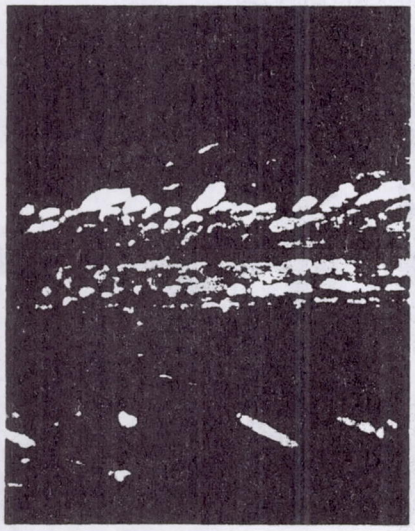

J + 3 (rotated view) 40x.

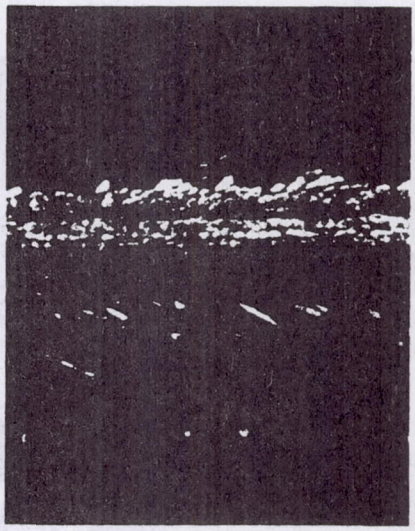

J + 3 (rotated view) 23x.

(b) Concluded.

Figure 11.—Continued.

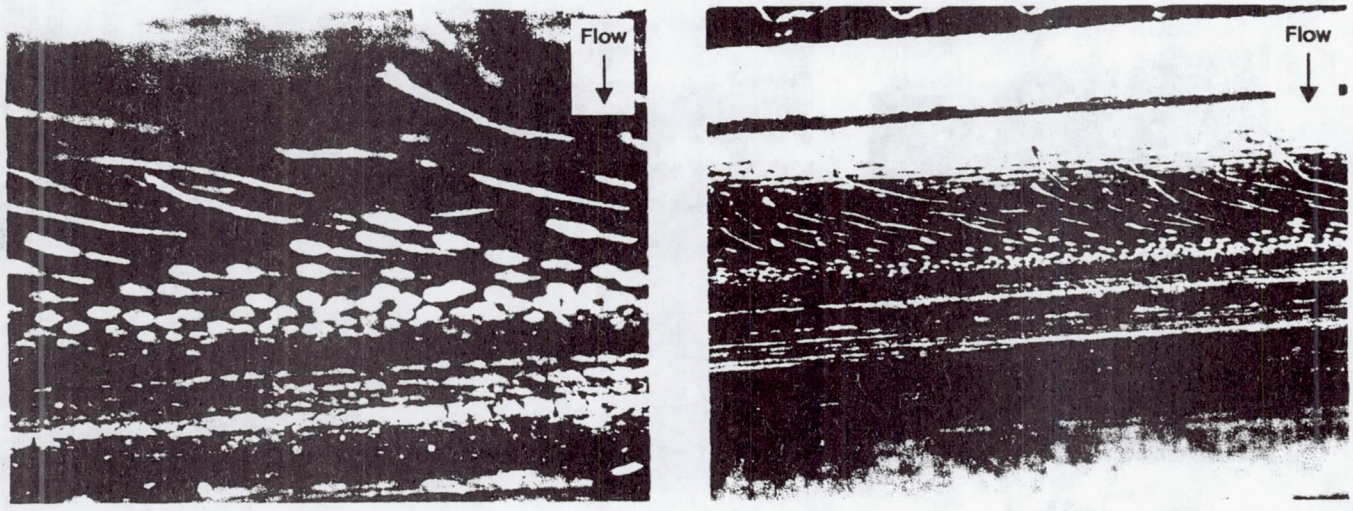

(c) Wear track and fence rub.

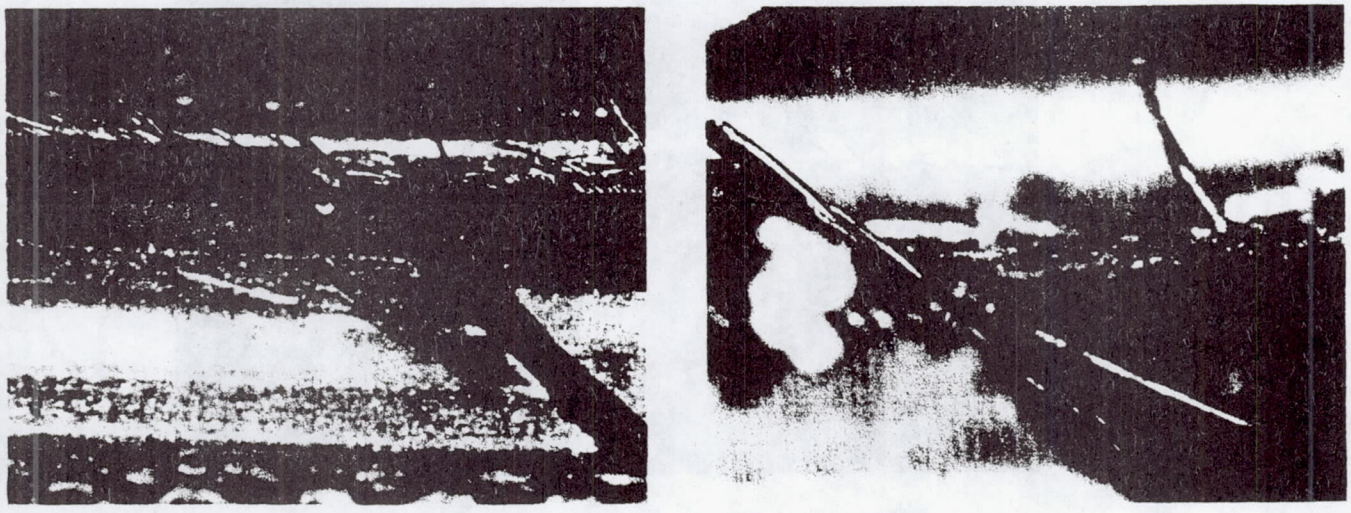

(d) Joint wear track.

Figure 11.—Concluded.

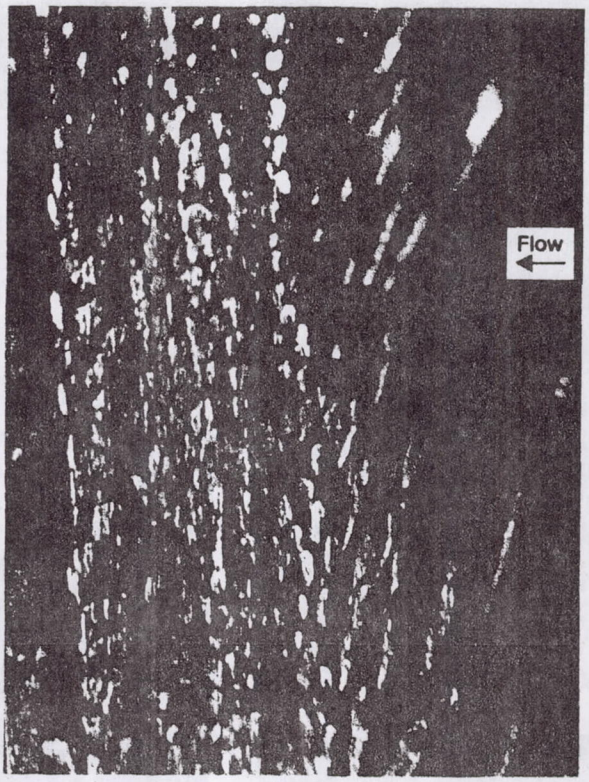

Figure 12.—Details of brush seal wear pattern.

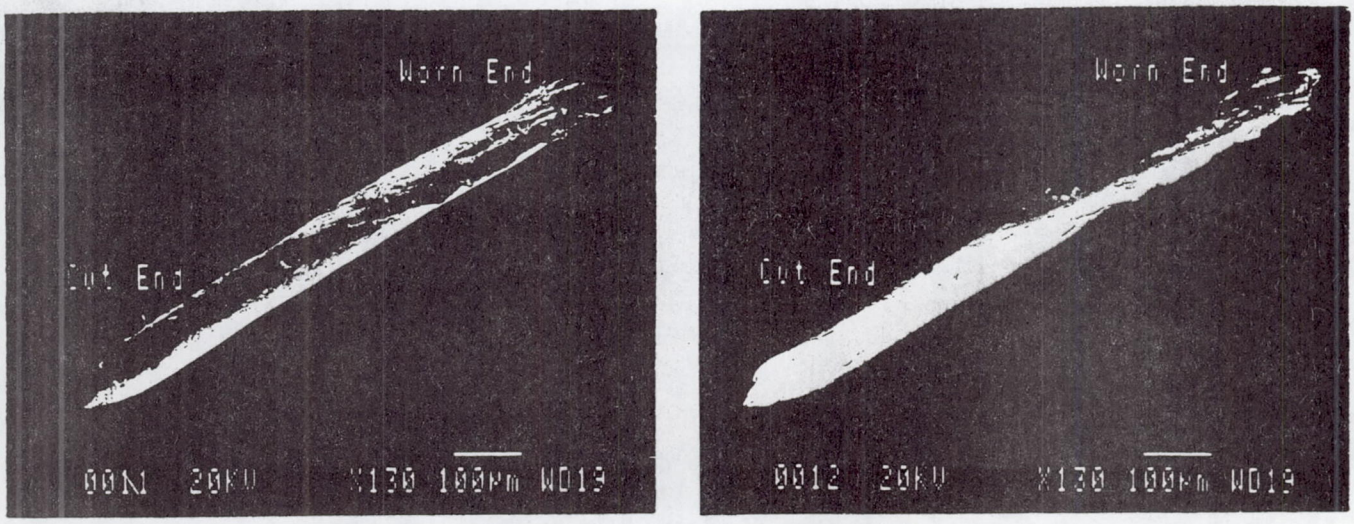

(a) Bristle 1 spread away from wear track.

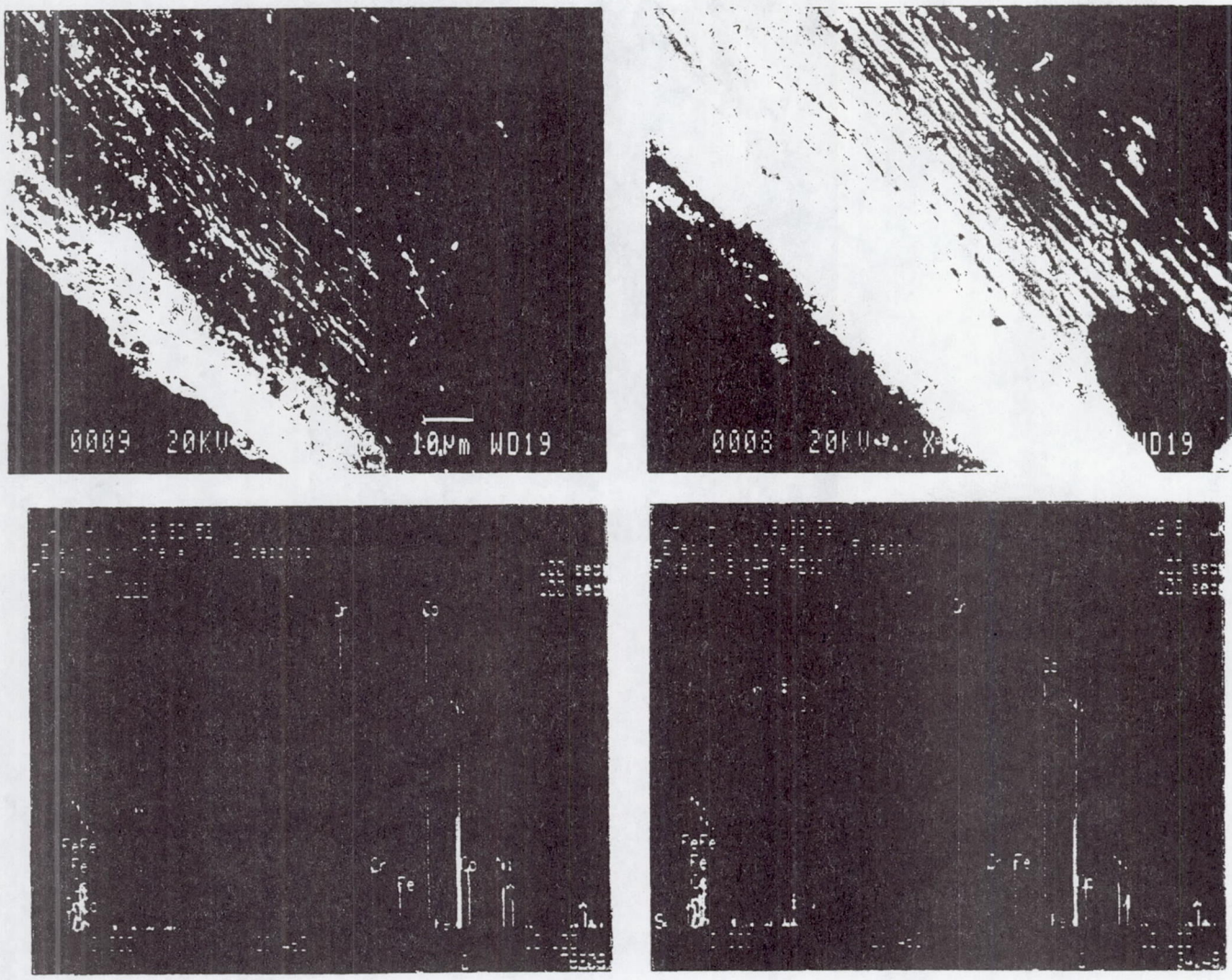

(b) Analysis of bristle 1.

Figure 13.—Post-test metallographic results for single bristle.

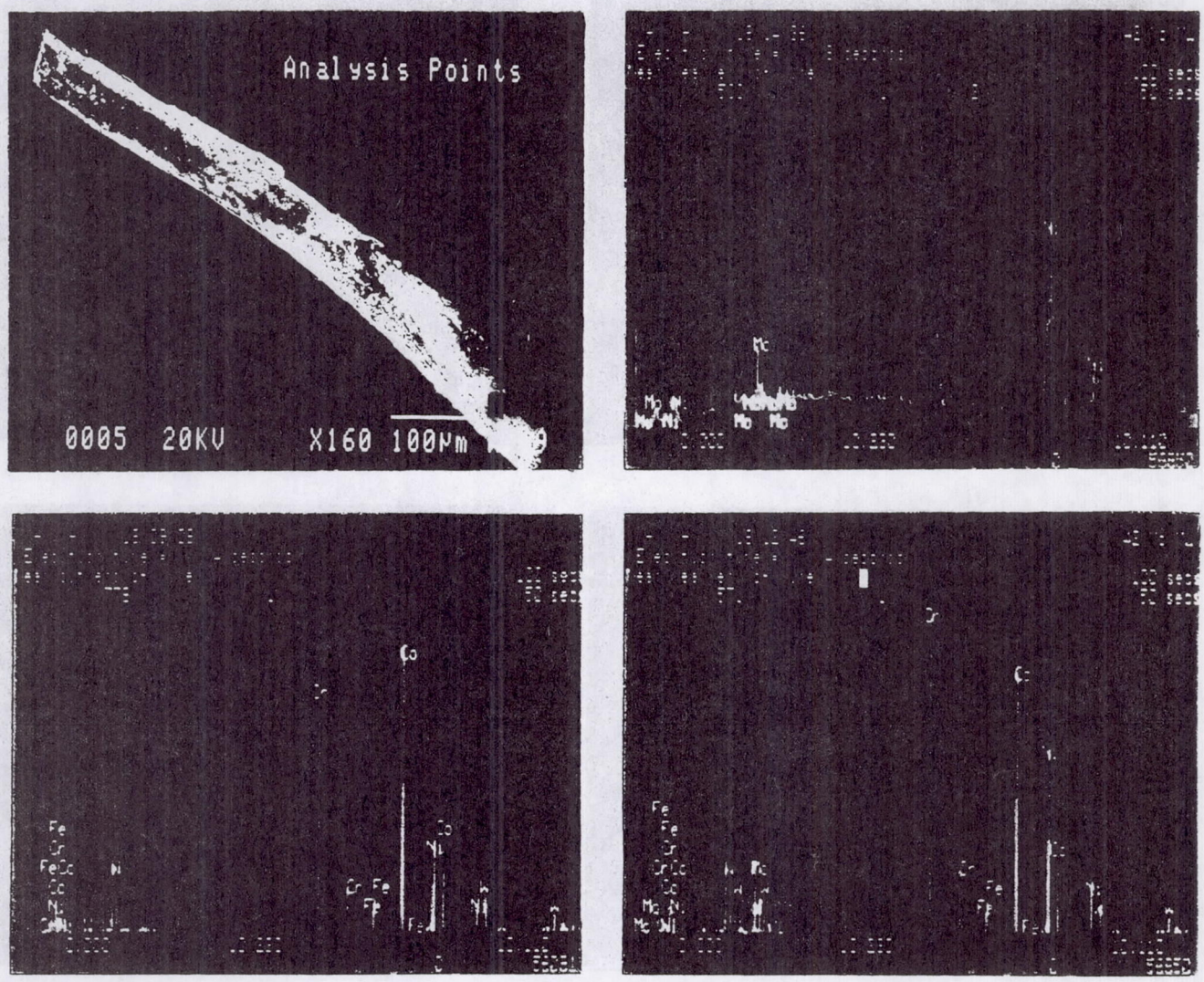

(c) Bristle 1 at increased resolution.

Figure 13.—Concluded.

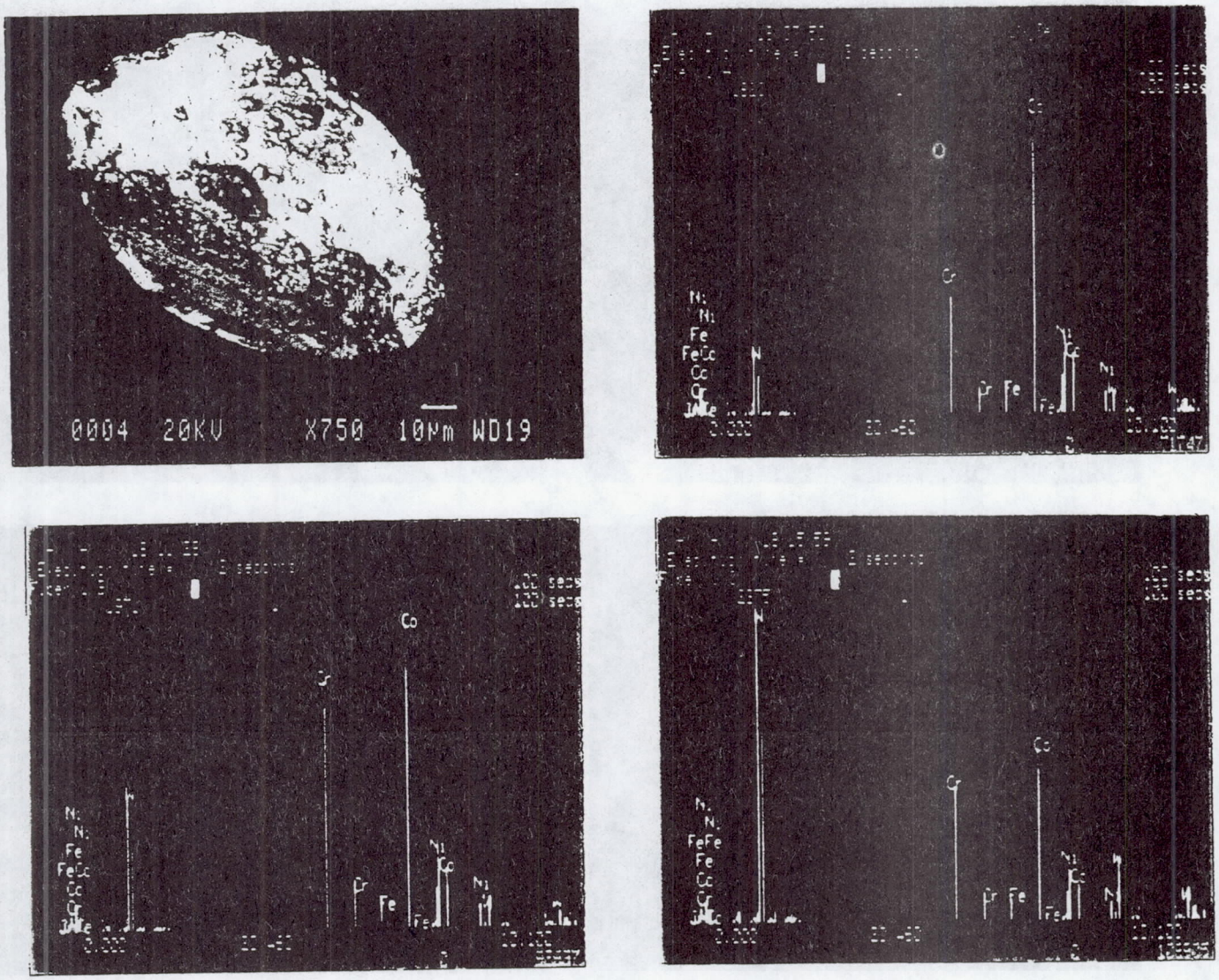

Figure 14.—Post-test metallographic results for bristle tip from wear track.

NASA
National Aeronautics and
Space Administration

MSFC Seal and Fluid Film Bearing Activities

Presented by Ted Benjamin
CFD Branch
Aerophysics Division
Structures and Dynamics Laboratory
George C. Marshall Space Flight Center
National Aeronautics and Space Administration

Presented August 6, 1992
at Brush Seals Systems Workshop
Lewis Research Center
National Aeronautics and Space Administration

Overview

- Highly-instrumented SSME HPOTP with hydrostatic bearing on Technology Test Bed
- Cryogenic fluid-film bearing tester
- Damping seal rotor support
- Damping seals for turbomachinery
- Experimental verification of rotordynamic analysis
- In-house CFD analysis

National Aeronautics and Space Administration

MSFC Seal Activities

Highly-instrumented SSME with HPOTP hydrostatic bearing on Technology Test Bed

Objective: Demonstrate feasibility of hydrostatic bearings for high pressure cryogenic turbopumps

- Joint Rocketdyne IR&D/MSFC activity
- Retrofit HPOTP pump-end with hydrostatic bearing for ball bearings
- Operated engine at multiple power levels with variable ramps and multiple LO_2 inlet conditions
- Bearing accumulated 723 seconds in 7 tests
- Rotordynamic stability maintained during all operational phases
- Proximity probe data indicated shaft contacted wall during both start and shutdown
- Post-test bearing wear data indicated minimum wear of 0.00109 inches over 7 test series

NASA
National Aeronautics and Space Administration

MSFC Seal Activities

Cryogenic Fluid Film Bearing Tester

Objective: Procure externally fed fluid-film bearing tester to test Earth-to-Orbit sized turbopump bearings in cryogenic fluids allowing for evaluation of bearings in realistic turbopump environment

- Should obtain repeatable and usable data
- Fluids of LH_2, LO_2, H_2O, and surrogates
- Only facility available to evaluate impartially and fully fluid film bearing concepts in cryogenic fluids
- Knowledge to be gained:
  - ◊ Important rotordynamic coefficients
  - ◊ Material characteristics, tribology of rubbing components
  - ◊ Basic load capacities

NASA
National Aeronautics and Space Administration

MSFC Seal Activities

Damping Seal Rotor Support

Objective: Obtain test rig to verify internally fed damping bearing predictions, validate rotordynamic codes

- Water as working fluid
- Experimentally determine dynamic coefficients and compare to in-house analytical predictions
- Include parametric changes to mechanical dimensions of seal and bearings as well as to fluid inlet and exit conditions
- Develop understanding of bearing performance as a function of parametric changes and analysis
- Preliminary design complete

NASA
National Aeronautics and Space Administration

MSFC Seal Activities

Damping Seals for Turbomachinery

Objective: Verify dynamic coefficient predictions of damping seals

- Rig used to determine dynamic coefficients of axially fed damping seals
  - 8 seal configurations tested
- Water as working fluid
- In-house bulk-flow codes closely match most of experimentally determined dynamic coefficients
- Performed at Wyle Laboratories

NASA
National Aeronautics and Space Administration

MSFC Seal Activities

Experimental Verification of Rotordynamic Analysis

Objective: Experimentally evaluate damping rotor supports for improvements in suppression of rotor whirl in turbopump

- Tests of 2 externally and 2 internally fed damping bearings in LO_2 surrogate fluid
- Provide head-to-head comparison between 4 damping bearing configurations
- Performed under contract to Rocketdyne
- Best combinations of bearing characteristics is candidate for replacing ball bearings in turbine end of SSME HPOTP

NASA
National Aeronautics and Space Administration

MSFC Seal Activities

In-house CFD Analysis

Objective: Mature CFD for fluid film applications to feed and support one-dimensional flow models

- Three-dimensional analysis on 60° slice of bearing
- Single-phase incompressible Navier-Stokes analysis assuming constant-γ H_2
- Rotational Reynolds number based on annulus width $\approx 4.8 \times 10^4$
- Multi-block solution in progress with FDNS code (Chen)
- K-ε turbulence models

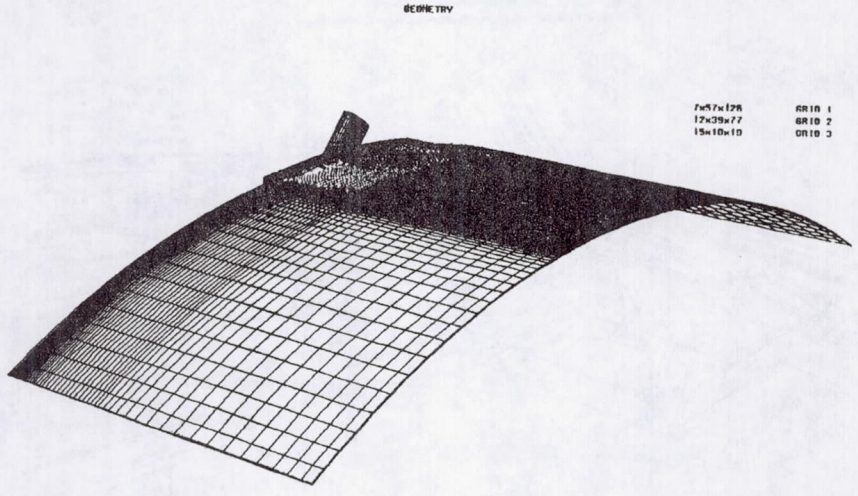

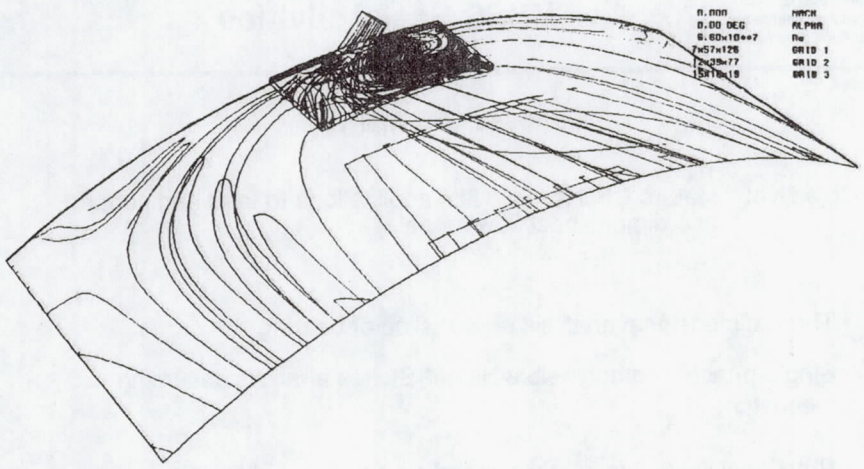

p12.1.img

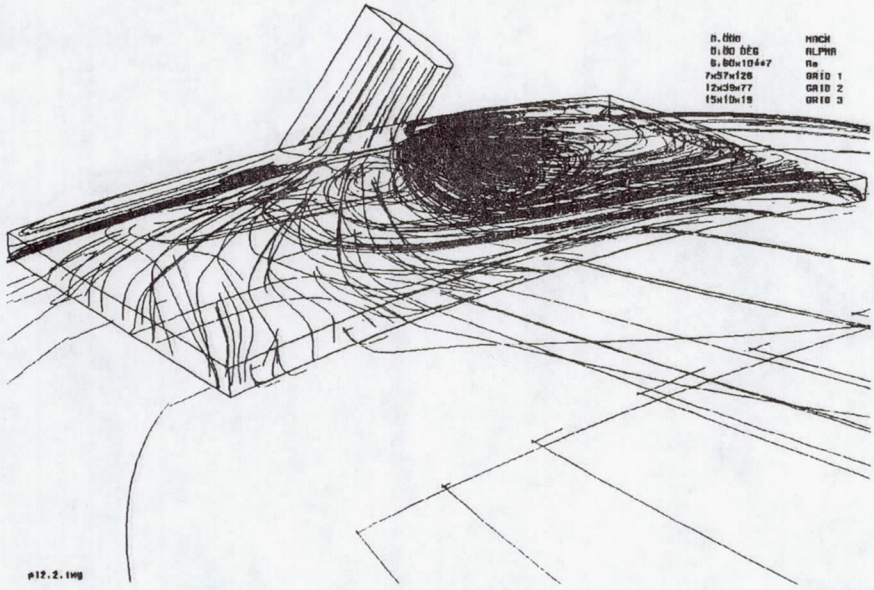

p12.2.img

PARTICLE TRACES

NLS HPFTP Hydrostatic Bearing

Preliminary Solution--40-degree Coolant Inlet Angle

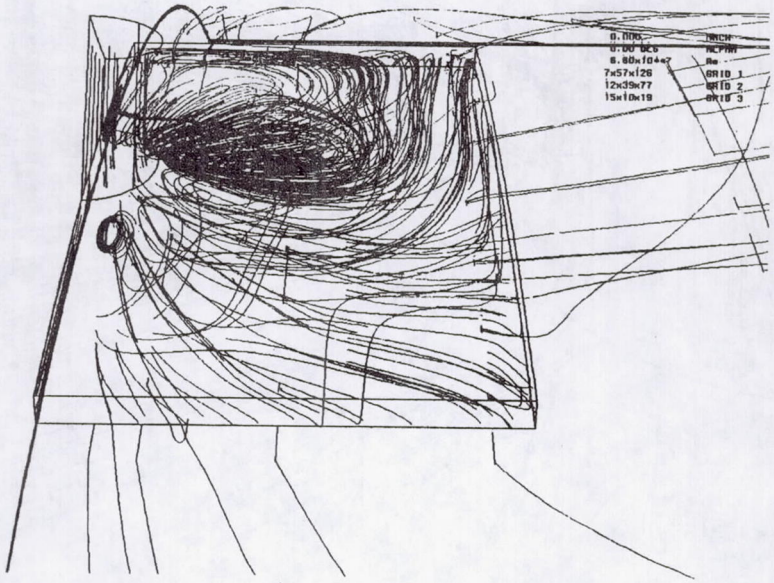

p12.3.ing

PARTICLE TRACES

NLS HPFTP Hydrostatic Bearing

Preliminary Solution--40-degree Coolant Inlet Angle

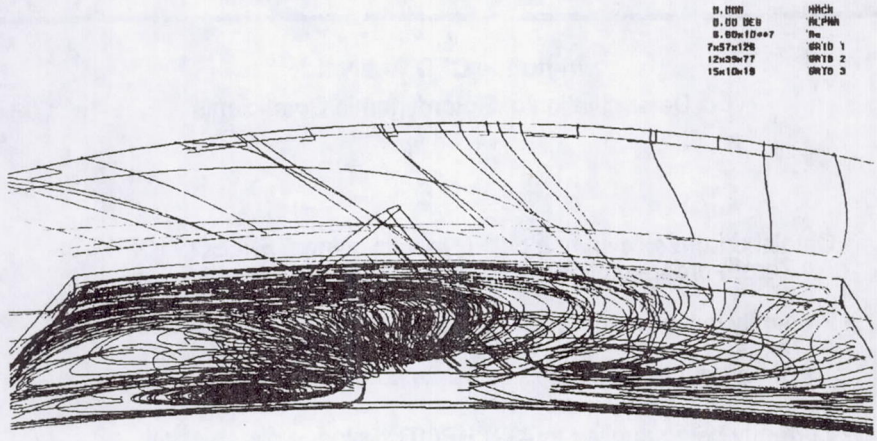

p12.5.ing

NASA
National Aeronautics and Space Administration

MSFC Seal Activities

In-house CFD Analysis
Determination of Rotordynamic Coefficients

- Obtained from axisymmetric CFD results using REFLEQS (CFDRC)
  - ◊ Zeroth-order solution
- Presently using perturbation method of Dr. Erian Baskharone (Texas A&M University) and Dr. Steve Hensel (former Texas A&M graduate student) to calculate coefficients
- Currently being applied to ATD HPOTP balance piston cavity

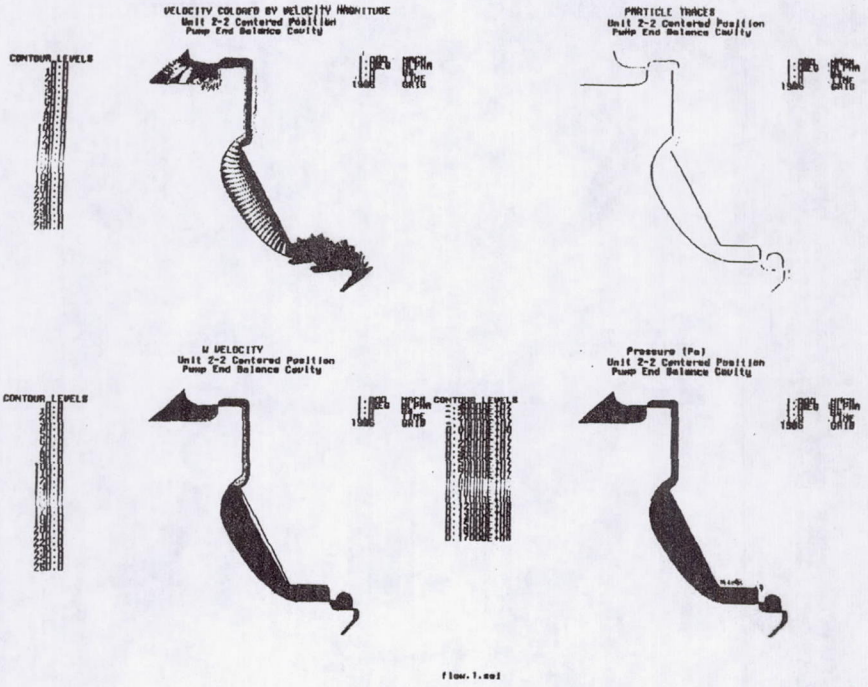
VELOCITY COLORED BY VELOCITY MAGNITUDE
Unit 2-2 Centered Position
Pump End Balance Cavity
CONTOUR LEVELS
PARTICLE TRACES
Unit 2-2 Centered Position
Pump End Balance Cavity
U VELOCITY
Unit 2-2 Centered Position
Pump End Balance Cavity
CONTOUR LEVELS
Pressure (Pa)
Unit 2-2 Centered Position
Pump End Balance Cavity
flow.1.sol

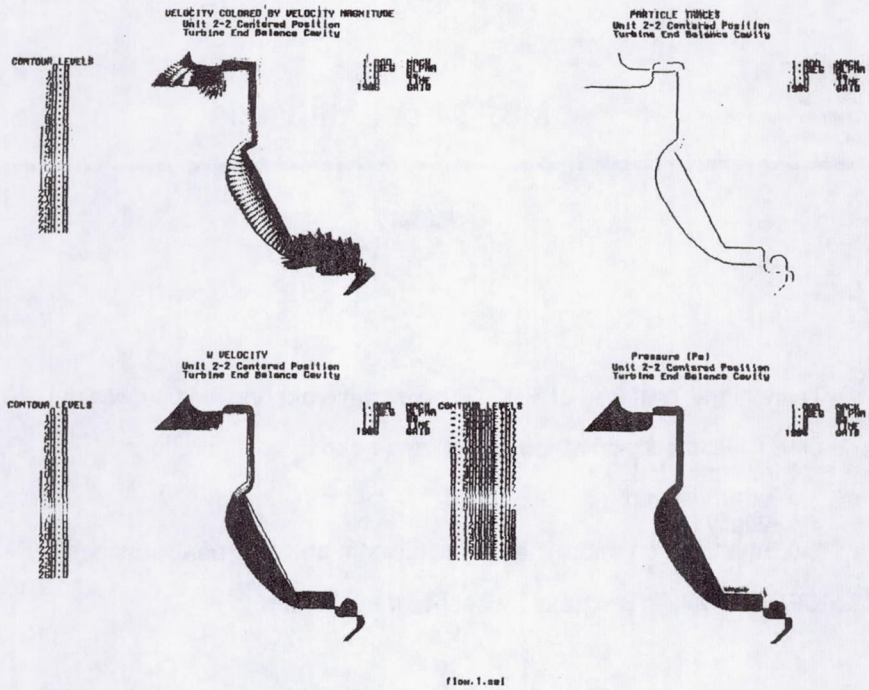
VELOCITY COLORED BY VELOCITY MAGNITUDE
Unit 2-2 Centered Position
Turbine End Balance Cavity
CONTOUR LEVELS
PARTICLE TRACES
Unit 2-2 Centered Position
Turbine End Balance Cavity
U VELOCITY
Unit 2-2 Centered Position
Turbine End Balance Cavity
CONTOUR LEVELS
Pressure (Pa)
Unit 2-2 Centered Position
Turbine End Balance Cavity
flow.1.sol

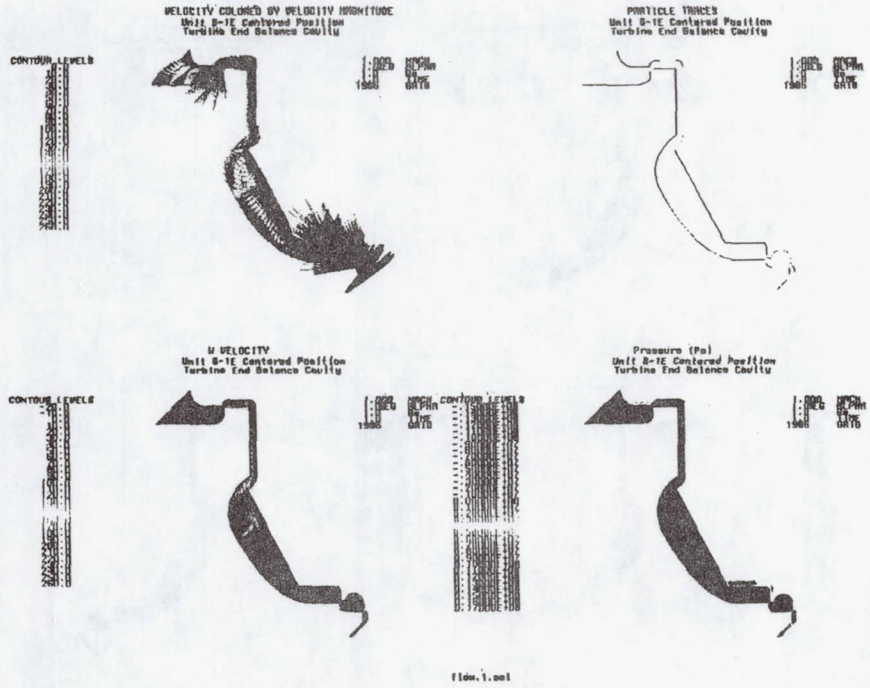

NASA
National Aeronautics and Space Administration

MSFC Seal Activities

Summary

- Technology Test Bed of HPOTP hydrostatic bearing was successful
- OAST tasks support range of seal and bearing configurations
  - ◊ Internally fed
  - ◊ Externally fed
  - ◊ Axially fed
  - ◊ Emphasis on rotordynamic coefficients and seal performances
- CFD analysis in progress for seal-flow evaluation

AIR FORCE BRUSH SEAL PROGRAMS

Capt Connie Dowler
Aero Propulsion & Power Directorate
Wright Laboratory
Wright-Patterson Air Force Base Ohio

Aggressive pursuit of increased performance in gas turbine engines is driving the thermodynamic cycle to higher pressure ratios, bypass ratios, and turbine inlet temperatures. As these parameters increase, internal air system and resultant thermodynamic cycle losses increase. This conflict of reducing internal airflows while increasing thermodynamic efficiency and performance is putting more emphasis on improvements to the internal flow system. One improvement that has been and continues to be pursued by the Air Force for both man-rated and expendable turbine engine applications is the brush seal. This presentation briefly describes both past and current brush seal research and development programs and gives a summary of demonstrator and developmental engine testing of brush seals.

OUTLINE

- PAST R&D PROGRAMS
- CURRENT R&D PROGRAMS
- DEMONSTRATOR ENGINE BRUSH SEALS
- F119 BRUSH SEALS
- SUMMARY

PAST AF BRUSH SEAL R&D PROGRAMS

- ALLISON: HIGH TEMPERATURE BRUSH SEALS
  - Inconel X-750 bristles wear better than Haynes 25 in hot dynamic contact with chrome-carbide journal
  - Initial build-up interference effects static leakage
  - Brush seal with hot running clearance has less leakage than 4-knife lab seal at same pressure ratio
  - Report #: WL-TR-91-2005
- TELEDYNE: BRUSH SEAL DESIGN
  - Brush seals provide a factor of 3 or more reduction in leakage flow over conventional lab seals
  - Brush seals retain a significantly reduced leakage over lab seals for time periods of limited-life engines
  - Brush seals can survive shaft excursions of over 0.025 inches without any performance loss
  - Report #: WRDC-TR-90-2123

PAST AF BRUSH SEAL R&D PROGRAMS (cont.)

- TEXAS A&M: BRUSH SEAL ROTORDYNAMICS
  - Last stage of seal group develops higher pressure drop than previous stages
  - Increasing inlet tangential velocity increases leakage slightly
  - Cross-coupled stiffness coefficient very low and generally negative (stabilizing)
  - Whirl frequency ratio indicates brush seal is extremely stable
  - Rotordynamic coefficients independent of seal spacing and inlet tangential velocity
  - Comparison with 8-cavity lab seal indicate brush seal will generally improve rotordynamic characteristics
  - Report #: WL-TR-91-2013 (original)
    corrected report in progress

CURRENT BRUSH SEAL R&D PROGRAMS

- EG&G SEALOL
  - Brush Seal Development Program
  - Advanced Brush Seal Development Program (New Start)
- PRATT & WHITNEY
  - High Speed Brush Seal Development Program (New Start)
- IN-HOUSE
  - Brush Seal Leakage Flow Modeling
  - Brush Seal Compressor Shroud Test

BRUSH SEAL DEVELOPMENT PROGRAM
EG&G SEALOL

OBJECTIVE:

Develop a comprehensive design methodology for application of brush seals to man-rated engines

APPROACH:

Conduct parametric testing of design variables for brush seals to define performance, fatigue, oxidation, and wear characteristics

ACCOMPLISHMENTS:

- Examined effect of bristle angle, bristle length, stiffness, staging, and packwidth on hysteresis, ΔP capability, leakage, wear
- Significant hysteresis with speed, but not pressure
- Increased Packwidth gave higher ΔP capability, lower leakage
- Multiple Stage Brush Seal Performance
  - Leakage reduction
  - Unequal pressure distribution
    - -- May be controlled by using mixed stiffness designs
    - -- Staging with higher packwidth seals most effective
- Tribopair Test and Evaluation
- Evaluating Advanced Designs to Reduce Hysteresis
- Designing Full-Scale Seal for Demonstrator Engine Test

PROJECT ENGINEER: Capt Connie Dowler, 513-255-8210

ADVANCED BRUSH SEAL DEVELOPMENT PROGRAM
EG&G SEALOL

OBJECTIVE:

Develop a comprehensive design methodology for application of advanced, high performance brush seals in man-rated engines

APPROACH:

Conduct experimental characterization of seal design and materials pairs and CFD modeling to maximize single- and multi-stage brush seal Δ P capability and axial and radial excursion accommodation. Investigate feasibility of non-contacting brush seal.

ACCOMPLISHMENTS:

New Start

PROJECT ENGINEER: Lt Carolyn Sunderland, 513-255-8210

HIGH SPEED BRUSH SEAL DEVELOPMENT PROGRAM
Pratt & Whitney

OBJECTIVE:

Provide verification of advanced brush seal technology needed to enable continued application of brush seals in IHPTET Phase II demonstrator engines.

APPROACH:

Conduct an application study using IHPTET Phase II engine design and mission flight cycle to determine surface speed and temperature requirements for brush seals. Design and fabricate brush seals for rig testing to verify their capability to operate at IHPTET Phase II conditions (~ 1400fps, 1400 F).

ACCOMPLISHMENTS:

New Start

PROJECT ENGINEER: Lt Carolyn Sunderland, 513-255-8210

BRUSH SEAL LEAKAGE FLOW MODEL
FLOW MODEL APPROACH

- 1-D MODEL, WITH RADIAL AND AXIAL FLOW CONSIDERED
- FLOW CORRELATIONS FROM KNUDSEN AND KATZ
  - Laminar Flow
  - Turbulent Flow
  - Transition Flow
- SINGLE CORRELATING PARAMETER: EFFECTIVE THICKNESS
- MODEL 1
  - Linear
  - Square Array Bristle Bed
- MODEL 2
  - Linear
  - Hexagonal Pack Bristle Bed
- MODEL 3
  - Modification of Model 2 to Account for Curvature Effects
  - Effective Thickness Constant Between Journal and Mean Diameter
  - Bristle Bed Configuration Varies
    - Increased Transverse Bristle Spacing
    - Increased Leakage Flow Area at Mean Diameter
    - Hexagonal Pack Bristle Bed

TYPICAL MODEL PERFORMANCE CHARACTERISTICS

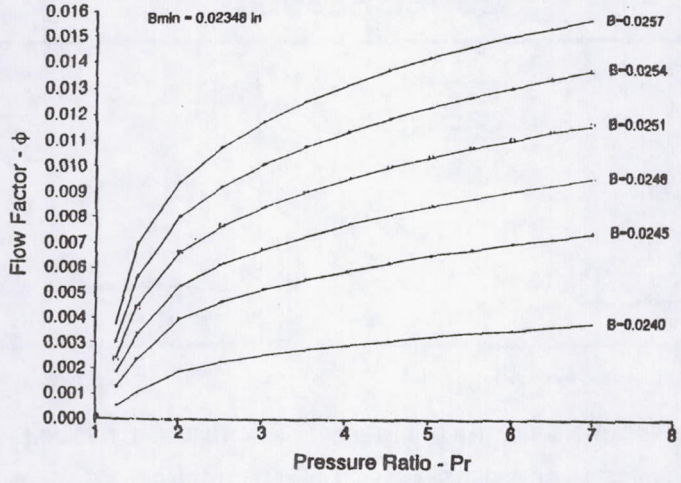

- SHAPE OF Ø VERSUS P_r IS EXPECTED CHARACTERISTIC CURVE
- FLOW INCREASES WITH B AS THE BRISTLE PACK OPENS UP
- TRANSITION FROM LAMINAR TO TURBULENT FLOW NEAR $P_r = 2$

LEAKAGE PERFORMANCE DATA

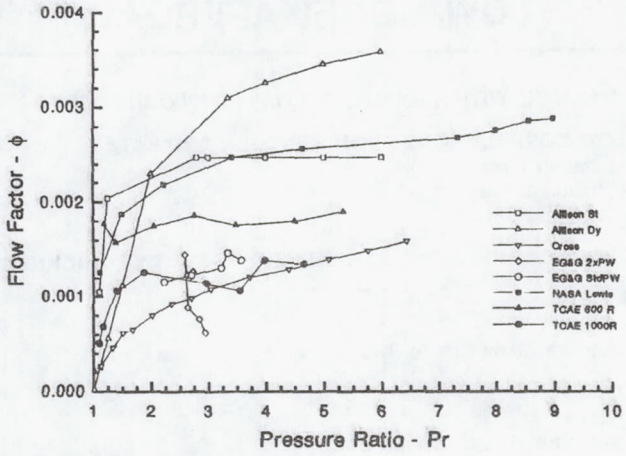

- HYSTERESIS EFFECT REMOVED
- ALLISON DATA ARE AVERAGED RESULTS FOR SEVERAL SEALS
- TELEDYNE CAE DATA ARE FOR A BASELINE BRUSH SEAL
- CROSS DATA PROVIDED CHECK ON EFFECT OF BRISTLE DENSITY
- NASA LEWIS DATA PROVIDED CHECK ON SEAL DIAMETER EFFECT

BRUSH SEAL LEAKAGE FLOW MODEL
MODEL RESULTS

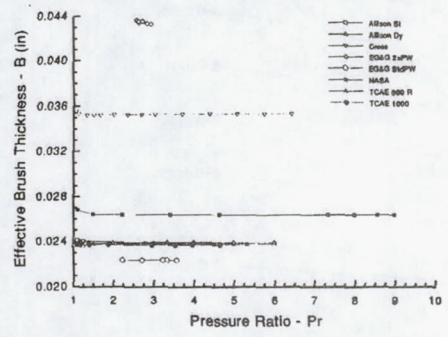

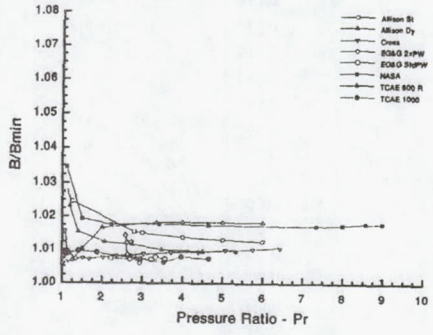

- WIDE RANGE OF B INDICATIVE OF DIFFERENCE IN ACTUAL SEAL THICKNESS
- B/Bmin INDICATOR OF BRUSH SEAL LEAKAGE EFFECTIVENESS
- EG&G DOUBLE PACKWIDTH SEAL LESS EFFICIENT THAN STANDARD DENSITY SEAL
- CROSS SEAL VERY EFFICIENT
- NASA SEAL LESS EFFICIENT THAN LARGER DIAMETER SEALS

BRUSH SEAL COMPRESSOR SHROUD TEST

- PART OF ADLARF TEST PROGRAM IN COMPRESSOR RESEARCH FACILITY
- TENTATIVELY SCHEDULED TO TEST JAN 93
- INVESTIGATING CAPABILITY OF BRUSH SEAL SHROUD TO IMPROVE
  - BLADE VIBRATIONS (DAMPING)
  - STALL MARGIN
  - EFFICIENCY
- PROJECT ENGINEER: Lt Carolyn Sunderland, 513-255-8210

DEMONSTRATOR ENGINE BRUSH SEAL TESTING

- TESTING TO DATE:
  - PRIMARILY IN TURBINE SECTION
  - HAYNES 25 BRISTLES
  - CHROME CARBIDE OR ALUMINUM OXIDE COATING
  - 20 TO 80% REDUCTION IN LEAKAGE OVER LAB SEALS
  - REDUCED HEAT GENERATION
  - GENERALLY GOOD DURABILITY
  - MAX CONDITIONS: 1275 FPS, 1130 F, 55 PSI ΔP
- FUTURE TESTING:
  - PLANNED FOR ALL DEMO ENGINES (ATEGG, JTDE, JTAGG, ETEC)
  - COMPRESSOR AND IGV LOCATIONS
  - BRUSH SEAL SHROUD
  - HIGHER SURFACE SPEED AND TEMPERATURE (>1400 F, >1400 fps)

F119 BRUSH SEALS

- BILL OF MATERIALS
  - 3 STATIC SEALS
  - HPT & LPT SHROUD
- TECHNOLOGY TRANSITION PLANS
  - HPT (3 Locations)
  - LPT (2 Locations)
  - REPLACE LAB SEALS WITH BRUSH SEALS AT ALL COMPRESSOR INTERSTAGE LOCATIONS
  - 0.9% TFSC IMPROVEMENT (TOTAL)

SUMMARY

- AF COMMITTED TO DEVELOPING AND TRANSITIONING BRUSH SEAL TECHNOLOGY
- EMPHASIZING BRUSH SEAL RIG TESTING (CONTRACT AND IN-HOUSE)
- PUSHING FOR INCORPORATION OF BRUSH SEALS IN ALL DEMONSTRATOR ENGINES
- WORKING WITH PROGRAM OFFICES TO TRANSITION BRUSH SEAL TECHNOLOGY TO OPERATIONAL AND DEVELOPMENT ENGINES

Navy GTE Seal Development Activity

by

Carl P. Grala
Naval Air Warfare Center
Aircraft Division- Trenton

Under the auspices of the Integrated High Performance Turbine Engine Technology Initiative, the Naval Air Warfare Center conducts advanced development programs for demonstration in the next generation of air-breathing propulsion systems. Among the target technologies are gas path and lube oil seals. Two development efforts currently being managed by NAWCAD are the High Performance Compressor Discharge Film-Riding Face Seal and the Subsonic Core High Speed Air/Oil Seal.

The High Performance Compressor Discharge Film-Riding Face Seal Program aims at reducing parasitic leakage through application of a film-riding face seal concept to the compressor discharge location of a Phase II IHPTET engine. An order-of-magnitude leakage reduction relative to current labyrinth seal configurations is expected. Performance goals for these seals are (i) 1200 F air temperature, (ii) 800 feet-per-second surface velocity, and (iii) 600 PSI differential pressure. The two designs chosen for fabrication and rig test are a spiral groove and a Raleigh step seal. Rig testing is currently underway.

The Subsonic Core High Speed Air/Oil Seal Program is developing shaft-to-ground seals for next-generation propulsion systems that will minimize leakage and provide full life. Significantly higher rotor speeds and temperatures will be experienced. Technologies being exploited include, hydrodynamic lift assist features, ultra light weight designs, and improved cooling schemes. Parametric testing has been completed, a final seal design is entering the endurance test phase.

MECHANICAL SYSTEMS TECHNOLOGY
S.O.A. vs FUTURE REQUIREMENTS

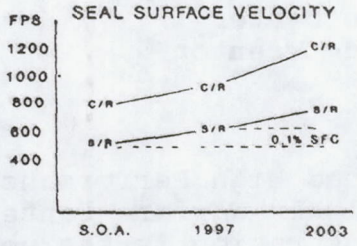

SPEED AND TEMPERATURE TRENDS HAVE AN ADVERSE EFFECT ON MECHANICAL SYSTEMS:

- STRESS CYCLES ACCUMULATE FASTER, LIFE IN HOURS GOES DOWN.
- INTERFACIAL HEAT GENERATION GOES UP WITH VELOCITY.
- MATERIALS ALLOWABLES DROP WITH INCREASING TEMPERATURE.
- REQUIRED WEIGHT REDUCTIONS MAGNIFY THE ENVIRONMENTAL CHALLENGE.

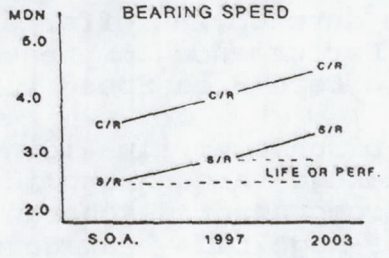

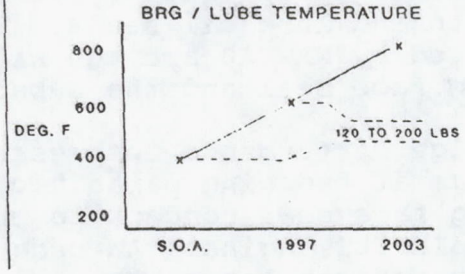

MECHANICAL SYSTEMS PROJECT

CHALLENGE:

* SIGNIFICANTLY EXPAND COMPONENT OPERABILITY
  - SPEED, TEMPERATURE, LOAD

* SIGNIFICANT COMPONENT/SYSTEM WEIGHT REDUCTIONS

* REACT TO CURRENT DESIGN PRACTICE DEFICIENCIES

MECHANICAL SYSTEMS PROJECT
(WR22-P64)

TRENTON, NEW JERSEY

TASK 1: RADIAL AND AXIAL BEARINGS

TASK 2: LUBE OIL SEALS

TASK 3: STATIC AND DYNAMIC GAS PATH SEALS

MECHANICAL SYSTEMS PROJECT
TASK 1: AXIAL AND RADIAL BEARINGS

TRENTON, NEW JERSEY

FLEET ISSUES ADDRESSED:

- INCREASED ENDURANCE FOR EXTENDED COVERAGE FOR ASW/ASUW/AEW/EW/C3/DRUG MISSIONS
- INCREASED STANDOFF RANGE FOR POWER PROJECTION ASHORE
- HIGH PERFORMANCE ENGINES FOR EMERGING SYSTEM REQUIREMENTS (AX, NATF, ASTOVL, SSF)
- IMPROVED LIFE CYCLE COST THROUGH IMPROVED RELIABILITY
- IMPROVED A/C AVAILABILITY

TECHNOLOGIES:

- MAGNETIC BEARINGS
- THRUST COMPENSATION
- RADIAL LOAD COMPENSATION
- INNOVATIVE DESIGN
- IMPROVED MATERIALS
- IMPROVED DAMPERS

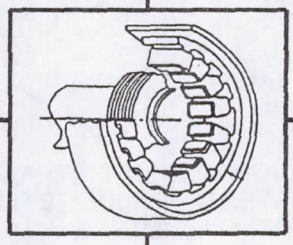

IHPTET/S&T RELIANCE JDL GOALS:

	PH I	PH 2	PH 3
TEMPERATURE (F)	400	600	800
BEARING SPEED (MDN)	2.5 3.7	3.0 4.2	3.5 4.5
WEIGHT	- 5 %	- 10 %	- 20 %

IHPTET/S&T RELIANCE JDL SYSTEM PAYOFFS:

	PH I	PH II	PH III
TIME ON STATION	+1.8%	+3.0%	+ 6 %
RANGE	+ 2 %	+ 4 %	+ 7 %
PAYLOAD	+ 18 %	+ 36 %	+ 50 %
FN / WT	+5.2%	+11.1%	+25.%

MECHANICAL SYSTEMS PROJECT
TASK 2: LUBE OIL SEALS

TRENTON, NEW JERSEY

FLEET ISSUES ADDRESSED:

- INCREASED ENDURANCE FOR EXTENDED COVERAGE FOR ASW/ASUW/AEW/EW/C3/DRUG MISSIONS
- *INCREASED STANDOFF RANGE FOR POWER PROJECTION ASHORE*
- HIGH PERFORMANCE ENGINES FOR EMERGING SYSTEM REQUIREMENTS (AX, NATF, ASTOVL, SSF)
- IMPROVED LIFE CYCLE COST THROUGH IMPROVED RELIABILITY
- IMPROVED A/C AVAILABILITY

TECHNOLOGIES:

- HYDRODYNAMIC LIFT ASSIST
- EXTREME LIGHTWEIGHT DESIGNS
- IMPROVED CARBON MATERIALS
- INNOVATIVE COOLING SCHEMES

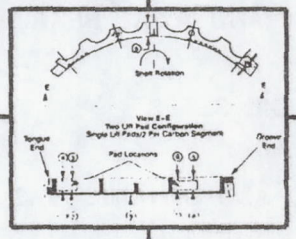

IHPTET/S&T RELIANCE JDL GOALS:

		PH I	PH 2	PH 3
TEMPERATURE (F)		400	600	800
SEAL SPEED (FPS)	S/R:	500	600	750
	C/R:	900	1100	1300
WEIGHT		- 5 %	- 10 %	- 20 %

IHPTET/S&T RELIANCE JDL SYSTEM PAYOFFS:

	PH I	PH II	PH III
TIME ON STATION	+1.8%	+3.0%	+ 6 %
RANGE	+ 2 %	+ 4 %	+ 7 %
PAYLOAD	+ 18 %	+ 35 %	+ 50 %
FN / WT	+5.2%	+11.1%	+25.%

MECHANICAL SYSTEMS PROJECT
LUBE OIL SEALS

TRENTON, NEW JERSEY

SUBSONIC CORE HIGH SPEED AIR/OIL SEAL

CONTRACTOR: PRATT & WHITNEY

COST: $ 430 K

OBJECTIVE: DEVELOP SHAFT-TO-GROUND SUMP SEAL SYSTEMS FOR IHPTET PHASE II CONDITIONS THAT MINIMIZE LEAKAGE, GIVE FULL LIFE.

GOALS:

- PHASE II CONDITIONS:
  - 600 FPS
  - 60 PSID
  - FULL LIFE
  - 750 F AIR
  - 400 F OIL

MECHANICAL SYSTEMS PROJECT
LUBE OIL SEALS

TRENTON, NEW JERSEY

APPROACH:
- ANALYTICALLY ASSESS MULTIPLE SEALS
- DETAIL DESIGN AND FABRICATE THE TWO BEST CANDIDATE SEALS
- 25 HRS OPERABILITY EACH, REVISE
- ENDURANCE TESTING

TECHNOLOGIES:
- HYDRODYNAMIC LIFT ASSIST (STEIN)
- ULTRA-LIGHTWEIGHT DESIGN (REXNORD)
- IMPROVED PACKAGING / COOLING

ADVANCEMENT BEYOND SOA:
- ORDER OF MAGNITUDE LEAKAGE REDUCTION RELATIVE TO LAB SEALS (.1% SFC PER)
- 30% SPEED CAPABILITY INCREASE

MECHANICAL SYSTEMS PROJECT

TRENTON, NEW JERSEY

STEIN HYDRODYNAMIC CIRCUMFERENTIAL NON-CONTACTING SEGMENTED SEAL

PROS:
- EXTENSION OF SUCCESSFUL SEGMENTED RING SEAL
- LOW LEAKAGE
- WEAR TO 6 MILS O.K.
- LIGHTWEIGHT
- WINDBACK ALLOWS MINIMUM LEAKAGE AND CONTAMINATION

CONS:
- MINIMAL EXPERIENCE WITH HYDRODYNAMIC LIFT GEOM. IN CARBON BORE.
- THERMAL CONEING AND MISALIGNMENT CONCERNS

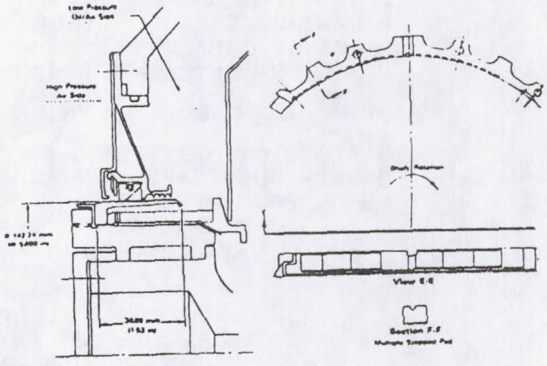

REXNORD CARTRIDGE-TYPE CONTACTING FACE SEAL

PROS:

- VERY LIGHTWEIGHT LOW DRAG DESIGN IMPROVES SPEED CAPABILITY.
- TOLERANT TO CONEING AND MISALIGNMENT.
- LOW TO MOD. LEAKAGE
- LOW OPERATING LOADS IMPROVE LIFE

CONS:

- NUMEROUS PARTS
- NARROW CARBON NOSE PRESENTS HANDLING DAMAGE RISK
- POSSIBLE LEAKAGE AT VERY LOW DELTA P's

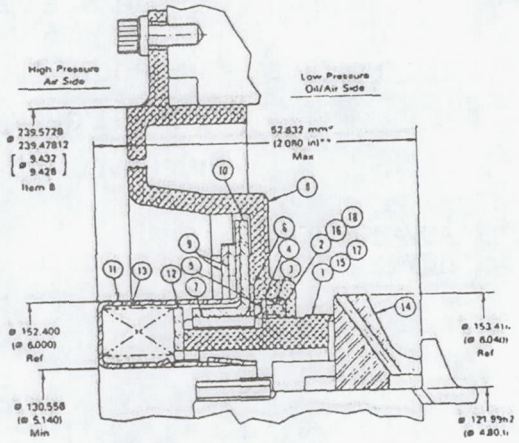

MECHANICAL SYSTEMS PROJECT

LUBE OIL SEALS

TRENTON, NEW JERSEY

STATUS:

- PHASE I OPERABILITY EVAL COMPLETE
  - MIXED RESULTS

- STEIN HYDRODYNAMIC CIRCUMFERENTIAL SEAL:
  - STATIC CAL DONE, VERY LOW LEAKAGE
  - RAN SUCCESSFULLY TO 600 FPS, 60 PSID !
  - LEAKGE CONSISTENTLY LOW, THEN -
    - BROKE EXTENSION SPRING - EASY FIX IN HAND

- REXNORD CARTIDGE-TYPE FACE SEAL:
  - STATIC CAL COMPLETED (INITIAL SEC. SEAL PROB)
  - VERY SUCCESSFUL THROUGH TWO DYNAMIC TESTS TO 600 FPS, 60 PSID !
    - ** LEAKAGE TOOK OFF, SEAL FAILED
      - INVESTIGATION IN PROGRESS.

SUMMARY:

- MINOR REVISIONS TO STEIN SEAL, HIGH CONFIDENCE FOR ENDURANCE PHASE
- ASSESSMET OF REXNORD SEAL IN PROGRESS, ENDURANCE PROSPECTS TBD
- HAVE SHOWN STABLE LOW LEAKAGE OPERATION AT AGGRESSIVE GOAL CONDITIONS FOR BOTH.

MECHANICAL SYSTEMS PROJECT
TASK 3: STATIC & DYNAMIC GAS PATH SEALS

TRENTON, NEW JERSEY

FLEET ISSUES ADDRESSED:

- INCREASED ENDURANCE FOR EXTENDED COVERAGE FOR ASW/ASUW/AEW/EW/C3/DRUG MISSIONS
- INCREASED STANDOFF RANGE FOR POWER PROJECTION ASHORE
- HIGH PERFORMANCE ENGINES FOR EMERGING SYSTEM REQUIREMENTS (AX, NATF, ASTOVL, SSF)
- IMPROVED LIFE CYCLE COST THROUGH IMPROVED RELIABILITY
- IMPROVED A/C AVAILABILITY

TECHNOLOGIES:

- FILM-RIDING FACE SEALS:
  - HYDRODYNAMIC, HYDROSTATIC
- BRUSH / FIBER SEALS
- ABRADABLE SEALS

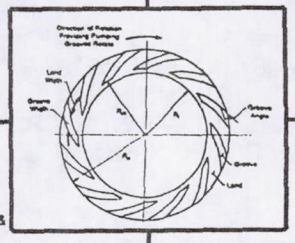

GOALS:

- NO FORMAL IHPTET GOALS, CONTRIBUTES TO COMPRESSOR & TURBINE GOALS.

	PH 1	PH 2	PH 3
TEMPERATURE (F)	800	900	1200
SPEED (FPS)	700	850	1200
WEIGHT	- 5 %	- 10 %	- 20 %

IHPTET/S&T RELIANCE JDL SYSTEM PAYOFFS:

	PH I	PH II	PH III
TIME ON STATION	+1.8%	+3.0%	+ 6 %
RANGE	+ 2 %	+ 4 %	+ 7 %
PAYLOAD	+ 18 %	+ 35 %	+ 60 %
FN / WT	+5.2%	+11.1%	+25.%

MECHANICAL SYSTEMS PROJECT
GAS PATH SEALS

TRENTON, NEW JERSEY

HIGH PERFORMANCE CD FILM-RIDING FACE SEAL

CONTRACTOR: ALLISON

CONTRACT NO.: N00140-39-C-2728

COST: $460 K

OBJECTIVE: DEVELOP/DEMO FILM RIDING CD FACE SEAL° FOR VERY HIGH PRESSURE RATIO PHASE II ENGINES.

GOALS:
- 1200 F AIR
- 800 FPS
- 600 PSID

MECHANICAL SYSTEMS PROJECT
GAS PATH SEALS

TRENTON, NEW JERSEY

APPROACH: APPLY FILM-RIDING FACE SEAL CONCEPT TO PM II C.D. APPLICATION, USING IMPROVED DESIGN ANALYTICS, IMPROVED MATERIALS ASSESS MULTIPLE LIFT FEATURES, FABRICATE & TEST

TECHNOLOGIES:
- TRANSIENT DYNAMIC FILM ANALYSIS
- SPIRAL GROOVE & RAYLEIGH PAD LIFT GEOMETRIES
- SILICON CARBIDE PRIMARY RING
- IMPROVED PRESSURE BALANCE

ADVANCED BEYOND SOA: REPLACES MULTIPLE LABYRINTH STAGES AT OVER AN ORDER OF MAGNITUDE LESS LEAKAGE

MECHANICAL SYSTEMS PROJECT

TRENTON, NEW JERSEY

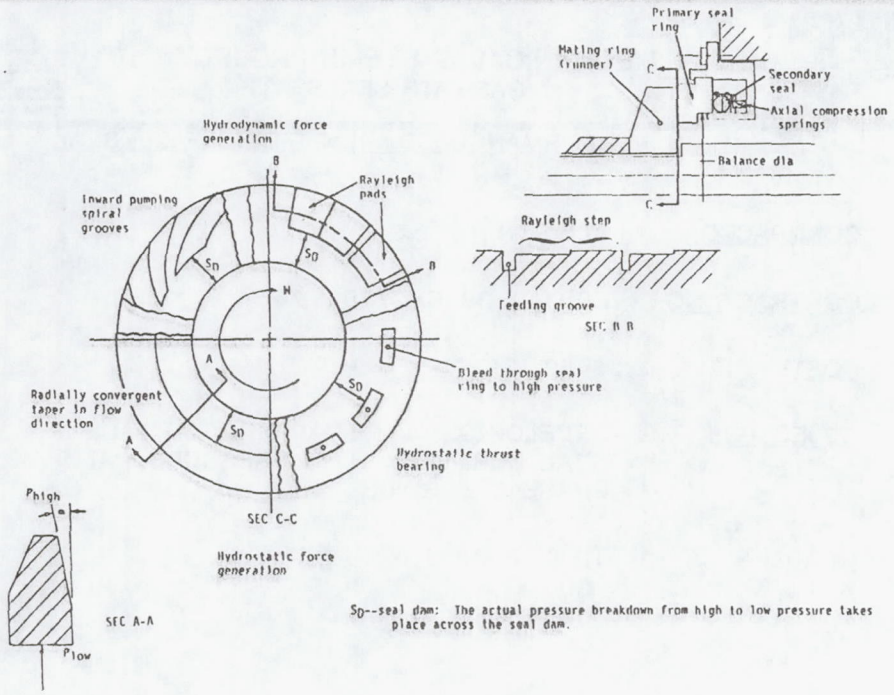

S_D--seal dam: The actual pressure breakdown from high to low pressure takes place across the seal dam.

MECHANICAL SYSTEMS PROJECT
GAS PATH SEALS

TRENTON, NEW JERSEY

TRANSITION/
APPLICATION:

* PHASE II JTAGG
* APPLICABLE TO ANY HIGH PRESSURE RATIO MACHINE

PAYOFFS:

* SIGNIFICANT CYCLE EFFICIENCY BENEFITS
  + 0.5 % THROUGH REDUCED LEAKAGE

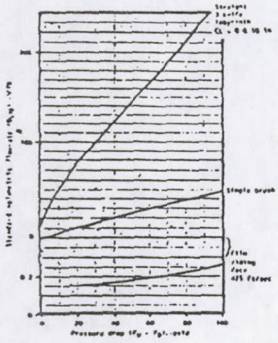

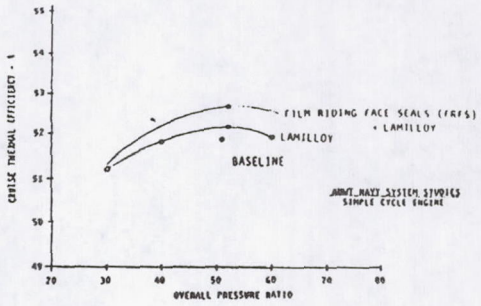

MECHNICAL SYSTEMS PROJECT
GAS PATH SEALS

TRENTON, NEW JERSEY

PROGRESS/STATUS:

•FABRICATION OF BOTH SEALS COMPLETE

•STATIC CAL. TESTING OF BOTH SEALS COMPLETE
  •VERY LOW LEAKAGE

•DURING EVALUATION OF CRANE SEAL - RIG INDUCED RUB OCCURRED - SEAL OK; REWORKABLE

•KAYDON SECONDARY SEAL FAILURE OCCURRED AWAITING REVISED HARDWARE

GAS SEAL CODE DEVELOPMENT AND ANALYSIS

P. Basu
EG&G

1. Developed opening force versus film thickness curves (F-h curves) at ID (hi) at different speeds for a given set of OD and ID pressures. The constant closing force line intersects each one of the above curves at the corresponding operating point. The slope of a F-h curve at the operating point gives that average film stiffness. (Fig. 1)

2. Developed film thickness profile along the interface at the operating point for a given combination of speed and pressure. This curve combined with the corresponding stiffness value would enable the designer to know whether the seal is operating with a safe and stable film at that speed and pressure. (Fig. 2)

3. Developed the operating film thickness (hi) versus system pressures for different speeds. This family of curves presents the operating film level over the entire envelope of operation in one picture. Hence, an unsafe operation at any off-design condition will become evident. (Fig. 3)

4. Developed leakage versus system pressure curves for different speeds. This family of curves is the most useful one for the purpose of correlating the experimental data with the code prediction. (Fig. 4)

5. Additionally, the code provides the pressure and Mach number distributions along the interface that are printed on a file for each operating point.

6. Seal distortion

   Since the seal face distortions are of the same order of magnitude as the average operating film thickness, the code iteratively determines the distortions using a finite element module. (Ref. 1)

7. Design

   A figner spring installed in a groove beneath the SiC inner diameter allowed for differential thermal expansion between retainer and seal ring while keeping the ring centered. Round smooth wire bent into shape to give centering force between rotating seal ring and the retainer. Also used to mount retainer on the shaft to accommodate centrifugal growth.

   Antimony impregnated carbon graphite stator ring is used. This provides high compressive strength and stability:

   The seals are designed to run with a very thin operating film (3-4 μm) to minimize leakage and maximize film stiffness.

For more information

1. Gardner, J., Basu, P., Muraki, R. (1992), Analysis, Design, Laboratory Testing of a High Pressure, High Speed, Reduced Axial Length Gas Seal, Proceedings of the 13th International Conference on Fluid Sealing.

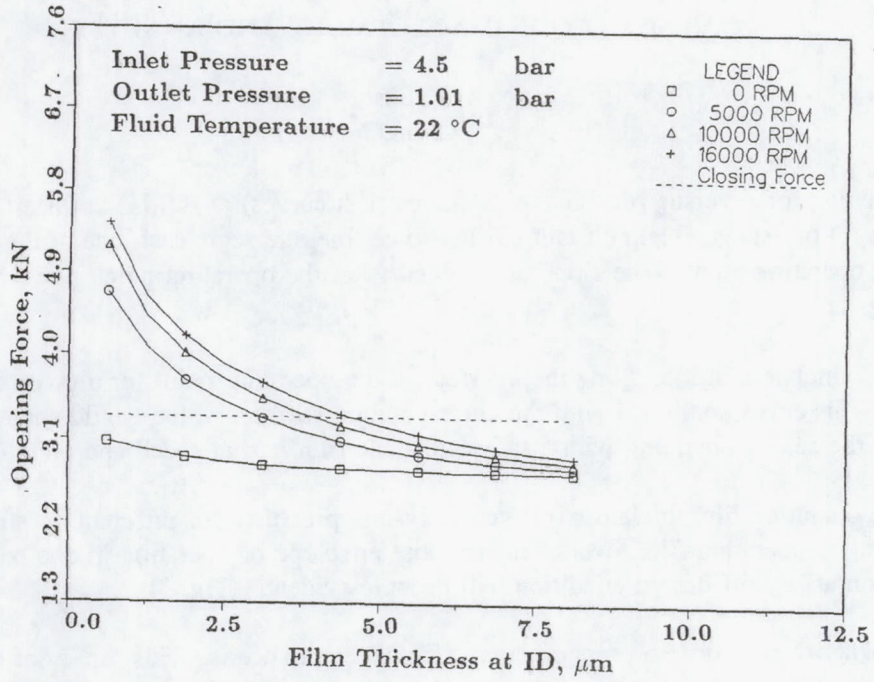

Figure 1. 'F-h' Curves

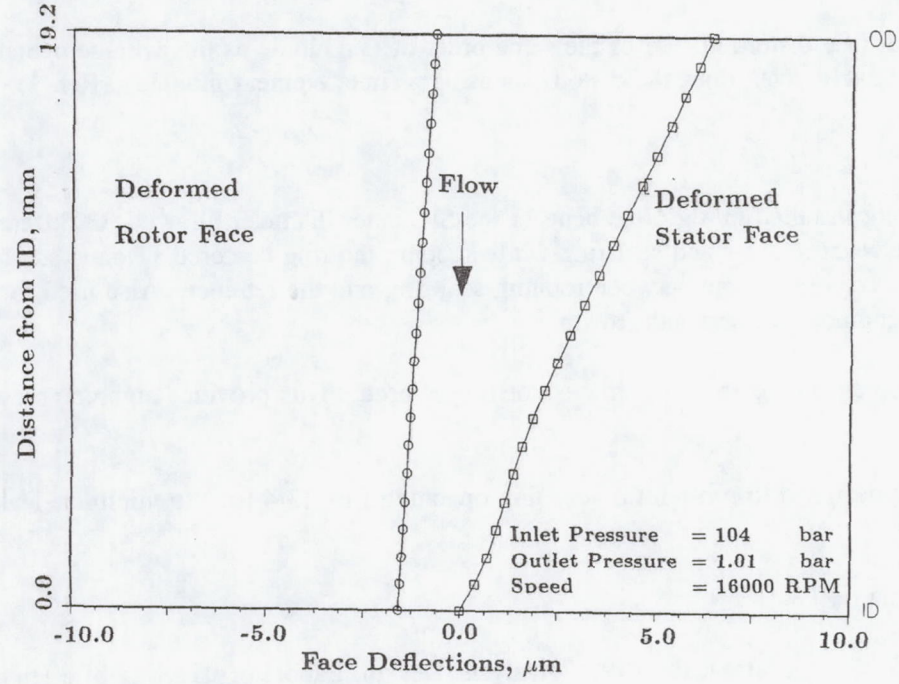

Figure 2. Film Thickness Profile

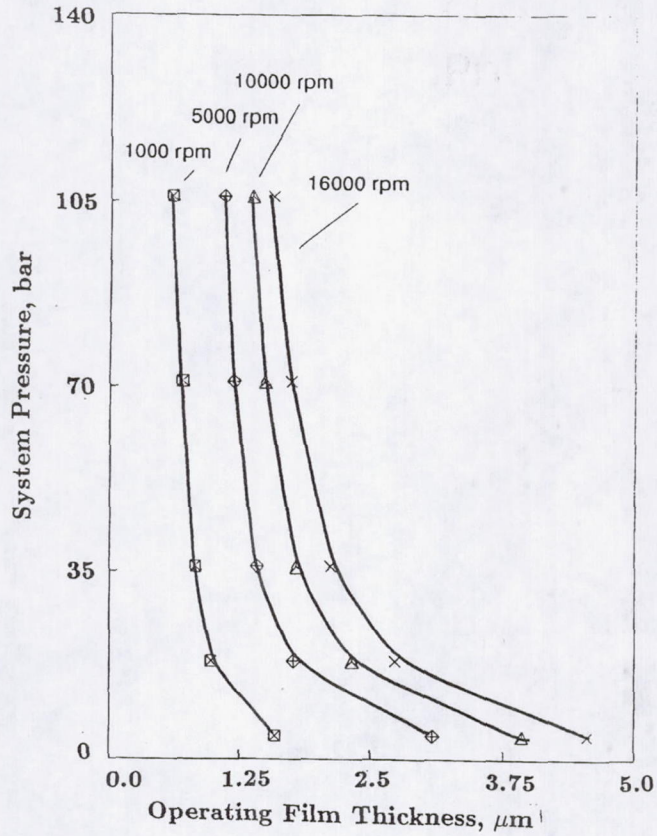

Figure 3. System Pressure versus Operating Film Thickness Plots

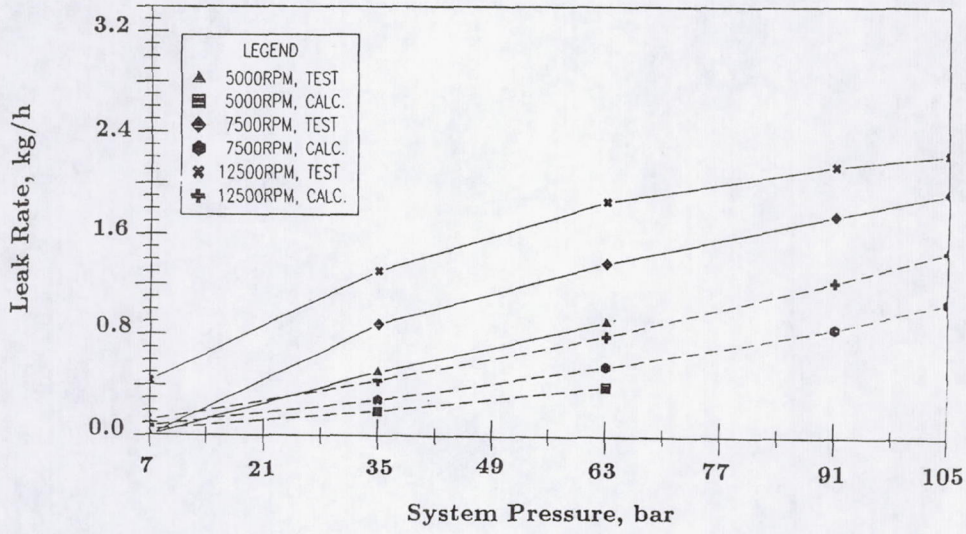

Figure 4. Leakage Correlation

Compliant Seal Development

From notes and discussion of talk by J. Gardner, EG&G
by R.C. Hendricks

The compliant metallic seal combines the noncontact feature of the labyrinth seal, the low leakage of a mechanical seal, and the compliant nature of the brush seal. It consists of several thin metallic elements or leaves mounted within a ring which is press fit into the housing, and in form, sort of resembles a lip seal sections wiping the shaft. A second set of overlapping cover leaves are placed on top of the shaft riding leaves which reduces leakage and provides stiffness. The leaves can be straight or angle cut. The shaft riding fingers are designed with mismatched curvature to provide lift off similar to the Rayleigh lift pads in mechanical seals with leading edge clearances nearly twice those of the trailing edge as shown by Fleming to be optimal for gas flows in convergent seal passages. Leading edge clearances range from 300 to 500 microinches.

Balance pockets beneath the leaves provide fluid film feed to the "Rayleigh lift" surface and the proper balance ratio (mechanical seal) when combined with the static pressure and film pressure. The leaves flex in the radial direction and accomodate thermomechanical behavior as well as axial motion and angular mialignment.

In the static mode, there is a net closing force on the leaves.

The seals were tested to 70 psi at speeds to 16,000 rpm or surface speeds to 330 fps and temperatures from ambient to 440F. A slow cycle through the rig critical at 10,000 rpm induced a radial vibration response of 0.004 to 0.005 inch were accomodated by the seal.

Preliminary performance data are encouraging demonstrating hydrodynamic liftoff and non contacting operation at pressure and speeds typical of gas turbine engines. The leakage performance data are significantly better than commerical labyrinth and brush seals which should be expected as this design incorporates the features of the low leakage face or mechanical seal along with the flexibility of the brush configuration.

For more information

1. Gardner, J., Basu, P., and Datta, A.: A New Compliant Seal Concept for Aerospace Applications, Fourth Int. Symp. on Transport Phenomena and Dynamics of Rotating Machinery (ISROMAC-4), Vol. A, April 5-8, 1992, Honolulu, Hawaii, Sponsored by Pacific Center of Thermal-Fluid Engineering.

FIGURE 1

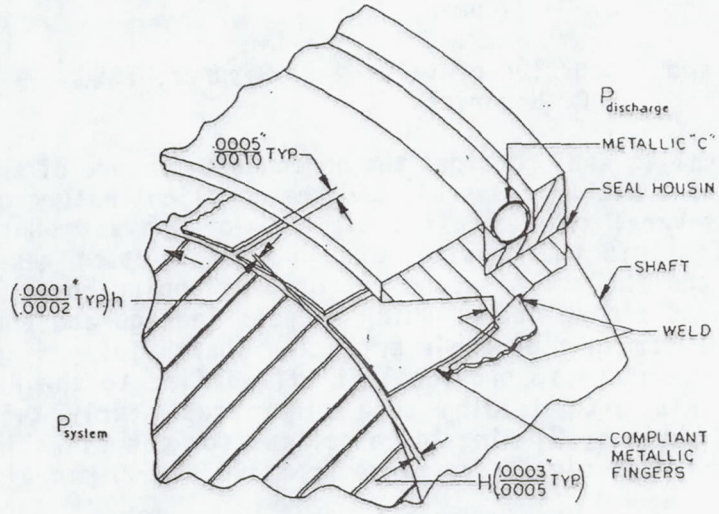

COMPLIANT METALLIC HYDRODYNAMIC SHAFT GAS SEAL

Typical Pressure Distribution for Straight Cut Compliant Seal without Slot Cover

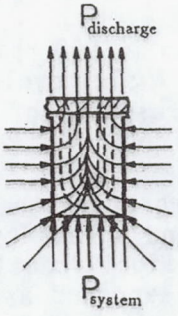

dotted lines represent lines of constant pressure between the shaft the underside of the compliant metallic members

solid lines represent the direction of the flow field

Figure 2a

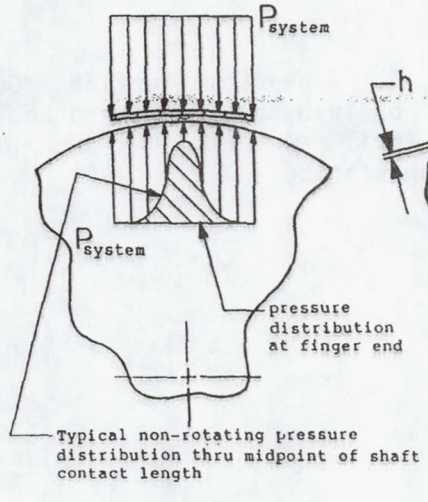

Figure 2b

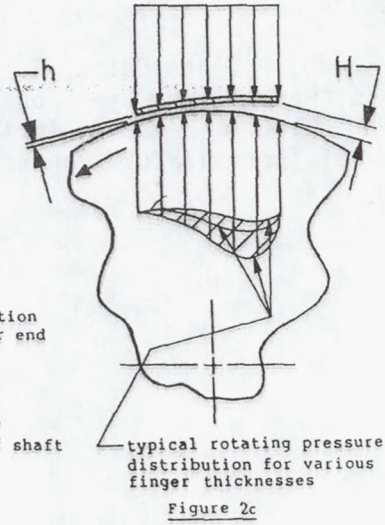

Figure 2c

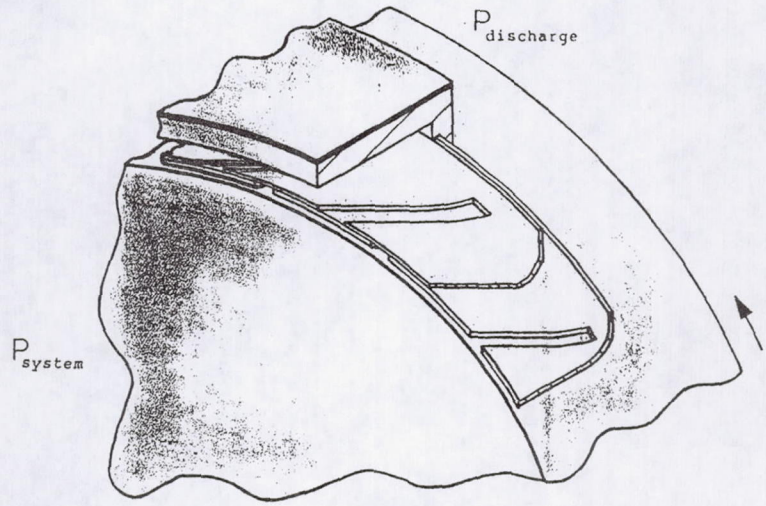

Angle Cut Compliant Seal with Slot Cover

Figure 3

Straight finger Compliant Seal with Rayliegh Pads and Slot Cover

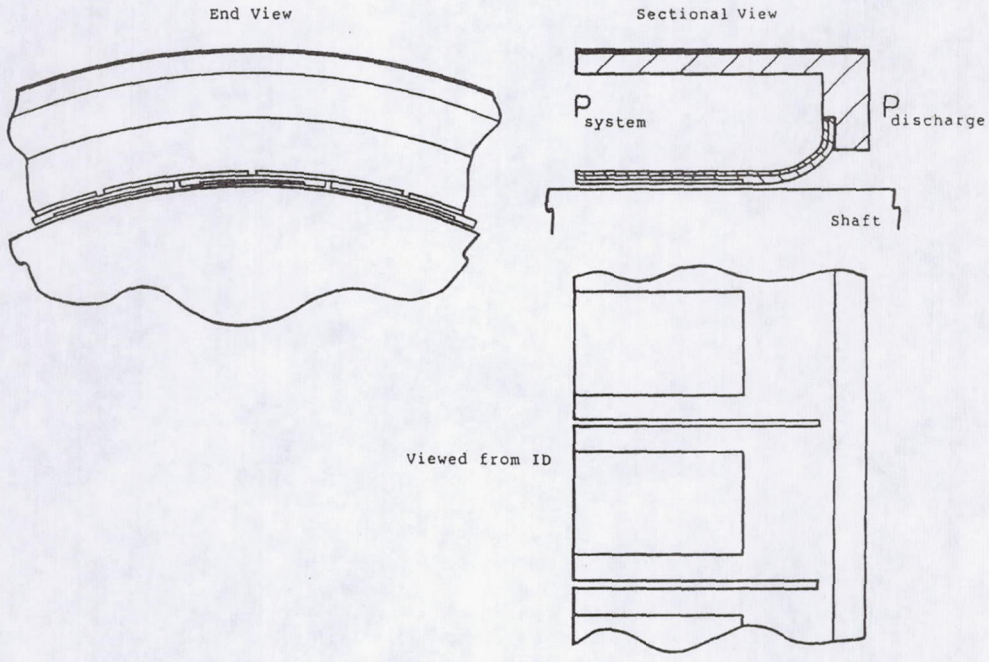

Figure 4

ACTIVELY CONTROLLED SHAFT SEALS FOR AEROSPACE APPLICATIONS

Richard F. Salant and Paul Wolff
School of Mechanical Engineering
Georgia Institute of Technology
Atlanta, Georgia 30332

NASA Research Grant NAG 3-974
NASA Technical Officer: M. P. Proctor

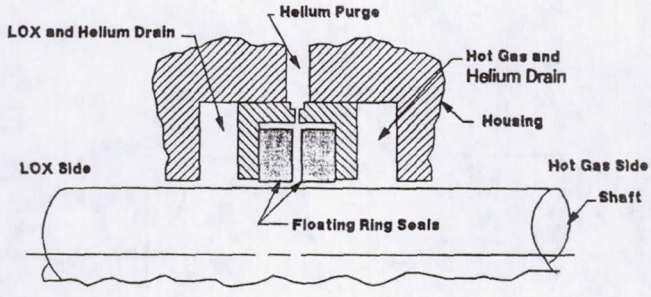

Helium Purge Assembly

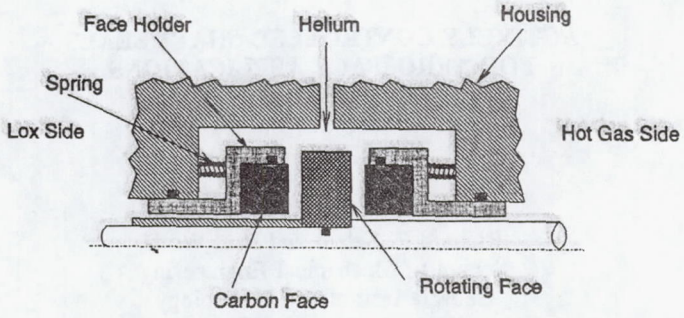

CONVENTIONAL MECHANICAL SEAL

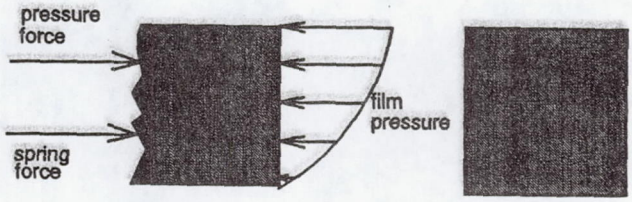

FLOATING FACE FIXED FACE

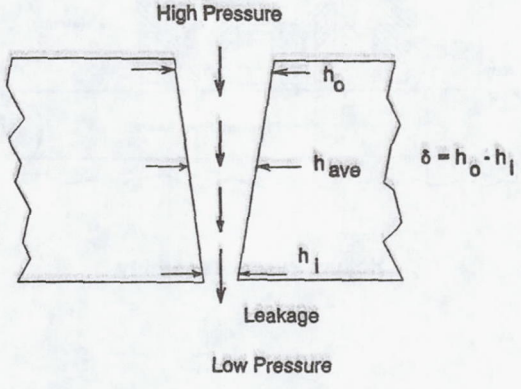

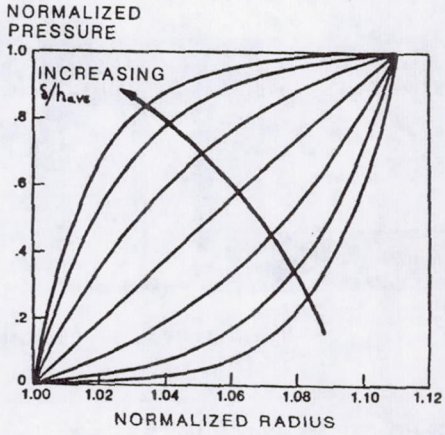

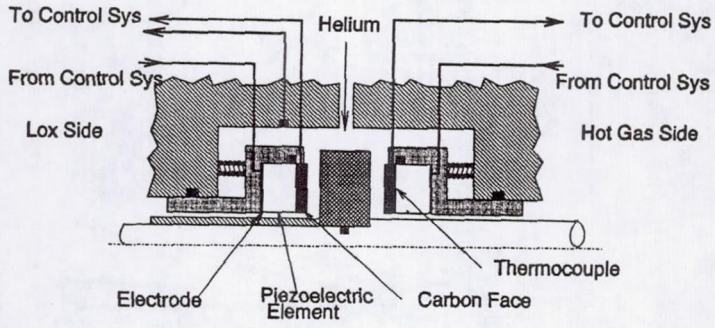

CONTROLLABLE SEAL

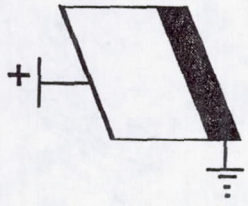

CONED DEFORMABLE FACE ASSEMBLY

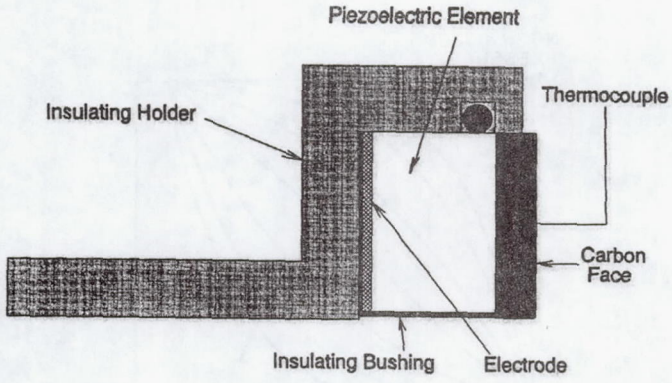

FACE HOLDER AND DEFORMABLE FACE ASSEMBLY

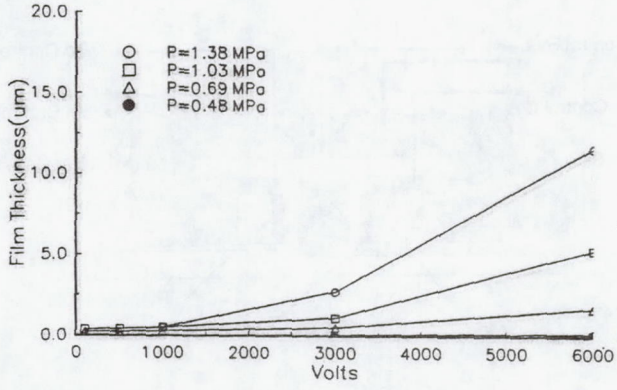

Variable Pressure Operation

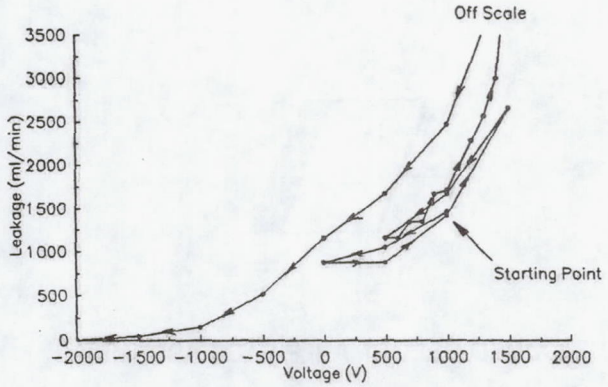

Leakage versus Voltage – Static Test

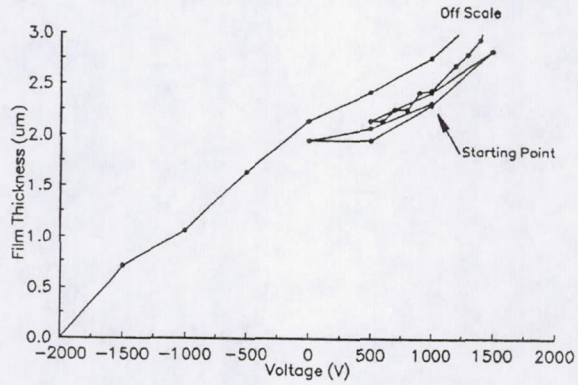

Film Thickness versus Voltage – Static Test

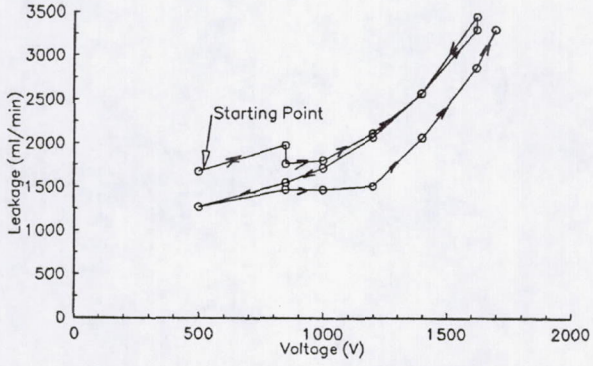

Leakage versus Voltage – Rotating Test

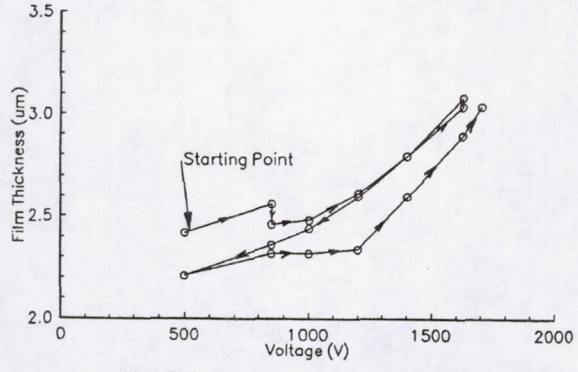

Film Thickness versus Voltage – Rotating Test

EXPERIMENTAL AND ANALYTICAL INVESTIGATION OF BRUSH SEALS

M.J. BRAUN
Professor

V.V. KUDRIAVTSEV
Visiting Scientist

NASA grant NAG 3-969

Project Manager: Mr. George Bobula
Vehicle Propulsion Directorate
US Army, MS 77-12

OBJECTIVES OF THE PRESENTATION:

- Report on the status of the project
- Discussion that will broaden your research and and help to interpret results

OBJECTIVES AND ACCOMPLISHMENTS

- Develop verified family of CFD codes for Analyzing Brush Seals

  -idealized(uncompliant) 2D configuration \/
  -compliant 2D geometry not
  -compliant 3D not

- Experimental Facilities for the adequate code verification

  -stationary bristles(cylinders) \/
  -moving bristles not

  additional experiments were designed specifically for code validation and investigation of features to be incorporated in the computer program

- Qualitative and quantitative analyses of the Fluid Flow in the Brush Seal Configuration

  -flow around one bristle, level 1 \/
  -flow around several bristles, level 2 \/
  -flow in the deep tube bundles, level 3 \/
  (intermediate pitch-to-diameter ratio)

  -flow through uncompliant brush prototypes, level 4 \/
  (small pitch-to-diameter ratio)

PRESENT CODE CHARACTERISTICS

- finite-difference primary variables (u,v,p) formulation
- collocated grid
- conservative formulation of the momentum equations
- conservative formulation of the pressure equation
- conservative fully populated of the boundary conditions
- steady-state solutions
- transient solutions
- 2nd and 3rd order convective schemes are implemented
- implicit under/over relaxation (if necessary, optional)
- accommodates an arbitrary geometrical configuration in Cartesian coordinates(non-contiguous boundaries)
- regular and nonregular grid
- graphical post-processor capabilities with PV-Wave (Unix)

MODEL ASSUMPTIONS:

- incompressible fluid, constant properties
- isothermal model
- leakage flow
  - $M < 0.3$
  - Re (low, intermediate)
- no shaft rotation
- stationary bristles

DETERMINED FLOW RESISTANCES THROUGH THE BRUSH SEAL

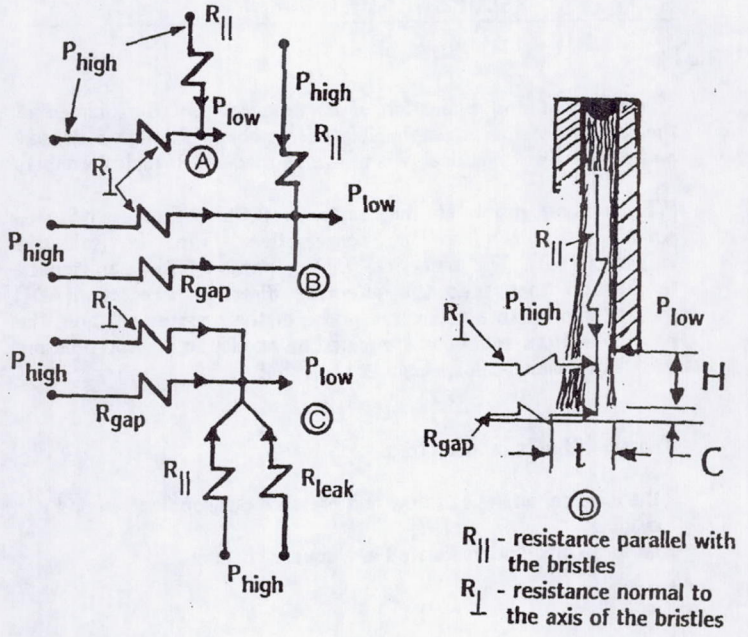

$R_{||}$ - resistance parallel with the bristles

$R_{\perp}$ - resistance normal to the axis of the bristles

3D VIEW OF THE LINEAR BRUSH IN THE CHANNEL

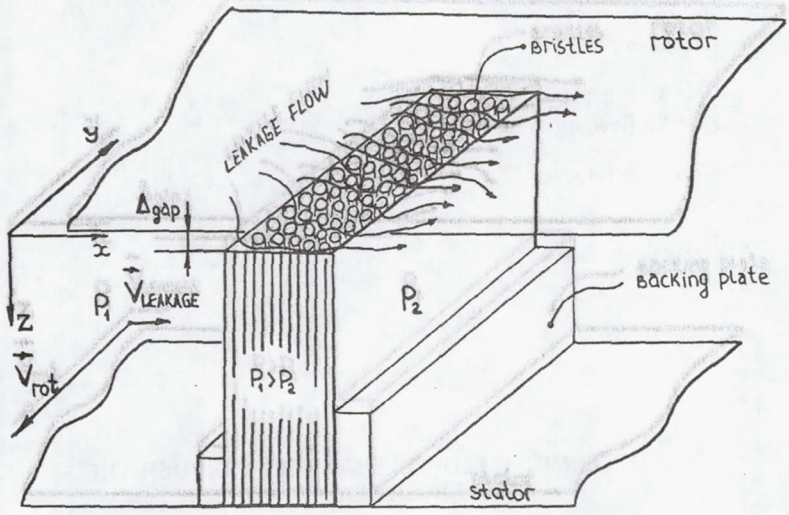

SCOPE OF THE WORK

- development and evaluation of a numerical procedure aimed at the solution of the incompressible flow problem through a densely packed array of cylindrical pins at low to medium Reynolds numbers

[The method promotes the solution of the 2-D Navier-Stokes equations written in a conservative form in primitive variables(u,v,p). The numerical implementation follows an implicit formulation that uses the alternate direction integration(ADI) method applied to a collocated grid. For the pressure solution, the two momentum equations are joined by an elliptic Poisson pressure equation(Roache, 1981, Ghia et al., 1983).]

The algorithm is applied to:

- the classical analysis of flow and pressure development around a cylinder
- an array of cylinders located in a square channel

- flow and pressure patterns are discussed parametrically with respect to the variation of the Reynolds number.

$$\frac{\partial U}{\partial T}+\frac{\partial(UU)}{\partial X}+\frac{\partial(UV)}{\partial Y}=-\frac{\partial P}{\partial X}+\frac{1}{Re}\left(\frac{\partial^2 U}{\partial X^2}+\frac{\partial^2 U}{\partial Y^2}\right)$$

$$\frac{\partial V}{\partial T}+\frac{\partial(VV)}{\partial Y}+\frac{\partial(UV)}{\partial X}=-\frac{\partial P}{\partial Y}+\frac{1}{Re}\left(\frac{\partial^2 V}{\partial X^2}+\frac{\partial^2 V}{\partial Y^2}\right)$$

$$\frac{\partial U}{\partial X}+\frac{\partial V}{\partial Y}=0$$

Taking the divergence of the X- and Y-momentum equations, and using continuity for simplification, one obtains a pressure equation that appears under a Poisson type format(Roache, 1981).

$$\nabla^2 P=-\frac{\partial^2(U^2)}{\partial X^2}-2\frac{\partial^2(UV)}{\partial X\partial Y}-\frac{\partial^2(V^2)}{\partial Y^2}+$$

$$+\left\{\frac{\partial D}{\partial T}+\frac{1}{Re}\left(\frac{\partial^2 D}{\partial X^2}+\frac{\partial^2 D}{\partial Y^2}\right)\right\}$$

D is the dilation term, $D=\frac{\partial U}{\partial X}+\frac{\partial V}{\partial Y}$.

During calculations, D represents the residual that has to shrink to zero if continuity is to be satisfied.

Boundary and Initial Conditions for the Momentum Equation.

⋆The boundary conditions on the lateral solid walls assume non-slip conditions and non-porous walls.

⋆The inflow velocity is uniform with U=1, and V=0(angle of incidence is zero). A reference pressure is assigned to one point on the inflow boundary.

Special Form of Open Boundary Condition(Exit Flow)

(i) the satisfaction of the continuity equation(specifically in the direction of the U velocity),

$$\frac{\partial U}{\partial X}=-\frac{\partial V}{\partial Y}$$

(ii) the condition for fully developed velocity gradient for the vertical component

$$\frac{\partial V}{\partial X}=0$$

(iii) satisfaction of the momentum equation(in the direction of U velocity)

$$\frac{\partial P}{\partial X}=-\left[\frac{\partial(UU)}{\partial X}+\frac{\partial(UV)}{\partial Y}\right]+\frac{1}{Re}\left(\frac{\partial^2 U}{\partial X^2}+\frac{\partial^2 U}{\partial Y^2}\right);$$

Boundary Conditions for the pressure Poisson Equation

★ The dynamic pressures P, are determined from the balance of the normal forces with the inertia and viscous forces. The effects of the terms $\frac{\partial U}{\partial T}$ and $\frac{\partial V}{\partial T}$ both at inflow and outflow boundaries have been considered negligible. The following formulation is totally independent of the internal boundary configuration, and thus applicable with no restrictions.

$$\frac{\partial P}{\partial X} = -\left[\frac{\partial (UU)}{\partial X} + \frac{\partial (UV)}{\partial Y}\right] + \frac{1}{Re}\left(\frac{\partial^2 U}{\partial X^2} + \frac{\partial^2 U}{\partial Y^2}\right);$$

On the non-contiguous internal boundaries of the pins, in addition to previous equation, one needs to add an expression for $\frac{\partial P}{\partial Y}$

$$\frac{\partial P}{\partial Y} = -\left[\frac{\partial (UV)}{\partial X} + \frac{\partial (VV)}{\partial Y}\right] + \frac{1}{Re}\left(\frac{\partial^2 V}{\partial X^2} + \frac{\partial^2 V}{\partial Y^2}\right)$$

At the channel's upper and lower walls the pressure boundary condition takes a simplified form due to the fact that U=V=0

$$\frac{\partial P}{\partial Y} = \frac{1}{Re}\left(\frac{\partial^2 V}{\partial Y^2}\right)$$

Initial conditions(T=0). The input velocities are given as U=1, V=0. The pressures are set initially to an arbitrary and operator chosen constant ($P=P_{ref}$=const).

NUMERICAL IMPLEMENTATION : ADI METHOD

• The discretization of the system of governing equations introduced above, follows the use of the ADI applied to a collocated grid. The procedure uses the full direct approximation of each term within the differential equation on every half time step, $\Delta\tau/2$. One obtains the following system of linear algebraic equations.

$$\frac{u^{n+1/2}-u^n}{\Delta\tau/2} = \frac{1}{Re}\left[A_{xx}(u)^{n+1/2} + A_{yy}(u)^n\right] + C_x(u)^{n+1/2} + C_y(u)^n + Q_x(p)^n$$

$$\frac{u^{n+1}-u^{n+1/2}}{\Delta\tau/2} = \frac{1}{Re}\left[A_{xx}(u)^{n+1/2} + A_{yy}(u)^{n+1}\right] + C_x(u)^{n+1/2} + C_y(u)^{n+1} + Q_x(p)^n$$

$$\frac{v^{n+1/2}-v^n}{\Delta\tau/2} = \frac{1}{Re}\left[A_{xx}(v)^{n+1/2} + A_{yy}(v)^n\right] + C_x(v)^{n+1/2} + C_y(v)^n + Q_y(p)^n$$

$$\frac{v^{n+1}-v^{n+1/2}}{\Delta\tau/2} = \frac{1}{Re}\left[A_{xx}(v)^{n+1/2} + A_{yy}(v)^{n+1}\right] + C_x(v)^{n+1/2} + C_y(v)^{n+1} + Q_y(p)^n$$

$$\frac{p^{s+1/2,n+1}-p^{s,n+1}}{\sigma} = A_{xx}(p)^{s+1/2,n+1} + A_{yy}(p)^{s,n+1} + Q(u,v)^{n+1}$$

$$\frac{p^{s+1,n+1}-p^{s+1/2,n+1}}{\sigma} = A_{xx}(p)^{s+1/2,n+1} + A_{yy}(p)^{s+1,n+1} + Q(u,v)^{n+1}$$

The spatial derivatives, with the exception of the convection terms and cross-derivatives, are approximated by a second order central finite-difference. For the convection terms the first-order conservative scheme proposed by Torrance(1968) is employed.

Solution Procedure

The solution follows according to the time-dependent alternative-direction method using a tridiagonal matrix elimination. The steps of the solution are as follows:

- solve in the x direction for U velocity at the n+1/2 time step
- solve in the y direction for the U velocity at the n+1 time step
- solve in the x direction for V velocity at the n+1/2 time step
- solve in the y direction for the V velocity at the n+1 time step
- solve the Poisson's pressure equation at the n+1 time step by means of the pseudo-transient method within the set of internal ADI iterations $n_{it}=1,...n_f$, :

(i) in the x direction at the s+1/2 pseudo-time step
(ii) in the y direction at the s+1 pseudo-time step

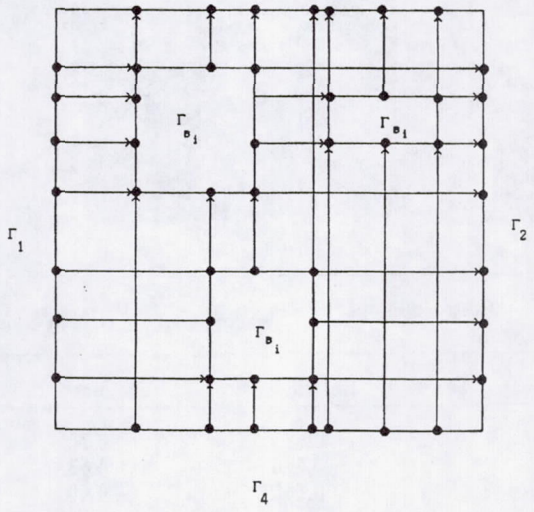

ACCURACY CONSIDERATIONS

- Qualitative comparison of calculated flowfield with experimental results of Bouard and Coutanceau(JFM,v.101, 1980)

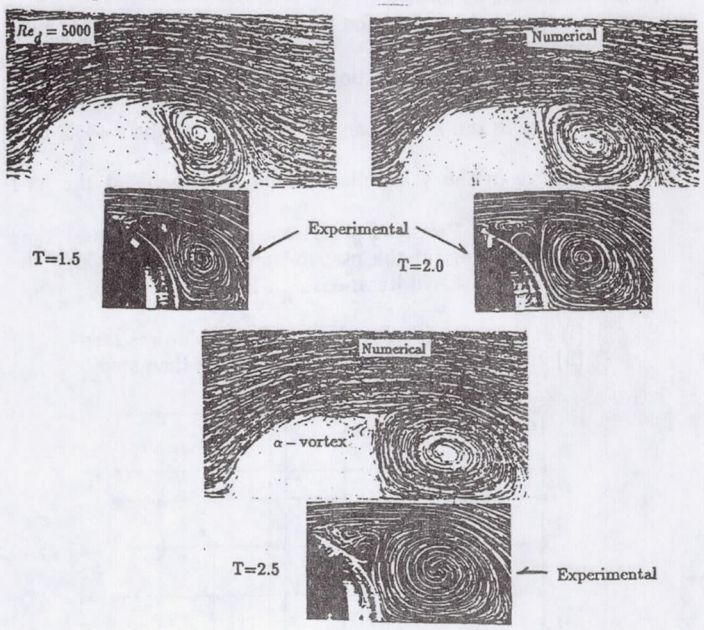

Pressure Drops, $\Delta P = P_{leading\ edge} - P_{trailing\ edge}$

Re_d	this study	Fornberg, 1980
100	0.689	0.70
200	0.670	0.63
300	0.640	0.60

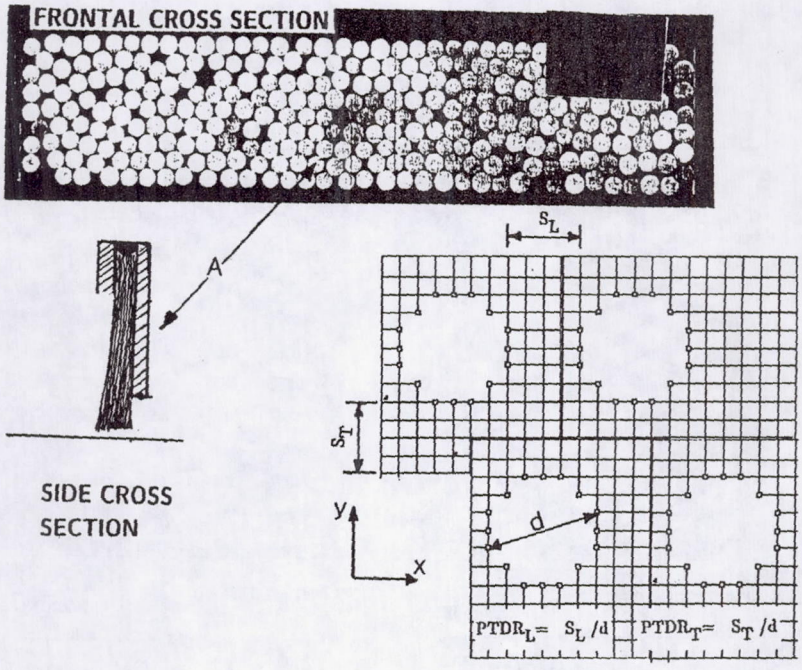

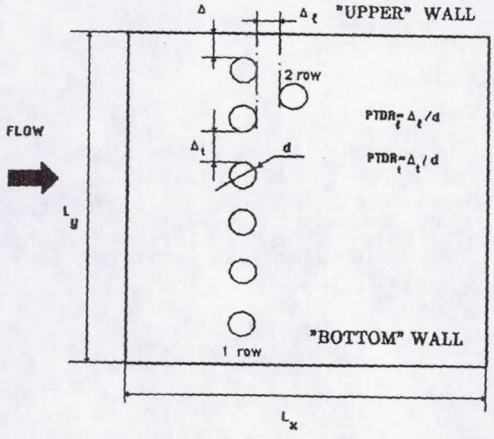

FIG. 1 CHARACTERISTIC CONFIGURATION

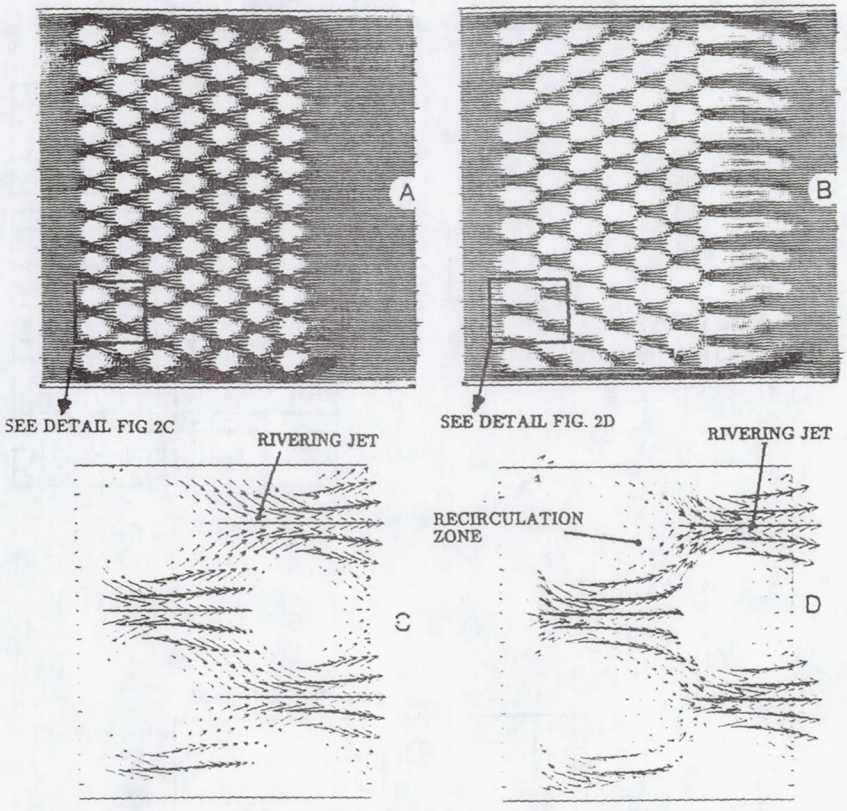

FLOW THROUGH BASIC ARRAY CONFIGURATION 7 ROWS X 11 PINS
A)Re_h=100; B) Re_h=2000:
C)DETAIL OF FLOW IN THE QUADRANT INDICATED IN FIG. 2A
D)DETAIL OF FLOW IN THE QUADRANT INDICATED IN FIG. 2B

PRESSURE MAPS INSIDE TUBES ARRAYS

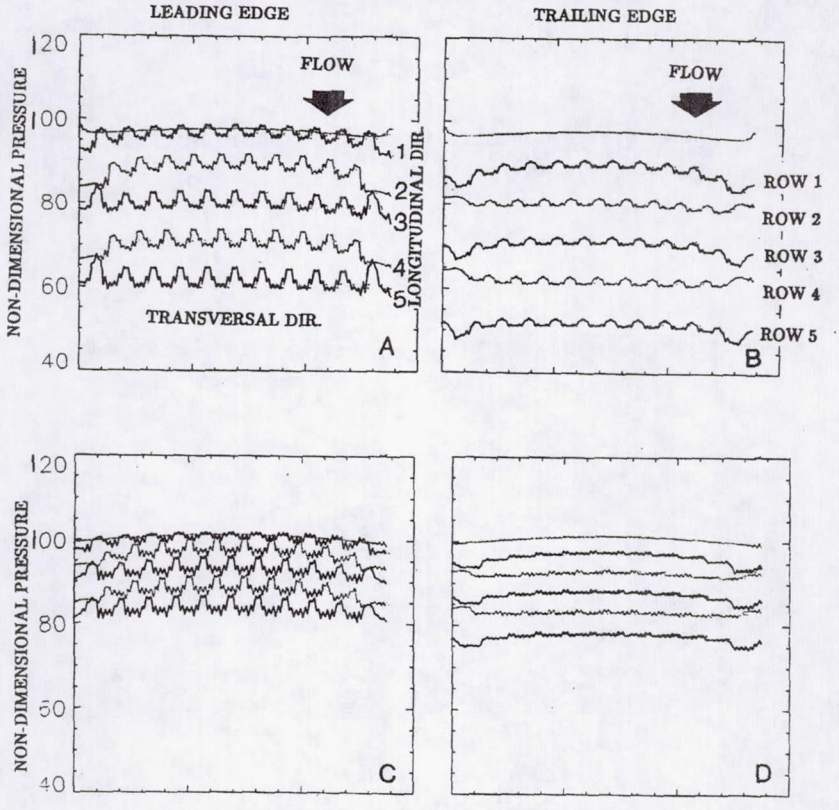

NON-DIMENSIONAL PRESSURE VARIATION IN THE TRANSVERSE DIRECTION
A), C) LEADING EDGE OF THE ROW, AT Re_h=100 AND Re_h=2000
B), D) TRAILING EDGE OF THE ROW, AT Re_h=100 AND Re_h=2000

Deep bank(72) cylinders, Level 3

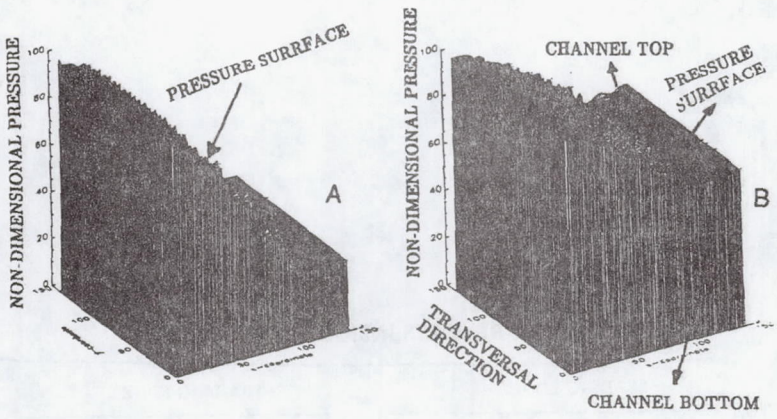

NON-DIMENSIONAL PRESSURE MAPS FOR PRESSURE DROPS IN THE BASIC ARRAY CONFIGURATION(7 ROWS X 11 PINS)
A)Re_h=100; B) Re_h=2000;

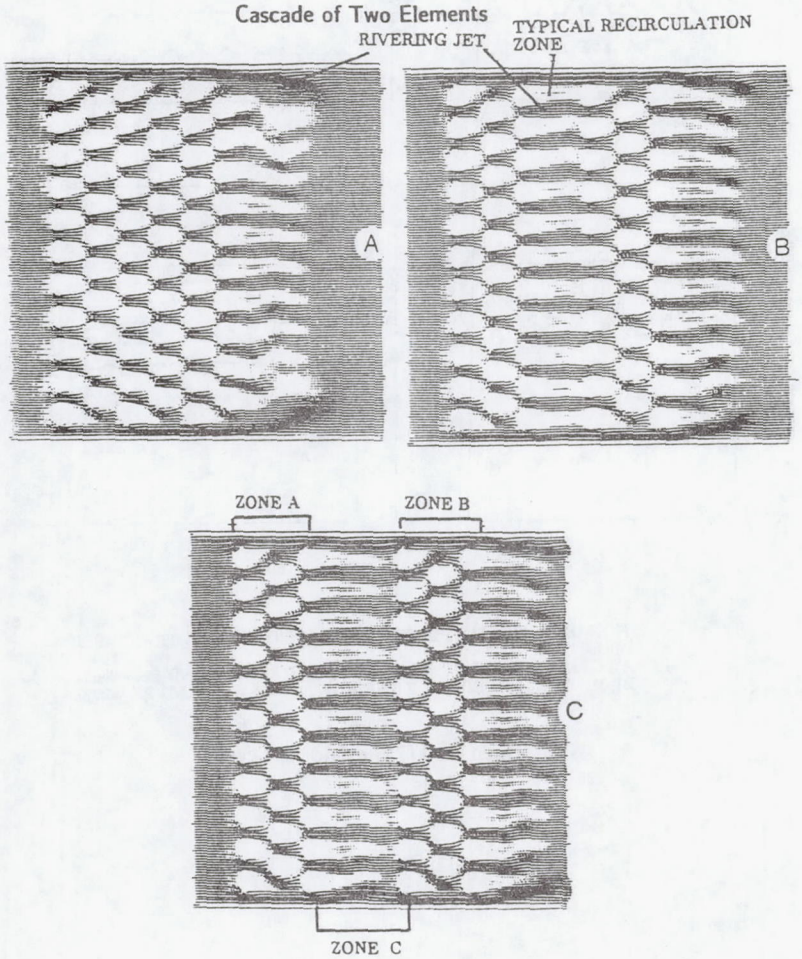

FLOW ACROSS ARRAY OF PINS AT RE_h=2000, $PTDR_L$=1, $PTDR_T$=1
A) SIX ROWS
B) CASCADE OF TWO ELEMENTS(THREE ROWS EACH), C=3d
C) CASCADE OF TWO ELEMENTS(THREE ROWS EACH), C=5d

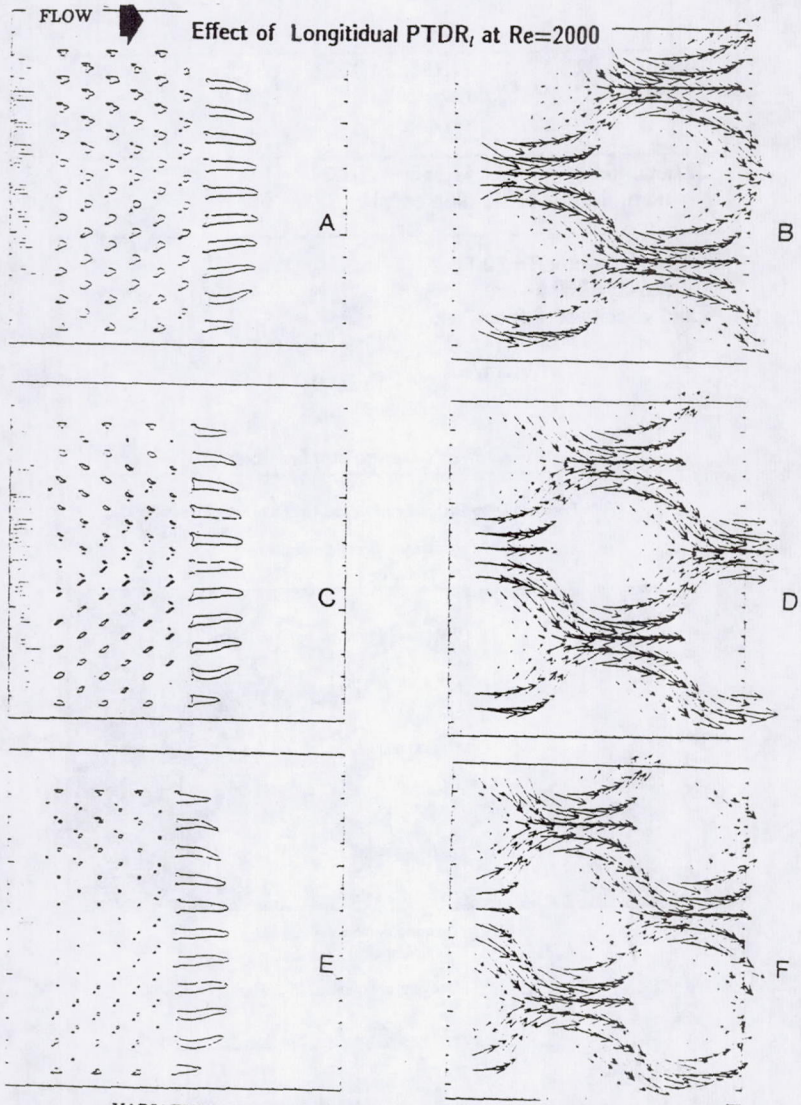

VARIATION OF THE FLOW FIELD STRUCTURE WITH THE CHANGE IN THE LONGITUDINAL PITCH

3 rows of pins

Re	P (psi)	P(Pa)	ρU^2	ΔP(nond)
91.3	2.263	15,602	7.09	2200.
195exp.	4.02	27,758	32.16	863.0
num.	4.31	(7% difference)		926.0
327exp.	6.82	47,056	91.29	516
num.	8.6	(26% difference)		650

Oil temperature: T=70 F
Oil density=950 kg/m^3
Fluid velocities: 8.6 cm/sek
18.5 cm/sek
31.0 cm/sek

Brush Design Applications

Pressure Drop Estimation For the Characteristic Brush Section

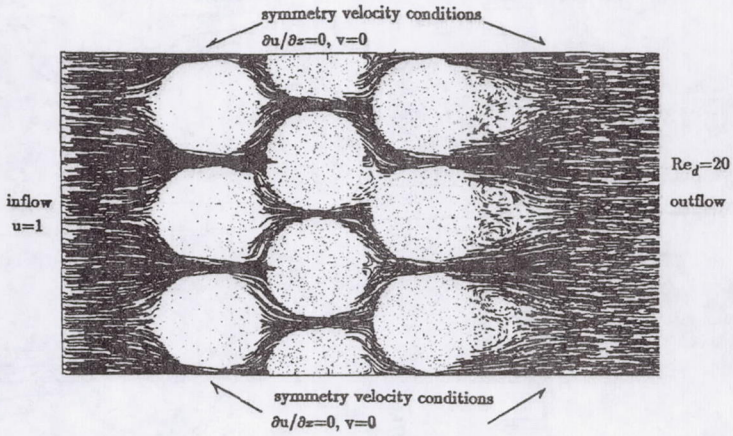

Converged Solution, n_{it}=5000

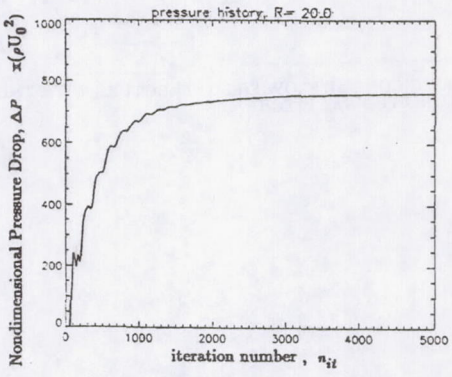

History of the Pressure Drop Convergence, Re_d=20

$PTDR_L$= $PTDR_T$=13.4

Alternative Configuration: Pin Array in the Channel

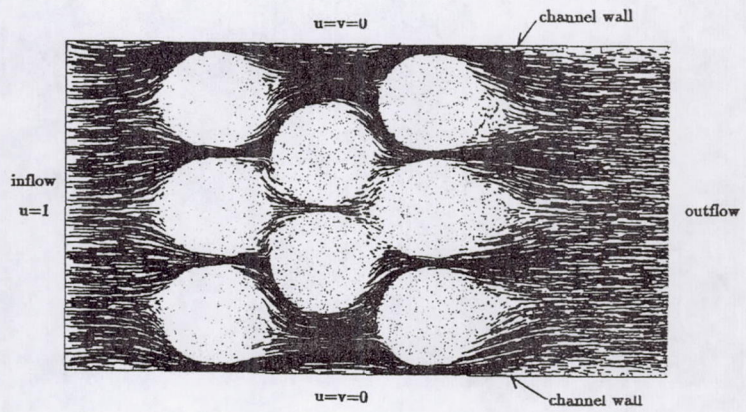

Re_d=20

$PTDR_L$= $PTDR_T$=11.8

CONCLUSIONS:

- approximate mathematical model with distributed parameters and without porous media assumption
- developed and evaluated a new computational algorithm for the solution of N-S equations in (u,v,p) formulation
- systematic analyses of the fluid flow in the brush sea components
- typical pressure and velocity distributions were estimated
- nonlinear behaviour of the pressure drop vs $PTDR_L$
- Pressure paradox for highly recirculative flows
- Capabilities of calculation of the pressure drop for a given bristle geometry and a typical brush segment
- PTDR is extemely influential in the nature of the overall flow inside the array and the subsequent pressure drops
- Pressure distribution inside the brush is non-symetrical and varies across the cross section
- New information on the flow structure within tube bundles. Butterfly flow formation. Near wall jets that are instrumental in the butterfly formation.
- transients are negligible, Re<1000

Simon Leefe August 14, 1992

DYNAMICS OF FACE SEALS FOR HIGH SPEED TURBOMACHINERY

Simon Leefe

Project Engineer

BHR Group Ltd.

Cranfield, Bedford, MK43 0AJ, England

ABSTRACT

Face seals in rocket engine fuel and oxidiser turbopumps have been the subject of intense investigation for over 25 years. Whilst advances have been made in the understanding of thin film lubrication between seal faces; valuable data has been produced on the friction and wear of material pairs in cryogenic environments; pioneering work has been done on the effect of lubricant phase change in seals; and many improvements have been made in mechanical seal design, relatively superficial attention has been given to the vibrational dynamics of face seals in high-speed turbomachinery.

BHR Group Ltd. (formerly BHRA) has recently completed the first stage of a study, commissioned by the European Space Agency, to investigate this area. This has involved the development of a two-dimensional adiabatic, turbulent lubrication model for thick gas film applications, the production of an integrated mathematical model of gas seal vibrational dynamics for thin film applications, implementation in software, the undertaking of an experimental programme to validate software against variations in operating conditions and design variables, and suggestions for improved seal design.

BHR Group Limited

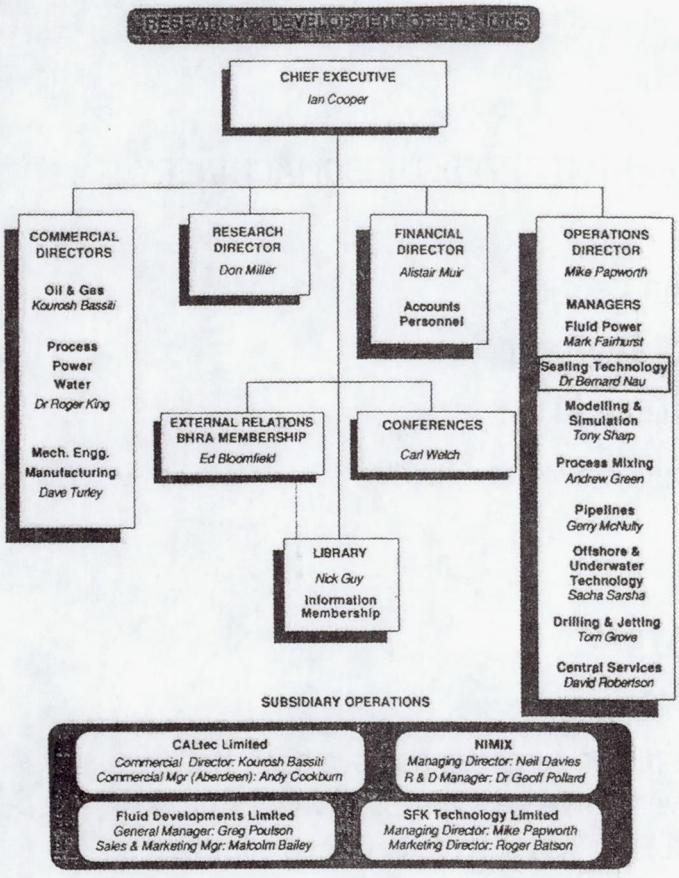

CALtec Limited - Oil & gas
NIMIX - Non-intrusive mixing equipment
Fluid Developments Limited - Abrasive jet cutting equipment
SFK Technology Limited - Software development

CURRENT PROJECTS

- Applications
  - rotary
  - reciprocating
  - static
- Technology
  - experimental
  - analytical
  - design studies
- Organisation
  - direct contract
  - consortium + Dept. of Trade and Industry
  - consortium + EEC
  - independent consortium

FLUID SEALING TECHNOLOGY

Independent facilities and expertise:-

- Seal Analysis:- thermal, mechanical, lubrication
- Seal testing:- oil, water, gas, cryogens, contaminants
- Pump Loops:- oil, water, slurry, water/air
- Site Measurements:- fixed, portable
- Design Audit:- analysis, critical review
- Rig Manufacture:- design, build, modification

bHR Group

PROJECT STRUCTURE

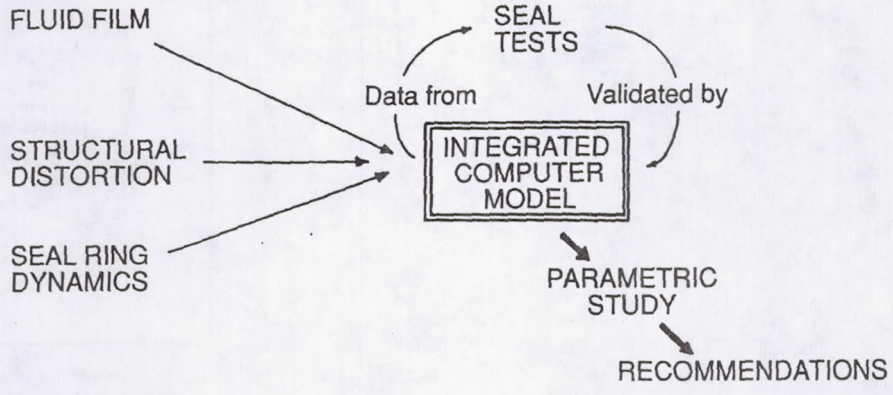

bHR Group

TURBOPUMP SEALING

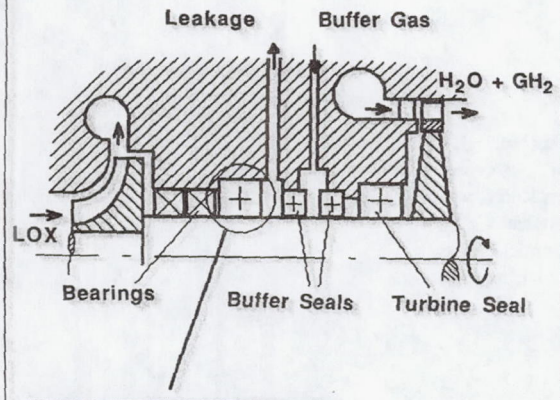

FACE SEAL OPTIONS:

- Plain
- Hydrostatic
- Self-acting

bH/Group

LITERATURE SURVEY
MAIN FINDINGS - SEALING PRACTICE

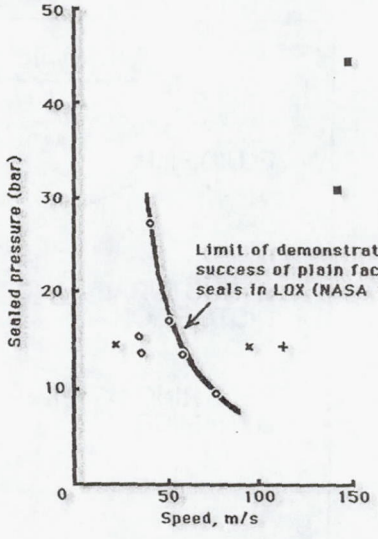

- ■ Self-acting face-seals in LOX (NASA evaluation)
- o Plain face-seals in LOX (demonstrated success)
- \+ Plain face seals in LH2 (Japanese test programme)
- × Plain face seals in GN2 (BHRG test programme)

bH/Group

LITERATURE SURVEY

MODELLING - FILM LUBRICATION ANALYSIS

Laminar, isothermal - Reynolds equation

- Liquid films - treatment of cavitation
- Gas films - grid design (adaptive, graded, etc.)
  - algorithm design (implicit, alternating, multigrid, 'interior co-location', etc.)

Turbulent lubrication - Hirs' bulk flow
- Constantinescu
- Ng & Pan

Non-isothermal (higher Mach number) compressible flow

- 1-D (radial) adiabatic model with radial taper and entrance effects - Zuk

Two-phase (boiling interface) films

- 1-D models
- Stability approached from consideration of equilibrium film thickness vs. opening force curves (i.e. not from dynamic analysis)

bHR Group

LITERATURE SURVEY

MODELLING - DYNAMICS

- [K] and [C] matrices from fluid film analysis then dynamics as a separate problem
- Integrated analysis - fluid film forces and moments calculated at each timestep
- Excitation mechanisms
- Number of vibrational degrees-of-freedom
- Thermal and vibrational transients - 3 or 4 orders of magnitude difference in timescale - separate problem

bHR Group

SCOPE OF MODEL

- Concentrate initially on DYNAMICS
- Gas seal assumed (2-D transient 2-phase prohibitive within commercial constraints)
- Transient structural distortions
- Full transient lubrication analysis
- Turbulent, adiabatic AND laminar, isothermal leakage flow
- Choked exit conditions catered for
- 4 vibrational degrees of freedom
- Mechanical damping

bH/Group

MATHEMATICAL MODEL

TURBULENT, ADIABATIC FLOW

Radial and circumferential velocities:

$$u_r = -\frac{G_r h^2}{\eta}\left(\frac{\partial p}{\partial r} - I_r\right) \quad \text{where} \quad I_r = \frac{\rho u_\theta^2}{r}$$

and (optional inertia)

$$u_\theta = -\frac{G_\theta h^2}{\eta}\frac{\partial p}{r\partial \theta} + \frac{r\omega}{2}$$

Iterate round instantaneous equations

G_r and G_θ from Hirs' bulk flow turbulent lubrication theory (or = 1/12, laminar)

Given in terms of Reynolds numbers "as seen by" rotor and stator (different)

Shear stresses from these Reynolds numbers

2-D adiabatic energy equation relates pressure to circumferential shear stress for density at current timestep

Timestepping

Substitute u_r and u_θ in continuity equation as 'knowns' and find density at next timestep

Use film thickness, h, at mid-timestep throughout procedure

bH/Group

MATHEMATICAL MODEL

LAMINAR, ISOTHERMAL FLOW

Compressible Reynolds equation with ideal gas assumption

$$\frac{\partial}{\partial r}\left\{ph^3\frac{\partial p}{\partial r}\right\} + \frac{\partial}{r\partial \theta}\left\{ph^3\frac{\partial p}{r\partial \theta}\right\} - 6\eta r\omega\frac{\partial}{r\partial \theta}\{ph\} = 12\eta\frac{\partial}{\partial t}\{ph\}$$

Time discretisation:

$$\frac{\partial}{\partial r}\left(p_n h^3_{n+\frac{1}{2}}\frac{\partial p_{n+1}}{\partial r}\right) + \frac{\partial}{r\partial \theta}\left(\frac{h^3_{n+\frac{1}{2}}}{2}\frac{\partial p^2_n}{r\partial \theta}\right) - 6\eta r\omega\frac{\partial}{r\partial \theta}\left(p_n h_{n+\frac{1}{2}}\right) = 12\eta\left\{\frac{(p_{n+1}+p_n)}{2}\frac{\partial h}{\partial t}\Big|_{n+\frac{1}{2}} + h_{n+\frac{1}{2}}\frac{(p_{n+1}-p_n)}{\delta t}\right\}$$

No energy equation required

Velocities and shear stresses from pressure gradients

- Check exit Mach number distribution for condition

$$M < \frac{1}{\sqrt{\gamma}}$$ (isothermal flow)

- Check Reynolds number distribution for condition

$$Re < Re_{critical}$$ (laminar flow)

bH/Group

EXCITATION MECHANISMS

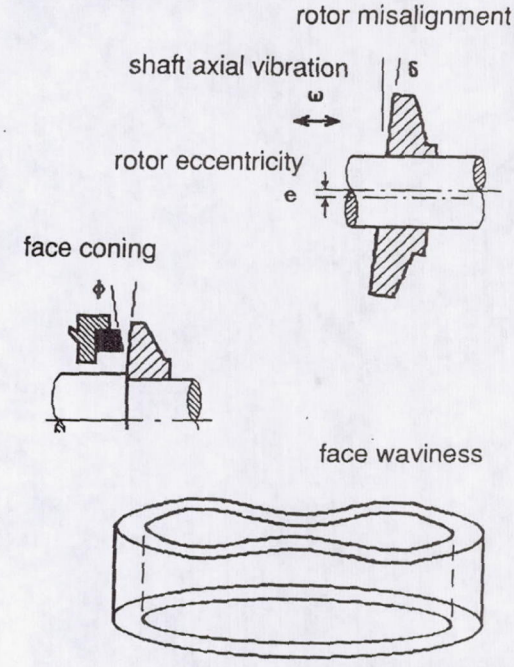

bH/Group

MATHEMATICAL MODELLING

FACE CONING

Sources:

- Pre-lapped taper and clamping forces

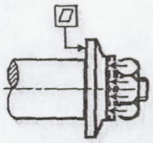

- Bellows load

- Rotor centrifugal inertia

- Change in ambient temperature for seal ring assemblies

- Sealed pressure differential

- Interfacial heat generation

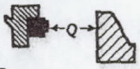

- Interfacial pressure distribution

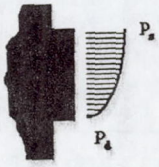

bH/Group

MATHEMATICAL MODELLING

INTERFACIAL PRESSURE CONING

1. F.E. Analysis

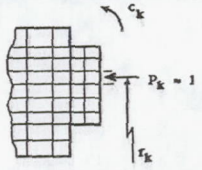

2. Pressure distn. over F.D. grid - circumfl. average → uniform pressure over annular rings corresponding to F.E. mesh

3. Use influence coefficients to calculate face coning

$$\Psi = \sum_k c_k \cdot P_k$$

bH/Group

VIBRATIONAL DEGREES OF FREEDOM

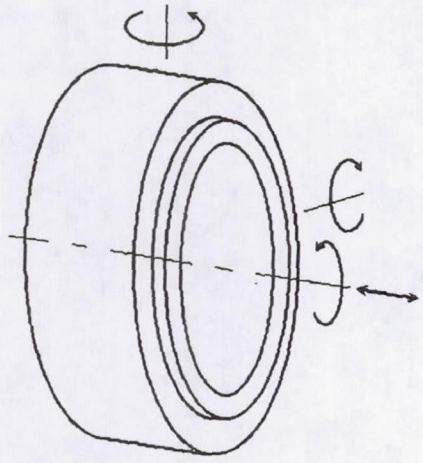

bHR Group

MATHEMATICAL MODELLING

DYNAMICS

Equations of motion time-discretised by Newmark's method:

$$[M]^{-1}\{F\}_{n+1} = \frac{4}{\delta t^2}\left(\{X\}_{n+1} - \{X\}_n\right) - \frac{4}{\delta t}\{\dot{X}\}_n - \{\ddot{X}\}_n$$

$\{\ddot{X}\}_{n+1}$

$$\{F\}_{n+1} = [K_L]\{X\}_{n+1} + \{F_{NL}\}_{n+1}$$

linear stiffness (bellows)

all nonlinear forces (fluid film and mechanical dampers)

Collect terms in $\{X\}_{n+1}$ and solve:

$$\{X\}_{n+1} = \left[[I] - \frac{\delta t^2}{4}[M]^{-1}[K_L]\right]^{-1}\left\{\frac{\delta t^2}{4}\left\{[M]^{-1}\{F_{NL}\}_{n+1} + \{\ddot{X}\}_n\right\} + \delta t\{\dot{X}\}_n + \{X\}_n\right\}$$

Inertia and stiffness matrices, [M] and $[K_L]$, are diagonal in the absence of lateral stiffness, so that inverses are trivial

bHR Group

MATHEMATICAL MODELLING

TIMESTEPPING

COMPUTATION	USES	TO PREDICT
Fluid film shape	$h_{n-\frac{1}{2}}$ $\dot{h}_{n-\frac{1}{2}}$ $\{X\}_n$ $\{\dot{X}\}_n$ Ψ_n	$h_{n+\frac{1}{2}}$ $\dot{h}_{n+\frac{1}{2}}$
Fluid film pressure distribution, p	p_n $h_{n+\frac{1}{2}}$ $\dot{h}_{n+\frac{1}{2}}$	p_{n+1}
Velocity and shear stress distributions	p_{n+1} $h_{n+\frac{1}{2}}$	$\boxed{u_{r_{n+1}}}$ $u_{z_{n+1}}$ $\tau_{r_{n+1}}$ $\boxed{\tau_{z_{n+1}}}$
Coning	p_{n+1}	Ψ_{n+1}
Fluid film forces and moments	p_{n+1} $\tau_{z_{n+1}}$ $\tau_{r_{n+1}}$	$\{F_{\substack{Fluid \\ film}}\}_{n+1}$
Mechanical damper forces and moments	$\{\dot{X}\}_n$ $\{\ddot{X}\}_n$ $\xrightarrow[\text{Expansion}]{\text{Taylor}}$ $\{\dot{X}\}_{n+1}$	$\{F_{Damper}\}_{n+1}$
		$\{F_{ML}\}_{n+1}$
Dynamics	$\{X\}_n$ $\{\dot{X}\}_n$ $\{\ddot{X}\}_n$ $\{F_{ML}\}_{n+1}$	$\boxed{\{X\}_{n+1}}$ $\{\dot{X}\}_{n+1}$ $\{\ddot{X}\}_{n+1}$

$\square$ = Output of fundamental importance

bH/Group

MATHEMATICAL MODELLING

APPROACH TO THERMAL TRANSIENT CONING

PROBLEM

Thermal diffusion timescale 2-4 orders of magnitude slower than timescale of vibrational dynamics

SOLUTION

- Off-line thermal transient F.E. analysis provides coning as a function of time
- Coning-time cuve 'sampled' at user-specified intervals to provide quasi-steady coning for vibrational analysis

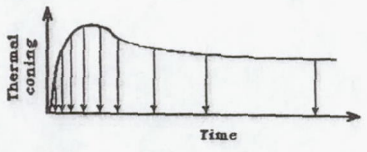

bH/Group

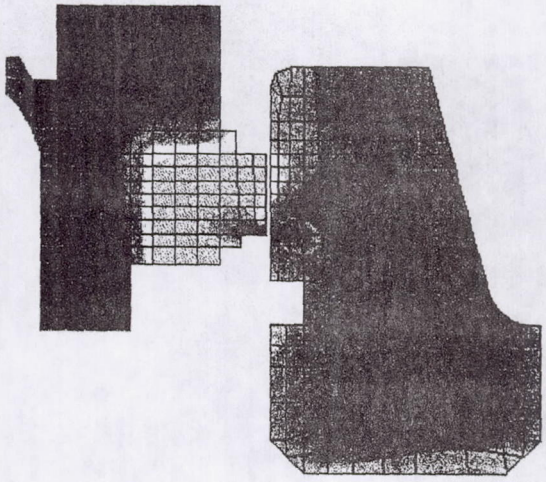

bHr Group

GENERIC SEAL TYPE

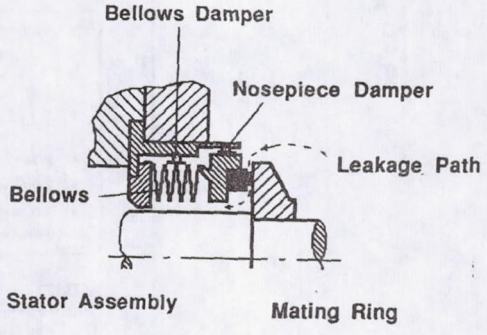

- Plain-faced balanced mechanical seals
- Bellows-type flexibly-mounted stator ring
- Rigidly-clamped rotor ring
- Coulomb friction vibration dampers

bHr Group

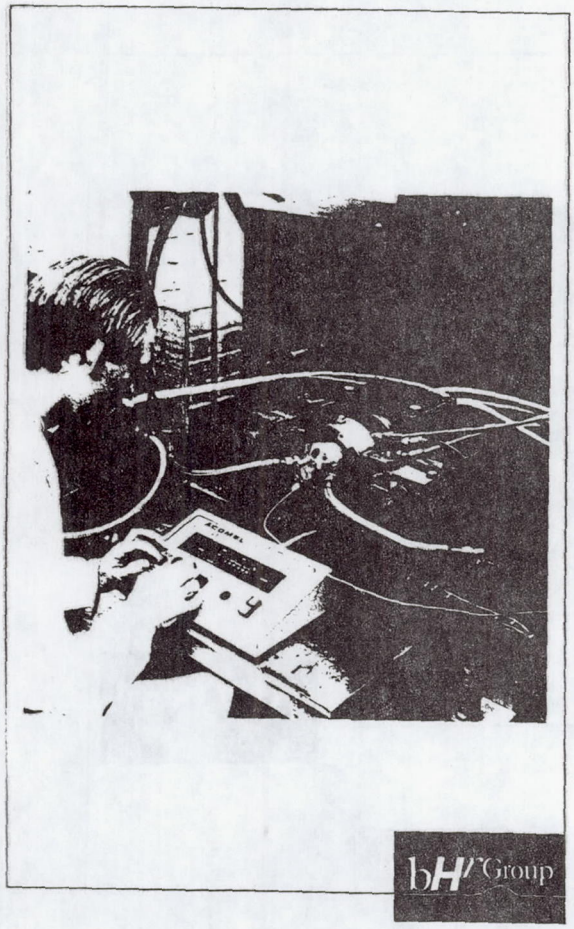

bHR Group

TEST PROGRAMME

SCOPE

- 42 tests covering:
  - face coning
  - rotor eccentricity
  - rotor out-of-squareness
  - degree of damping

  } room temp, 14000 rpm, 5,10,15 bar
- Effects of high and low temperature investigated
- Tests at high speed (60,000 rpm)
- All tests on typical plain face seal, modified to suit required conditions (face diameter = 30mm)

FACILITY

- Hot gas (to around 220°C) supply
- Cold gas supply (boiling to room temp)
- Liquid cryogen supply possible
- High pressure (rated to 20 bar) up to 14000 rpm
- High speed (60,000 rpm) at lower pressure

bHR Group

TEST PROGRAMME

MISALIGNMENT AND ECCENTRICITY

MISALIGNMENT

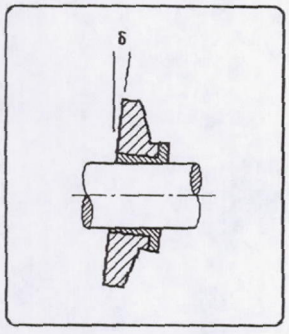

ECCENTRICITY

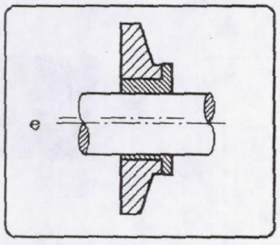

bHr Group

Accurate tracking of run-out

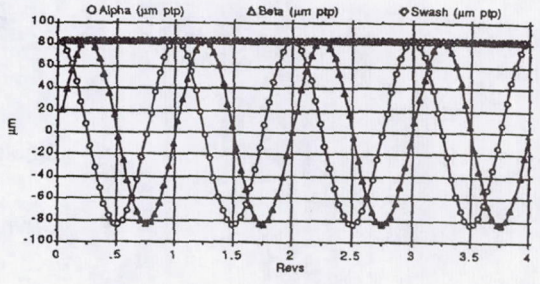

Stability reached quickly

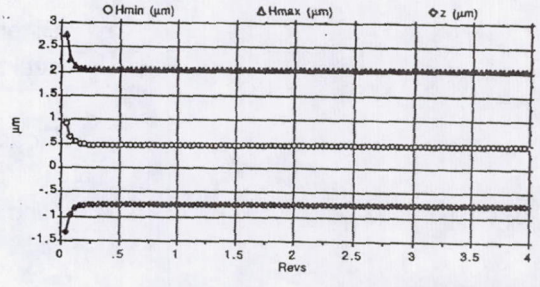

bHr Group

ANIMATION SEQUENCE

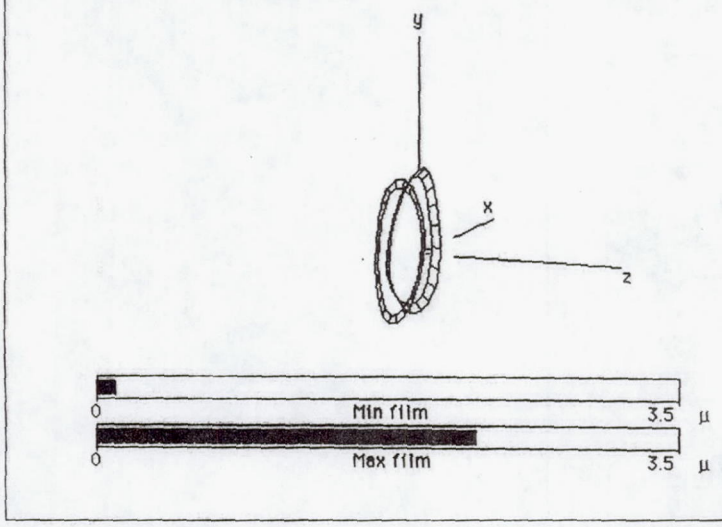

bH Group

AREAS SUITABLE FOR FURTHER DEVELOPMENT

- Liquid lubricant film
- Cavitating film
- Mechanical contact
- Circumferential EHD
- Different spring and secondary seal types
- Floating rotor types
- Ring seal geometries

bH Group

Dynamic Coefficients for Multiple Brush Seals

From notes and discussion of talk by D. Childs Texas A&M Univ.
by R.C. Hendricks

The cross sectional view of the Dressman-Childs apparatus is given as figure 1. This is the same apparatus as described by Childs et al., ref. 1, and used to determine the rotordynamic coefficients for a variety of seal configurations and test conditions. The working fluid is compressed air.

The experimental test sections for four, five, and six brush seal configurations are illustrated in figures 2, 3, and 4 respectively, see ref. 2.

While the dynamics of the 4-stage system was reported by Connors et al. ref. 3, with good reliability, the results of the extensions to other brush seal sets has not proven satisfactory. The data are inconsistent, e.g., the leakage for 4-brushes is less than for 6-brushes, however for all cases, the whirl frequency ratio was near or less than zero. But again the performance of the 4-brush configuration was dynamically better than that of the other configurations.

These results are not yet resolved and as such are given to provide the Seals Workshop with some information about multiple brush configurations - at least be aware that multiple brush seals require attention even though dual brush seals are operating with high resolve, there are only a few results for more than two brushes in the literature and NO other dynamic data to determine or assess rotordynamic coefficients.

For more information

1. Childs, D.W., Nelson, C.C., Nicks, C., Scharrer, J., Elrod, D., and Hale, K., 1986, "Theory Versus Experiment for th Rotrodynamic Coefficients of Annular Gas Seals: Part 1-Test Facility and Apparatus, "Trans. ASME J. of Tribology, V. 108, pp. 426-432.

2. Griffin, M., Kelynhans, G., Alexander, C., Pierce, T. and Childs, D.W.
Experimental Rotordynamic Coefficient Results for a 4-Stage Brush Seal
TL-SEAL-17-92 #363, May 92.
Experimental Rotordynamic Coefficient Results for a 5-Stage Brush Seal
TRC-SEAL-7-92 #353, May 92.
Experimental Rotordynamic Coefficient Results for a 6-Stage Brush Seal
TRC-SEAL-8-92 #354, May 92.
Turbomachine Laboratories, Texas A&M Univ., College Station Texas 77843

3. Conner, K.J., and Childs, D.W.: AIAA 90-2139, "Brush Seal Rotordynamic Damping Characteristics" AIAA/SAE/ASME/ASEE 26th Joint Propulsion Conference, July 16-18 1990 / Orlando, FL.

Table 1 Test Points

Rotor Speed ω (rpm)	Inlet Pressure P_t (bar)	Pressure Ratio P_n (-)	Inlet Preswirl in the Direction of Rotor Rotation
1 - 5000	1 - 7.90	1 - 0.55	1 - None
2 - 12000	2 - 13.1	2 - 0.40	2 - Intermediate
3 - 16000	3 - 18.3	3 - 0.25	3 - High
		4 - 0.14	

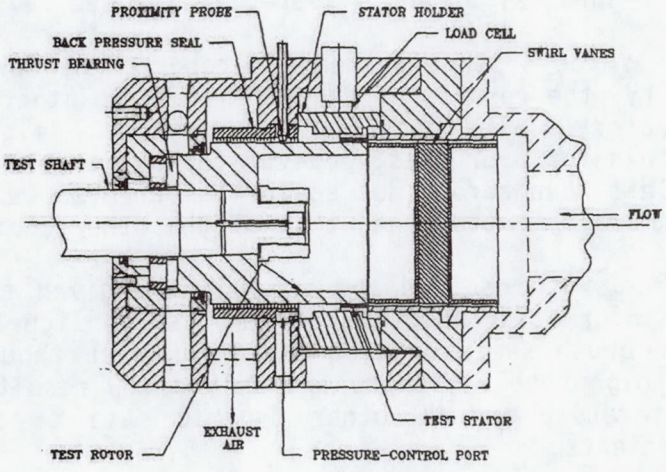

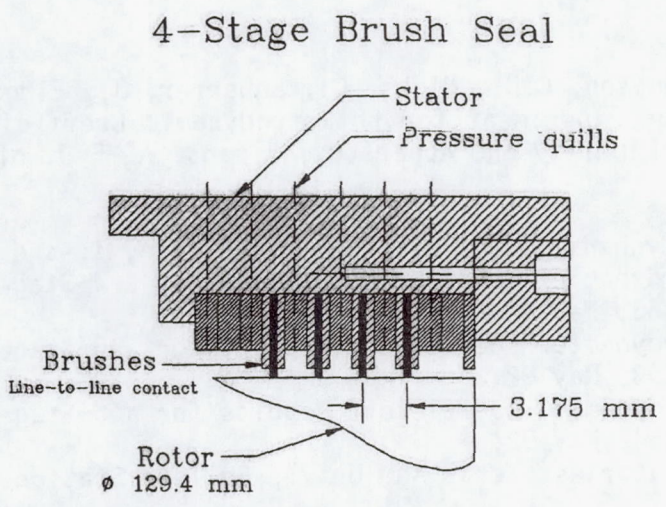

Figure 8 Geometry and dimensions of seal insert, all dimensions in millimeters

Fig. 8 illustrates the brush seal insert geometry used in this study.

Uncertainty Analysis

An experimental uncertainty analysis based on Holman (1978) for the measured experimental values is used in this study. The expression for the total uncertainty of a measured value is given below in equation (8).

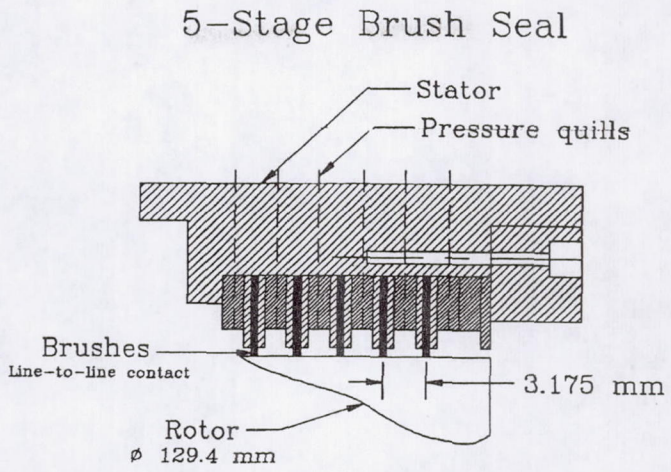

Figure 8 Geometry and dimensions of seal insert, all dimensions in millimeters

Fig. 8 illustrates the brush seal insert geometry used in this study.

Uncertainty Analysis

An experimental uncertainty analysis based on Holman (1978) for the measured experimental values is used in this study. The expression for the total uncertainty of a measured value is given below in equation (8).

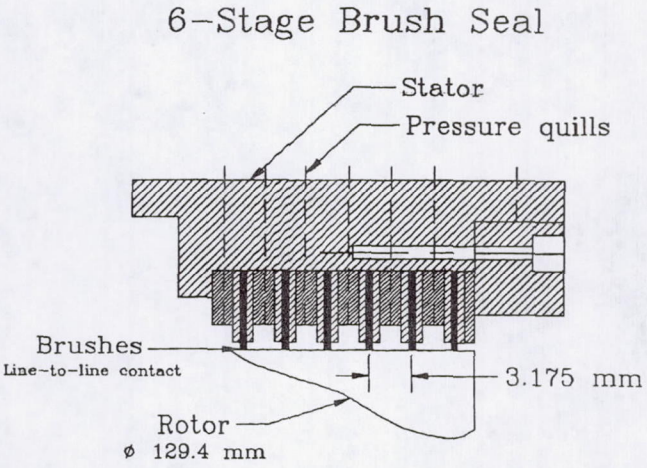

Figure 8 Geometry and dimensions of seal insert, all dimensions in millimeters

Fig. 8 illustrates the brush seal insert geometry used in this study.

Uncertainty Analysis

An experimental uncertainty analysis based on Holman (1978) for the measured experimental values is used in this study. The expression for the total uncertainty of a measured value is given below in equation (8).

RESULTS OF CRYOGENIC BRUSH SEAL TESTING

Presented by J. Scharrer, Rocketdyne

and

R.C. Hendricks, National Aeronautics and Space Administration

Five-Brush Seal Configuration Leakage as a Function of Pressure for Selected Rotor Speeds

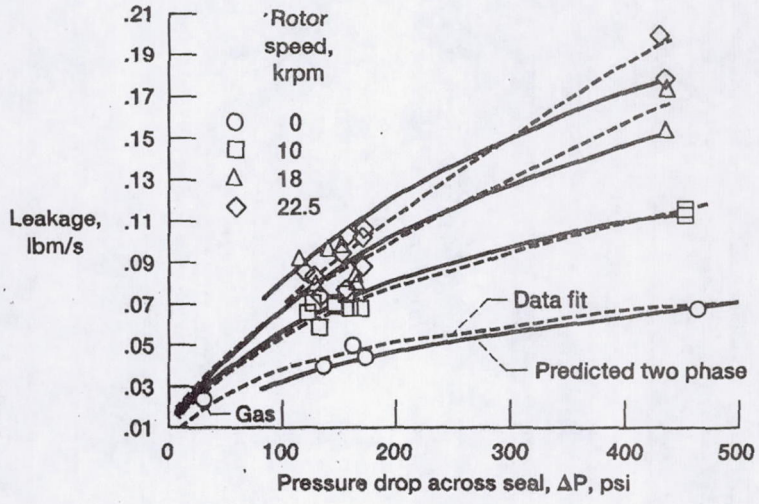

Schematic and Section View of Multifunction Tester

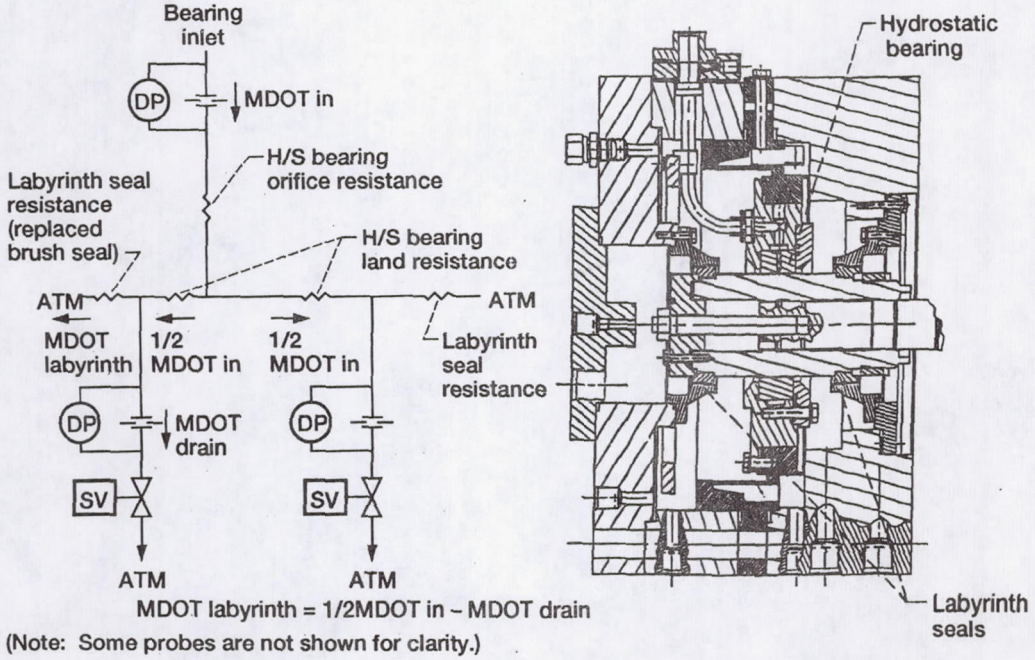

(Note: Some probes are not shown for clarity.)

MODELING BRISTLE LIFT-OFF IN IDEALIZED BRUSH SEAL CONFIGURATIONS

VIJAY MODI
DEPARTMENT OF MECHANICAL ENGINEERING
COLUMBIA UNIVERSITY
NEW YORK, NEW YORK 10027

1. Introduction

In the last decade, brush seals have emerged to be one of the most promising technologies for the reduction of leakage flow in gas turbine engines. Recent bench tests indicate a possibility of an order of magnitude reduction in leakage flow over multiknife labyrinth seal, Holle and Krishnan (1990). Additional potential for performance benefit arises from mechanical and maintenance considerations. The efficiency of a labyrinth type seal depends upon the clearance between the tip of the knife and the bore but this radial clearance may be difficult to control due to thermal and dynamic conditions. A brush seal on the other hand is compliant, and hence has the ability to recover after excursions, Flower (1990). An important question that remains to be answered is the relationship between brush configuration/operation parameters and some measure of its compliance. One measure of compliance is the clearance that develops between the bristle tips and the rotating element due to the pressure differential across the seal and due to the aerodynamic drag.

We attempt in this paper to develop a model for the flow through brush seals and determine their elastic behavior in order to predict the dependence of brush/journal clearance on geometry and operating conditions. Several idealizations regarding brush seal configuration, flow conditions and elastic behavior are made in the analysis in order to determine closed form parametric dependence. This formulation assumes that there is no initial interference between the bristle tip and the rotor. Also interbristle, bristle-backing plate and bristle-rotor friction is neglected. The bristle bundle or the brush seal as it is alternately called is assumed homogeneous and isotropic on a macroscopic scale so that a physical property like permeability is uniform. The fluid is assumed to be homogeneous, incompressible, viscous and is flowing under steady conditions.

A schematic of a brush seal is shown in figure 1. If the nominal bristle-shaft interference is absent then under static conditions the bristles may deflect axially due to the imposed pressure differential. This axial deflection may create a clearance permitting leakage flow in excess of that which occurs through the porous matrix

formed by the bristle bundles. Under dynamic conditions the Couette flow created by shaft motion could be strong enough to cause bristle deflection and once again a clearance may develop.

The paper proposes a means to determine this clearance (or at least describe its parametric dependence on geometry and operating conditions) under static as well as dynamic conditions. The study can be thought of as consisting of three separate modeling efforts. First a flow model that describes the coupled parallel flow through the porous medium made of bristle bundles and the clearance region. This development follows the earlier work of Beavers and Joseph (1967), Beavers et al. (1970), Williams (1978) and Rudraiah (1985). This model provides the macroscopic description of the flow field, i.e., a filter velocity in the porous medium. Second, a model to relate this macroscopic flow field to a local flow field and its associated drag on the bristle is developed. This model also permits us to determine an expression for the permeability in order to characterize the physical property of the bristle bundle in absence of an experimentally determined value. The forces on a single bristle due to this macroscopic flow field are then estimated assuming idealized microscopic flow behavior and a phenomenological description of drag on a bristle. Third, the elastic behavior is modeled to estimate the deflection of the bristle tip due to the flow field or the impressed axial pressure differential. A description of the clearance would in principle require a simultaneous solution of the three models. It is, however, assumed here that the physical property permeability remains unchanged both due to the presence of leakage flow through and around the bristle bundle as well as due to the deformation of the bristles themselves. Given this, it is then necessary to solve only the flow and elastic models simultaneously to determine the clearance.

2. Circumferential Deflection

To determine the circumferential deflection of the bristles we must first estimate the forces on each bristle. The forces in the circumferential direction are due to drag caused by the flow around the bristle bundle. This flow is in turn driven by the Couette flow in the bristle-shaft clearance as a result of the circumferential slip velocity of the shaft itself. In the absence of a clearance, the shaft motion imposes a circumferential velocity boundary condition directly at the bristle-shaft interface. A model to determine the flow field in both these circumstances is introduced next. This development assumes that the clearance h_0 if any is known. Its actual value will be determined later along with considerations of the elastic behavior.

2.1 Flow Model

Let us consider the geometry shown in figure 2, with a porous medium of height h underlying a channel formed by a clearance of height h_o. The clearance is bounded above by an impermeable wall moving to the right at u_o and the porous region is bounded below by an impermeable stationary wall. The formulation presented here follows that in Rudraiah (1985). The basic equations describing the flow are obtained after the following approximations are made.

i) The fluid is homogeneous and incompressible.

ii) The flow in the channel and in the porous medium is driven by a shear produced due to the motion of the upper plate. This flow is steady, laminar and fully developed.

iii) The porous medium formed of bristle bundles is homogeneous and isotropic on a macroscopic scale.

iv) The flow in the porous medium is adequately described by the Brinkman equations and this flow is coupled to the channel flow by a boundary condition given by Williams (1978).

Following Rudraiah (1985), we write equations for u, velocity in the gap and $\hat{u}$, filter velocity in the porous medium as:

$$\frac{d^2u}{dy^2} = 0 \quad \text{and} \quad \frac{d^2\hat{u}}{dy^2} - \frac{1}{\lambda k}\, u = 0 \tag{1}$$

where λ is a positive constant and k is the permeability of the porous medium. The velocity $\hat{u}$ in the porous medium is related to u by

$$u = (1-\phi)\,\hat{u} \tag{2}$$

where $(1-\phi)$ is the porosity. Following Williams (1978), at the clearance-porous medium interface we assume that:

$$\frac{du}{dy} = (1-\phi)\lambda\,\frac{d\hat{u}}{dy} \tag{3}$$

The remaining boundary conditions are the usual no-slip conditions at impermeable walls and are:

$$u = u_o \text{ at } y = h_o$$
$$u = 0 \text{ at } y = -h \tag{4}$$

Solving (1) subject to (2), (3) and (4) we obtain the velocity distributions in the clearance and the porous regions to be

$$u = u_o\left[1 - \frac{\lambda\delta\,(h_o - y)}{(\tanh\delta h + \lambda\delta h_o)}\right] \qquad y > 0$$
$$\hat{u} = \frac{u_o}{(1-\phi)(\tanh\delta h + \lambda\delta h_o)}\left[\sinh\delta y + \frac{\cosh\delta y}{\coth\delta h}\right] \qquad y < 0 \tag{5}$$

where $\delta = (\lambda k)^{-1/2}$. Here $\delta h = h\,(\lambda k)^{-1/2} >> 1$ is used. This relies on λ to be of order unity and h to be a macroscopic length scale assumed to be several times greater than $k^{1/2}$ (which is typically of order d_o, the characteristic dimension of the porous matrix, i.e. bristle diameter). Hence we may approximate $\hat{u}$ by

$$\hat{u} = \frac{u_o}{\eta}\,e^{\delta y} \qquad y < 0 \tag{6}$$

where $\eta = (1-\phi)(1+\lambda\delta\, h_o)$. The exponential behavior of the filter velocity implies that it decays to the Darcy value (which in this case is zero) within a boundary layer of length scale $1/\delta$, where $1/\delta$ is of the order of $k^{1/2}$.

Here $\hat{u}$ represents a filter velocity, a macroscopic quantity defined in order to avoid the more difficult question of what is the true velocity of the fluid in the porous region between the bristles. We now make certain idealizations about the bristle bundle geometry and subsequently model the flow through the interbristle pores in order to determine the viscous drag force directly as a function of the filter velocity.

2.2. Permeability Model

The drag force on a bundle of cylindrical bristles clearly depends upon the flow through the pores which in turn depends upon the particular geometric configuration. Let us first examine the situation for two particular geometric arrangements. Let us assume that the cross-section of the bundle remains same in the direction along the bristle axis and that the flow is normal to these axes. Let ϕ be the solidity or here the area fraction and Z be the number of nearest neighbors.

Then ϕ and Z are respectively $\pi/4 = 0.79$ and 4, for a square array and $\pi/2\sqrt{3} = 0.907$ and 6 for a hexagonal array. For these arrays there is no possibility of any transverse flow since all neighboring cylinders are in contact. Typical solidities ϕ for brush seals are between 0.7 and 0.8, indicating a fairly close packed geometry. It is very likely that the manufacture of bristle bundles and their relative movement in the presence of leakage flow lead to bristle configurations that are close to random. A particular means to generate a closely packed random array is by the following two step process, described by Sangani and Yao (1988). In the first step, the process of dropping a large number of equal-diameter cylinders in a container is simulated. Note that in the configuration so generated any cylinder is in contact with its nearest neighbors. Let ϕ_t be the solidity of such a closely packed random array. Berryman (1983) summarizes the results of several simulations and reports ϕ_t in the range of 0.81-0.89, with most studies quoting a value of approximately 0.82. Sangani and Yao (1988) have also simulated such arrays recently with upto 1600 cylinders in a container and they report a value of $\phi_t = 0.824$ and $Z = 4.2$. In the second step, the diameters of all the cylinder centers are shrunk by a constant amount $2\varepsilon r$, while keeping the location of all cylinder centers fixed. Here r is the bristle radius. The value of ε is chosen so that the new configuration has the measured solidity ϕ. For this special kind of array the gap between neighboring cylinders is uniform and is given by $2\varepsilon r$ where

$$\varepsilon = 1 - \left(\frac{\phi}{\phi_t}\right)^{1/2} \tag{7}$$

The resistance offered to the flow by the gap between pairs of nearly touching cylinders determine the overall drag and hence the effective permeability of the medium. The analysis below is due to Sangani (1990). The pressure drops as fluid squeezes through a gap of width $2\varepsilon r$ at a volume flow rate Q, as shown in figure 3. Here Q is the two-dimensional volume flow rate. The profile of the cylinder surface can be approximated by

$$\frac{f(x)}{r} \approx \varepsilon + \frac{x^2}{2r^2} \quad \text{for} \quad \frac{x}{r} \to 0\ (\varepsilon^{1/2}) \tag{8}$$

Assume that inertia terms are negligible and that the viscous forces in the streamise direction are small compared to those in the normal direction. Hence the equation governing the x- direction velocity component $\hat{u}$ reduces to

$$\mu \frac{\partial^2 \hat{u}}{\partial y^2} \approx \frac{dp}{dx} \tag{9}$$

Integrating the above equation with $\hat{u} = 0$ at $y = f(x)$ and $\partial\hat{u}/\partial y = o$ at $y = o$ we obtain

$$\hat{u} = -\frac{1}{2\mu} \frac{dp}{dx} [f^2(x) - y^2)] \tag{10}$$

Integrating the above velocity profile over the gap and identifying it with volume flow rate Q, we obtain

$$(\Delta p)\ \text{gap} = \frac{9\pi\mu Q}{8\sqrt{2}} \frac{\varepsilon}{r^2}^{-5/2} \tag{11}$$

Thus the force exerted per unit length and width in direction of flow is Δp. The direction of flow however is normal to the line segment joining the centers of the cylinder pair in question. If such a line segment is oriented at an angle θ_i as shown in figure 4, then the force vector F_i per unit length arising over width 2r due to each gap for volume flow rate Q_i is given by

$$F_i = \frac{9\pi\mu Q_i}{8\sqrt{2}} \frac{\varepsilon_i^{-5/2}}{r^2} (2r) \tag{12}$$

The component of the force (per unit length) in the direction of mean flow (assumed to be along $\theta_i=0$) is then obtained after noting that $Q_i = (2\hat{u}\sin\theta_i)\, r$

$$F_{1i} = |F_i| \sin\theta_i = \frac{9\pi\mu\varepsilon^{-5/2}}{8\sqrt{2}}\ 2\hat{u}\sin^2\theta_i \tag{13}$$

Here $\hat{u}$ is the filter velocity or the superficial velocity. Hence, the mean force $\langle F_1 \rangle$ is given by

$$\langle F_1 \rangle = \frac{9\pi\mu\hat{u}Z}{8\sqrt{2}}\ \varepsilon^{-5/2} \tag{14}$$

where Z is the average number of nearest neighbors and the mean value of $\sin^2\theta_i$ averaged over all θ_i is 1/2. If the number of cylinders per unit cross-section area is $4\phi/\pi d_o^2$ where d_o is the diameter then

$$|\nabla p_1| = \langle F_1 \rangle \frac{4\phi}{\pi d_o} = \frac{9Z\phi\mu}{2\sqrt{2}} \varepsilon^{-5/2} \frac{\hat{u}}{d_o^2} \tag{15}$$

If one was interested in the permeability k of the medium defined as $k = \mu\hat{u}/|\nabla p|$ then

$$k = \frac{2\sqrt{2}}{9Z\phi} d_o^2 \varepsilon^{5/2} \tag{16}$$

which is identical to the expression in Sangani and Yao (1988) except for ϕ in the denominator.

2.3 Elastic Behavior Model

The expression in (15) permits us to calculate $|\nabla p|$, as a function of the filter velocity u which may vary along the bristle axis as given by (6). Hence, we are in a position to determine the loading on the bristle due to the inter-bristle flow driven by the Couette flow in the clearance region. We define a co-ordinate system shown in figure 5. The deflection of the bristle tip, Δ_t, can be obtained from straightforward application of linear elasticity theory. The radial component of the deflection $h_o = \Delta_t \cos\beta$ is then the clearance, and is given by

$$h_o = \Delta_t \cos\beta = \frac{9Z}{2\sqrt{2}} \varepsilon^{-5/2} \frac{\mu u_o}{\eta} \frac{\cos\beta}{(\sin\beta)^3} \frac{1}{EI} \frac{1}{\delta} \frac{h^3}{3} \tag{17}$$

Recall that $\eta = (1-\phi)(1+\lambda\delta h_o)$, $\delta = (\lambda k)^{-1/2}$, $I = \pi d_o^4/64$. Since the above equation is implicit in h_o, consider $h_o >> k^{1/2}$ first, so that $\lambda\delta h_o >> 1$ providing an explicit form,

$$\left(\frac{h_o}{d_o}\right)^2 = \frac{9Z}{2\sqrt{2}} \left[1 - \sqrt{\phi/\phi_t}\right]^{-5/2} \frac{\mu u_o}{(1-\phi)} \frac{k}{d_o^2} \frac{\cos\beta}{(\sin\beta)^3} \frac{h^3}{3EI} \tag{18}$$

If permeability k is experimentally determined for the medium then that measured value can be used in the above expression. The recommended values of ϕ_t

and Z are 0.82 and 4.2 for a random array of cylinders. Hence the expression is valid for $\phi < \phi_t(=.82)$. If, however, k is not known, permeability can be estimated from (16) allowing us to determine h_o from

$$\left(\frac{h_o}{d_o}\right)^2 = \frac{\mu u_o}{\phi(1-\phi)} \frac{\cos\beta}{(\sin\beta)^3} \frac{h^3}{3EI} \qquad ho >> \sqrt{k} \tag{19}$$

In the absence of any clearance h_o vanishes and any initial increase in h_o must occur with $h_o << k^{1/2}$. Under circumstances that permit us to assume $\lambda \delta h_o << 1$ we obtain

$$\frac{h_o}{d_o} = \frac{9Z}{2\sqrt{2}} \left[1 - \sqrt{\phi/\phi_t}\right]^{-5/2} \frac{\mu u_o}{(1-\phi)} \frac{\sqrt{\lambda k}}{d_o} \frac{\cos\beta}{(\sin\beta)^3} \frac{h^3}{3EI} \tag{20}$$

Once again k can either be measured or evaluated from equation (16). In the above expression in addition to Z and ϕ_t we also need an empirical estimate for the constant $\lambda^{1/2}$. The constant $\lambda^{1/2}$ can be identified with α in Beavers and Joseph (1967) and is a dimensionless quantity depending on the material parameters which characterize the structure of the porous medium within the boundary region where the filter velocity decays to zero, its Darcy value. The value of α reported by Beavers and Joseph are for Foametal and Aloxite, with effective pore sizes varying between 0.013 inches and .045 inches. The value of α for these materials was found to vary between 0.1 and 4 with lower values observed at lower pore sizes.

Preliminary estimates of the clearance due to tangential loading can be made from either (19) or (20) and if it turns out that h_o is of the order of $k^{1/2}$ then the quadratic equation (17) can be solved for h_o. Before discussing the results for the tangential deflection we will develop the analysis for axial deflection. This will permit us to determine their relative magnitudes and establish conditions under which, it may be possible to neglect the clearance due to deflection in one of the directions.

3. Axial Deflection

The axial deflection of the bristles is due to the pressure differential along the axis of the rotating element. It is the purpose of the brush seal to minimize what would otherwise be a leakage flow due to this pressure differential. The axial loading on the bristle is straightforward to estimate since the pressure differential impressed upon the bristle bundle can be assumed to remain unaltered in the presence of leakage flow. If the pressure differential is $\Delta p = P_h - P_e$ over the width w of the

bristle bundle (in the axial direction) then the force per unit length, q, acting on the bristle is given by $q = \Delta p\, d_o^2/w$. This force acts uniformly over the overhanging length a of the bristle, i.e. exposed portion between the backing ring of inner diameter D_b and the shaft, diameter D_s. Since the bristle bundle is clamped at the retaining plate inner diameter D_r, the bristle behavior can be modeled as a bar clamped at origin and simply supported at D_b with an overhanging distributed load between D_b and D_s. If we define L to be the bristle length between the retaining ring ID and the backing ring ID, $L = (D_r - D_b)/2 \sin \beta$ then the bristle geometry with its axial loading diagram is as shown in figure 6. We wish to determine the displacement, Δ_h, due to the axial deflection of the unloaded member, as shown in figure 7. This quantity is the clearance produced due to the axial loading and would be observed in a static leakage test. In dynamic tests the clearance would be produced by a combination of effects, the tangential as well as the axial loading.

Linear elasticity theory assumes small angles of rotation for the beam and thus would only permit the calculation of the vertical displacement Δ_v while Δ_h would remain zero. Typical axial loading and the bristle length to diameter ratios are however, such that it becomes necessary to use large deflection theory in order to model the problem. Thus the differential equation of the deflection curve becomes

$$\left[\frac{\dfrac{d^2y}{dx^2}}{\left[1+\left(\dfrac{dy}{dx}\right)^2\right]^{3/2}}\right] = -\frac{M(x)}{EI} \qquad (21)$$

The exact shape of the elastic deflection curve given by the solution to this equation, is called the elastica. The mathematical solution to the problem of determining the elastica has been obtained for many different types of beams and loading conditions, see Frisch-Fay (1962). The solutions to the specific loading of interest here was not available in the existing literature. A particular difficulty is that the problem is statically indeterminate and the reaction force where the bristle is simply supported is unknown. While a linear theory may provide a value of the reaction, it will be approximate at best. This value, however, could be of use as an initial guess in an iterative determination of the reaction force into vertical component R and horizontal component $R\tan\theta$, where $\tan\theta$ is the bristle slope at the support, see figure 7. To determine Δ_h we need to solve for the elastica and

terminate the curve at a point where the length of the curve is (L + a). Here we assume that any elongation of the bristle is negligible or of an order smaller than that under consideration. In the deformed position of the bristle the axial loading is no longer applied over the overhang initial length 'a' but over the overhang length $a' = a - \Delta_h$ in the deformed position. The direction of the axial force, however, continues to remain vertical in the deformed position.

Solution to the problem described above requires us to integrate (21), with a moment distribution function M(x) given by

$$M(x) = qa'\,(a'/2 + L-x) - R(L-x) - R\tan\theta\, y \qquad 0 < x < L$$
$$M(x) = (q/2)\,(L + a' - x)^2 \qquad L < x < L + a \qquad (22)$$

where a' and $\tan\theta$ are unknown and are determined as part of the solution y(x). The reaction force, however, is still unknown because the problem is statically indeterminate. This difficulty is easily overcome, especially since the solution is perhaps most easily obtained on a computer. An initial guess of R is made from linear theory. The preliminary solution thus obtained however, will in general fail to pass through the support at (L,0). The magnitude of the reaction force is gradually changed until the elastica does pass through, (L,0). It is convenient to normalize x and y with length L, i.e. $x^* = x/L$ and $y^* = y/L$. Dropping asterisk now equations (21) and (22) become

$$y''/(1+y'^2)^{3/2} = -M(x) \quad \text{with } y(o) = o \; y'(o) = 0, \text{ where}$$
$$M(x) = C_{eff}\left\{1/2 + (1/a')\,(1-x)\right\} - \alpha\,(1-x) - \alpha \tan\theta\, y \qquad 0 < x < 1$$
$$M(x) = (C_{eff}/2)\,(1/a')^2\,(1 + a'-x)^2 \qquad 1 < x < 1 + a/L \qquad (23)$$
$$\text{where } C_{eff} = C\,(a'/a)^2,\ C = qa^2L/EI \text{ and } \alpha = RL^2/EI$$

The problem shown above was solved numerically for various values of the loading parameter C and the overhang ratio a/L. The elastica curves for a/L = 0.2 are shown in figure 8. Note that the axis in the y-direction is stretched considerably for clarity. The quantity of interest here is the clearance Δ_h the variation of which with loading parameter C is shown in figure 9 for several overhang ratios a/L. Note that the small deflection theory value of Δ_h is identically zero for all C. We observe that the departure from this value as loading is increased depends upon the overhang parameter. It turns out that for typical gas turbine applications brush seals may be operating in a parameter range where Δ_h is rapidly increasing with C and a/L.

The actual value of the reaction force is not of immediate interest once the axial deflection is known, however, it may be of use in the following manner. Earlier analysis to determine the circumferential deflection assumed that the friction at the bristle-backing ring interface was negligible. The bristle orientation under axial loading shown in figure 8 indicates that the only point of contact may be at the inner edge of the backing ring where the normal force acting on the bristle is given by R/cos θ. An estimated value of the static Coulomb friction coefficient would permit an approximate evaluation of the tangential restraining force. This force would act on the bristle layer in contact with the backing ring. While in this paper we do not account for this friction force in the calculation of the circumferential deflection the value of R and θ may prove useful for future work.

4. Discussion

Under dynamic conditions the actual deflection would be due to both the circumferential and axial loads and a vector sum of forces has to be used to solve the three-dimensional elastica problem. Additional simplification is possible if we can demonstrate that the deflection in one of the directions is small compared to the other. An explicit expression for their relative magnitude is not available because of the lack of a closed form formula for the axial deflection.

The numerical results of figure 9 establish that the behavior of Δ_h (C, a/L) is indeed nonlinear, and may be of importance in the design of brush seal systems. In addition to the expected non linearity in the response to loading parameters C the displacement h is also sensitive to a/L ratios. Thus it is not just the overhang length that is relevant even though it is the length exposed to a pressure differential but also the size of the retaining plate. The analysis carried out here while making several idealizations may provide insight into the dependence of the clearance on geometry and operating conditions.

ACKNOWLEDGMENTS

I would like to thank Dr. Prithwish Basu of E G & G Sealol for introducing the author to the problem and providing significant insight along the way. I am also grateful to Mr. Albert Bonamio and Dr. Hayri Cabuk for some of the calculations reported here.

BIBLIOGRAPHY

1. Beavers, G. S., and Joseph, D. D., "Boundary Conditions at a Naturally Permeable Wall", Journal of Fluid Mechanics, Vol. 30, 1967, pp 197-207.

2. Beavers, G. S., Sparrow, E. M., and Magnuson, R. A., "Experiments on Coupled Parallel Flows in a Channel and a Boundary Porous Medium", ASME Journal of Basic Engineering, Vol. 92, Series D, No. 1, 1970, pp. 843-848.

3. Berryman, J., Phys. Rev. A 27, 1983, p. 1053.

4. Flower, R., "Brush Seal Development System", AIAA paper 90-2143, 26th Joint Propulsion Conference, July 16-18, Orlando, Florida, 1990.

5. Frisch-Fay, R., "Flexible Bars", Butterworths, Washington, 1962.

6. Holle, G. F., and Krishnan, M. R., "Gas Turbine Engine Brush Seal Applications", AIAA paper 90-2141, 26th Joint Propulsion Conference, July 16-18, Orlando, Florida, 1990.

7. Rudraiah, N., "Coupled Parallel Flows in a Channel and a Bounding Porous Medium of Finite of Thickness", ASME Journal of Fluids Engineering, Vol. 107, 1985, pp. 322-328.

8. Sangani, A. S., Personal Communication, 1990.

9. Sangani, A. S. and Yao, C., "Transport Process in Random Arrays of Cylinders. Part II Viscous Flow", Physics of Fluids, Vol. 31, 1988, pp. 2435-2444.

10. Williams, W. O., "Constitutive Equations of a Flow of an Incompressible Viscous Fluid Through a Porous Medium", Quarterly of Applied Mathematics, 1978, pp. 255-267.

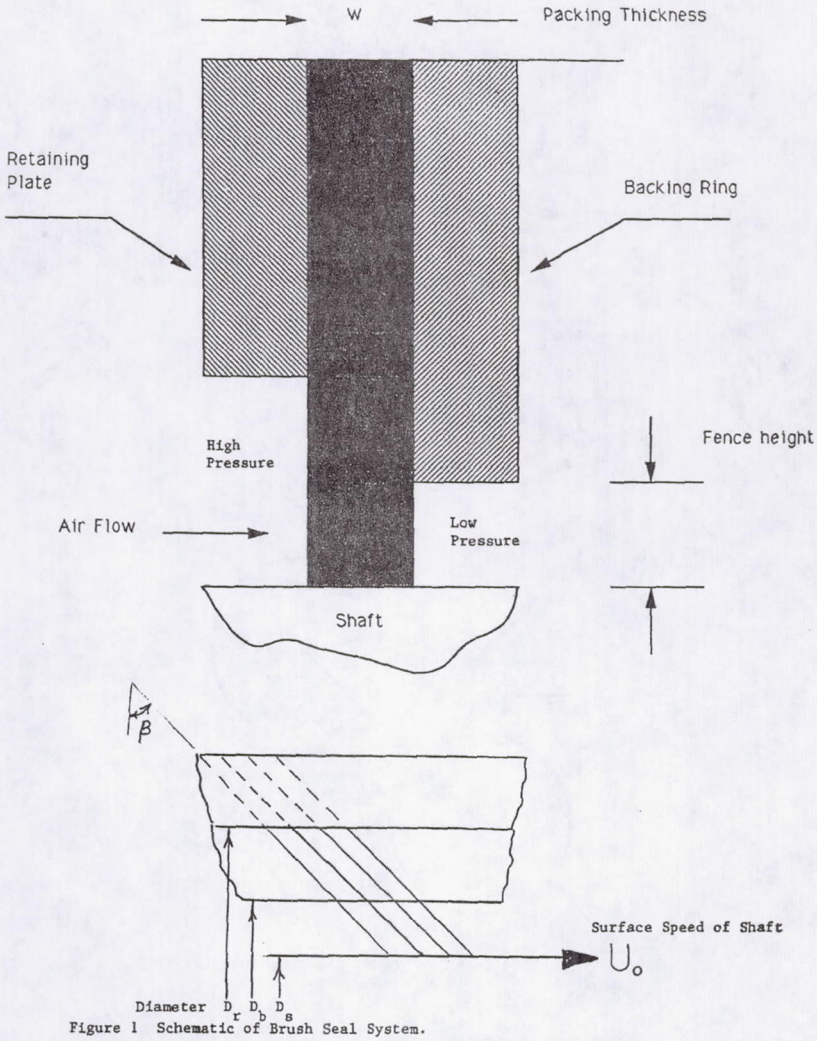

Figure 1 Schematic of Brush Seal System.

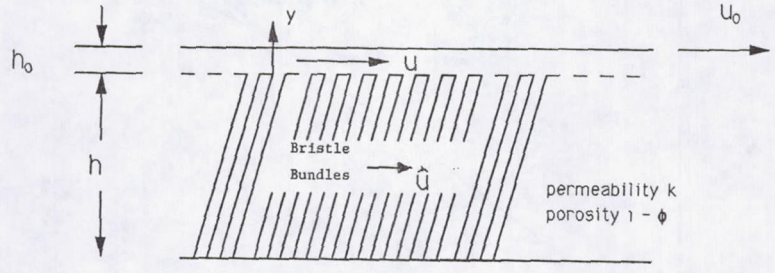

Figure 2

Physical model of clearance channel bounded by shaft on one side and porous bristle bundle on other.

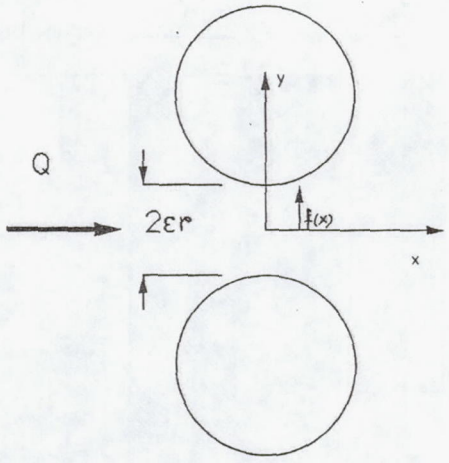

Figure 3 Schematic of Volume Flow Q through a gap of size 2εr

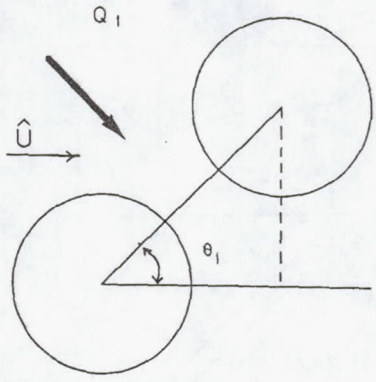

Figure 4 A pair of neighbouring cylinders in a random array.

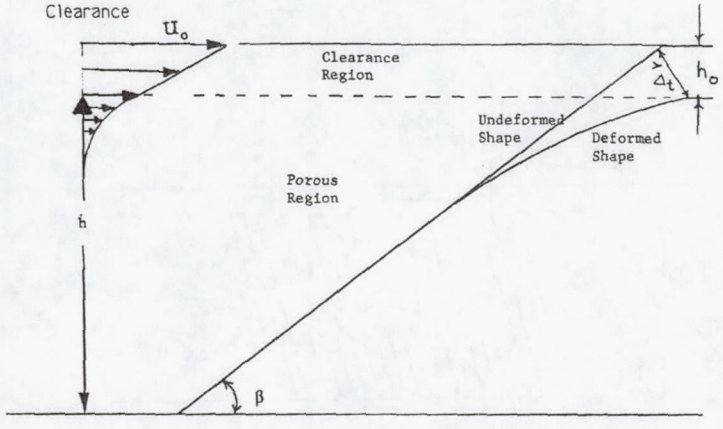

Figure 5 Schematic diagram of clearance region and the porous bristle bundle matrix. Velocity distributions in each are shown at left. Bristle displacement is normal to its axis.

$h_o = \Delta_t \cos\beta$

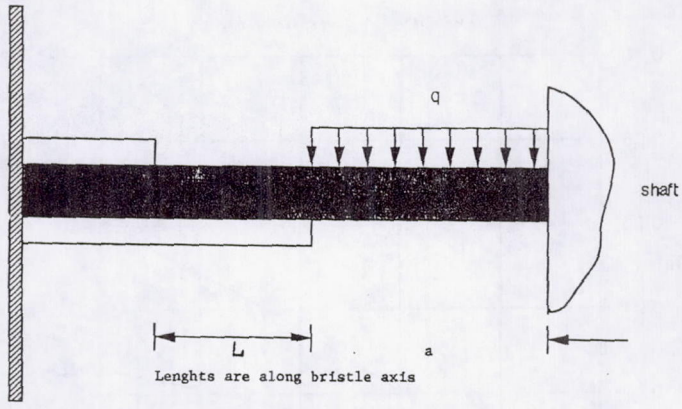

Figure 6 Axial loading diagram for a single bristle.

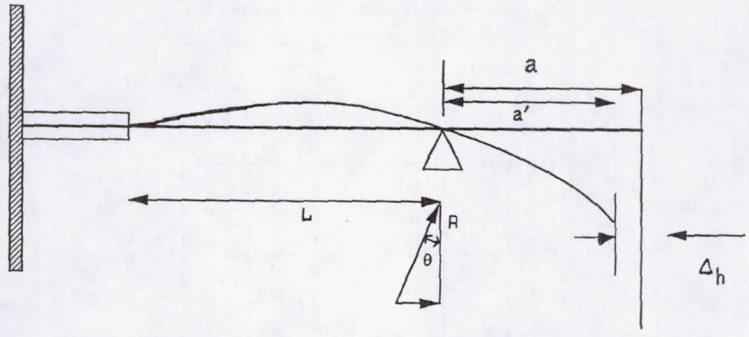

Figure 7 Schematic diagram showing the deformed shape of the bristle under axial loading. Horizontal displacement is such that the length of the bristle is unchanged under loading.

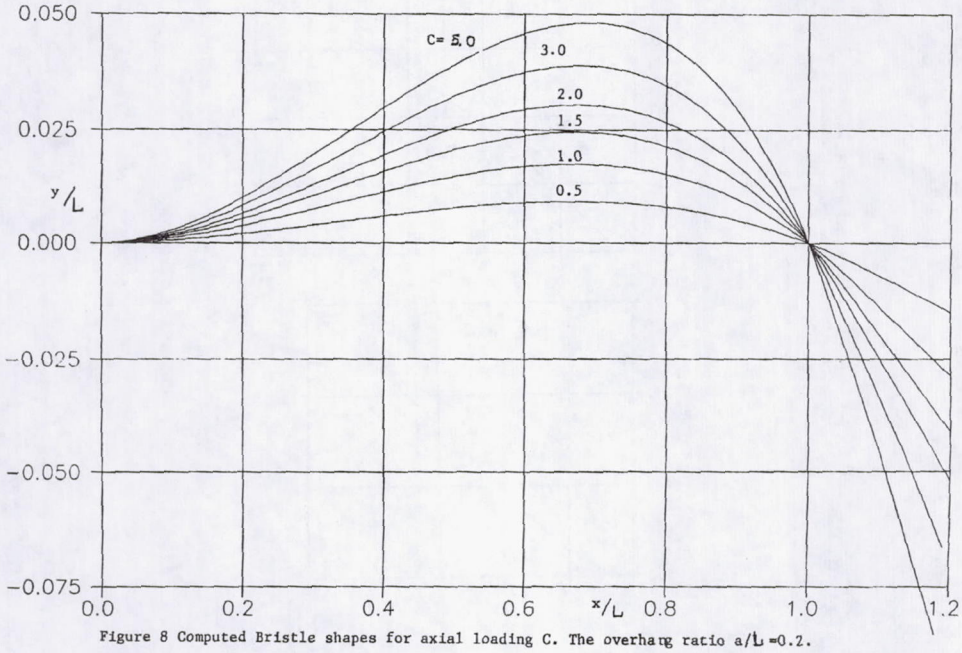

Figure 8 Computed Bristle shapes for axial loading C. The overhang ratio a/L =0.2.

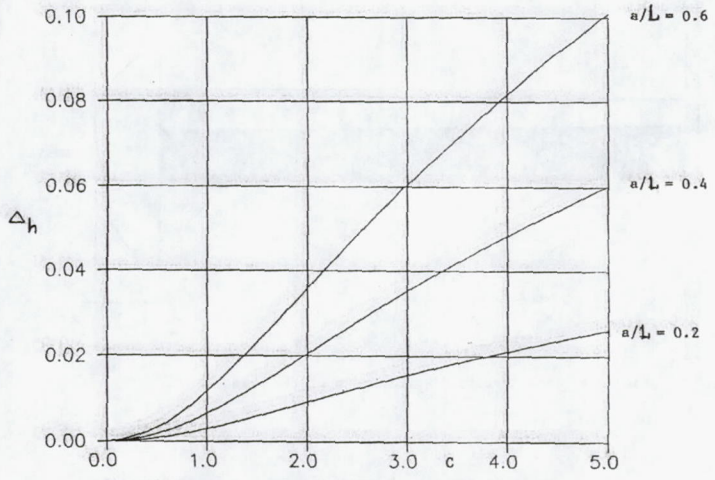

Figure 9 Clearance generated due to axial loading for various values of C. a/L = 0.2,0.4,0.6

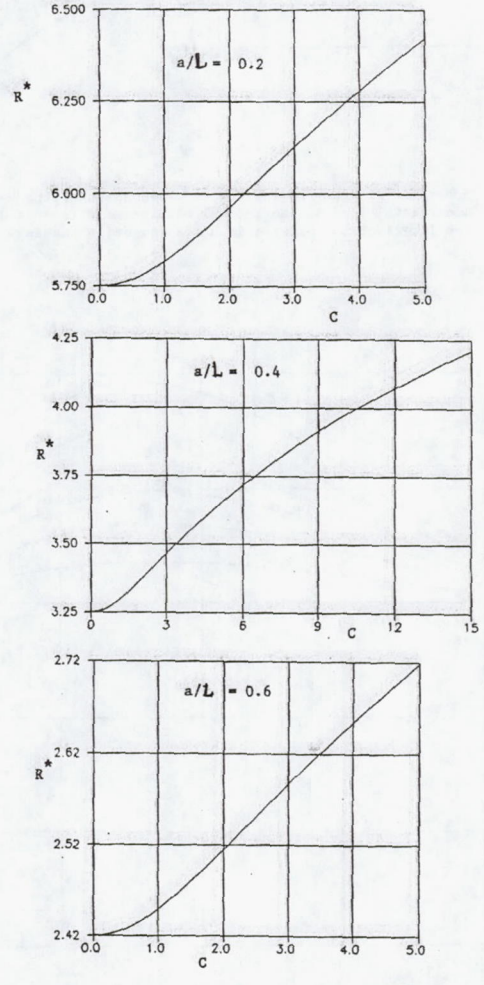

Figure 10 Variation of the Normalized reaction force R^* where $R^* = (RL^2/EI)/ C_{eff}$

Brush Seals For Turbine Engine Fuel Conservation

Contract No. N00140-90-C-3199
W. Voorhees, U.S. Navy/NAWC Program Engineer

August 6, 1992

Presented At:

Brush Seal System Workshop
NASA Lewis Research Center
Cleveland, Ohio

R. Korzun
W. Ostergren

GE Aircraft Engines
Lynn, Massachusetts

GEAE Brush Seal Program Presentation Summary

Brush Seals for Turbine Engine Fuel Conservation

General Electric Aircraft Engines (GEAE) has an ongoing program sponsored by NAWC (Contract No. N00140-90-C-3199) for the evaluation of brush seals. This is a summary of the program status as presented during the Brush Seal System Workshop at the NASA Lewis Research Center in Cleveland, Ohio on August 6, 1992 by Ron Korzun.

The objective of the program is to design, procure and test brush seals intended to be suitable for replacing the inner and outer balance piston seals in the T407 turboprop engine. An existing T407 low pressure turbine rig was modified to conduct the brush seal testing. The rig which includes the power turbine shaft accurately simulates the dynamics of the engine. A picture and cross section of the rig are shown in Figures 1 and 2.

Figure 1. T407 Rig Assembled in Test Platform

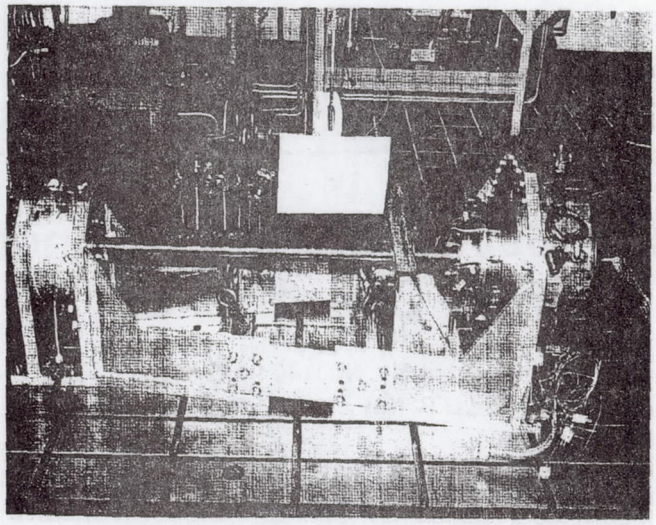

GE Aircraft Engines

Figure 2. T407 IBP and OBP Brush Seal Dynamic Test Rig

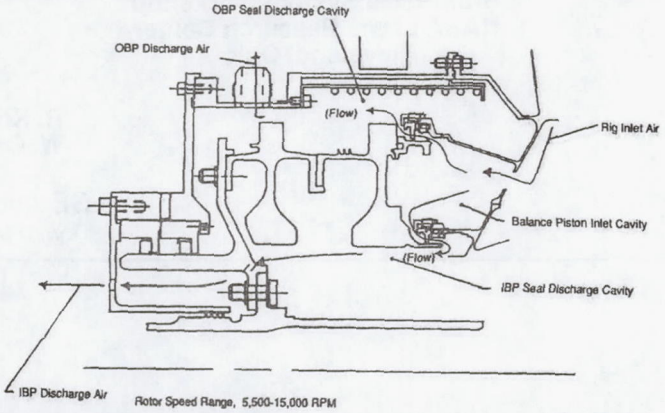

The design of the seals was conducted with the assistance the seal supplier EG&G Sealol. Some design parameter and features are presented in Figures 3 and 4.

Figure 3. Seal Design and Fit - Ups

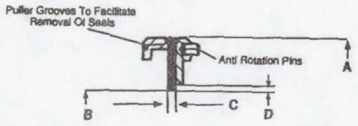

	OBP	IBP
Brush Seal Inner Diameter Cold (B)	10.1"	5.6"
Brush To Runner Diametral Interference - Cold (B)	.006	.006
Brush To Runner Diametral Interference - Hot (B)	.010	.010
Brush Axial Pack Width (C)	.025	.050
Backing Plate GAP (D)	.051	.044
Diametral Interference Fit With Stator Support - Cold (A)	.006	.004
*Maximum Stress – Seal Support	18 KSI	25 KSI
*Maximum Stress –Brush Seal	13 KSI	17 KSI

* At SS IRP, Nominal Fit Up

GE Aircraft Engines

Figure 4. Key Brush Seal/Rig Features

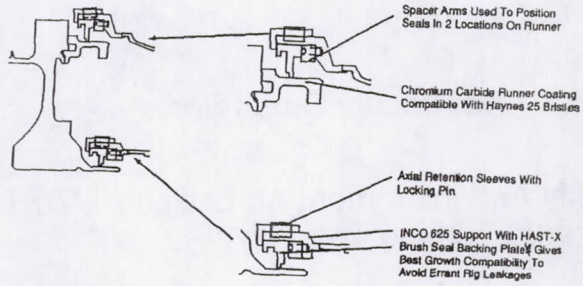

The test plan calls for cyclic test to evaluate the leakages at operating pressures and temperatures. The test plan also calls for the evaluation of the effect of seal pack width and rotor eccentricity. The brush seal design goals are to achieve or exceed a 50% leakage reduction versus labyrinth seals. This must be accomplished without affecting rotor life. The test will also evaluate runner coating wear, heat generation and corrosion.

The project is carried out under the direction of Bill Voorhees, the NAWC Project Engineer with the assistance of Guy Ullman, the NAVAIR Project Engineer and Carl Grala, the NAWC Component Engineer. At GEAE Warren Ostergren is the program manager. Ron Korzun is the design engineer and Bert Campbell is the test engineer. EG&G Sealol's support has come from program manager, Chuck Nevola and design engineer, Bob Johnson.

As of the August review, the build of the test rig for its initial testing was in process. GEAE looks forward to presenting the results of the test program during a future NASA workshop.

Program Objective

Design, Procure, And Test Brush Seals Intended To Be Suitable For Replacing The Inner And Outer Low Pressure Balance Piston Labyrinth Seals In the T407 Turboprop Engine.

Program Approach

- Design And Procure Brush Seals
- Modify And Instrument An Existing T407 Low Pressure Turbine Test Rig
- Conduct Cyclic Tests To Evaluate Seal Leakage At Operating Pressures And Temperatures
- Evaluate Effect Of Seal Pack Width And Rotor Eccentricity

Project Organization

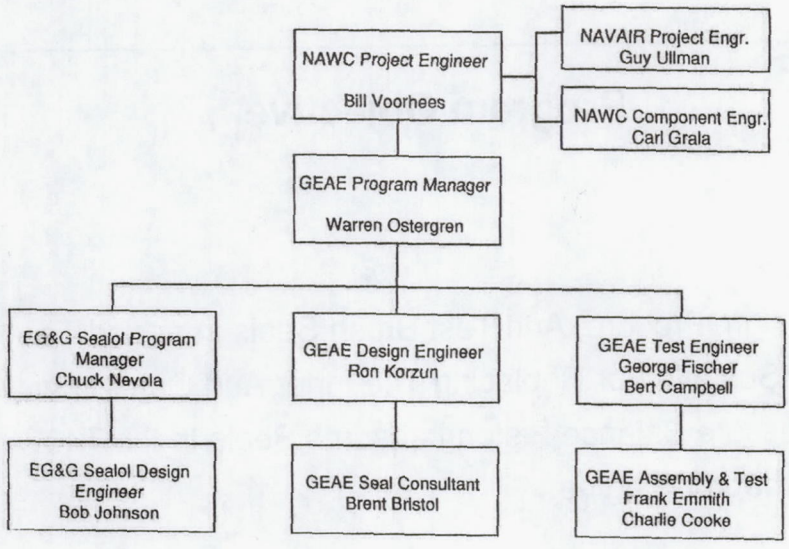

Brush Seal Design Goals

- Achieve Or Exceed Predicted Leakage Reduction Versus Labyrinth Seals
  - OBP - 59% Reduction
  - IBP - 45% Reduction
- Rotor Part Life Not Limited By Brush Contact
  - Runner Coating Wear
  - Heat Generation
  - Corrosion

T407 IBP And OBP Brush Seal Dynamic Test Rig

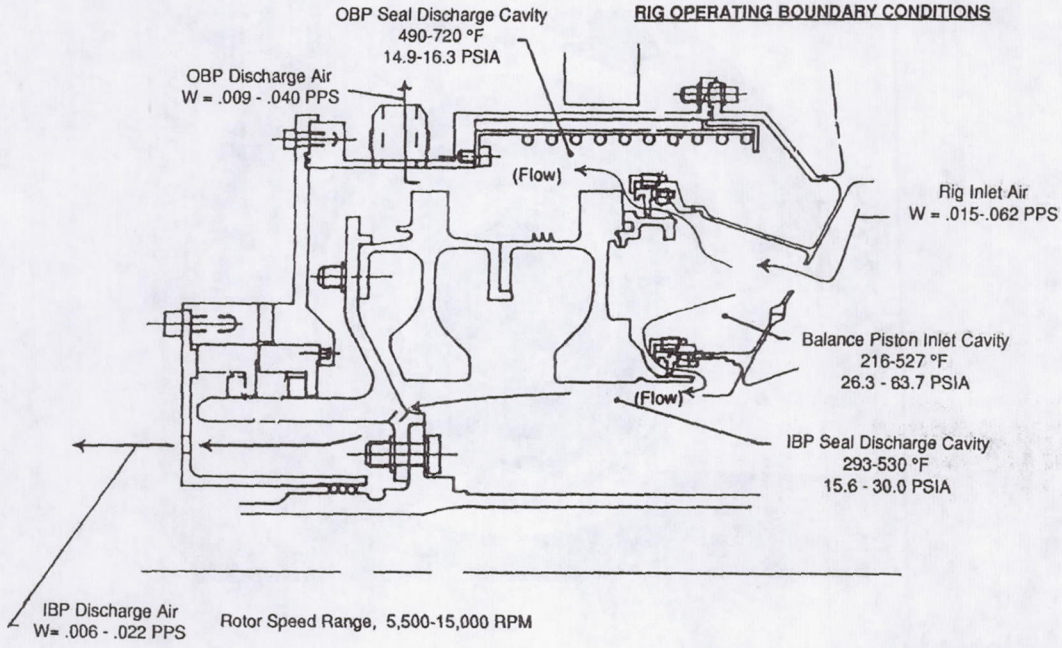

Power Turbine Rotor Assembly

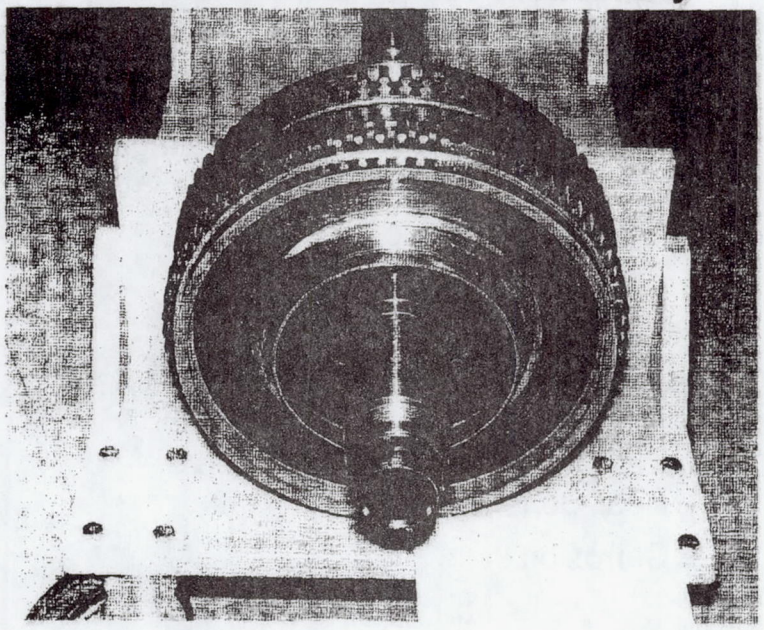

Exhaust Frame Stator Assembly With Brush Seals Installed

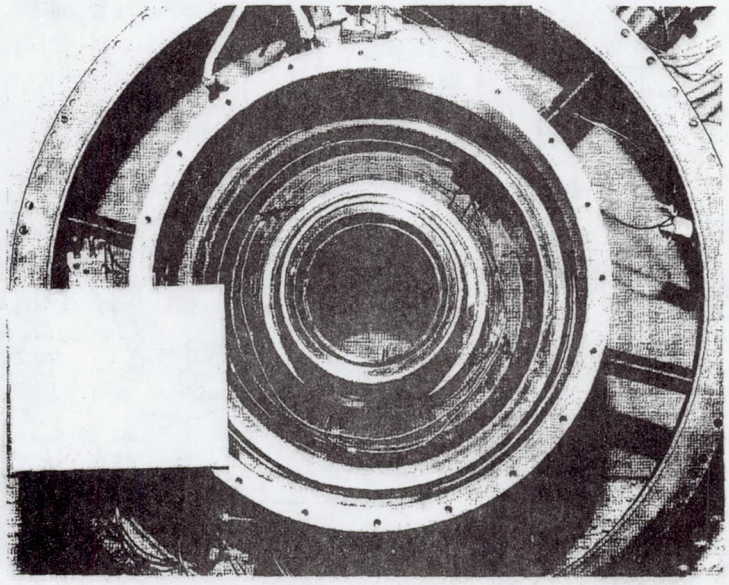

Exhaust Frame/Outer Housing Assembly

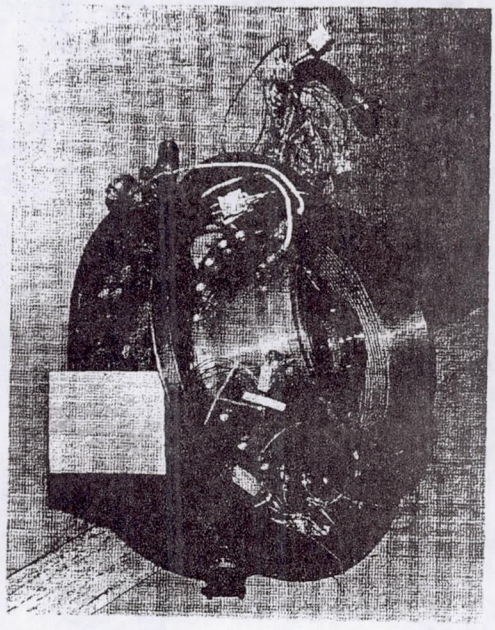

T407 Rig Assembled In Test Platform

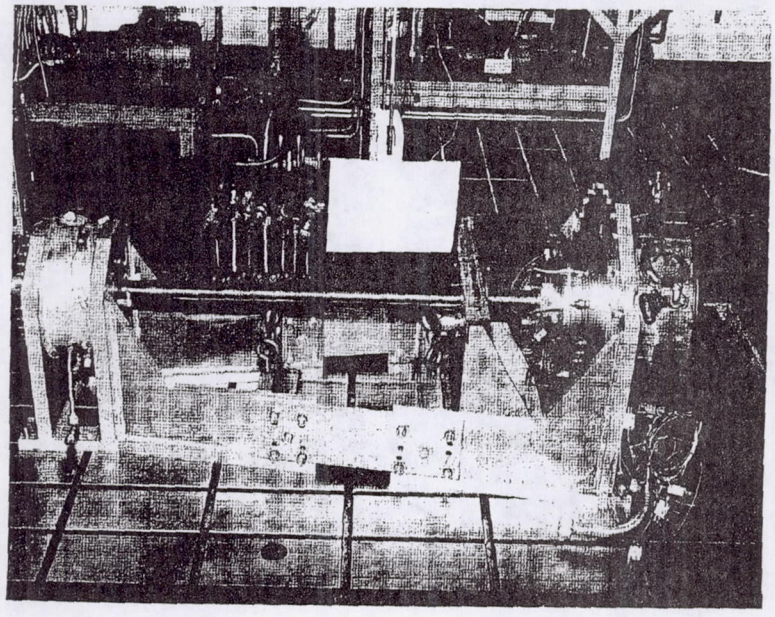

Key Brush Seal/Rig Features

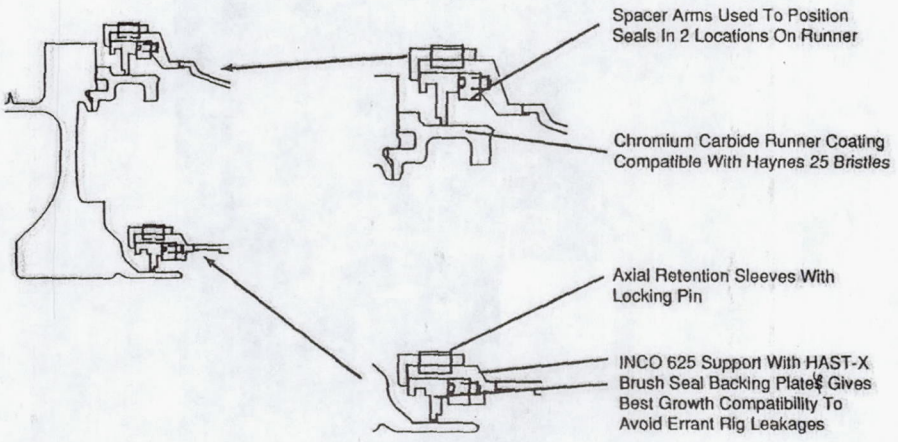

Outer Balance Piston Brush Seal

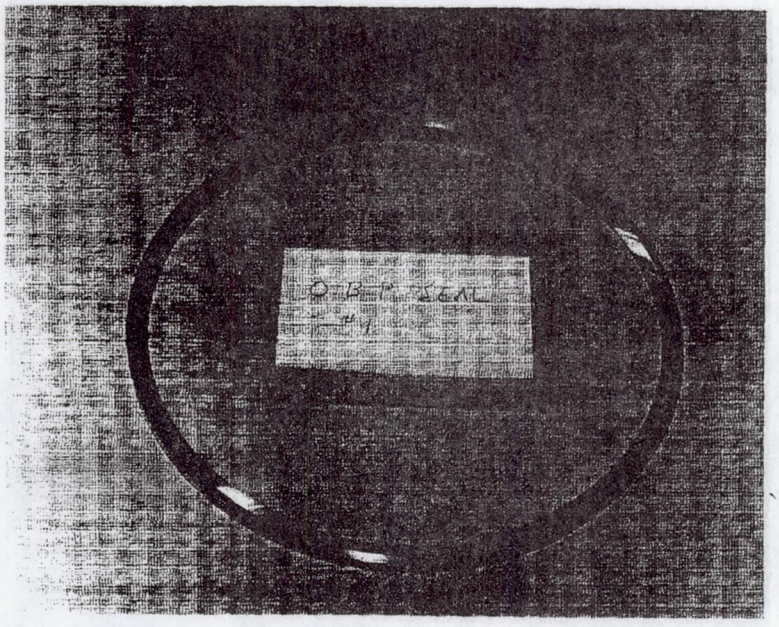

Inner Balance Piston Brush Seal

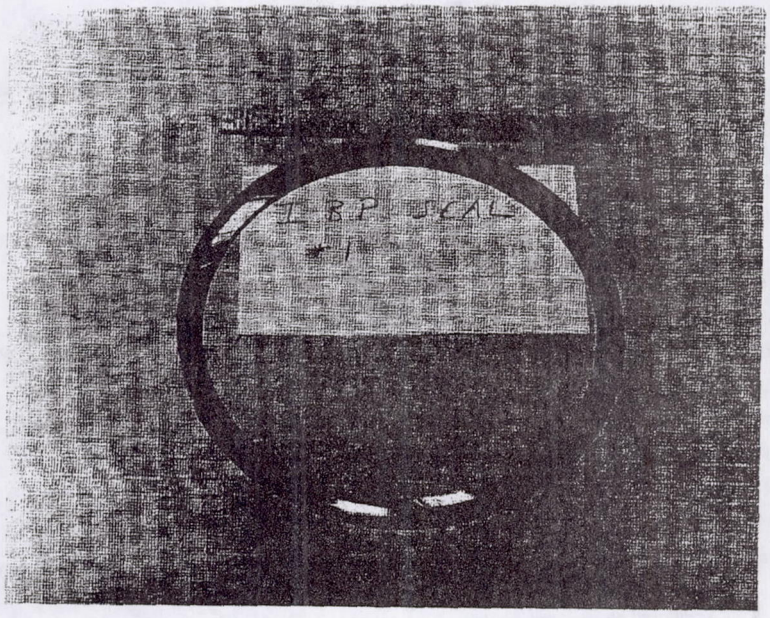

Seal Design and Fit - Ups

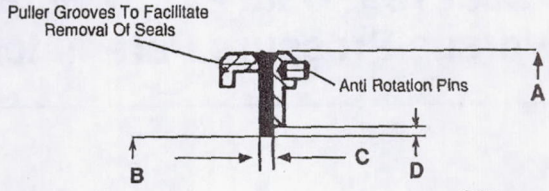

	OBP	IBP
Brush Seal Inner Diameter Cold (B)	10.1"	5.6"
Brush To Runner Diametral Interference - Cold (B)	.006	.008
Brush To Runner Diametral Interference - Hot (B)	.010	.010
Brush Axial Pack Width (C)	.025	.050
Backing Plate GAP (D)	.051	.044
Diametral Interference Fit With Stator Support - Cold (A)	.006	.004
*Maximum Stress – Seal Support	18 KSI	25 KSI
*Maximum Stress –Brush Seal	13 KSI	17 KSI

* At SS IRP, Nominal Fit Up

- Brushes Maintain Contact With Rotor At All Operating Conditions
- Backing Plate Distance Sized For Worst Case Conditions Expected In Field
- Backing Interference Maintained At All Operating Conditions - Avoid Leakage
- Stress Is Acceptable - Below .2% Yield Strength

Brush Seal Data Used To Size T407 Brush Seals

	GE	Sealol	Technical Literature
Test Conditions			
Pressure Drop	0-80	15-25	20
Temperature (F)	70	70	600
Surface Speed (Ft/S)	430	375	668
Seal Parameters			
Diameters	5.1, 11.3	5.4	5.1
Backing Plate Height	.04-.130	.047	.02,.03
Pack Thickness	.018-.027	.025	.027
Bristle Diameter	.002,.0028	.0028	.0028
Bristle Angle	45-56	36-56	45
No. Of Stages	1	1	1, 2

- The above ranges stated are for the test data which was readily available (10/91) to use in evaluating the T407 Seals
- Additional studies are continually in process at GEAE (Ruston) and at Sealol

Brush Seal Test Data - Flow Parameter Versus Pressure Parameter

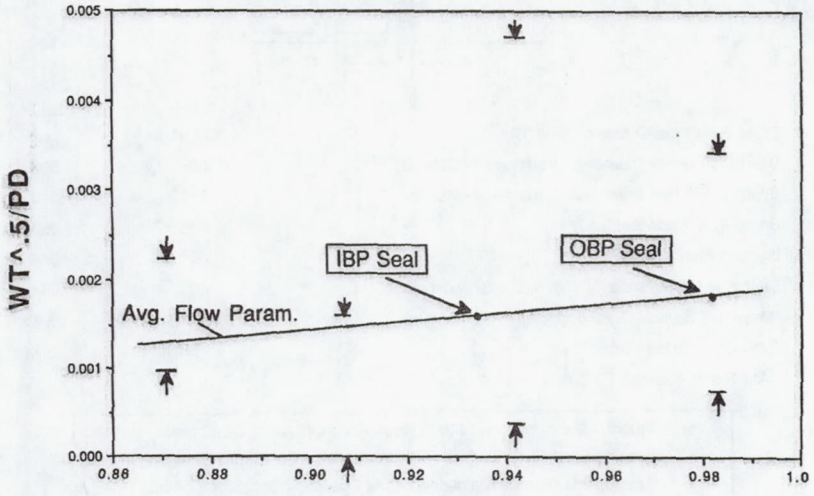

Test Plan Schedule

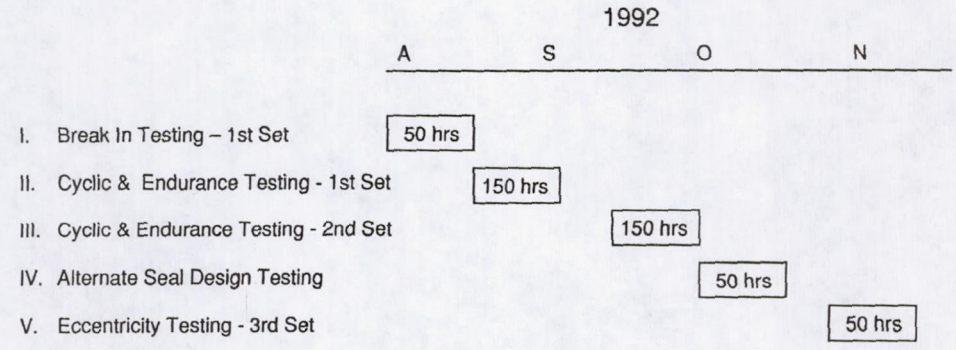

Test Plan Includes Extensive Testing On Three Sets Identical Seals And One Alternate Design.

Summary

- OBP And IBP Brush Seal Designs Completed And Fabricated
- LPT Dynamics Rig Modifications Completed
- Test Plan Defined
- Test Cell Checkout Completed
- Testing To Begin In August

Tribopair Evaluation of Materials for Brush Seal Applications

From notes and discussion of talk by J. Derby , EG&G
by R.C. Hendricks

Derby and England investigated several brush seal system tribopairs from bristle materials Haynes 25, Inconel 718, and proprietary materials called Alloys A, B, C, D, and E and coatings chromium carbide, Triboglide, tungsten carbide, chromium oxide, aluminum oxide, Tribaloy, Tribomet T-104C.

Haynes 25 is a cobalt chromium nickel tungsten based superalloy that forms an oxide resistive Cr2O3 film.

Inconel 718 is a precipitation hardenable nickel chromium superalloy good to 1300 F.

Alloy A (Ni Cr Al base superalloy solid-solution strengthened) is being used in gas turbine hot spots and develops a tenacious Cr2O3 and Al2O3, yittria-modified oxide layer.

Alloy B (solid-solution, and carbide strengthened Ni Cr, W based superalloy) with good strength at elevated temperatures developing an Cr2O3 oxide film that is enhanced by lanthanum, and used in combustion cans.

Alloy C (mechanically alloyed, oxide dispersion strengthened, Fe, Cr, Al based superalloy) has excellant resistance to oxidation due the a tenacious Y2O3 stabilized Al2O3 and Cr2O3 film, good to perhaps 2100 F.

Alloy D (solid-solution strengthened by addition of W and precipitation of M6 and M23C6 carbides Co, Cr, W, Ni based superalloy) is one of the first sheet alloys developed for aircraft engines. Adding lanthanum is reported to modify the protective oxide layer up to 2000 F.

Alloy E (age hardened Ni, Mo, Cr based superalloy without gamma prime precipitate and hardening believed based on Ni2(cr,Mo) stoichiometry) with service temperatures to 1400 F.

Although not reported Haynes 125 is known to have a higher use temperatue but more data are required on tribological pairing.

Chromium carbide has superior wear and friction performance. Sprayed coatings contain Cr3C2 and Cr7C3 mixtures produce an increase in hardness. The CrO was applied using HVOF.

Triboglide is a CrC containing additives of 12 wt. percent barium and calcium fluoride solid lubricants based on the work of Sliney at NASA-LeRC. Spray parameters (standoff, angle, powder size, feed rate, temperature) were investigated and use of HVOF was prefered.

Tungsten carbide contains a Co binder and exibits phases WC, W2C, and Co3W3C with decarbonization of some WC above 900F. Union Carbide D-Gun was preferred with 8-percent Co binder.

Chromium oxide has higher friction but used within the industry has low thermal expansion and thermal conductivity.

Aluminum oxide was applied using air plasma spray (APS) with a bond coat of 0.001-0.002 inch.

Tribaloy T-800 is a Co based with Mo, Cr, and Si additives and APS and HVOF applied followed by a heat treatment.

Tribaloy T-104C is Co based that is electrodeposited such that CrC particles are codeposited in the coating. Exhibits good friction and wear characteristics and is almost entirely metallic (good rotor adherence).

The tests were performed using a 2.0 inch diameter, 0.040 inch-two-lobed-cam rotor at 1200F at speeds of 10, 20, and 30 krpm, providing about 15E9 fatigue cycles. The interface was assumed to be line to line at the mean equivalent diameter although no preload information was given.

In a second of tests at 0-pressure drop, conducted at 2, 20, 40, and 60 krpm at 800 F the nominal brush-rotor clearance was -0.010 inch-radial.

Inconel 718 and Haynes 25 bristles form unstable Cr2O3 layers with leading edge alloy fractures. Alloy A is least damaged by fatigue cycles and most oxidative resistant.

Oxide coatings exhibit microfracturing and grain pullout which promotes wear and cobalt alloy bristles perfromed poorly due to a transformation from hexagonal close to face centered at 400C (750F).

Alloy A/Triboglide (15-20 microinch Ra) provided good friction behavior vs sliding speed (varies from 0.14 to 0.25) with Inco 718/Triboglide constant at 0.3. The Haynes 25 /Triboglide is good at surface speeds of 100 to 350 ft/s while Haynes 25/CrC increased linearly from 0.23 to 0.45 at 500 ft/s.

As an editorial note, there does exist some transition from hexagonal close pack to cubic crystal structure between 350 C and 400 C. Within this temperature range the wear increases and is up to ten times higher in a vacuum (ref. 2). In air the formation of oxides tends to mitigate wear and for low sliding speeds wear actually decreases as temperature is increased (ref. 3). However data at both elevated temperature and surface speed are needed.

For more information

1. Derby, J., and England, R.: AIAA 92-3715, "Tribopair Evaluations of Brush Seal Applications," AIAA/SAE/ASME/ASEE 28th Joint Propulsion Conference, July 6-8, 1992, Nashville, Tennessee.

2. Buckley, D.H.; and Johnson, R.L.: Friciton and Wear of Hexagonal Metals and Alloys as Related to Crystal Structures and Lattice Parameters in Vacuum. ASLE Trans. 9, 121-135 (1966).

3. Murray, F.S.; and Calabrese, S.J.: Low Speed Sliding Behavior of Metal-Ceramic Couples at Temperatures to 800 C. Lubrication Engr., V. 49, 5, pp. 387-397 (1993).

NASA LEWIS RESEARCH CENTER SEAL WORKSHOP IN CLEVELAND/OHIO, 5 - 6 AUGUST 1992

DAMPING SEAL BEARINGS

George L. von Pragenau, Huntsville/Alabama, (205) 536-6832

PRESENTATION TOPICS

1. ABOUT TECHNOLOGY	9. HPOTP DAMPING SEAL BEARINGS
2. HIGH PRES. FUEL TURBOPUMP (HPFTP)	10.HPOTP DAMPING SEAL BEARING ENGINE TESTS
3. HIGH PRES. OXYGEN TURBOPUMP (HPOTP)	11.HYDROSTATIC BEARING
4. HIGH PRESSURE TURBOPUMP WHIRL DATA	12.DAMPING BEARINGS
5. BASIC ROTORDYNAMIC MODEL	13.HPOTP/HPFTP TURBINE DAMPING BEARINGS
6. ROTOR SPEED LIMIT	14.SEALS & BEARINGS DYNAMIC & LEAKAGE DATA
7. DAMPING SEAL	15.GENERIC BEARING COMPARISON
8. SPACE SHUTTLE PUMP SEAL HISTORY	16.OUTLOOK

ABOUT TECHNOLOGY

TECHNOLOGY IS A STATE OF READINESS TO REALIZE DREAMS BEYOND OUR LIMITS.

LASTING TECHNOLOGY COMES BY FAITH IN GOD, HIS INSPIRATION, LOVING CARE, RISK, STAMINA, PATIENCE, LABOR, COOPERATION, APPRECIATION, AND LIBERTY.

TECHNOLOGY THRIVES ON SOUND ENGINEERING; YET DARES OLD LIMITS, SEEMLY IN CONFLICT, TO FIND WAYS OUTSIDE THE STATUS QUO TO A BRIGHTER FUTURE.

HIGH PRESSURE FUEL TURBOPUMP (HPFTP)

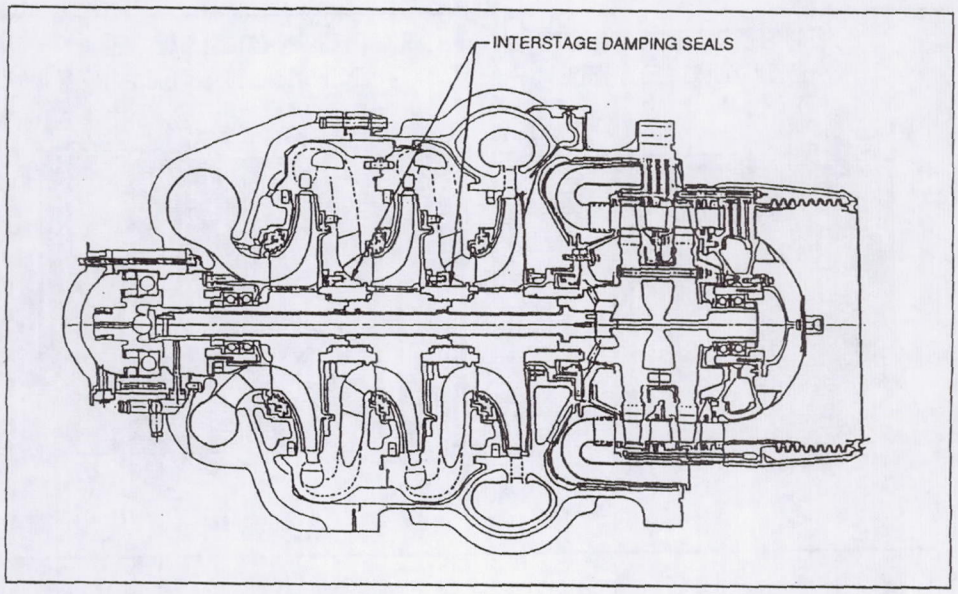

HIGH PRESSURE OXYGEN TURBOPUMP (HPOTP)

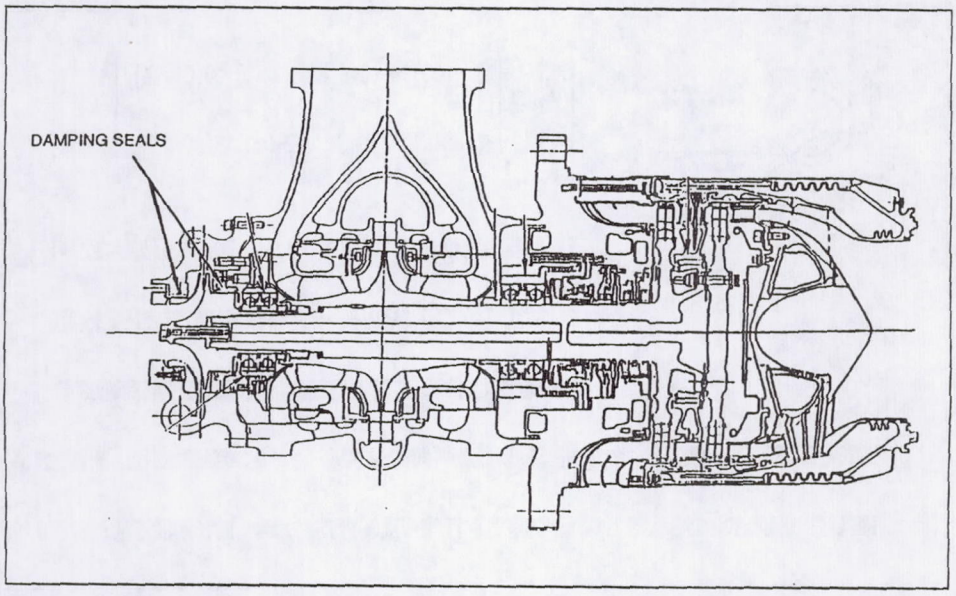

HIGH PRESSURE TURBOPUMP WHIRL DATA

HIGH PRESSURE FUEL TURBOPUMP
HPFTP 2106R3 50 % WHIRL

HIGH PRESSURE OXYGEN TURBOPUMP
HPOTP 0303 90 % WHIRL

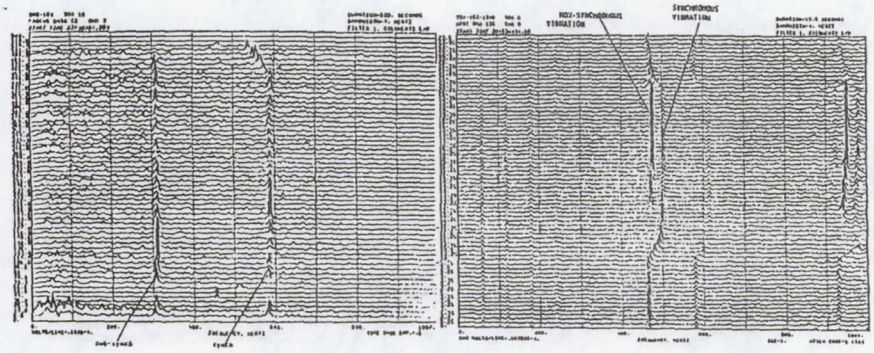

BASIC ROTORDYNAMIC MODEL

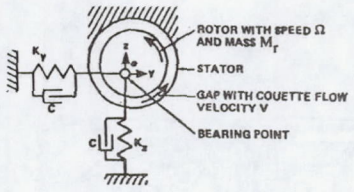

$$\begin{vmatrix} F_y \\ F_z \end{vmatrix} = \begin{vmatrix} K_y-(c\underline{Q})^2M+sC+s^2M_r & Q+c\underline{Q}(C+s2M) \\ -Q-c\underline{Q}(C+s2M) & K_z-(c\underline{Q})^2M+sC+s^2M_r \end{vmatrix} * \begin{vmatrix} y \\ z \end{vmatrix}$$

F_i EXTERNAL ROTOR FORCES y, z ROTOR DISPLACEMENTS

C SEAL INDUCED DAMPING c=v/w COUETTE FLOW RATIO

K_i BEARING+SEAL STIFFNESSES M_r ROTOR MASS PLUS M

$\underline{Q}$ ROTOR SPEED IN RADIANS M SEAL FLOW INDUCED MASS Q OTHER WHIRL DRIVERS

s LAPLACE OPERATOR RADIANS v COUETTE FLOW VELOCITY w ROTOR SURFACE SPEED

ROTOR SPEED LIMIT

RESONANCE FREQUENCY (RADIANS)	$w_o = \{[K_y+K_z+(c\underline{Q})^2 2M+c\underline{Q}4MQ/C]/2M_r\}^{0.5}$
DETERMINANT AT RESONANCE	$D_o = [c\underline{Q}+Q/C]^2*[C^2+(c\underline{Q}2M)^2] - w_o^2*[C^2+(c\underline{Q}2M)^2] - [K_y-K_z]^2/4$
STABILITY CONDITION ($D_o < 0$)	$[c\underline{Q}+Q/C]^2*[C^2+(c\underline{Q}2M)^2] < w_o^2*[C^2+(c\underline{Q}2M)^2] + [K_y-K_z]^2/4$
SPEED LIMIT FOR UNIFORMITY	$\underline{Q} < (w_o - Q/C)/c = \underline{Q}_o$ FOR $K_y = K_z$
APPROXIMATE SPEED LIMIT	$\underline{Q} < w_o/c$ FOR $K_y = K_z$ AND $w_o*C >> Q$

AT THE WHIRL ONSET SPEED $\underline{Q}_o$ THE ROTOR BECOMES UNSTABLE AND WHIRLS. NOTICE THAT HIGH DAMPING C AND A LOW CUETTE FACTOR c INCREASE THE SPEED LIMIT. DAMPING SEALS MEET BOTH REQUIREMENTS. TYPICALLY c IS 0.20. FOR SMOOTH SEALS AND JOURNAL BEARINGS c IS 0.50.

DAMPING SEAL

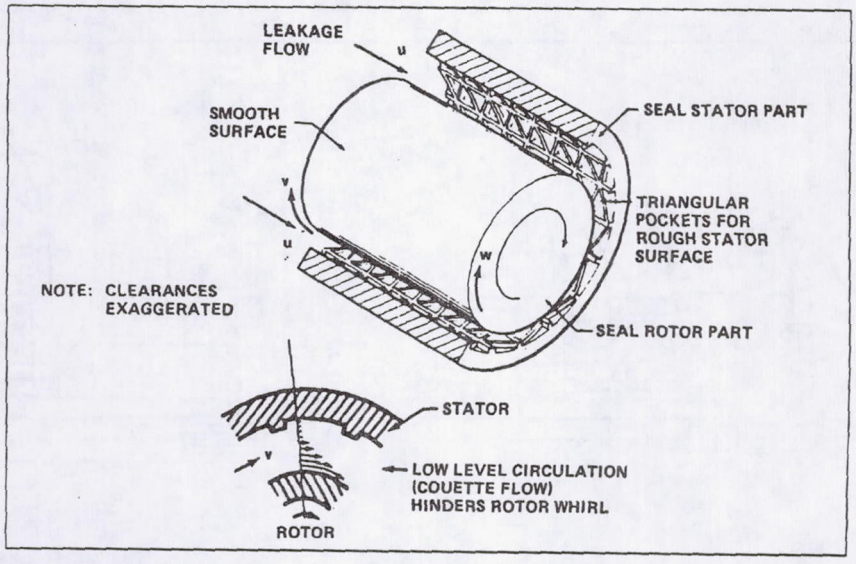

SPACE SHUTTLE PUMP SEAL HISTORY

EARLY IN 1976 THE HIGH PRESSURE FUEL TURBOPUMP (HPFTP) SPEED LIMIT WAS 22,000 RPM TO AVOID A 175 Hz SUBSYNCHRONOUS ROTOR WHIRL. THE REQUIRED OPERATIONAL SPEED IS 36,000 RPM.

STIFFER BALL BEARING SUPPORTS AND TWO STIFFER SMOOTH SHAFT SEALS (INSTEAD OF LABY SEALS) RAISED THE 1st CRITICAL SPEED TO 18,000 RPM AND THE WHIRL TO AN INTERMITTENT 300 Hz.

DAMPING SEALS WERE INVENTED 1981 TO ELIMINATE THE 50 % SUBSYNCH. WHIRLS OF SMOOTH SEALS. DAMPING SEALS WERE INSTALLED 1989 IN THE HPFTP. COULOMB FRICTION DEVICES WERE ABANDONED.

ONE HIGH PRESSURE OXYGEN TURBOPUMP (HPOTP) EXPLODED 8 SEPTEMBER 1977 FROM A 95 % SUB-SYNCHRONOUS WHIRL, CAUSED BY INTERNAL ROTOR FRICTION, THE MOST VIOLENT WHIRL-DRIVER.

SINCE THE 1st REFLIGHT, DISCOVERY ON 29 SEPTEMBER 1988, EVERY HPOTP FLIGHT PUMP HAS DAMPING SEALS IN THE PREBURNER PUMP (PBP) INLET AND DISCHARGE TO AVOID THE 95 % WHIRL.

HIGH BALL WEAR LIMITS THE HPOTP TO 2 FLIGHTS AND IGNITED A FIRE 23 JUNE 1989 IN A TEST. TESTS W/O BALL BEARINGS CONFIRMED THAT DAMPING SEALS ARE SUPERIOR HIGH SPEED BEARINGS.

HPOTP DAMPING SEAL BEARINGS WITH AND W/O BALL BEARINGS

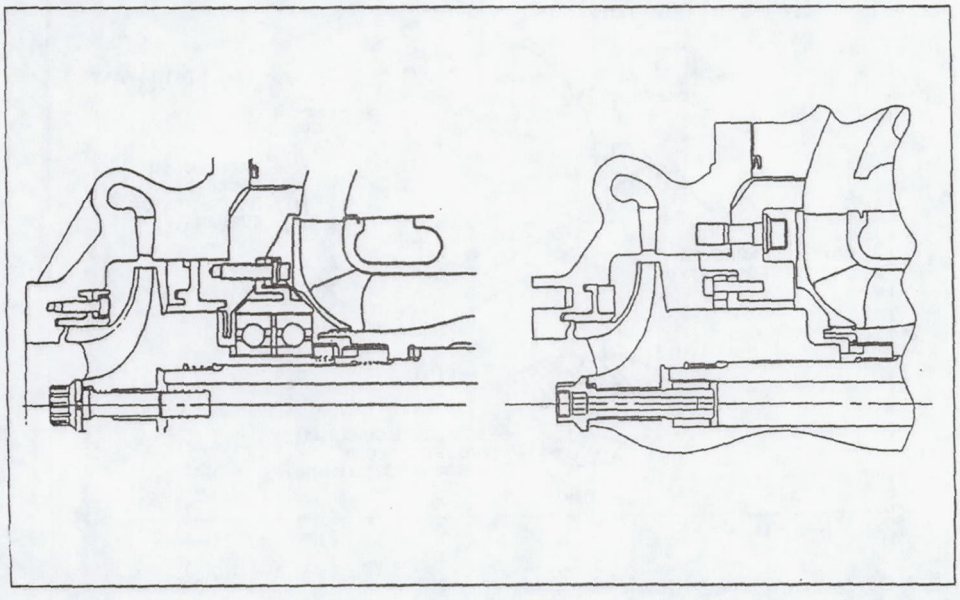

HPOTP DAMPING SEAL BEARING ENGINE TESTS WITH BALL BEARINGS

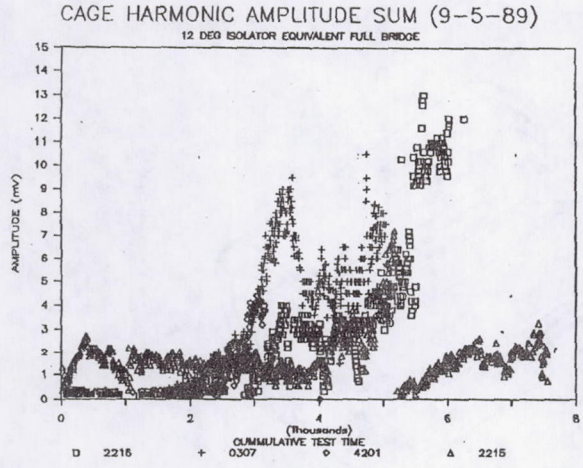

HPOTP PUMP END BEARING TEST SAMPLE

HPOTP 0307#	ENGINE NUMBER	TEST NO.	TIME SEC.	SUM SEC.
R3	2105	901-501	519	519
R3		502	520	1039
R3		503	520	1559
R3		504	520	2079
R3		505	520	2599
R3		506	520	3119
R3		* 507	590	3709
R4	2106	902-405	200	3909
R4		406	200	4109
R4		407	200	4309
R4		408	200	4509
R4		409	200	4709
R4		410	520	5229
R4	0210	750-283	300	5529
R4		** 284	300	5829

* BALL BEARING PRELOAD AND SUPPORT WAS LOST AT 3509 SEC. OF TEST TIME.

** PUMP END BEARING TEST TIME WAS 5829 SEC. WITH 2320 SEC. (8 STARTS AND 9 STOPS) ON THE DAMPING SEAL BEARING. THE TURBINE END BEARING REACHED 8303 SEC. TEST TIME.

HPOTP DAMPING SEAL BEARING ENGINE TESTS W/O BALL BEARINGS

NASA MSFC AND ROCKETDYNE CONDUCTED 7 SUCCESSFUL ENGINE TESTS FROM 12 MARCH TO 11 JUNE 1992 WITH THE DAMPING SEAL BEARING FUNCTIONING AS A HIGH PRESSURE SHAFT SEAL, CRITICAL DAMPER, AND STIFF BEARING; REPLACING A LABY. SEAL AND PREBURNER PUMP (PBP) DUPLEX BALL BEARING.

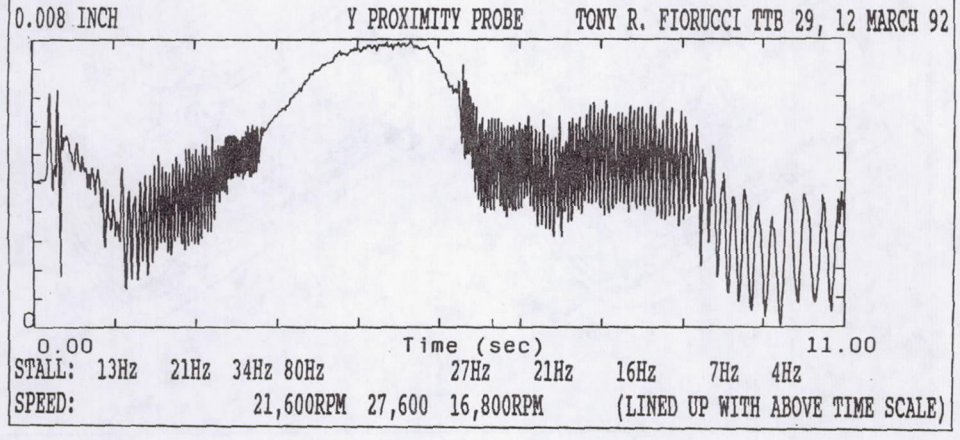

HYDROSTATIC BEARING

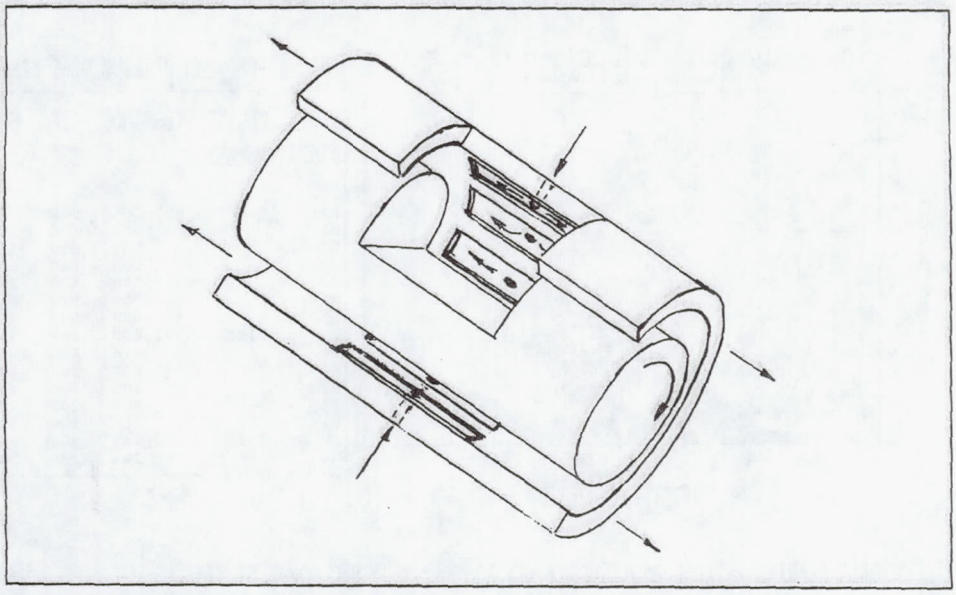

DAMPING BEARINGS

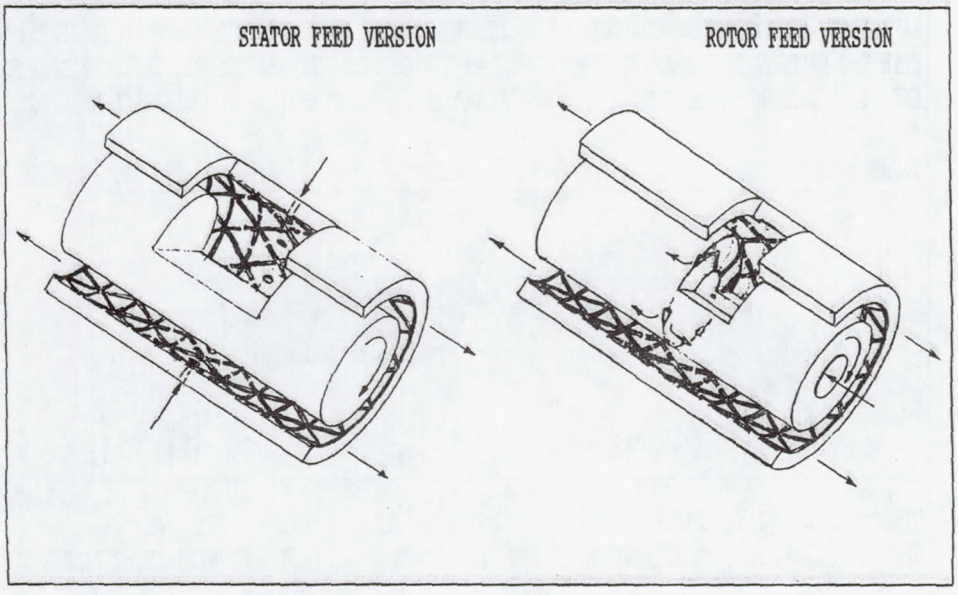

HPOTP (LEFT) / HPFTP (RIGHT) TURBINE DAMPING BEARINGS

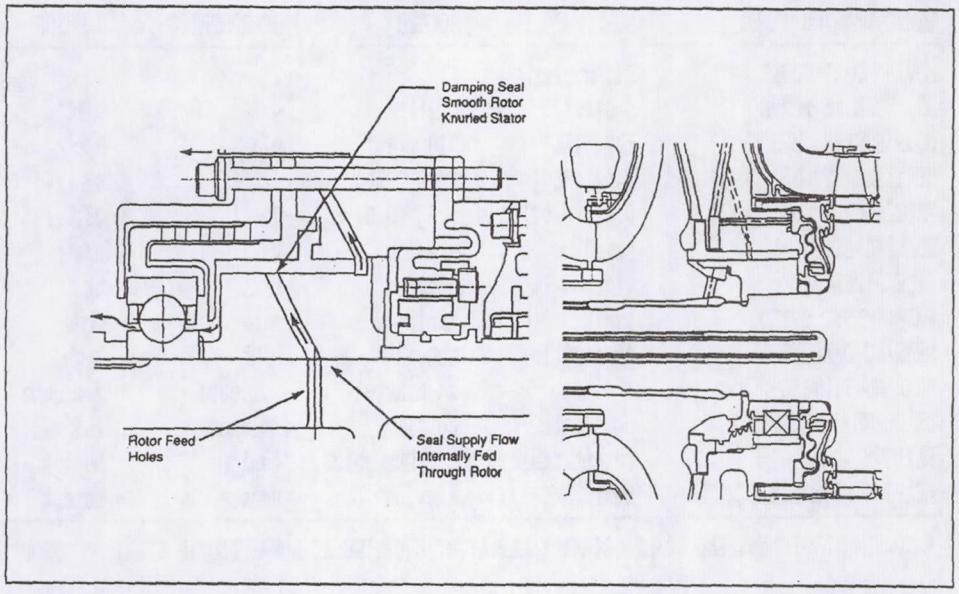

SEALS & BEARINGS DYNAMIC & LEAKAGE DATA

SEALS AND BEARINGS	STIFFNESS MN/m (klb/in)	DAMPING kNs/m (lb s/in)	WHIRL FREQUENCY RATIO	LEAKAGE kg/s (lb/s)
HPOTP PBP DUPLEX BALL BEARING	70 (400)	3.5 (20)	n/a	2.7 (6)*
HPOTP PBP DISCH.LABYRINTH SEAL	3.5 (20)	4.0 (23)	0.50	2.3 (5)
HPOTP PBP DISCH.DAMPING SEAL	100 (580)	53 (300)	0.19	2.7 (6)
HPOTP TURBINE HYDROSTATIC BEARING	1100 (6000)	400 (2300)	0.50	18 (39)
HPOTP TURBINE DAMPING BEARING	1200 (6800)	670 (3800)	0.27	9.1 (20)
HPFTP SMOOTH SEAL	68 (390)	28 (160)	0.50	0.6 (1.4)
HPFTP DAMPING SEAL	26 (150)	44 (250)	0.17	0.3 (0.7)
HPFTP TURBINE ROLLER BEARING	610 (3500)	none	n/a	1.1 (2.5)*
HPFTP TURBINE HYDROSTATIC BEARING	510 (2900)	89 (510)	0.50	2.3 (5.0)
HPFTP TURBINE DAMPING BEARING	530 (3000)	160 (920)	0.18	1.1 (2.5)

* LEAKAGE THROUGH BALL AND ROLLER BEARINGS ARE COOLANT FLOWS. HPOTP IS THE HIGH PRESSURE OXYGEN TURBOPUMP. PBP IS THE PREBURNER PUMP OF THE HPOTP. HPFTP IS THE HIGH PRESSURE FUEL TURBOPUMP. HPOTP AND HPFTP DATA ARE FOR 30,000 RPM AND 36,000 RPM, RESPECTIVELY.

GENERIC BEARING COMPARISON

ITEMS\BEARING TYPES	BALL	ROLLER	HYDROSTATIC	DAMPING
MOVING PART COUNT	33, duplex	17	1	1
DN, BORE mm x RPM	$< 2*10^6$	$< 2*10^6$	$< 10^7$	$< 10^7$
HOOP STRESS MPa (ksi)	172 (25)	310 (45)	n/a	n/a
HERTZIAN ST. MPa (ksi)	2412 (350)	2412 (350)	41 (6)	41 (6)
PRECISION um (mil)	0.5 (0.02)	0.5 (0.02)	25 (1)	25 (1)
ROLLING STABILITY	skidding	skewing	n/a	n/a
HIGH SIDELOAD	wear	skewing	ok	ok
WHIRL ONSET SPEED	limit	limit	limit	none
BEARING DAMPING	negligible	none	high	high
BEARING TILTING	< minute	<< minute	> minute	> minute
DEADBAND/TIGHT FIT	conflict	conflict	relaxed	relaxed
FAILURE MODE	catastrophic	catastrophic	benign	benign
BEARING LIFE LIMIT	wear	skewing	none *	none *

* NO WEAR AT FULL SPEED. ONLY OCCASIONALLY LIGHT BRUSHING AT LOW SPEED IN START AND STOP.

OUTLOOK

GOD'S LIBERATING CREATIVITY IS JOYFULLY ACKNOWLEDGED IN FAILURE TO RECOVER (& IN SUCCESS).

DAMPING SEALS SUPPRESS ROTOR WHIRL AS PROVEN WITH SPACE SHUTTLE MAIN ENGINE (SSME) PUMPS.

DAMPING SEAL BEARINGS PROVED TO BE SUPERIOR HIGH SPEED BEARINGS IN SEVERAL SSME TESTS.

DAMPING SEAL & BEARING SIZES AND FLOWS READILY RETROFIT SEALS, BALL AND ROLLER BEARINGS.

DAMPING SEAL & BEARING OFFER COMPARATIVELY INFINITE LIFE AND SIMPLIFY TURBOPUMP DESIGNS.

CRITICAL SPEEDS BECOME NONCRITICAL AND CATASTROPHIC FAILURE MODES BECOME RATHER BENIGN.

DILEMMAS BECOME DESIGN OPTIONS AND FABRICATION/ASSEMBLY/MAINTENANCE OFFER GREAT SAVINGS.

NASA AND ROCKETDYNE HAVE THE OPPORTUNITY TO SAVE $10 MILLION/YEAR ON SHUTTLE FLIGHTS.

CROSS-FORCES FROM LABYRINTH SEALS. MECHANISMS AND UPSTREAM COUPLING

By

Knox Millsaps
and Manuel Martinez-Sanchez

MIT, Gas Turbine Laboratory

OUTLINE

- EXPERIMENTAL DATA AND THEORETICAL ANALYSIS OF ROTORDYNAMIC FORCES IN SINGLE-CAVITY LABYRINTHS.
- PARAMETERS VARIED: INLET SWIRL, PRESSURE RATIO, WHIRL SPEED, SPIN SPEED, SEAL LENGTH, LAND SURFACE (SMOOTH VS. HONEYCOMB).
- DATA WERE SEAL CAVITY REAL-TIME PRESSURE DISTRIBUTIONS

MAJOR FINDINGS

- PRESSURE FORCES ARE SUM OF IDEAL COMPONENT, PROPORTIONAL TO RELATIVE SWIRL, PLUS FRICTION-INDUCED COMPONENT, PROPORTIONAL TO SWIRL CHANGE
- THE IDEAL COMPONENT VANISHES WHEN FLUID SWIRL EXACTLY FOLLOWS TRAVELLING WAVE OF GAP VARIATION DURING WHIRL. THIS COMPONENT IS SOLELY RESPONSIBLE FOR DAMPING
- THE VISCOUS COMPONENT ALTERS CROSS-STIFFNESS, BUT NOT DAMPING
- DAMPING DATA CAN BE EXTRACTED FROM STATIC TESTS WITH VARYING SWIRL
- UPSTREAM NONUNIFORMITIES DUE TO SEAL ECCENTRICITY STRONGLY FEED BACK INTO CAVITY PRESSURE PATTERN

CROSS-FORCE MECHANISMS

(1) **INVISCID**

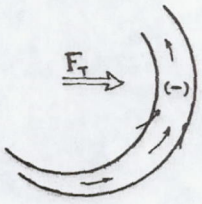

- WITH ECCENTRIC ROTOR, TANGENTIAL FLOW IN CAVITY SEES VARYING CROSS SECTION
- IN REGIONS OF INCREASING AREA, CONTINUITY REQUIRES ADDITIONAL FLOW TO BE BROUGHT FROM UPSTREAM (OR A REDUCED DISCHARGE DOWNSTREAM)
- THIS THEN MEANS LOW P IN THESE AREAS, WHICH INTEGRATES TO FORWARD-WHIRLING FORCE.

- THIS ARGUMENT ASSUMES CONSTANT VELOCITY. BERNOULLI EFFECTS MODIFY (REDUCE) IT, BUT BASICS REMAIN
- THE RELEVANT TANGENTIAL VELOCITY IS <u>WITH RESPECT TO THE WHIRLING FRAME</u>, I.E., $V^* - \Omega R$. THIS IS THE ORIGIN OF <u>DAMPING</u> (FORCE = 0 WHEN $V^* = \Omega R$)

CROSS-FORCE MECHANISMS

(2) **VISCOUS**

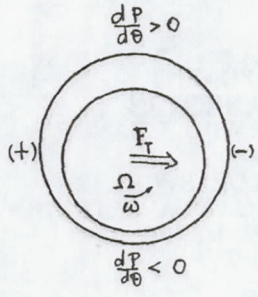

- BECAUSE OF WALL FRICTION, V* (IN CAVITY) CAN BE SMALLER (OR LARGER, AT HIGH ω) THAN V_i^* (INLET)
- ASSUMING $V^* < V_i$, INCOMING LEAKAGE FLUID ENERGIZES CAVITY FLOW $\left(\frac{dP}{d\theta} > 0\right)$
- MORE FLOW ENTERS IN WIDER GAP REGION, SO P PEAKS 90^o AFTER IT. THIS RESULTS IN FORWARD-WHIRLING FORCE
- NOTE ESSENTIAL VELOCITY HERE IS $V_i - V^*$, <u>REGARDLESS OF</u> Ω. SO THIS FORCE COMPONENT IS INDEPENDENT OF WHIRL (<u>NO DAMPING</u>)

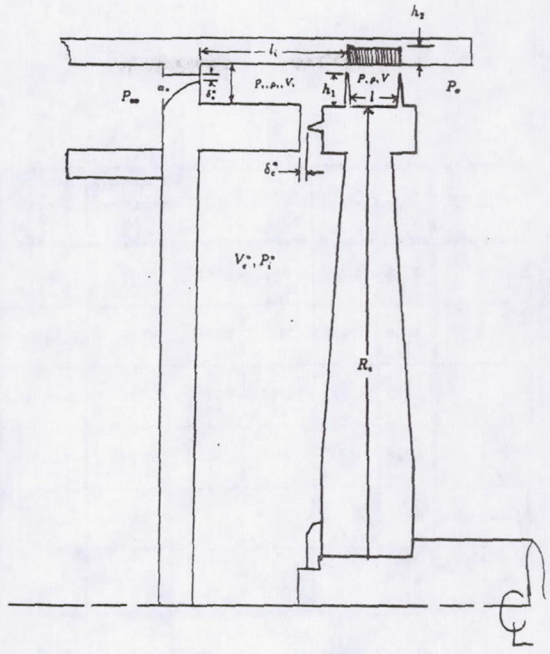

Figure 2-6: Test section schematic showing the geometry and flow variables when the swirl vanes feed into an upstream swirl cavity. Also shown is the leakage path to the large center cavity.

SIMPLIFIED THEORETICAL PREDICTIONS

- **ASSUMING UNIFORM INLET AND EXIT CONDITONS, AND NEGLECTING A FEW MINOR TERMS, WE CALCULATE**

$$\frac{F_N}{\pi R_s \ell \Delta P} \cong -\frac{1}{2}\,\frac{K-\left(1-\frac{1}{\alpha}\right)}{1+(\alpha\beta)^2+\frac{1}{\mu^2_1}\left(\frac{\ell h}{R_s \delta_1}\right)^2}\left(\frac{r}{\delta_1}\right)$$

$$\frac{F_T}{\pi R_s \ell \Delta P} \cong \frac{1}{2}\left(\frac{\ell h}{R_s \delta_1}\right)^2 \frac{\left(\frac{V_i - V^*}{v_x}\right)+\left(\frac{V^* - \Omega R_s}{v_x}\right)\left(\frac{\delta_1}{h}\right)}{1+(\alpha\beta)^2+\frac{1}{\mu^2_1}\left(\frac{\ell h}{R_s \delta_1}\right)^2}\left(\frac{r}{\delta_1}\right)$$

WHERE $K = \frac{\delta_1}{\mu_2}\frac{\partial \mu_2}{\partial \delta_2}$ SENSITIVITY OF CARRY-OVER TO GAP)

$\alpha = \frac{\delta_2}{\delta_1}$ (SEAL DIVERGENCE, EQUAL TO 1 FOR US)

V_i = INLET TANGENTIAL VELOCITY

V^* = CAVITY TANGENTIAL VELOCITY

$V_x \cong \sqrt{\Delta P / \rho}$ = AXIAL FLOW SPEED IN GAP

Ω = WHIRL SPEED

NOTE: $C_{xx} = \frac{\partial F_T}{\partial \Omega} = -R_s \frac{\partial F_T}{\partial V^*}$ THIS YIELDS Cxx FROM STATIC DATA

BUILD#	$\frac{\partial K^{**}_{xx}}{\partial \sigma}$	$\frac{F_T(\Omega_d)}{P}$	$\frac{F_{TT}(\Omega_d)}{P}$	C^{**}_{xx}	From Static Correlation $C_{xx}\left(\frac{Ns}{m}\right)$	Measured Directly $C_{xx}\left(\frac{Ns}{m}\right)$
2	0.372	7763	953	0.289	22.70	19.95
3	0.416	27821	3162	0.371	82.19	75.80
4	0.283	20001	3162	0.247	56.13	48.54
5	0.338	7053	953	0.231	20.33	15.81
Composite	0.357					
Data of Benckert	0.357 0.423 0.265					

Table 7.1 The first column shows the cross-stiffness correlation for all builds and for the static data of Benckert [28] The next two columns show the total cross force and frictional component evaluated at $\Omega_d = 300\left(\frac{rads}{sec}\right)$ and design pressure ratio. The next column is the measured nondimensional direct damping coefficient. The final two columns give the damping calculated from the cross-stiffness coefficient and the average value that was directly measured.

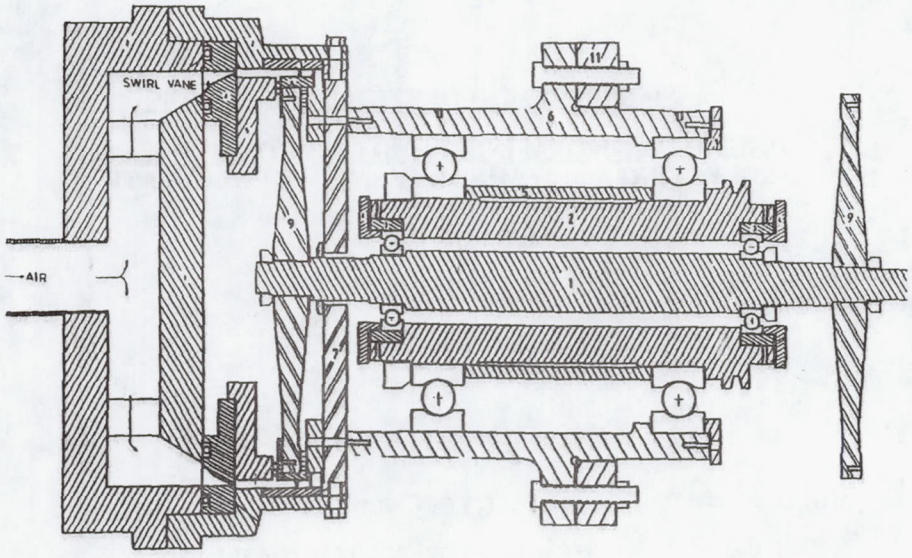

Figure 4-3: Cross section of nested spindle Spin/Whirl producing rotating rig and test section assembly.

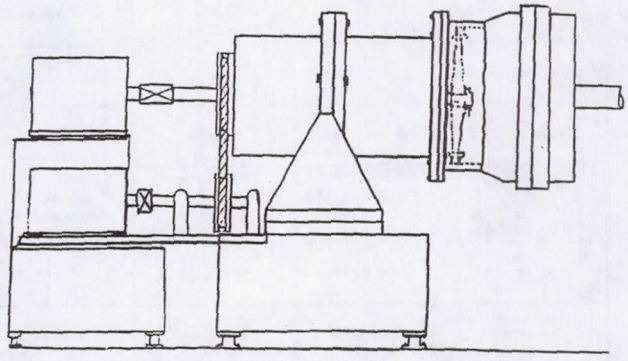

Figure 4-8: Layout of the core facility showing the drive systems for both the spin and whirl.

(δ-mils) $\bar{\epsilon} = \frac{\delta}{r_c}$	VANE ANGLE	PRESSURE RATIO π_c	SPIN SPEEDS ω (Hz.)	WHIRL SPEEDS Ω (Hz.)
(1.0) 0.0370	0°plate	1.27, 1.38, 1.46 1.65, 1.83	0	±7.52, ±20.87 ±33.17, ±48.15
(1.0) 0.0370	15°plate	1.25, 1.39, 1.42 1.65, 1.84	0	±7.52, ±20.87 ±33.17, ±48.15
(1.0) 0.0370	30°	1.27, 1.38, 1.44 1.66, 1.82	0	±7.52, ±20.87 ±33.17, ±48.15
(1.0) 0.0370	60°	1.25, 1.40, 1.46 1.66, 1.85	0	±7.52, ±20.87 ±33.17, ±48.15
(3.8) 0.1407	0°plate	1.13, 1.21, 1.27 1.38, 1.48, 1.65	0	±7.52, ±20.87 ±33.17, ±48.15
(3.8) 0.1407	0°plate	1.73, 1.79, 1.94 2.07, 2.29, 2.40	0	±7.52, ±20.87 ±33.17, ±48.15
(3.8) 0.1470	0°plate	1.48	±44.87, ±66.52	±7.52, ±20.87 ±33.17, ±48.15
(3.8) 0.1470	15°plate	1.24, 1.40, 1.55 1.64, 1.81	0	±7.52, ±20.87 ±33.17, ±48.15
(3.8) 0.1407	15°plate	1.55	±44.87, ±66.52	±7.52, ±20.87 ±33.17, ±48.15
(3.8) 0.1470	30°	1.23, 1.38, 1.55 1.66, 1.76	0	±7.52, ±20.87 ±33.17, ±48.15
(3.8) 0.1470	30°	1.55	±44.87, ±66.52	±7.52, ±20.87 ±33.17, ±48.15
(3.8) 0.1407	60°	1.11, 1.19, 1.23 1.38, 1.55, 1.66	0	±7.52, ±20.87 ±33.17, ±48.15
(3.8) 0.1407	60°	1.79, 1.88, 2.02 2.21, 2.30, 2.38	0	±7.52, ±20.87 ±33.17, ±48.15
(3.8) 0.1407	60°	1.54	±44.87, ±66.52	±7.52, ±20.87 ±33.17, ±48.15
(7.3) 0.2704	0°plate	1.20, 1.38, 1.58 1.67, 1.88	0	±7.52, ±20.87 ±33.17, ±48.15
(7.3) 0.2704	15°plate	1.21, 1.38, 1.55 1.67, 1.93	0	±7.52, ±20.87 ±33.17, ±48.15
(10.7) 0.3963	0°plate	1.23, 1.39, 1.52 1.65, 1.79	0	±7.52, ±20.87 ±33.17, ±48.15
(10.7) 0.3963	60°	1.25, 1.40, 1.46 1.66, 1.85	0	±7.52, ±20.87 ±33.17, ±48.15
(13.1) 0.4852	0°plate	1.27, 1.38, 1.46 1.65, 1.83	0	±7.52, ±20.87 ±33.17, ±48.15
(13.1) 0.4852	15°plate	1.25, 1.39, 1.42 1.65, 1.84	0	±7.52, ±20.87 ±33.17, ±48.15
(13.1) 0.4851	30°	1.27, 1.38, 1.44 1.66, 1.82	0	±7.52, ±20.87 ±33.17, ±48.15
(13.1) 0.4851	60°	1.25, 1.40, 1.46 1.66, 1.85	0	±7.52, ±20.87 ±33.17, ±48.15

Table 5.5: Test Matrix for build #3.

VARIABLE	ABSOLUTE UNCERTAINTY	RELATIVE UNCERTAINTY	COMMENTS
Kulite Sensitivity, $\frac{\partial V}{\partial P}$	±7.1 Pa	±1.4% - ±2.2% of $\hat{P}$	linearity, hysteresis and calibration
Repeatability $\hat{P}$	$2\sigma_{F_N} = 0.304N$ $2\sigma_{F_T} = 0.146N$	±8.5% ±4.6%	95 % Confidence
Inlet swirl V_i Build#3 design	$0.0 \pm 0.75\frac{m}{s}$-0° $28.4 \pm 2.2\frac{m}{s}$-15° $49.7 \pm 3.6\frac{m}{s}$-30° $69.6 \pm 4.4\frac{m}{s}$-60°	undefined 7.7 % 7.2 % 6.3 %	mass flow, alignment, repeatability, calibration
P_i, P^o, P^o	±344 Pa Max	0.5 % each MAX	Total accuracy
Spin speed ω	±2.1 RPM	±0.1 % MAX	@ 1275 RPM
Whirl speed Ω	±4.5 RPM	±0.9 % MAX	@ 520 RPM
Temperature T	1° F	0.2 %	To calculate density
$\frac{r}{r}$ and $\frac{r}{r}$	1.0± 0.2 mils 3.8± 0.2 mils 7.3± 0.1 mils 10.7± 0.1 mils 13.1± 0.2 mils 17.1± 0.3 mils	5.5% 1.5% 0.6% 0.2% 0.3% 0.3%	Most probable error due to non-circularity of orbit and casing.
l, h, R_s	±0.001 in. MAX	0.5 % MAX	Machining tolerances
δ_e^o	0.012±0.008 in.	+67% -50%	Uncontrolled axial clearance
Digitization	$\frac{1}{2}\frac{1}{4096}$	0.4% MAX	

Table 5.8: Table of uncertainties used in calculating the overall confidence interval for the force data.

TYPICAL RESULTS FOR ZERO INLET SWIRL

- DATA SHOWN FOR CONF. #3 (SMOOTH, LONG SEAL)
- RESTORING DIRECT FORCE, INDEPENDENT OF SWIRL, SCALING WITH ΔP
- STABILIZING CROSS FORCE, ZERO AT ZERO WHIRL RATE, PROPORTIONAL TO WHIRL
- $\frac{F_T}{\Delta P} \sim \frac{\Omega R}{\sqrt{\Delta P}}$, SO DATA CAN BE COLLAPSED TO ONE LINE

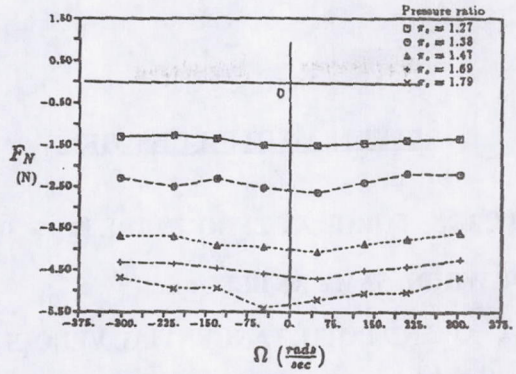

Figure 7.13: Experimentally obtained direct force, F_N, vs. the whirl frequency, for five different inlet pressures, π_s =1.27, 1.38, 1.47 1.69 and 1.79. These data are from build #3 with 0° inlet swirl and $\omega = 0$.

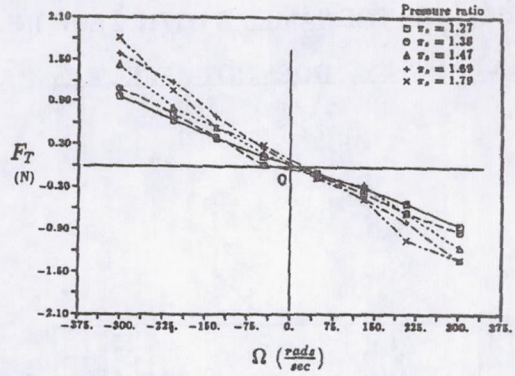

Figure 7.14: Experimentally obtained cross force, F_T, vs. the whirl frequency, for five different inlet pressures, π_s =1.27, 1.38, 1.47, 1.69 and 1.79. These data are from build #3 with 0° swirl and $\omega = 0$.

K+E 10 X 10 TO THE CENTIMETER 10 X 25 CM. KEUFFEL & ESSER CO. MADE IN U.S.A. 46 1510

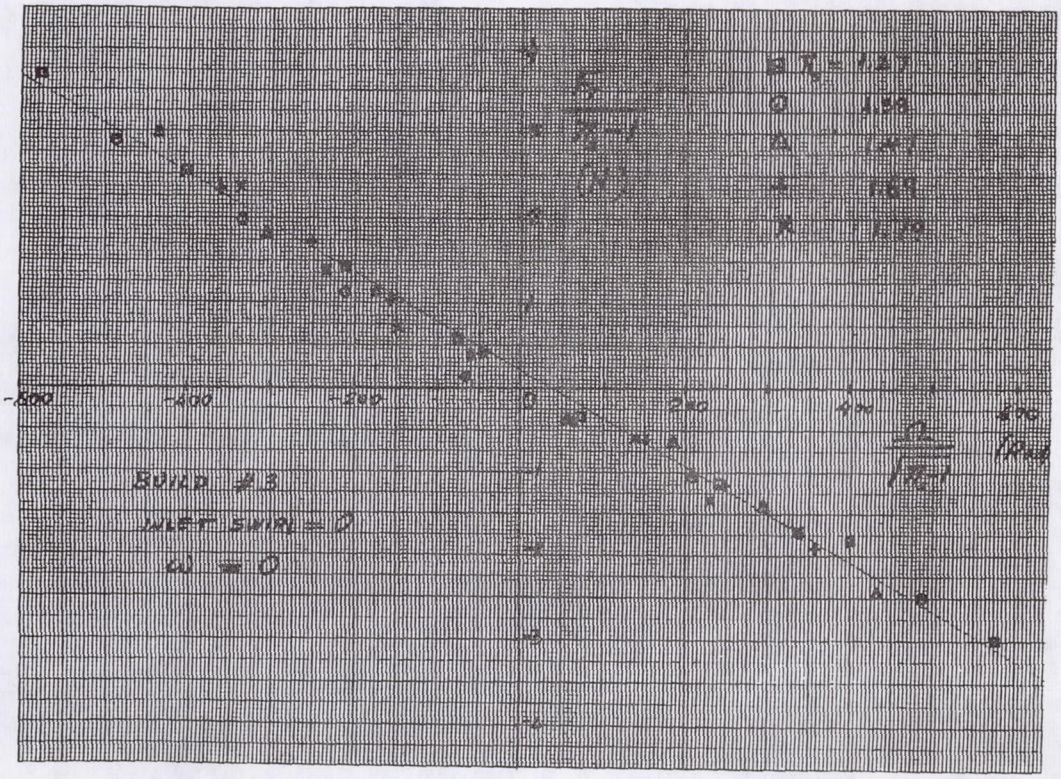

RESULTS WITH INLET SWIRL

- NONZERO CROSS FORCE AT ZERO WHIRL $(K_{xy} \neq 0)$.
- EFFECT OF WHIRL SAME AS BEFORE.
- SINCE $F_T \sim \Delta P$ AND BOTH, TANGENTIAL VELOCITY AND ΩR SCALE AS $\sqrt{\Delta P}$, PLOT OF $\frac{F_T}{\Delta P}$ VS. $\frac{\Omega}{\sqrt{\Delta P}}$ STILL COLLAPSES DATA
- SLOPE $\frac{\partial(F_T / \Delta P)}{\partial(\Omega_s / \Delta P)}$ IS THE SAME AS WITH ZERO INLET SWIRL. SWIRL INCREASES K_{XY}, DOES NOT AFFECT C_{XY}.

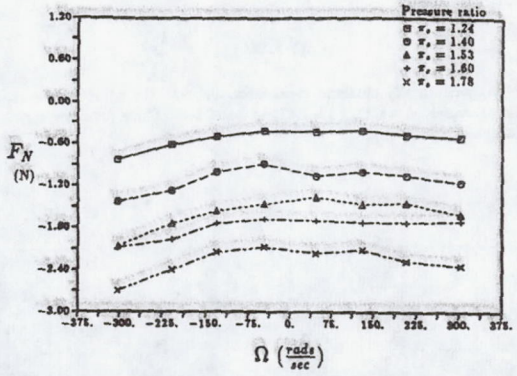

Figure 7.17: Experimentally obtained direct force, F_N, vs. the whirl frequency for five different pressure ratios. These data are from build #3 with 8.6° inlet swirl and $\omega = 0$.

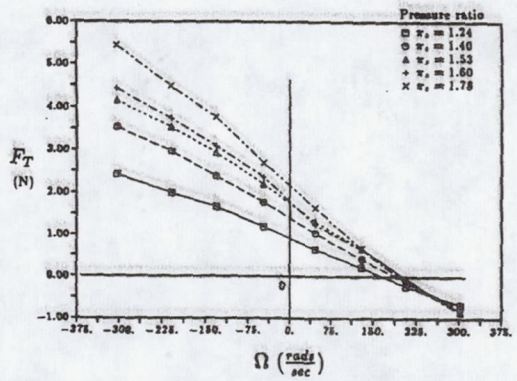

Figure 7.18: Experimentally obtained cross force, F_T, vs. the whirl frequency, for five different pressure ratios. These data are from build #3 with 8.6° inlet swirl and $\omega = 0$.

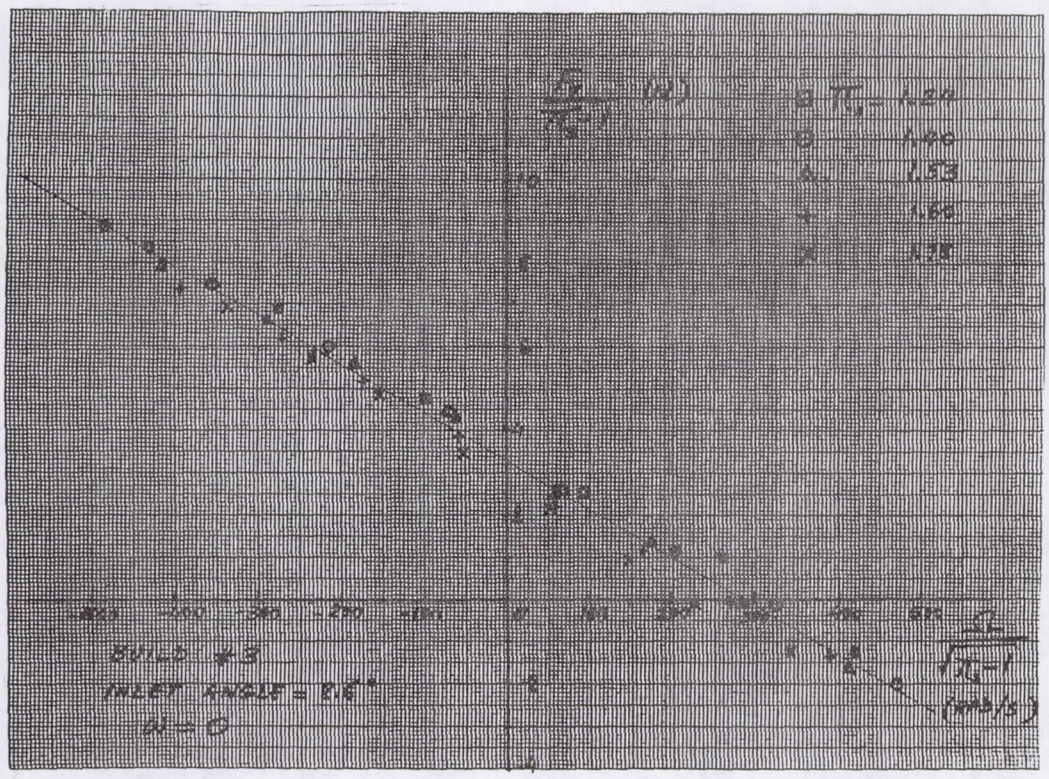

SHAFT ROTATION-THE FRICTIONAL EFFECT

- ROTATION IN THE INLET SWIRL DIRECTION REDUCES CROSS-FORCE K_{XY} (AND VICE-VERSA)
- REDUCTION IS THE SAME AT ALL WHIRL SPEEDS (NO CHANGE IN DAMPING C_{XX}
- EFFECT DUE TO VARIATIONS OF THE TANGENTIAL VELOCITY CHANGE $V^* - V_i$ BETWEEN INLET AND GLAND

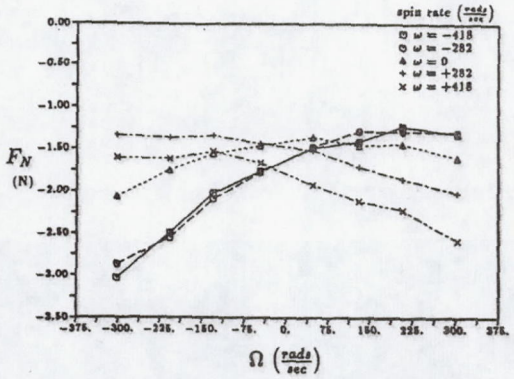

Figure 7.19: Experimentally obtained direct force, F_N, vs. the whirl frequency for five different spin rates, $\pi_s = 1.53$. These data are from build #3 with 8.6° inlet swirl.

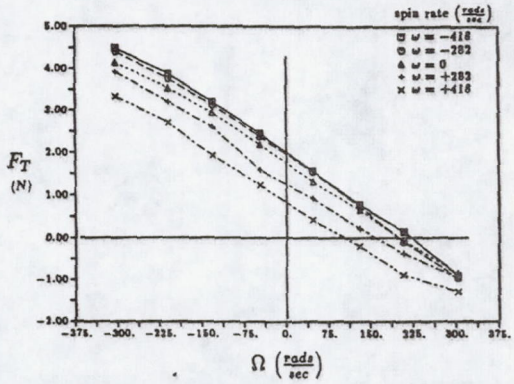

Figure 7.20: Experimentally obtained cross force, F_T, vs. the whirl frequency, for five different spin rates, $\pi_s = 1.47$. These data are from build #3 with 8.6° inlet swirl.

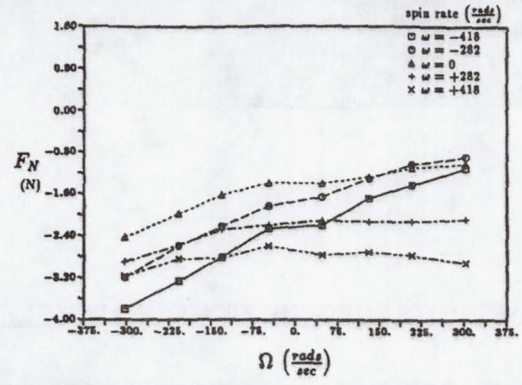

Figure 7.21: Experimentally obtained direct force, F_N, vs. the whirl frequency for five different spin rates, $\pi_s = 1.55$. These data are from build #3 with 21.4° inlet swirl.

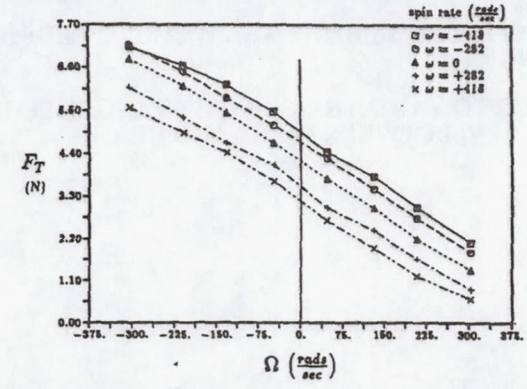

Figure 7.22: Experimentally obtained cross force, F_T, vs. the whirl frequency, for five different spin rates, $\pi_s = 1.55$. These data are from build #3 with 21.4° inlet swirl.

EFFECTS OF HONEYCOMB LAND

- SOME REDUCTION (~ 25%) OF CROSS FORCE. PROBABLY DUE TO CARRYOVER DISRUPTION. THEORY GIVES 17% REDUCTION WITH K = 0.
- MAJOR REDUCTION, EVEN REVERSAL, OF DIRECT FORCE (BECOMES NEGATIVE SPRING). SINCE F_N DUE ALMOST ENTIRELY TO CARRYOVER DISRUPTION.
  - DATA SHOWN FOR CONF. #4 (LONG, HONEYCOMB) FOR COMPARISON TO #3 (LONG, SMOOTH)
  - EFFECTS FOR SHORT SEAL (#5 VS. #2) ARE WEAKER.

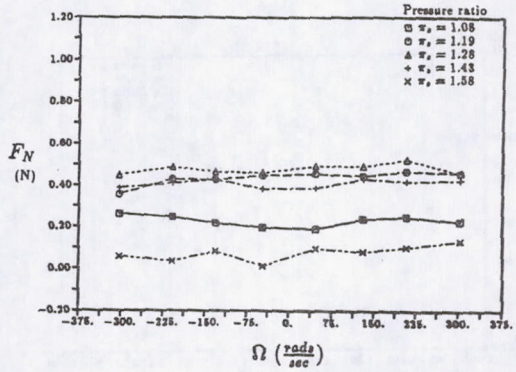

Figure 7.23: Experimentally obtained direct force, F_N, vs. the whirl frequency for five different pressure ratios. These data are from build #4 with 0° inlet swirl and $\omega = 0$.

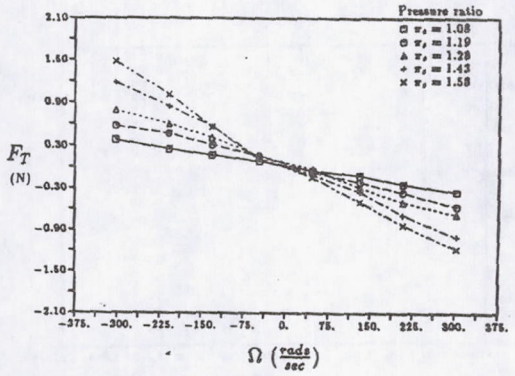

Figure 7.24: Experimentally obtained cross force, F_T, vs. the whirl frequency, for five different pressure ratios. These data are from build #4 with 0° inlet swirl and $\omega = 0$.

NON-DIMENSIONAL ROTORDYNAMIC COEFFICIENTS

- **FORCES FITTED AS**

$$\frac{F_N}{\hat{r}} = -K_{xx} - C_{xy}\,\Omega + M_{xx}\,\Omega^2$$

$$\frac{F_T}{\hat{r}} = K_{xy} - C_{xx}\,\Omega$$

- **COEFFICIENTS MADE NONDIMENSIONAL BY**

$$K_{ij}^{**} = \frac{K_{ij}\,\delta_1}{\ell\, R_s\,(P_1 - P_s)}$$

$$C_{ij}^{**} = \frac{C_{ij}\,\delta_1}{\ell\, R_s^2\,\sqrt{\rho_1\,(P_1 - P_s)}}$$

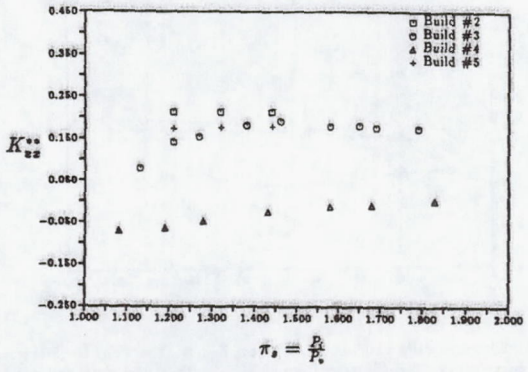

Figure 7.29: The effect of pressure ratio on the nondimensional direct stiffness coefficient, K_{xx}^{**}, for builds #2(narrow rotor-smooth land) , #3(wide rotor-smooth land), #4(wide rotor - honeycomb land) and #5(narrow rotor - honeycomb land). The inlet swirl for all cases is 0° and ϵ_1=0.1407.

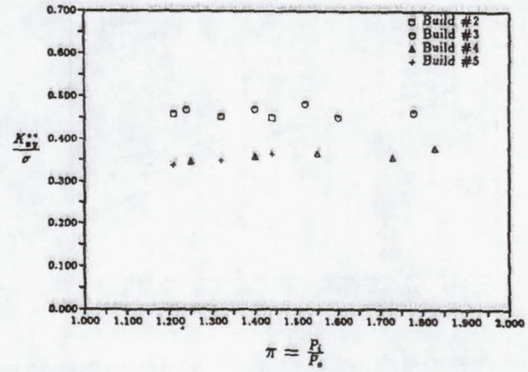

Figure 7.30: The effect of pressure ratio on the nondimensional cross stiffness coefficient, $\frac{K_{xy}^{**}}{\sigma}$ for build #2, #3, #4 and #5. All were taken with the 15° swirl orifice plate and ϵ_1=0.1407.

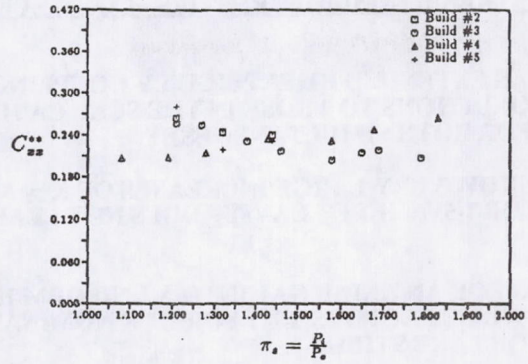

Figure 7.31: The effect of pressure ratio on the direct damping coefficient, C^{**}_{xx}, for builds #2(narrow rotor-smooth land) , #3(wide rotor-smooth land), #4(wide rotor - honeycomb land) and #5(narrow rotor - honeycomb land). The inlet swirl for all cases is 0° and ϵ_1=0.1407.

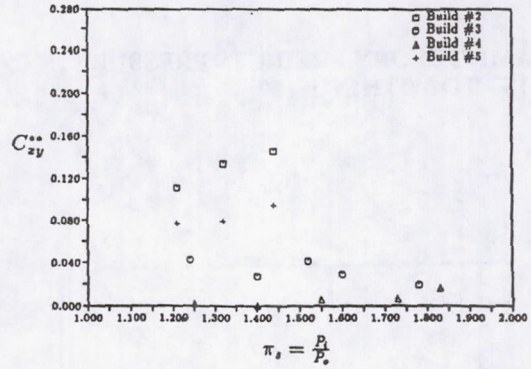

Figure 7.32: The effect of pressure ratio on the nondimensional cross damping coefficient, C^{**}_{xy} for build #2, #3, #4 and #5. All were taken with the 15° swirl orifice plate and ϵ_1=0.1407.

EFFECTS OF UPSTREAM NONUNIFORMITIES

- **PREVIOUS STUDIES HAVE ASSUMED UNIFORM P_i ,V_i**

  OUR RESULTS STRONGLY SUGGEST THIS IS NOT IN GENERAL A GOOD ASSUMPTION

- **SINCE EFFECT NOT SUSPECTED, NO PRESSURE DATA WERE TAKEN UPSTREAM, AND NO SPECIAL CARE WAS TAKEN TO MEASURE OR MAINTAIN A CONSTANT AXIAL GAP IN UPSTREAM FACE SEAL (NOMINAL ~ 10 mil)**

- **LINEARIZED THEORY IGNORING UPSTREAM EFFECTS PREDICTS ALL TRENDS CORRECTLY, BUT YIELDS K_{XY}, C_{XX} VALUES 2-3 TIMES TOO LOW**

- **THIS SAME DISCREPANCY HAD BEEN PREVIOUSLY NOTED BY SEVERAL RESEARCHERS WHEN TRYING TO CALCULATE δP IN THE FIRST CAVITY OF MULTICAVITY SEALS**

UPSTREAM NONUNIFORMITIES - CONTINUED

- MODEL WAS EXTENDED BY EXPLICITLY COUPLING THE INLET CAVITY CONDITIONS TO THOSE IN THE SEAL CAVITY, SOLVING FOR BOTH SIMULTANEOUSLY.
- RESULTS SHOW VERY LARGE INCREASES OF K_{XY} AND C_{XX} (FACTORS OF 3-5) IF INLET CAVITY DOES NOT LEAK INTO HUB AREA.
- ALLOWING FOR AN AXIAL GAP INTO A UNIFORM HUB VOLUME REDUCES THESE FACTORS, BUT FOR OUR NOMINAL 10 mil GAP, THE FACTORS ARE STILL 2-3.
- WE ALSO REDUCED FIRST-CAVITY DATA OF BENCKERT-WACHTER. DISCREPANCY BETWEEN DATA AND THEORY CAN BE REMOVED IF AN AXIAL GAP OF ~ 10 mil IS CONSISTENTLY ASSUMED.

NOTE: THE SAME THEORY PREDICTS PRESSURE IN CAVITIES OTHER THAN 1ST TO WITHIN ± 15%

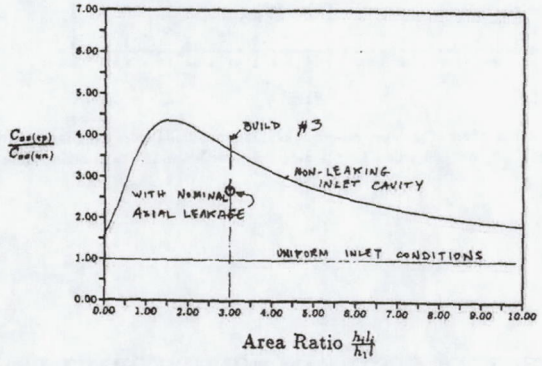

Figure 3-41: Ratio of direct damping with upstream coupling to that with no coupling vs. swirl cavity to seal gland area ratio. The maximum occurs ≈ 1.35 and the damping ratio comes to within 1% at a area ratio of 75.

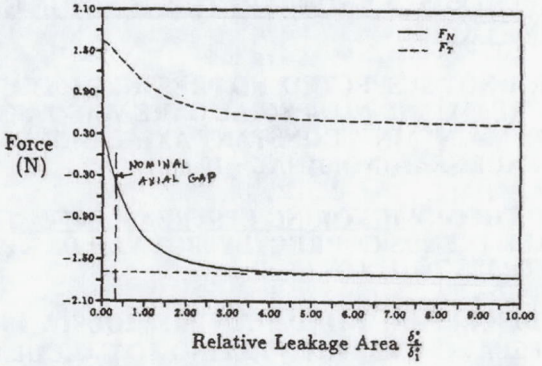

Figure 3-42: Predicted direct and cross force at $\Omega = 0$ from the fully coupled model vs. the relative axial clearance ratio, $\frac{\delta_2^*}{\delta_1^*}$. The geometry is the same as for build #3. π_s=1.4, $\alpha_s = 15°$, $\epsilon_1 = 0.1407$ and $\omega = 0$.

CONFIG.	$F_T(meas.)$	$F_T(\delta_c^* = 0)$	$F_T(\delta_c^* = \infty)$	Matched δ_c^*
1	10.21(N)	16.28(N)	4.99(N)	0.008"
2	8.28(N)	16.15(N)	4.25(N)	0.011"
3	11.91(N)	15.51(N)	4.09(N)	0.010"

Table 7.2 Comparison of the data of Benckert and Wachter [28] to the coupled model predictions. All cases are for standard conditions. P_i = 1.58 (bar), P_o = 1 (bar) and α_v = 28.4°. The first column shows the experimental value. The second column gives the value predicted with full coupling, that is no leakage flow. The third column has the predictions for constant upstream boundary conditions. The last column gives the value of the axial space needed for the model to match the experimentally obtained value.

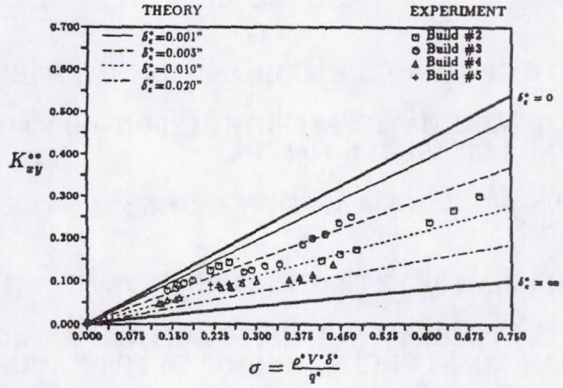

Figure 7.34: K_{xy}^{**} vs. σ for the experimental data and theory. The axial gap, δ_c^*, is used as a parameter. All experimental values fall between the theory with $0.004"(0.0001m) < \delta_c^* < 0.017(0.0004m)$. The top thick line is for full coupling (ie. no leakage). The bottom one is for uniform inlet conditions (ie. no coupling). The calculations are for build #3 geometry.

DISCUSSION

- THE SENSITIVITY OF CROSS-FORCES TO UPSTREAM CONDITIONS WILL NECESSITATE ACCOUNTING FOR THESE IN DESIGN WORK.
- THIS WAS RELATIVELY SIMPLE FOR OUR GEOMETRY (NO BLADES), BUT WILL NOT BE SIMPLE FOR REALISTIC TURBINE SHROUD GEOMETRY.
- THESE NONUNIFORMITIES ARE THEMSELVES DUE TO THE ROTOR ECCENTRICITY, SO NOT A-PRIORI KNOWN.

  - MORE RESEARCH IS NEEDED IN THIS AREA -

CONCLUSIONS

LABRYRINTH CROSS-FORCE MECHANISMS CLARIFIED

- INVISCID (KINEMATIC) EFFECTS RESPONSIBLE FOR DAMPING. DAMPING INSENSITIVE TO SPIN.
- VISCOUS MECHANISM AFFECTS CROSS-STIFFNESS, NOT DAMPING.
- DAMPING CAN BE EXTRACTED FROM STATIC DATA.
- INDUCED UPSTREAM NON-UNIFORMITIES CAN MORE THAN DOUBLE CROSS FORCES. THIS NEEDS TO BE ACCOUNTED FOR.
- DIRECT FORCES MAINLY DUE TO CARRYOVER VARIATIONS
- HONEYCOMB LAND REDUCES DIRECT FORCES STRONGLY, CROSS-FORCES WEAKLY.

STABILITY OF TWO-PHASE FACE SEALS

From notes and discussion

of talk by J. Yasuna, CMU

by R.C. Hendricks

A variable temperature model which considers squeeze film effects and thermal transients that was developed for two phase flows (1, 2) was extended to examine the axial stability of two-phase mechanical seals that tracks the axial response through position and velocity of the rotor from the perturbed state (3).

Step increases in film thickness usually engendered a response that decayed as the rotor asympototically approached the initial steady state condition.

Step decreases in film thickness that are large enough brought about monotone opening (seal failure) and other forms of failure through film collapse or "poping open" due to the onset of instabilities.

In certain conditions the response to small step decreases leads to stable film thicknesses and rotor goes to steady state or some orbital state.

Small amounts of coning tend to stabilize the configuration, even for large disturbances. The magnitude of the thermal response parameter is important to response time and overshoot.

Model is limited through 1-D heat transfer and a conjugate solution would appear more appropriate and must incorporate the thermomechanical behavior of the seal rotor and stator interface, which includes seal "waviness." The distinct liquid-vapor boiling interface and laminar flow assumptions are also limitations, but the "smeared" two-phase interface with flow turbulence and transient behavior is quite complex but necessary for a better understanding of the dynamics.

For more information

1. Hughes, W.F., Basu, P., Beatty, P.A., Beeler, R.M., and Lau, S.: Dynamics of Face and Annular Seals With Two-Phase Flow, NASA CR 4256, 1989.

2. Yasyna, J.A., and Hughes, W.F.: A Continuous Boiling Model for Face Seals, Trans. ASME J. Tribology April 1990, Vol. 112, pp 266, 274.

3. Yasuna, J.A., and Hughes, W.F.: Squeeze Film Dynamics of Two-Phase Seals, Trans. ASME J. Tribology April 1992, Vol. 114, pp 236, 247.

HIGH PRESSURE COMPRESSOR DELIVERY BRUSH SEAL OF THE INTERNATIONAL AERO ENGINES (IAE) V2500-A1 GAS TURBINE ENGINE

Peter A. Withers
Rolls-Royce plc
Filton, Bristol

High pressure compressor delivery brush seal of the international aero engines (IAE) V2500-A1 gas turbine engine

The V2500-A1 is the first production aero gas turbine to be certificated with brush seals. The engine has brush seals in three positions of which the HPC seal discussed in this short presentation has the most arduous duty.

Foil 1 shows the Rolls-Royce brush seal development "milestones" prior and subsequent to the entry into service of the V2500-A1 in 1989. Prior to the 1970's the potential of brush seals was known but limited by materials (early tests were conducted with Nylon bristles). Extensive R&D ws conducted during the 1970's, continuing in parallel with demonstrator engine testing in the early 1980's. By the mid 1980's sufficient technology and confidence in brush seals had been acquired to commit to application and development in the civil V2500-A1 engine with certification and entry into service in the late 1980's.

Foil 2 shows the HPC brush seal in relation to the HPC delivery, the seal providing control of turbine zone ventilation and temperatures, lower sfc, and in conjunction with the labyrinth shown, a balance piston, for control of bearing thrust load.

Foil 3 and 4 show constructional details of the brush seal and its associated journal, with Foil 5 showing the nominal operating conditions which are quite arduous. Rolls-Royce experience shows that to obtain good seal life it is essential to finish the journals aluminium oxide coating by grinding and lapping to a surface finish of better than 0,5 micrometers CLA.

The V2500-A1 engine designed with this HPC delivery, and two other, brush seals was successfully developed and certificated, Foil 6. During development the seals were found to quickly run in to a stabilised condition and provided the journal coating surface finish was good the seal would run indefinitely. Whilst craze/axial cracking of the aluminium oxide coating was observed this has not so far proved to be a problem.

Foils 7 and 8 show the service experience to date. No unscheduled removals of brush seals have occurred and the intention is not to remove seals for inspection until 5,000 engine cycles, (current high time engine is 3,600 cycles). A few engines have been stripped for other reasons and visual inspection of the seals on these engines have been shown the seals to be in good condition.

With the successful development and encouraging service experience of brush seals in the V2500-A1, Rolls-Royce will continue in the 1990's to exploit the advantages of brush seals through R&D, demonstrator engines and further engine applications.

R-R BRUSH SEAL DEVELOPMENT "MILESTONES"

PRE 1970's	–	POTENTIAL OF BRUSH SEALS KNOWN BUT LIMITED BY MATERIALS
1972 →	–	R & D OF BRUSH SEALS
1980's	–	DEMONSTRATOR ENGINE TESTS
1985–1988	–	DEVELOPMENT FOR A CIVIL ENGINE APPLICATION
1989 →	–	SERVICE APPLICATION IN CIVIL ENGINE
1990's	–	CONTINUING R & D AND APPLICATIONS

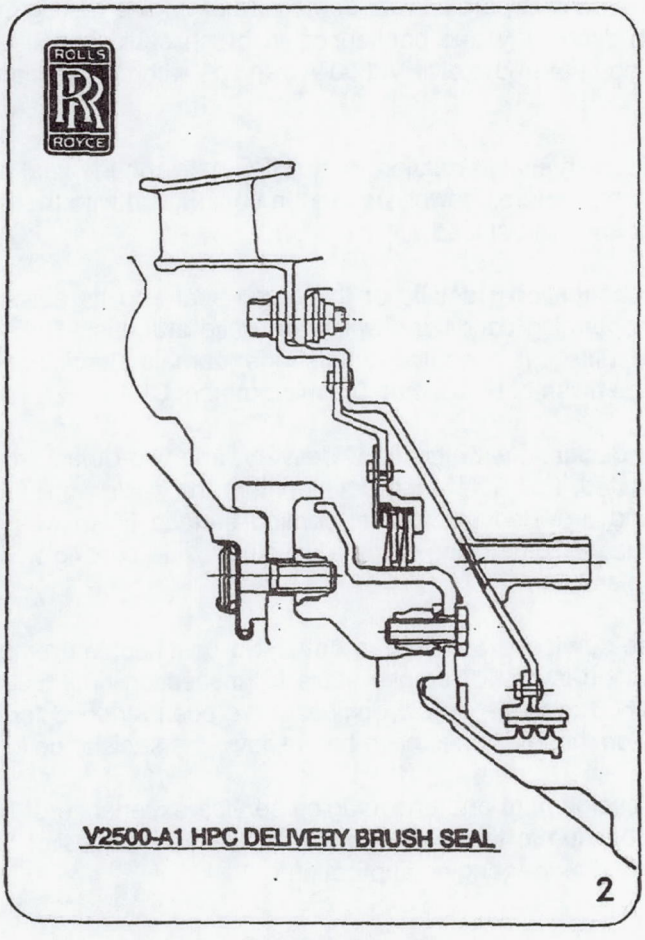

V2500-A1 HPC DELIVERY BRUSH SEAL

2

V2500-A1 HPC DELIVERY BRUSH SEAL DETAILS

1. THE JOURNAL

- JOURNAL DIAMETER – 315 mm
- JOURNAL COATING – PLASMA SPRAYED ALUMINIUM OXIDE
- FINISHED BY GRINDING AND LAPPING TO A SURFACE FINISH OF BETTER THAN 0,5 MICRO METERS CLA.

3

V2500-A1 HPC DELIVERY BRUSH SEAL DETAILS

2. THE BRUSH SEAL

- NUMBER OF SEALS IN SERIES – 2
- BRISTLE FIT AT BUILD – RADIAL CLEARANCE
- BRISTLE LAY ANGLE – 45°
- BRISTLE LENGTH – 15 mm
- BRISTLE WIRE DIAMETER – 0,071 mm NOMINAL
- NUMBER OF BRISTLE ROWS PER SEAL – 11
- BRISTLE DENSITY – 2250 TO 2650 PER 25 mm
- BRISTLE WIRE MATERIAL – HAYNES 25
- BACKING RING CLEARANCE – 1,2 mm (RADIAL)

4

V2500-A1 HPC DELIVERY BRUSH SEAL DETAILS

3. OPERATING CONDITIONS

- SURFACE VELOCITY – 250 m/s
- DIFFERENTIAL PRESSURE – 430 kPa
- TEMPERATURE – > 550 °C

5

V2500-A1 HPC DELIVERY BRUSH SEAL

DEVELOPMENT/CERTIFICATION

- THE V2500–A1 ENGINE WAS SUCCESSFULLY DEVELOPED AND CERTIFICATED WITH BRUSH SEALS
- OBSERVATIONS FROM THE DEVELOPMENT PROGRAMME:
  - SEALS QUICKLY RUN IN TO A STABILISED CONFIGURATION AND THEREAFTER , IF THE ROTOR CONDITION IS GOOD , THE SEAL WILL RUN INDEFINITELY
  - CRAZE/AXIAL CRACKING OF THE ALUMINIUM OXIDE JOURNAL COATING AT THESE EXACTING TEMPERATURES AND SPEEDS IS NORMALLY SEEN
  - BRISTLES WAXED OPEN FOR ENGINE ASSEMBLY

6

V2500-A1 HPC DELIVERY BRUSH SEAL IN SERVICE

1. RUNNING EXPERIENCE (TO END MAY 1992)

- 77 A1's IN SERVICE
-

	HOURS	CYCLES
TOTAL	354,300	212,100
HIGH TIME	7200*	3600*

*NOT SAME ENGINE – DIFFERENT USEAGE

7

V2500-A1 HPC DELIVERY BRUSH SEAL IN SERVICE

2. SEAL CONDITION

- FIRST SCHEDULED SERVICE REMOVALS WILL NOT TAKE PLACE BEFORE 5,000 CYCLES
- NO UNSCHEDULED REMOVALS OF BRUSH SEALS
- ON ENGINES STRIPPED FOR OTHER REASONS THE CONDITION OF THE BRUSH SEALS HAS BEEN GOOD

8

TEXTRON SPECIALTY MATERIALS
CONTINUOUS SILICON CARBIDE FILAMENT

BRUSH SEALS SYSTEMS WORKSHOP
NASA LEWIS RESEARCH CENTER
AUGUST 6, 1992

Melvin A. Mittnick
Textron Specialty Materials
2 Industrial Avenue
Lowell, MA 01851
Tel: 508/454-5746
Fax: 508/934-7597

TEXTRON Specialty Materials

BACKGROUND

- *TEXTRON SPECIALTY MATERIALS DEVELOPS AND PRODUCES ADVANCED FILAMENTS AS REINFORCEMENTS FOR CERAMIC AND METALLIC MATRICES*
  - BORON MONOFILAMENT - CVD
  - SILICON CARBIDE MONOFILAMENT - CVD
  - *CARBON FIBER TOWS*
  - TiB_2, TiBC, BN, Si_3N_4 FIBERS + COATINGS

TEXTRON Specialty Materials

STRENGTH COMPARISONS OF ADVANCED MATERIALS

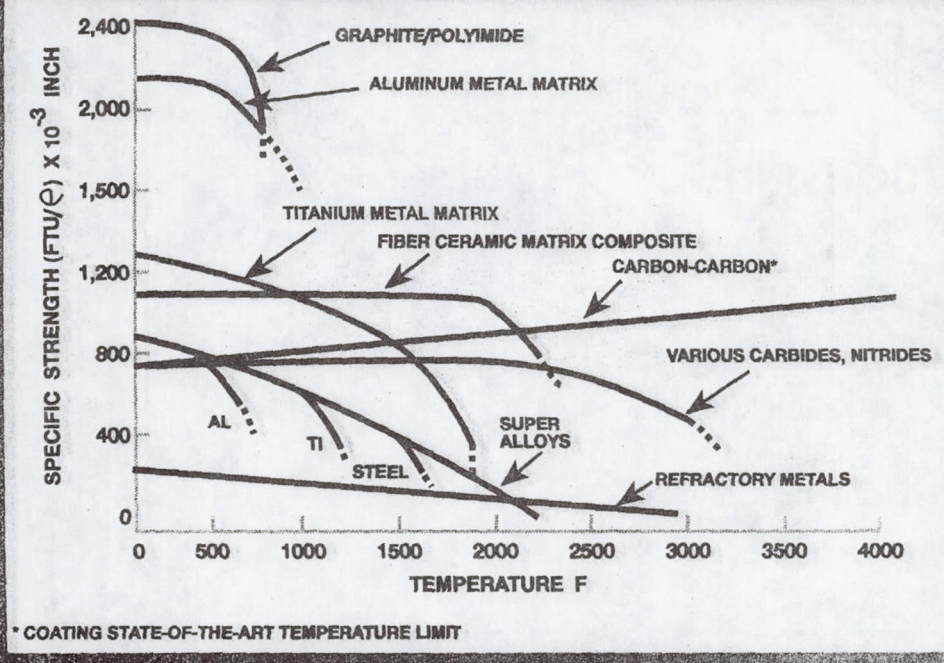

* COATING STATE-OF-THE-ART TEMPERATURE LIMIT

TEXTRON Specialty Materials

TURBINE ENGINE APPLICATIONS FOR FIBER REINFORCED METALS

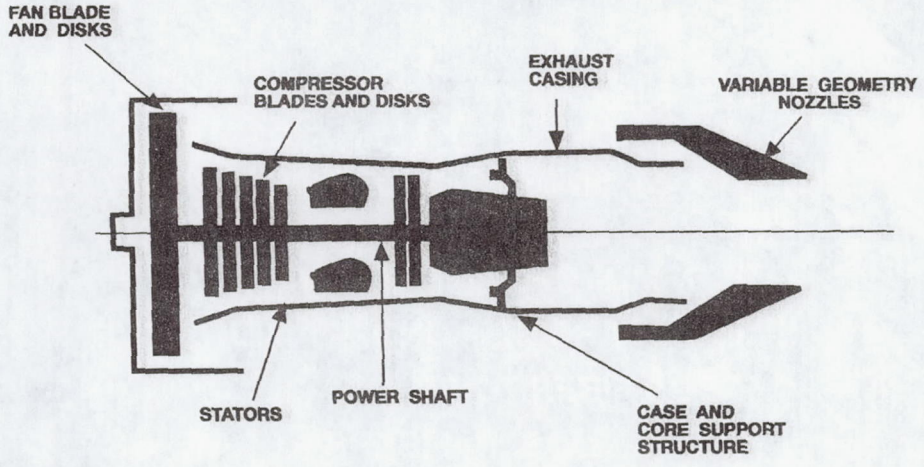

TEXTRON Specialty Materials

SILICON CARBIDE ON CARBON FILAMENT

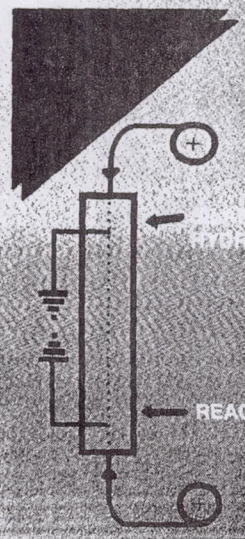

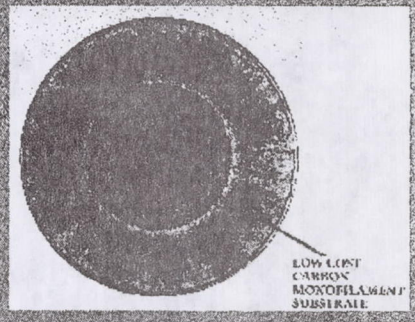

- SILANES ~ LOW COST
- FASTER DEPOSITION RATES
- PROVEN REACTOR TECHNOLOGY

- 500 Ksi, 58 Msi (STRENGTH & STIFFNESS)
- DENSITY, 0.110 LB/IN³
- HIGH TEMP STABILITY > 1600°F USE TEMP.
- CARBON CORE FOR HIGH STRENGTH/LOW COST
- COMPATIBILITY WITH METALS

TEXTRON Specialty Materials

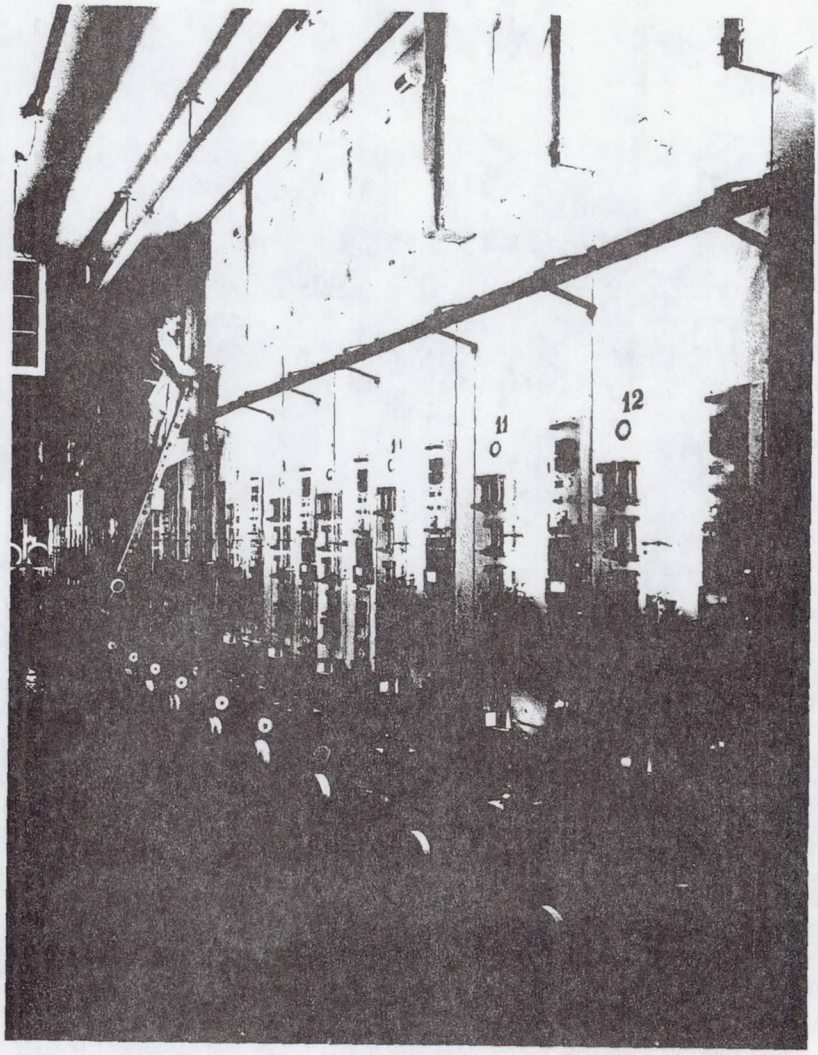
11
12

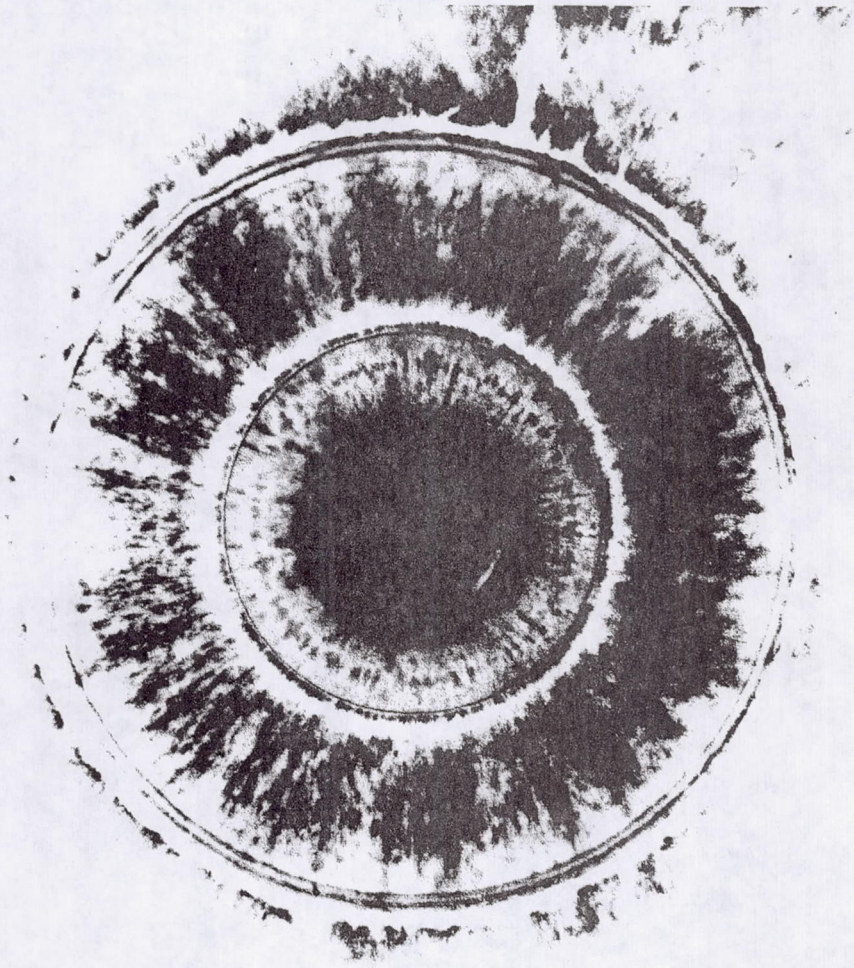

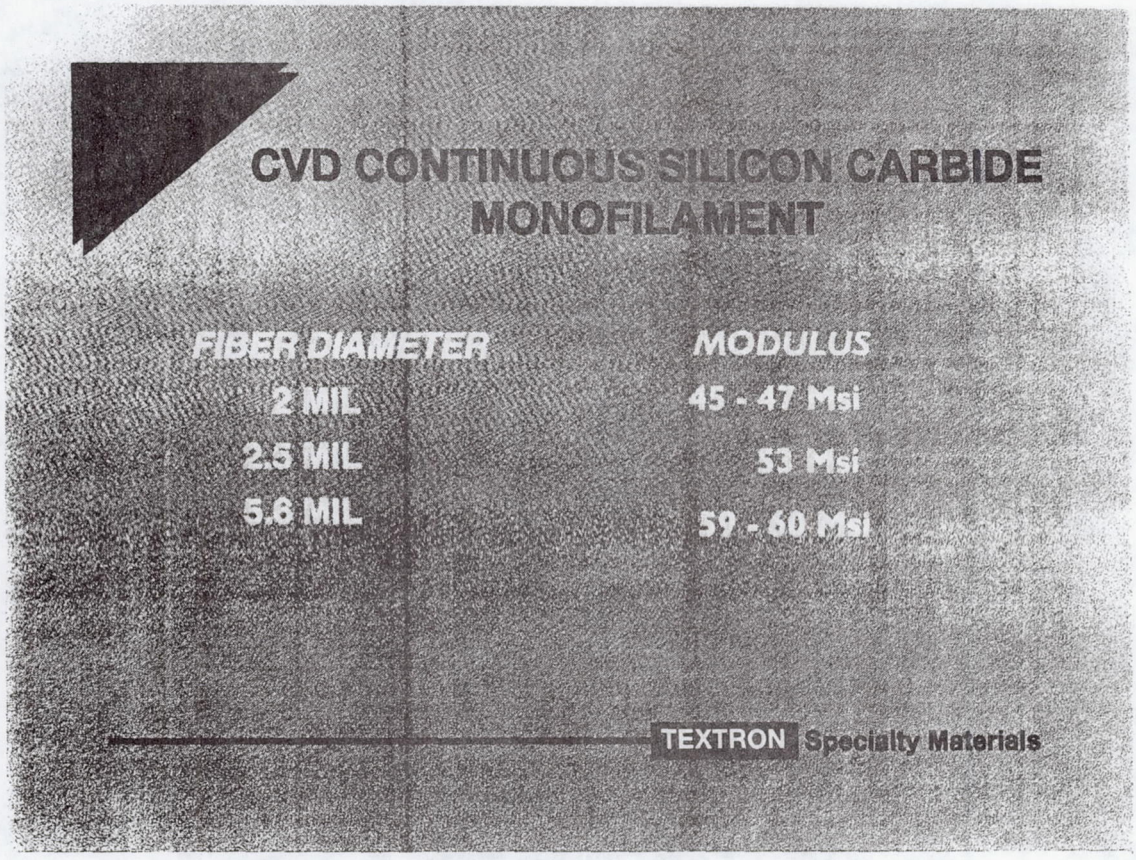
CVD CONTINUOUS SILICON CARBIDE MONOFILAMENT
FIBER DIAMETER
2 MIL
2.5 MIL
5.6 MIL
MODULUS
45 - 47 Msi
53 Msi
59 - 60 Msi
TEXTRON Specialty Materials

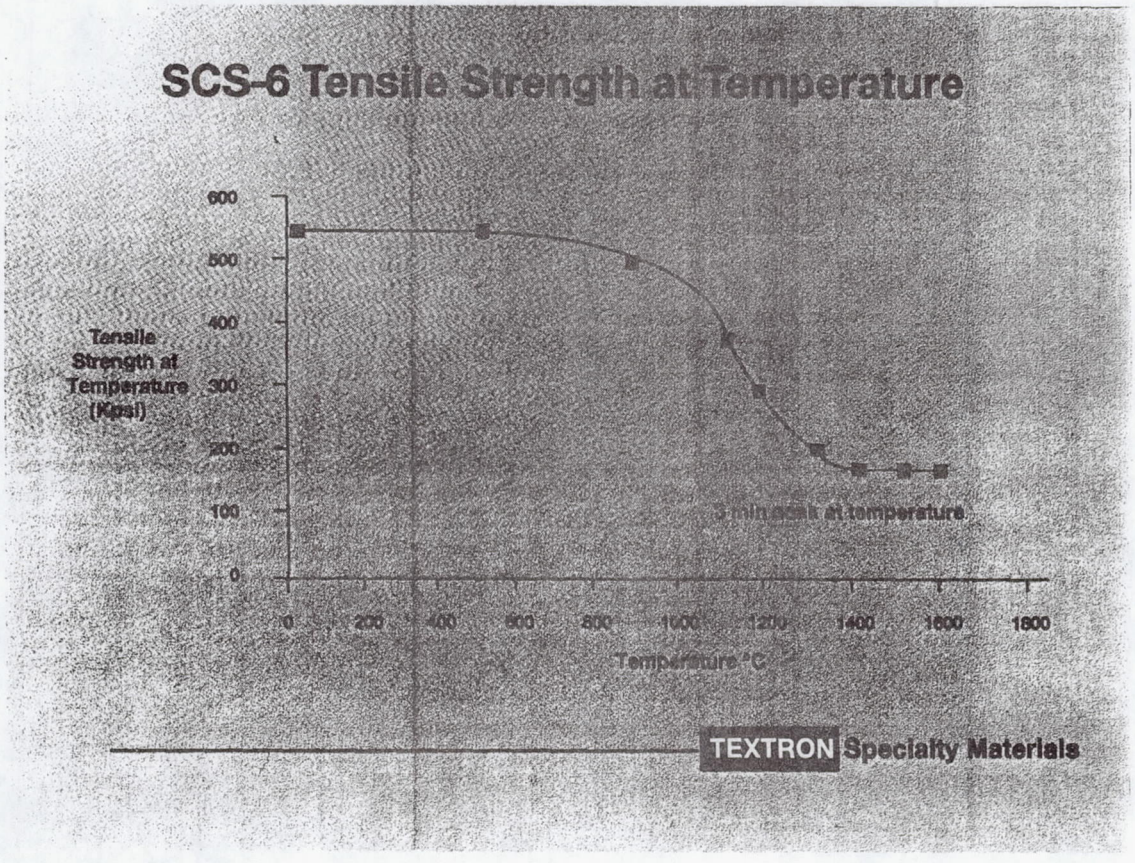
SCS-6 Tensile Strength at Temperature
Tensile Strength at Temperature (Kpsi)
600
500
400
300
200
100
0
0
200
400
600
800
1000
1200
1400
1600
1800
Temperature °C
TEXTRON Specialty Materials

= SiC =

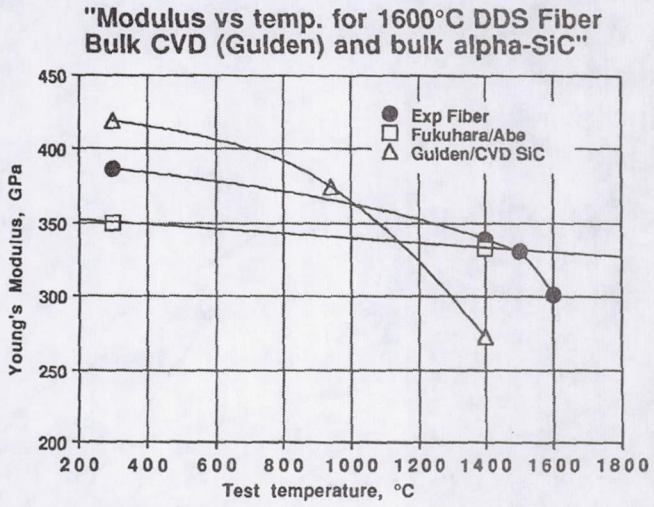

Figure 15. Plot Young's modulus (GPa)of fiber made at 2912°F(1600°C) from DDS and hydrogen,versus temperature (°C) compared with literature data (ref. 24, 25). Good agreement is evident. Gulden work was on CVD material.

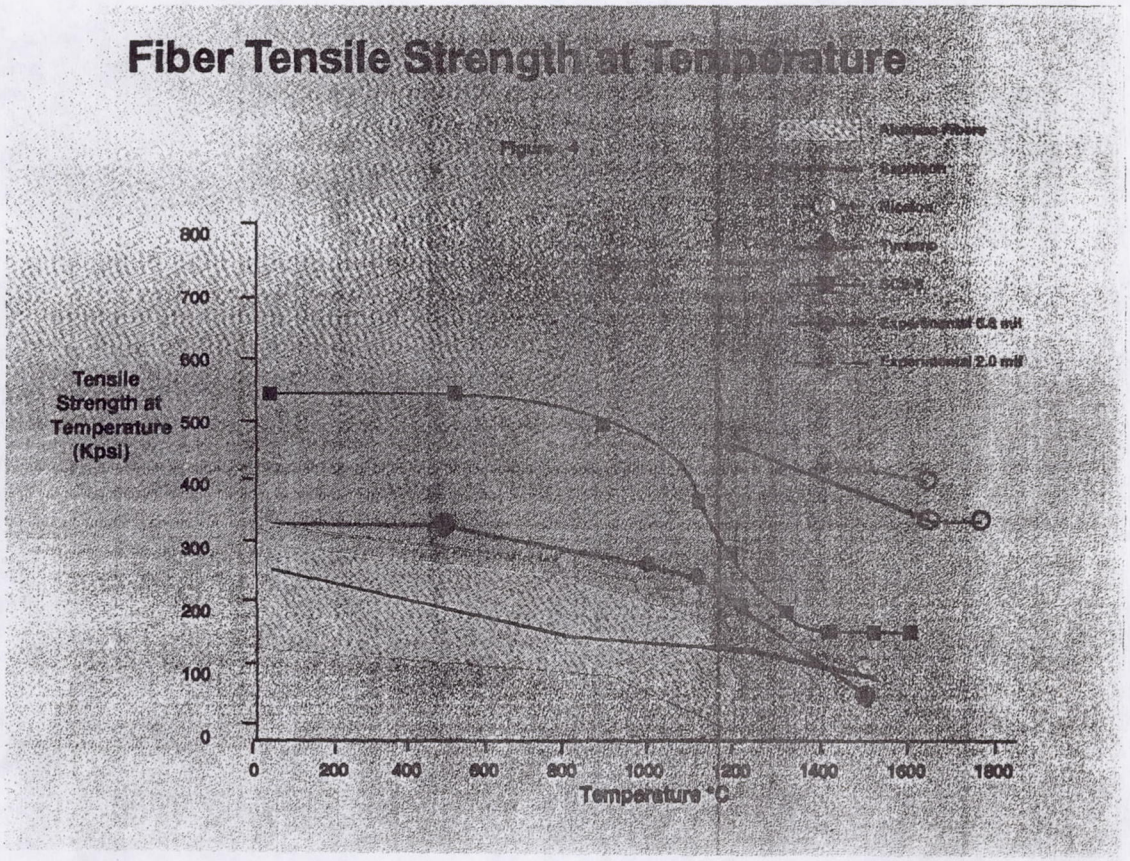

Figure 7

Comparison of creep rates at various loads for CVD and single crystal materials.
From G. Corman
AF Report
August 1990

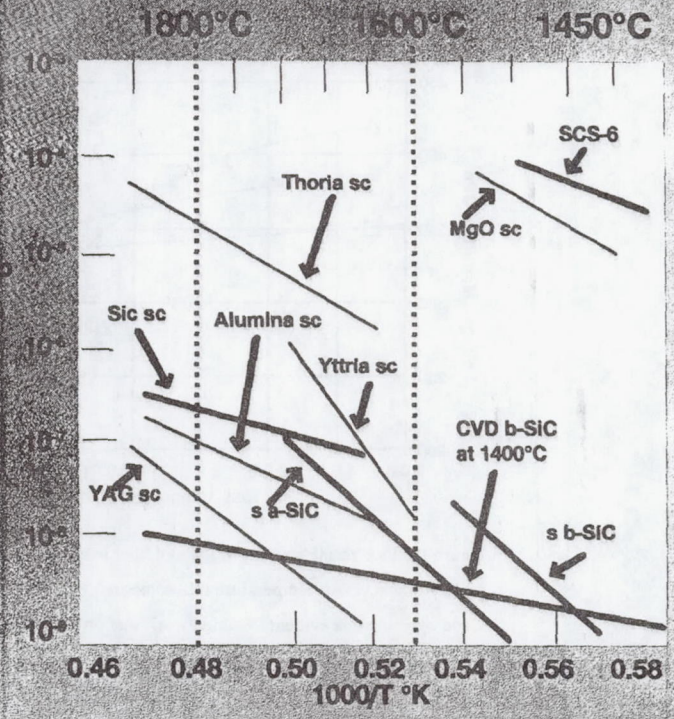

sc = single crystal
a = alpha
b = beta

FIBER SUMMARY

- FIBERS IN PRODUCTION (SCS-2™, 6, 8 AND 9)
- SCS-6™ - STANDARD FIBER FOR TITANIUM & CERAMICS
- SCS-9™ - DEVELOPMENT OF 3 mil DIAMETER FIBER
  - MADE ≃ 100 LBS
- PLANNED PRODUCTION FOR 1992 ≃ 500 LBS. (SCS-6™, 8 & 9)
- PLANT CAPACITY ≃ 1500 LBS/YEAR (BUILDING CAPABITY ≃ 20-30K LB/YEAR)

TEXTRON Specialty Materials

REPORT DOCUMENTATION PAGE

Form Approved
OMB No. 0704-0188

1. AGENCY USE ONLY (*Leave blank*)	2. REPORT DATE	3. REPORT TYPE AND DATES COVERED
	October 1993	Conference Publication

4. TITLE AND SUBTITLE

Seals Flow Code Development–92

5. FUNDING NUMBERS

WU–590–21–11

6. AUTHOR(S)

A.D. Liang and R.C. Hendricks

7. PERFORMING ORGANIZATION NAME(S) AND ADDRESS(ES)

National Aeronautics and Space Administration
Lewis Research Center
Cleveland, Ohio 44135–3191

8. PERFORMING ORGANIZATION REPORT NUMBER

E–8172

9. SPONSORING/MONITORING AGENCY NAME(S) AND ADDRESS(ES)

National Aeronautics and Space Administration
Washington, D.C. 20546–0001

10. SPONSORING/MONITORING AGENCY REPORT NUMBER

NASA CP–10124

11. SUPPLEMENTARY NOTES

Responsible person, Anita Liang, (216) 433–7439.

12a. DISTRIBUTION/AVAILABILITY STATEMENT

Unclassified - Unlimited
Subject Categories 16 and 99

12b. DISTRIBUTION CODE

13. ABSTRACT (*Maximum 200 words*)

A two-day meeting was conducted at the NASA Lewis Research Center on August 5 and 6, 1992, to inform the technical community of the progress of NASA Contract NAS3–25644. This contract was established in 1990 to develop industrial and CFD codes for the design and analysis of seals. Codes were demonstrated and disseminated to the user community for evaluation. The peer review panel which was formed in 1991 provided recommendations on this effort. The technical community presented results of their activities in the area of seals, with particular emphasis on brush seal systems.

14. SUBJECT TERMS

Seals; Numerical; Code; Flow

15. NUMBER OF PAGES

296

16. PRICE CODE

A–13

17. SECURITY CLASSIFICATION OF REPORT	18. SECURITY CLASSIFICATION OF THIS PAGE	19. SECURITY CLASSIFICATION OF ABSTRACT	20. LIMITATION OF ABSTRACT
Unclassified	Unclassified	Unclassified	

NSN 7540-01-280-5500

Standard Form 298 (Rev. 2-89)
Prescribed by ANSI Std. Z39-18
298-102